MÖSSBAUER AND SPECTROSCOPIC STUDIES OF YEAST CYTOCHROME OXIDASE

Thesis by

Hsin Wang

In Partial Fulfillment of the Requirements

for the Degree of

Doctor of Philosophy

California Institute of Technology

Pasadena, California

1987

(Submitted September 19, 1986)

Acknowledgements

I wish to thank my adviser, Professor Sunney Chan, for his support, guidance, and patience in this work. I am grateful that he granted me so much independence and freedom. On the other hand, I have also benefited a great deal from his meticulous way of reasoning and his emphasis on the connection of the experimental findings with the broad picture of the oxidase field.

I wish to thank Chan group oxidase workers of many generations for their assistance during my graduate years. Especially I would like to thank Dave Blair, Craig Martin, Jeff Gelles, Tom Stevens, Steve Witt, and John Manthey. Above all, I would like to thank Dave. I have learned a great deal about low temperature kinetics, redox properties, and, not the least, English from him. Every single word of this thesis has been read by him. If this thesis has any clarity at all, it is because of Dave. I also wish to thank him for involving me in the spectroelectrochemical studies with Walther Ellis in Gray's group, which ended with fruitful results and benefitted us all. Recently we recounted the events of helping fix each other's alternators. I felt the warmth of the friendship and was very moved.

I wish to thank Craig and Jeff for their help on computers. Craig's login.com and EPR routines have been very convenient for my work. Not less importantly, he has given me much assistance on cars and the English language. Tom taught me the ABC's of yeast-cell growth and the isolation of the yeast enzyme, and I thank him. I wish to thank Steve for discussions regarding the CO-photolysis and the reoxidation of yeast oxidase, and friendship. I thank John Manthey for allowing me to use his vacuum line in Dr. Hager's laboratory in Urbana. John and I also engaged in stopped-flow optical studies on yeast oxidase, using the Union Giken instrument in Drs. Hager and Sligar's laboratories (Urbana). Unfortunately I was not able to include this effort in my thesis. I also wish to thank his wife, Teresa, for the wonderful time at the

Reagans' in Davenport.

I wish to thank Professor Harry Gray for his interest in the redox properties of cytochrome oxidase. I wish to thank Walther Ellis for the collaboration with Dave and me. Walther picked up most of the sample loading responsibilities, from which Dave and I wisely retracted after a few practice runs. I am also impressed by the load on his neck machine.

My gratitude towards Professor Peter Debrunner is endless. During my visits to his laboratory in the University of Illinois at Urbana, he always gave me the first priority to his instruments. He also generously let me bring all the necessary computer programs back to Caltech. We had very close interactions during my visits. Through his clever and quiet inquiries, I was able to think through the problems more clearly. I feel totally at ease with him and I am not afraid to ask him any simple questions. Especially during last spring, I called him almost every week and he guided me through electronic theories to an extent that I thought I would never understand. Certainly this was a most pleasant experience. Several times, I stayed at his house. He and his wife, Sigrid, had shown me such a warmth and hospitality that I can never forget.

I would also like to thank his group, who have given me assistance on numerous occasions. Especially I would like to thank Chuck Schulz, Howie Dhonau, and Mike Hendrich. Chuck taught me everything I know about Mössbauer instruments and the use of Mössbauer computer programs. At the last stage of my analysis, he provided me with simulations using his recent relaxation program, for which I am very grateful. Howie spent endless hours on the high-field instrument. The result of this effort is presented in Chapter 2. Mike and I measured the low-field EPR transition (the so-called $g = 12$ signal) with a parallel-field cavity. At my request, he also plotted them for me. Unfortunately I was not able to include them in my thesis.

I wish to thank Professor Hans Frauenfelder, who granted me precious

instrument time to study the CO-recombination behavior of yeast oxidase. I also wish to thank his student Todd Sauke, Ben Cowen, Joel Berendzen, and Erramilli Shyamsunder for assistence. It was a fun experience to work on the photolysis experiments and to work with Todd. He pointed out a simple method to calculate the rate constant of CO-recombination, of which I was convinced after I derived the rate equations myself.

During my visits in Urbana, Professors Hager, Switzer, and Sligar generously let me use their facilities, for which I am most grateful.

I have been an NMR operator in the NSF Southern California NMR facility at Caltech for 5 years, and I wish to thank Drs. James Yesinowski, Hellmut Eckert, and Raphael Zidovetzki for the great time I enjoyed. Especially I would like to thank James for generously providing me a shelter in the last month of my stay in Pasadena, since the house in which I lived for many years was sold and turned over to the new owner two weeks before my Ph.D. defense. Without him, it would have been much more difficult. James was also very helpful in my career decision, for which I am grateful. I also wish to thank Jin-Feng Wang for teaching me to operate the NMR instrument and Paula Watnick for helpful assistance.

I wish to express my gratitude towards Nam-sun and Patty Wang. I was fortunate to know them. I cherish all the good time that I spent with them, especially the long trips that I took with them. They have made my life in Caltech much happier. I also wish to thank Nam for his assistance with computers. When I first came here, I was equipped with the computer language but not the operating knowledge; Nam helped me to fill this essential gap, for which I am grateful.

Finally and most importantly, I would like to thank my mother and my sister for their love.

ABSTRACT

Cytochrome oxidase from baker's yeast is investigated by Mössbauer spectroscopy, complemented by EPR, flash photolysis, and spectroelectrochemical studies. While the Mössbauer spectrum of cytochrome *a* can be described with one set of parameters, at least three components were identified for cytochrome a_3 in the native enzyme: a functional coupled site, a high spin ferric ion with the antiferromagnetic coupling disrupted, and a low spin ferrous ion. Photolysis experiments indicate that the CO-recombination at the functional cytochrome a_3 in yeast is a slow process with an activation energy of 33 kJ/mol, similar to that observed previously in the beef heart enzyme. The structure of this site is therefore very similar in both enzymes. However, the Mössbauer spectrum of the this site in yeast cannot be explained by the current spin Hamiltonian model that describes the widely accepted spin-coupling hypothesis. The shortcoming of this model is pointed out and discussed. The assignment of the reduced low spin heme to a degraded form of cytochrome a_3 is strengthened by photolysis studies, which reveal a second fast CO-rebinding site with a peak activation energy (13 kJ/mol) similar to that of myoglobin, and by spectroelectrochemical measurements, which demonstrate that the redox potential of the degraded cytochrome *a* is low rather than high as previously thought. Based on these findings in yeast oxidase and previous inactivation reports on beef heart oxidase, a global change in the structures of all of the metal centers during denaturation is suggested. The redox behavior of the normal cytochrome *a* in the CO-inhibited enzyme is well-explained by a 2-site interaction model which has also been applied successfully in the beef heart enzyme. The redox potential of cytochrome *a* in yeast is found to be roughly 45 mV higher than that in beef heart. A comparative EPR and Mössbauer study of the reoxidation of the fully-reduced yeast enzyme is also presented. The reoxidation course is well-described by the mechanism proposed for the beef heart enzyme and a few intermediates are suggested by the Mössbauer study.

TABLE OF CONTENTS

LIST OF ILLUSTRATIONS

INTRODUCTION

The cytochrome oxidase studied in this thesis is a cytochrome aa_3 type of oxidase. It is the terminal enzyme in the respiratory chain, which is located in the inner membrane of the mitochondrion in eukaryotic organisms. Recently, it has also been isolated from the cell membrane of several procaryotic microorganisms (1). The enzyme is a transmembrane protein and mediates the transfer of electrons between reduced cytochrome *c* and molecular oxygen. The overall reaction is given by:

$$4 \text{ ferrocytochrome } c + O_2 + 4H^+ \longrightarrow 4 \text{ ferricytrochrome } c + 2H_2O.$$

The oxidase receives its reducing equivalents from cytochrome *c* on the cytosol side, while four protons in the matrix are consumed per turnover. In addition, evidence is mounting that the enzyme is also a proton pump (2) with protons pumped across the membrane from the matrix to the cytosol side during turnovers. Thus, a transmembrane pH and/or potential gradient is established, which is used by ATPase to produce ATP.

Cytochrome oxidase has two iron centers and two copper centers. One iron, cytochrome a_3, and one copper, Cu_B, constitute the oxygen binding site. The other two centers, cytochrome *a* and Cu_A, are responsible for transferring

electrons from cytochrome *c* to the oxygen binding site and possibly are also involved in the proton-pumping acitvities (3). Recent reports (4,5) indicate the presence of strong binding sites for zinc and magnesium (stoichiometry 1:1 per oxidase molecule). As zinc and magnesium have not been located in bacterial cytochrome oxidases, their functions are probably peripheral.

Both iron-containing prosthetic groups are heme *a*'s, whose structure is shown in Figure 1. The special features of heme *a* are the formyl group in position 8 and the long isoprenoid chain in position 2 of the porphyrin ring. The presence of formyl group is suggested to increase the redox potential of these centers. By the same argument, the production of extremely high oxidation states such as compound I, which is commonly observed in peroxidases and catalase (6), is considered unfavorable. Although the two heme *a* centers are not covalently bound to the protein, efforts to reconstitute them back in the protein have not been successful. Cytochrome *a* is a low-spin center and has been proposed to be liganded by two axial histidines (7), which is supported by a recent ENDOR* study (8) on an isotopically labelled yeast cytochrome oxidase. Cytochrome a_3 is a high-spin center. The fifth ligand is a histidine (9). It is thought to be exchange-coupled to Cu_B to form an $S = 2$ center. The bridging ligand in the resting conformation has been suggested to be a histidine (10), an oxo (11), or a sulfur group (12).

Among the four metal centers, only cytochrome *a* and Cu_A display distinct EPR signals. The oxygen-binding site, cytochrome a_3 and Cu_B, is thought to be EPR-silent because of the coupled spin. However, an EPR signal at $g = 12$ has been proposed to arise from this coupled center (13) and was supported by EPR lineshape simulation studies (14,15). The optical spectrum of cytochrome oxidase is dominated by the overlapping absorptions from the two heme centers.

---

* The abbreviations used are: ENDOR, electron-nuclear double resonance; EPR, electron paramagnetic resonance.

Figure 1. The structure of heme *a*.

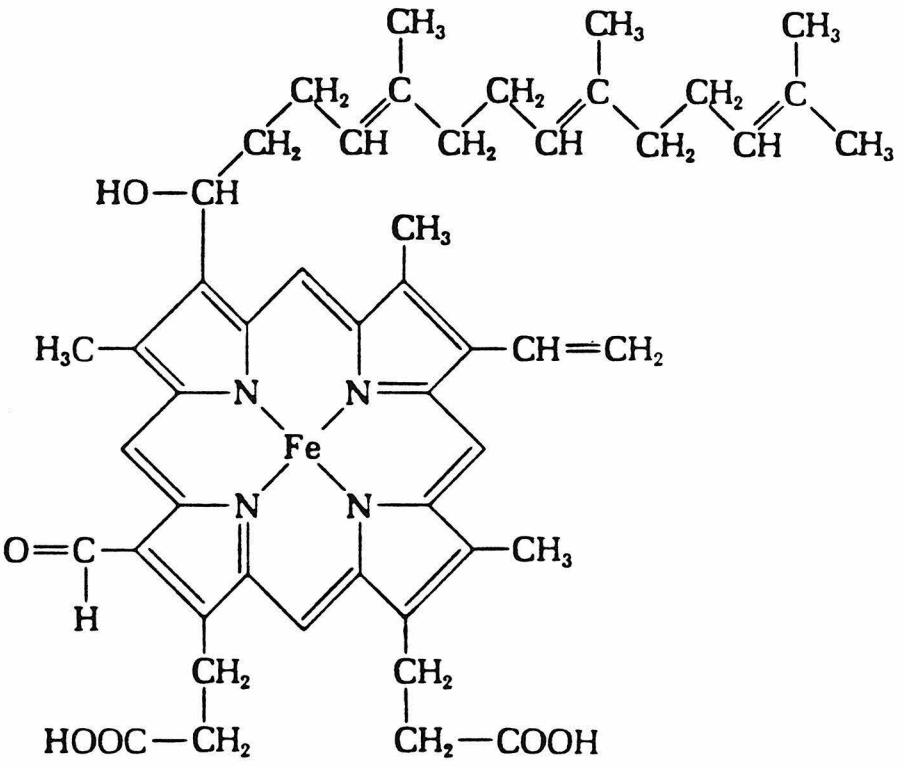
CH3
CH3
CH3
CH2
C
CH2
C
CH2
C
CH2
CH
CH2
CH
CH2
CH
CH3
HO—CH
CH3
H3C
CH=CH2
N
N
Fe
N
N
O=C
H
CH3
CH2
CH2
HOOC—CH2
CH2—COOH

This overlapping of the heme absorptions has led to severe misunderstandings about the structure of this enzyme until the last decade (2,16). Cu_A displays a weak band at 830 nm. A weak shoulder at 655 nm is probably associated with the coupled cytochrome a_3–Cu_B site (17,18).

Over the last ten years, impressive progress toward elucidating the chemical mechanisms of the redox processes catalyzed by the enzyme has also been achieved (2,19,20) mostly through optical and EPR studies. Unfortunately, in the studies of reaction intermediates, few EPR signals arise from the oxygen binding site and even fewer arise from cytochrome a_3.

Therefore, it is highly desirable to have direct access to the oxygen-binding site. We approach this problem by studying the ^{57}Fe enriched enzyme using Mössbauer spectroscopy, complemented by other spectroscopic studies. Since it is impractical to enrich the beef heart enzyme with ^{57}Fe, we have chosen the enzyme from baker's yeast for the Mössbauer work. The current knowledge about the subunit structure of yeast cytocochrome oxidase is summarized in Table 1. Yeast oxidase has nine subunits (21), as opposed to 13 in the beef heart enzyme (22). The physical properties of yeast oxidase are very similar to those observed in beef heart oxidase. However, a partial reduction has been detected in the resting oxidized state in virtually all the purified enzyme preparations (23). Since all iron centers are observed by Mössbauer spectroscopy, an extensive treatment is given to this partially reduced material as well as other minor contaminants, so that an accurate picture concerning the functional enzyme could be obtained. The partial reduction is found to be related to a denaturing process, which causes a global change in the structures of all of the metal centers. This phenomenon has not heretofore been understood.

We shall present in Chapter 1 the purification procedure and a general characterization of yeast cytochrome oxidase by optical and EPR studies. The Mössbauer studies of the native enzyme, in the resting oxidized and NADH-

Table 1. The Subunit Structure of Cytochrome Oxidase from Baker's Yeast

Subunit	Electro-phoresis[1]	DNA sequence[2]	HPLC & amino acid composition[3]	Coding origin
I	40,000	56,000	-	Mitochondrion
II	33,000	28,480	-	Mitochondrion
III	22,000	30,340	-	Mitochondrion
IV	14,500	-	13,600	Cytoplasm
V	12,700	-	12,200	Cytoplasm
VI	12,700	-	12,500	Cytoplasm
VII	4,600	-	6,500	Cytoplasm
VIIa	-	-	6,500	Cytoplasm
VIII	-	-	5,800	Cytoplasm
Subtotal		115,000	57,100	
Total	139,000			

1. Poyton, R.O. & Schatz, G. (1975). *J. Biol. Chem.* **250**, 752–761.
2. Bonitz, S.G., Coruzzi, G., Thalenfeld, B.E., & Tzagoloff (1980). *J. Biol. Chem.* **255**, 11927–11947; Coruzzi, G. & Tzagoloff, A. (1979). *ibid.* **254**, 9324–9330; Thalenfeld, B.E. & Tzagoloff, A. (1980). *ibid.* **255**, 6173–6180.
3. Power, S.D., Lochrie, M.A., Sevarino, K.A., Patterson, & Poyton, R.O. (1984) *J. Biol. Chem.* **259**, 6564–6570.

reduced states, are presented in Chapter 2. The spectral features of the low-spin ferric cytochrome *a* is deconvolved from the spectrum through simulations using a spin Hamiltonian model and a theory of low-spin ferric ions. The spectral features of cytochrome a_3 are fit with several hypotheses concerning the structure of the oxygen-binding site. The reduced material is identified unambiguously with a high-field measurement and its origin is assigned to a denatured form of cytochrome a_3. Both the functional and the denatured cytochrome a_3 are found to react with CO. The Mössbauer and photolysis studies of the CO-inhibited yeast enzyme are presented in Chapter 3. The CO-recombination behavior is found to be different for the two types of cytochrome a_3. A complete knowledge of the CO-inhibited enzyme is necessary, since it is the starting point of reoxidation studies. Chapter 4 presents a comparative EPR and Mössbauer study of the reoxidation of the fully reduced yeast enzyme. The reoxidation course is well described by the mechanism proposed for the beef heart enzyme, and a few intermediates are suggested by the Mössbauer study. In the last chapter, a comparative spectroelectrochemistry study of the redox potential of the cytochrome *a* in the beef heart and yeast oxidase is presented. The Nernst titration is well-explained by a 2-site interaction model (interaction between cytochrome *a* and Cu_A) proposed for the beef heart enzyme. Contrary to the assertion (23) that yeast oxidase becomes inactive because of a high redox potential that has developed at cytochrome *a*, the normal functioning yeast cytochrome *a* is found to have a redox potential roughly 45 mV higher than that in the beef heart enzyme, and the true cause of inactivation are two-fold: (1) an abnormal cytochrome *a* forms during the process of denaturation, which has a redox potential too low to be matched with cytochrome *c*; and (2) a reduction and spin transformation takes place at cytochrome a_3 such that the reaction with dioxygen at this site becomes unfavorable.

REFERENCES

1. Poole, R.K. (1983). *Biochim. Biophys. Acta* **726**, 205–243.
2. Wikström, M., Krab, K., and Saraste, M. (1981). *Cytochrome Oxidase: A Synthesis*, Academic Press, London.
3. Blair, D.F., Gelles, J., & Chan, S.I. (1986). *Biophys. J.* , in press.
4. Einarsdóttir, Ó. & Caughey, W.S. (1984). *Biochem. Biophys. Res. Commun.* **124**, 836–842.
5. Einarsdóttir, Ó. & Caughey, W.S. (1985). *Biochem. Biophys. Res. Commun.* **129**, 840–847.
6. Saunders, B.C. (1973). In *Inorganic Biochemistry* (G.L. Eichhorn, ed.), Vol. **2**, Elsevier, Amsterdam, pp. 988–1019.
7. Blumberg, W.E., & Peisach, J. (1971). In *Probes of Structure and Function of Macromolecules and Membranes* (B. Chance, T. Yonetani, & A.S. Midvan, eds.), Vol. 2, Academic Press, New York, pp. 215–229.
8. Martin, C.T., Scholes, C.P., & Chan, S.I. (1985). *J. Biol. Chem.* **260**, 2857–2861.
9. Stevens, T.H. & Chan, S.I. (1981). *J. Biol. Chem.* **256**, 1069–1071.
10. Palmer, G., Babcock, G.T., & Vickery, L.E. (1976). *Proc. Nat. Acad. Sci., U.S.A.* **73**, 2206–2210.
11. Blumberg, W.E., & Peisach, J. (1979). In *Cytochrome Oxidase* (T.E. King, Y. Orii, B. Chance, & K. Okunuki, eds.), Elsevier, Amsterdam, pp. 153–159.
12. Powers, L., Chance, B., Ching, Y., & Angiolillo, P. (1981). *Biophys. J.* **34**, 465–498.
13. Brudvig, G.W., Stevens, T.H., Morse, R.H., and Chan, S.I. (1981). *Biochemistry* **20**, 3912–3921.
14. Hagen, W.R. (1982). *Biochim. Biophys. Acta* **708**, 82-98.
15. Brudvig, G.W., Morse, R.H., and Chan, S.I. (1986). *J. Mag. Res.* **67**,

189–201.

16. Malmström, B.G. (1974). *Quart. Rev. Biophys.* **6**, 389–431.
17. Beinert, H., Hansen, R.E., & Hartzell, C.R. (1976). *Biochim. Biophys. Acta* **423**, 339–355.
28. Karlsson, B. & Andréasson, L.-E. (1981). *Biochim. Biophys. Acta* **635** 73–80.
19. Blair, D.F., Martin, C.T., Gelles, J., Wang, H., Brudvig, G.W., Stevens, T.H., and Chan, S.I. (1983). *Chemica Scripta* **21**, 43-53.
20. Blair, D.F., Witt, S.N., & Chan, S.I. (1985). *J. Amer. Chem. Soc.* **107**, 7389–7399.
21. Power, D.S., Lochrie, M.A., Sevarino, K.A., Patterson, T.E., & Poyton, R.O. (1984). *J. Biol. Chem.* **259**, 6564–6570.
22. Kadenbach, B. & Merle, P. (1981). *FEBS Lett.* **135**, 1–11.
23. Siedow, J.N., Miller, S., and Palmer, G. (1981). *J. Bioenerg. Biomemb.* **13**, 171-179.

CHAPTER 1

PURIFICATION & CHARACTERIZATION OF CYTOCHROME OXIDASE FROM BAKER'S YEAST, Saccharomyces cerevisiae

INTRODUCTION

In this chapter, we shall describe the purification procedure for the isolation of cytochrome oxidase from baker's yeast, and shall examine optical and EPR* properties of the enzyme thus purified. Optical studies indicate a partial reduction in the resting oxidized enzyme. Similar results have been reported by Siedow *et al.* (1) on the yeast enzyme from many different preparations. We will present Mössbauer evidence concerning the nature of this reduction in the next chapter.

Special attention will be given to the so-called '$g = 12$' signal. This signal is seen only in the resting state of the enzyme. In 1981, Brudvig *et al.* (2) proposed that this signal arose from transitions between $M_S = \pm 1$ sublevels in the $Fe_{a_3}^{3+}$–Cu_B^{2+} coupled $S = 2$ state. Their recent simulation results (3) strongly support this idea. On the other hand, Hagen (4) reported the study of this signal in the beef heart enzyme by parallel field EPR spectroscopy and supported a ferryl model ($S = 2$) for cytochrome a_3 in the resting oxidized

* Abbreviations used are: EPR, electron paramagnetic resonance; NADH, β-nicotinamide adenine dinucleotide; PMS, phenazine methosulfate

state, in which the EPR-detected transitions take place between $M_S = \pm 2$ sublevels. Clearly it would be desirable to resolve this issue by Mössbauer spectroscopy. Toward this end, it is important to locate such an EPR signal in yeast cytochrome oxidase.

Most researchers, however, agree that this resting conformation is probably not physiologically relevant. Greenaway *et al.* (5) first reported that the intensity of the $g = 12$ signal increased as the purification proceeded. On the other hand, Antonini *et al.* (6) have demonstrated that when the reduced cytochrome oxidase is reoxidized by a pulse of O_2, the enzyme assumes a 'pulsed' conformation, which has a higher activity than the resting enzyme. Brudvig *et al.* (2) noted that the $g = 12$ signal developed after reoxidation with a half-life of 1 hour. Therefore they proposed that the resting conformation was a dead-end conformation. Presumably a strong ligand is bridging between cytochrome a_3 and Cu_B in the resting state, which inhibits the reaction with O_2. This bridging ligand may be responsible for an antiferromagnetic coupling between cytochrome a_3 and Cu_B, which is suggested by magnetic susceptibility measurements (7–9) and by the absence of more typical Cu or Fe EPR signals. Although the resting conformation may not be an active form of cytochrome oxidase, it is very interesting from the physical point of view. Thus we conducted a Mössbauer study of the resting yeast cytochrome oxidase and will present the results in the next chapter.

Biochemically, it would be more meaningful to study the 'pulsed' state. However, very little information about the structure of this state is available. In this chapter, we shall also present a room temperature reoxidation study by EPR, in order to locate the 'pulsed' state in yeast cytochrome oxidase. The development of the $g = 12$ signal will also be followed. Due to the limited quantity of the yeast enzyme, many observations were made on one sample. Therefore some of the enzyme was lost to denaturation during the 'freeze-thaw' proce-

dure. However, the changes of the EPR signals during degradation provided important insights into the Mössbauer results.

MATERIALS AND METHODS

All chemicals used in the enzyme purifications were of enzyme grade when available; otherwise, they were reagent grade. All the chemicals used in the growth of yeast such as vitamins, amino acids, and galactose were the highest grades available from Sigma.

Large Scale Yeast Growth

The wild type *Saccharomyces cerevisiae* haploid strain D273–10B yeast cells were grown in a 350-liter fermenter, which was connected to a Sharples continuous flow centrifuge. The media contained yeast nitrogen-base component (10), 11 g each of uracil and adenine, 11 g of penicillin, and 17 g streptomycin. In addition, 95% ethanol was added as an additional carbon source at a rate of 1 gallon/day. A freshly grown yeast culture was used to inoculate the 350-liter fermenter to a level of about 10^6 cells/ml, and growth was allowed to proceed to about 5×10^8 cells/ml. All yeast growth was carried out at 30°C. The yield of yeast cells after 36 hours of growth was about 2–2.5 kg, wet weight.

Isolation of Yeast Mitochondria

Mitochondria were isolated from yeast by a procedure that was modified from the methods of Tzagoloff (11), Shakespeare & Mahler (12), and George-Nascimento & Poyton (13). A ~50% suspension of yeast cells in 0.4 M sucrose, 50 mM Tris-acetate, 2 mM EDTA, pH7.8 was pumped through a Dyno-Mill Cell Disintegrator (Model KDL) at 2.4 liters/h. This procedure resulted in the breakage of at least 80% of the yeast cells. The suspension that emerged from the disruption chamber was centrifuged at $4,000 \times g$ for 10 min to remove intact

cells and cell debris. The supernatant was adjusted to pH 5.3 with acetic acid and centrifuged at $54,000 \times g$ for 45 min. The mitochondria pellets were then resuspended in 50 mM phosphate, 1%KCl, 1 mM EDTA, pH 7.4 and stored at -80°C until use.

Isolation of Yeast Cytochrome Oxidase

Yeast cytochrome oxidase was isolated from mitochrondria by the method of Stevens *et al.* (14). This method used cholate to solubilize the isolated mitochondria. A crude enzyme was obtained after repeated fractionations with ammonium sulfate. The crude enzyme was then dialyzed and centrifuged to remove denatured materials. A cytochrome *c*-Sepharose 4B affinity column, prepared according to published precedures (15,16), was used to further purify the enzyme. It was found that washings with a 0.5% and a 2% cholate buffers (both containing Tris and EDTA, pH 7.4) were effective in removing contaminating materials. The enzyme was then eluted in a 0.2 M KCl solution containing Tween-20 and Tris, pH 7.4. This procedure has been described in detail elsewhere (14,17).

In the present study, the elution of protein from the cytochrome *c* affinity column was monitored continuously at 280 nm with a Gilson HM UV-Visible dual beam spectrophotometer. The eluted fractions were checked for cytochrome oxidase by measuring the absorbance difference between 603 nm and 630 nm in the presence of dithionite (18). The green fractions were collected, and the solution was brought to 25% ammonium sulfate saturation and centrifuged at $20,000 \times g$ for 10 min. The supernatant was then adjusted to 33% ammonium sulfate saturation and centrifuged again at $20,000 \times g$ for 10 min. The pellet was readily dissolved in a small volume of 0.5% Tween-20, 50 mM Tris, pH 7.4 buffer. The enzyme was dialyzed against the same buffer to remove ammonium sulfate, frozen in liquid nitrogen, and stored at -80°C

until use.

Protein Assays

Protein concentrations were determined by the method of Lowry *et al.* (19). Heme *a* concentrations were determined either by pyridine hemochromogen assay (20), assuming an extinction coefficient of 26.0 mM^{-1} cm^{-1} at 587 nm; or by the difference in absorbance between 603 nm and 630 nm after reduction with sodium dithionite (18), assuming an extinction difference of 16.5 mM^{-1} cm^{-1}. The results from these two procedures are in good agreement. The activity of the cytochrome oxidase was measured polarographically with a YSI model 53 oxygen electrode in a pH 7.4 medium containing 50 mM phosphate buffer, 0.5% Tween-80, 0.2 mg/ml of cytochrome *c*, and 30 mM ascorbate at 30°C.

Absorption spectra of yeast cytochrome oxidase were recorded on a Cary 219 spectrophotometer at room temperature. EPR spectra were recorded at the University of Illinois at Champaign-Urbana, on a Bruker ER200 X-band spectrometer, which was equipped with an Oxford Instruments helium flow cryostat.

Reoxidation Study by EPR Spectroscopy

Yeast cytochrome oxidase (0.35 mM) was degassed thoroughly, covered with argon, and then reduced by a slight excess (*ca.* 1.25 equiv.) of NADH (β-nicotinamide adenine dinucleotide, reduced form, from Sigma) in the presence of a small amount of PMS (phenazine methosulfate, also from Sigma). After complete reduction, an equal volume of oxygenated buffer was added to the sample, mixed well, and pipetted into an EPR tube. The sample was frozen within 1 min and the EPR spectrum was measured. The sample was then thawed several times to study the development of various EPR signals.

EPR intensity of the oxidized cytochrome *a* was quantitated as peak area at $g = 3$. Intensities of the $g = 12$ and $g = 6$ signals were measured as peak to

trough distances, and normalized respectively against the intensities observed in the resting enzyme, which account for 40% and 10% of one spin, respectively (*cf.* 'Results' section). Due to overlap of the Cu_A signal and a copper signal that is typical of inorganic coppers, the quantitation of Cu_A is rather difficult. The latter signal is identical to the so-called 'adventitious' copper signal. As will be demonstrated below, this copper is derived from the protein. Therefore it is neither adventitious nor inorganic. We shall term it as type 2 copper. The situation is worst around $g = 2$, since the intensity of the $g_\perp$ signal of the type 2 copper was significant. We did not attempt the quantitation of the Cu_Asignal. Inspection of the spectra indicates that the recovery of Cu_A intensity after the reoxidation is quite fast, comparable to that of cytochrome *a*. The increase in the peak-to-trough distances of the copper signals relative to those in the initial resting state will be interpreted in terms of an increase in the content of the type 2 copper. The latter signal probably arises from a form of degraded Cu_B(see below), and will be labeled as such in the figure.

RESULTS

Purification of Yeast Cytochrome Oxidase

The progress of a typical preparation of yeast cytochrome oxidase is summarized in Table 1. We note a substantial enhancement in heme *a* content after the purification of the protein on the cytochrome *c* affinity column. Figure 1 shows the specific affinity of this column toward yeast oxidase; here the eloution profiles of protein and oxidase are compared. While a substantial amount of protein eluted at low salt concetrations, most of the cytochrome oxidase elutes at higher (0.2 M KCl) salt concentrations. The final heme *a* content of 8.7 nmol of heme *a*/mg of protein compares well with typical values of 9–11 reported for preparations of beef heart cytochrome oxidase. The turnover rate of the purified enzyme is 11 electrons transferred per second per oxidase molecule,

comparable to other preparations of yeast cytochrome oxidase (1,21).

Optical Properties of Yeast Cytochrome Oxidase

Optical spectra of a typical preparation of the yeast enzyme are shown in Figure 2. The resting oxidized enzyme had a Soret maximum at 423 nm, about 5 nm red-shifted compared with that of beef heart enzyme. The α band (at 598 nm) had a higher absorbance than the β band (around 540 nm), which is unexpected since in the purified beef heart enzyme the two bands are of roughly equal intensity. Siedow *et al.* (1) has shown that the higher α band intensity can be lowered by reaction with ferricyanide and is thus a sign of partial reduction in the resting enzyme. This result is confirmed in our enzyme. In addition to the Soret, α, and β bands, a minor absorption can be discerned at 655 nm, which has been proposed (5,22,23) to arise from the coupled cytochrome a_3–Cu_B site. (Spectroelectrochemical studies indicate that some intensity at 655 nm is derived from cytochrome *a* as well (*cf.* Figure 4 of Chapter 5).)

The optical spectrum of the ascorbate-reduced yeast enzyme is very similar to that of the reduced beef heart enzyme. It reveals that this preparation of cytochrome oxidase is free of detectable contamination from cytochrome *c* and c_1 as evidenced by the A_{602}/A_{550} ratio of 2.4. The A_{423}/A_{442} ratio is 0.4; thus the amount of nonreducible oxidase (24) is low. These ratios are close to those reported by Lemberg (25) for beef heart cytochrome oxidase. However, a small peak can be located at 562 nm when dithionite is used as the reductant (spectrum not shown), indicating a contamination from cytochrome *b*. Under such conditions, the A_{423}/A_{442} ratio in the Soret band increases to 0.52. This is due to the wavelength shift of the absorption maxima during reduction (from 415 nm to 428 nm) of the contaminating cytochrome *b*. The concentration of cytochrome *b* in the purified yeast oxidase, estimated by the method of Vanneste (26), is 3–4.5% of the total hemes in typical preparations.

Table 1. Purification of Yeast Cytochrome Oxidase

	Total protein	Specific activity	Heme *a*/ protein
	mg	nmol O_2/mg/sec	nmol/mg
Mitochondrial particles	18,800	1.04	ND*
First ammonium sulfate fractionation (30 to 45%)	2,200	4.96	0.48
Second ammonium sulfate fractionation (28 to 39%)	680	2.62	0.96
Combined peak fractions of cytochrome oxidase with affinity column eluate	43	11.5	5.9
Purified yeast Cytochrome oxidase	30	11.9	8.7

* ND, not determined.

Figure 1. Elution profiles of yeast cytochrome oxidase (bottom, solid circles) and total proteins (top). Elution buffers were 10 mM Tris-acetate, 1 mM EDTA, pH 7.4, containing 0.5% cholate, A; 2% cholate, B; 0.5% Tween-20, 0.02 M KCl, C; 0.5% Tween-20, 0.2 M KCl, D; or 0.5% Tween-20, 1.0 M KCl, E. Methods of monitoring concentrations of protein and yeast cytochrome oxidase are described in the text.

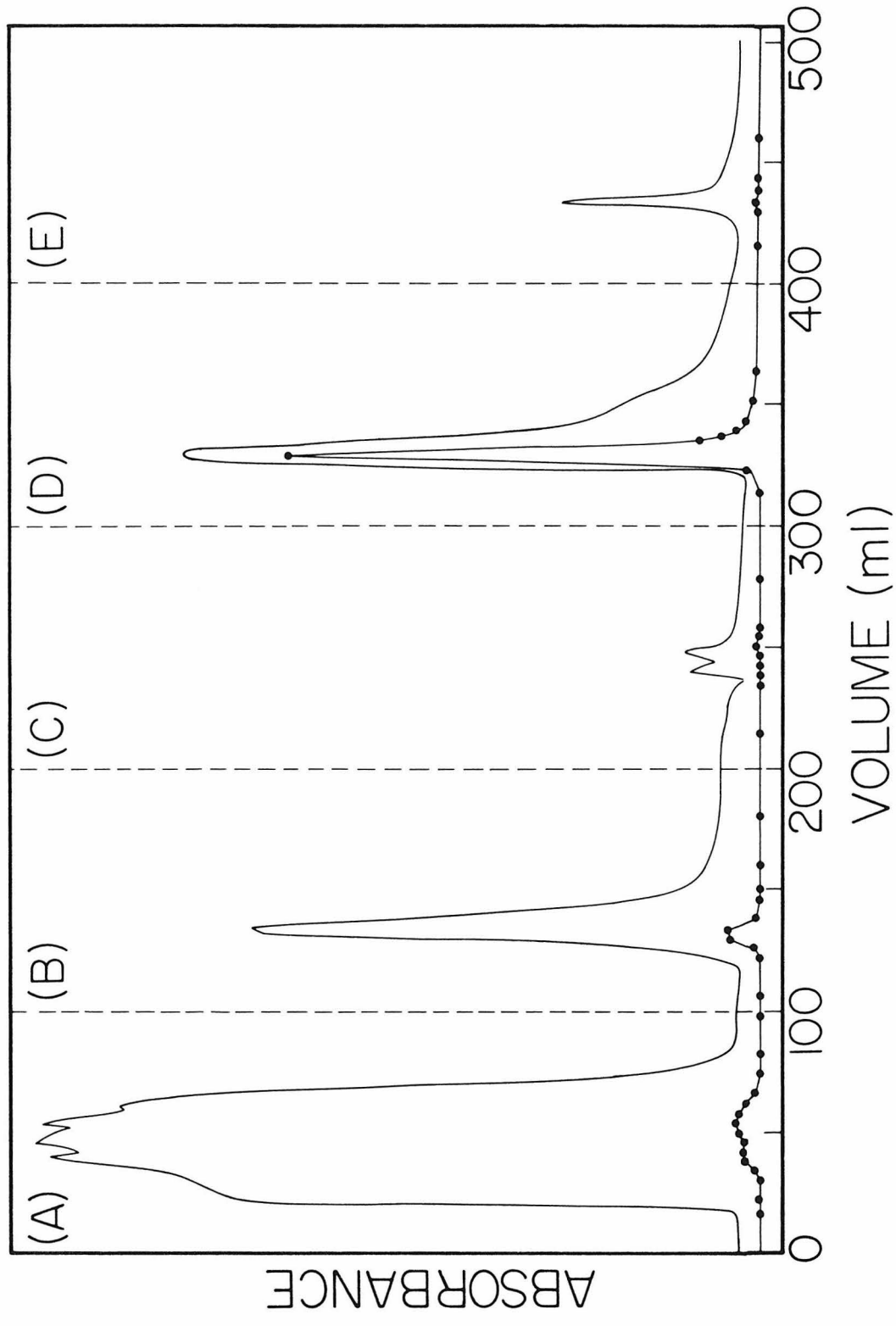
(A)
(B)
(C)
(D)
(E)
0
100
200
300
400
500
VOLUME (ml)
ABSORBANCE

Figure 2. Optical spectra of yeast cytochrome oxidase (21 μM). A, resting oxidized enzyme; B, enzyme reduced with 20 mM ascorbate and 0.2 mM *p*-phenylenediamine.

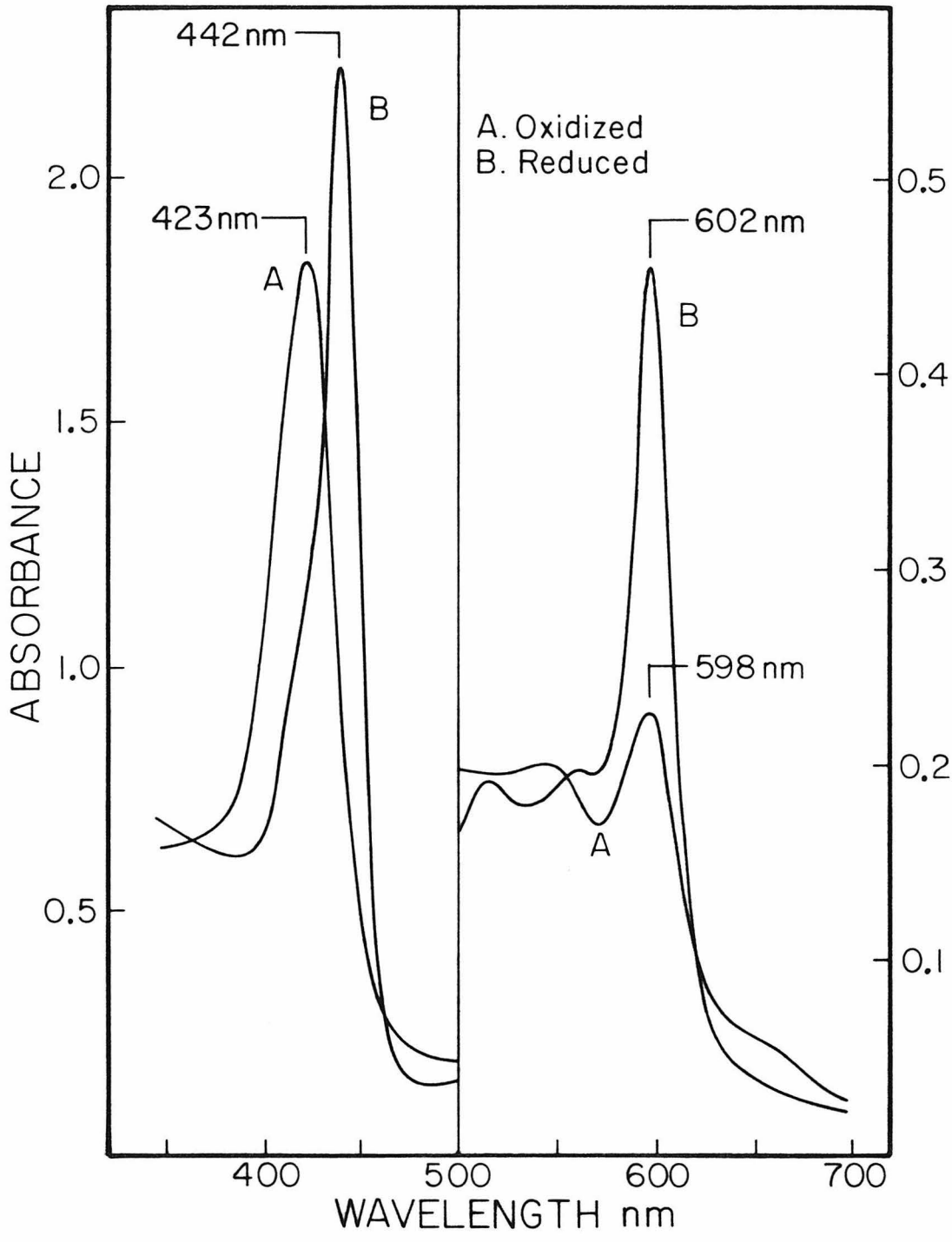
442 nm
B
A. Oxidized
B. Reduced
423 nm
A
602 nm
B
598 nm
A
ABSORBANCE
2.0
1.5
1.0
0.5
0.5
0.4
0.3
0.2
0.1
400
500
600
700
WAVELENGTH nm

EPR Properties of Yeast Cytochrome Oxidase

The EPR spectrum of a purified yeast cytochrome oxidase sample is shown in Figure 3. The EPR spectrum of the beef heart enzyme, prepared by the Hartzell & Beinert (27) method, is shown in Figure 4 for comparison. The oxidized cytochrome *a* of the yeast oxidase displays signals at $g = 2.98$, 2.25, and 1.49, very similar to those observed in the beef heart enzyme ($g = 3.0$, 2.3, and 1.46). Significant amounts of high spin signals near $g = 6$ are generally observed in the purified yeast enzyme. At least two kinds of high spin signals are present. An axial component is found at $g = 6$, whose intensity is lowered upon adding cyanide to the sample. Therefore this signal might represent a cytochrome a_3 site where the exchange coupling between cytochrome a_3 and Cu_B has been disrupted. For the rhombic signal, only the low-field peak, g_y, is observed at 6.7. This signal is insensitive to cyanide addition. These high spin centers have relatively low reduction potentials, as the EPR signals remained when the enzyme was reduced by excess NADH (spectrum not shown). The concentration of the high spin hemes varies from preparation to preparation. Together they typically account for ~10% of one heme when compared with the cytochrome *a* signal at $g = 3$ by the method of Aasa & Vänngård (28).

The three *g*-values for $Cu_A{}^{2+}$ in yeast cytochrome oxidase (2.14, 2.0, and 1.99) are also similar to those found in the beef heart enzyme. The lineshape is slightly different, probably due to the presence of the type 2 copper, which can be located around $g = 2.3$. In the presence of excess NADH, Cu_A is reduced and the EPR spectrum of the type 2 signal can be observed. Its *g*-values are at 2.30, 2.08, and 2.04, and a hyperfine coupling of 140 Gauss is found for the low-field ($g_{||}$) component (spectrum not shown). These parameters are similar to those found in inorganic copper signals. This species cannot be removed by dialyzing the sample against a buffer containing EDTA. In addition, it was found to react with cyanide (EPR spectrum not shown). Therefore it may

Figure 3. EPR spectrum of yeast cytochrome oxidase (0.35 mM). Conditions: Temperature, 9 K; microwave frequency, 9.433 GHz; microwave power, 0.1 mW; modulation amplitude, 16 Gauss; Gain, 8×10^4. The expanded region was measured with a gain of 2.5×10^6 and is a result of averaging 16 Scans.

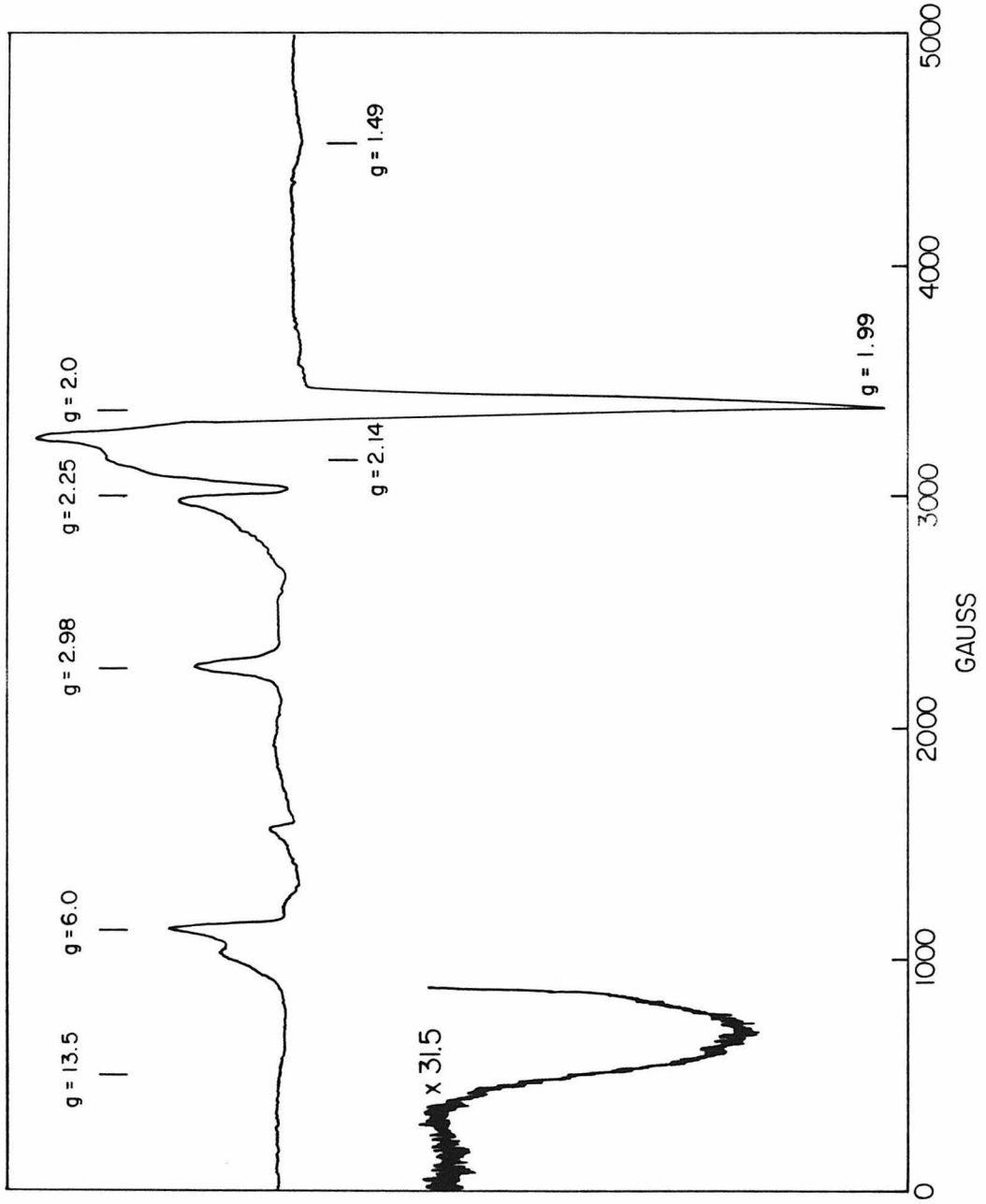
g = 13.5
g = 6.0
g = 2.98
g = 2.25
g = 2.0
g = 2.14
g = 1.49
g = 1.99
x 31.5
0
1000
2000
3000
4000
5000
GAUSS

Figure 4. EPR spectrum of beef heart cytochrome oxidase (0.23 mM). Conditions: Temperature, 9 K; microwave frequency, 9.433 GHz; microwave power, 0.1 mW; modulation amplitude, 16 Gauss; Gain, 1.6×10^5. The expanded region was measured with a gain of 2.5×10^6 and is a result of averaging 4 scans.

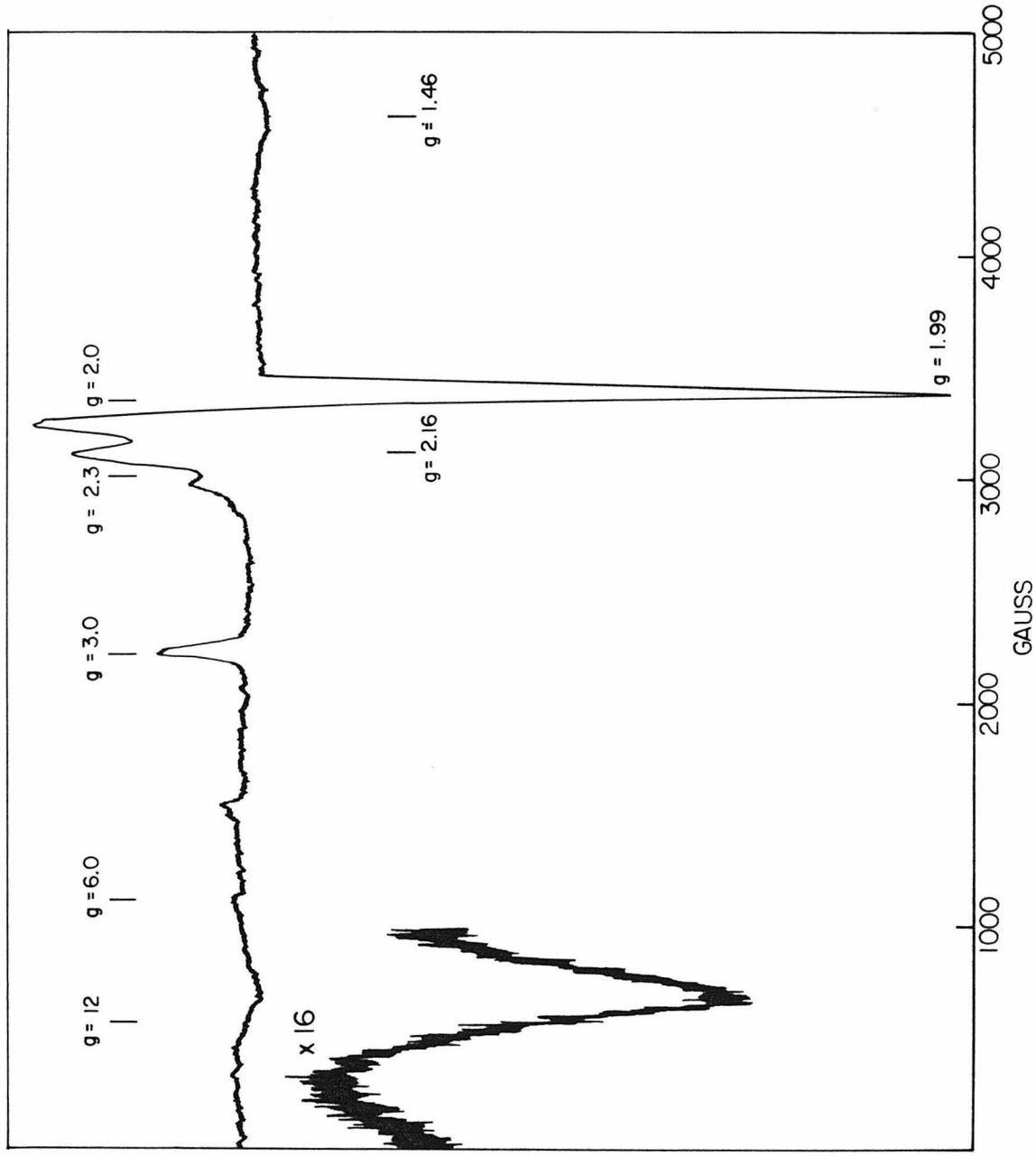
g = 12
g = 6.0
g = 3.0
g = 2.3
g = 2.0
g = 2.16
g = 1.99
g ≠ 1.46
x 16
1000
2000
3000
4000
5000
GAUSS

represent a denatured form of the a_3 site. However, there is no correlation between this copper signal and the high spin heme signals. For example, it was found that in one preparation, the high spin heme signal accounted for less than 5% compared with cytochrome *a* and the 'adventitious' copper accounted for 24% compared to Cu_A.

Yeast cytochrome oxidase exhibits a weak, broad EPR signal at $g = 13.5$. This band occurs in the same region of the spectrum as the $g = 12$ signal in the beef heart enzyme, and they are probably of the same origin. The expanded spectra in this region indicate that the intensity of $g = 13.5$ signal, when compared with the intensity of cytochrome *a* at $g = 3$, is roughly 40% of that of the $g = 12$ signal in beef heart oxidase. We shall refer to the signal observed at $g = 13.5$ in the yeast enzyme as the $g = 12$ signal, since it is the most familar term to researchers in this field.

Reoxidation of Yeast Cytochrome Oxidase at Room Temperature

The recovery or growth of various EPR signals at several time intervals after the reduced sample reacted with dioxygen at room temperature is shown in Figure 5. It shows that although close to 90% cytochrome *a* intensity was recovered within 1 min, no $g = 12$ signal could be detected at that time. However, a maximum intensity, 83% compared to the resting enzyme, was observed after one hour. The recovery of Cu_A intensity was comparable to cytochrome *a*, although accurate estimates are difficult to obtain. The slow recovery of the $g = 12$ intensities implies either that the reoxidation of the a_3 site is slow or that reoxidation leads to an intermediate state such as the 'pulsed' state, which then decays toward $g = 12$ state. Optical studies of the reoxidation of the same enzyme (spectra not shown) indicate that at 25 min after the reaction with dioxygen, the ratio of the α and β bands A_{598}/A_{540} is 1.5, significantly higher than the ratio observed in the resting oxidized yeast cytochrome oxidase

(typically, 1.2), and the Soret peaked at 426 nm. Since the 'pulsed' state of beef heart heart (6) is known to exhibit a higher extinction at the α band than the β band and a Soret maxima around 428 nm, our optical results suggest the presence of a 'pulsed' state although partial reduction cannot be ruled out. On the other hand, at 30 min after reoxidation, EPR study shows that a significant amount of the $g = 12$ conformation is produced (*cf.* Figure 5). Taken together, the optical and EPR results indicate clearly that the isolation of a pure 'pulsed' state in yeast cytochrome oxidase is quite difficult.

Figure 5 also shows the effects of denaturation during the 'freeze-thaw' process. The $g = 12$ signal did not recover its full intensity. A drop in the $g = 12$ intensity was accompanied by a sharp increase in the type 2 copper intensity after several 'freeze-thaw' cycles. The intensity of the high spin heme signals remained relatively unchanged, however. Since the intensities of the type 2 copper signal were measured as increases of copper signal intensities over the resting enzyme, this signal is most likely associated with Cu_B. The cytochrome a_3 in the degraded molecules cannot be accounted for by any EPR signals in the spectrum; accordingly, we surmise that cytochrome a_3 is reduced in the degraded enzyme, and it must be in the low-spin form. This conclusion is supported by the lack of relaxation effect on the Cu_B signal.

DISCUSSION

The EPR signals of cytochrome *a* and Cu_A in the yeast cytochrome oxidase are very similar to those in the beef heart enzyme, indicating that structures of these two metal centers are also alike. The detections of a low field EPR signal (at $g = 13.5$) and the 655 nm absorption band suggest that the ligand field structures of the a_3 sites in the two resting enzymes are also very similar. Although the lineshapes of the $g = 12$ signal of the beef heart enzyme and the $g = 13.5$ signal of the yeast enzyme are somewhat different, only a subtle

Figure 5. The recovery or growth of various EPR signals after the reoxidation of the reduced yeast cytochome oxidase by dioxygen at room temperature. The methods used to quantitate each species from the EPR spectra have been described in the 'Materials and Method' section. EPR spectra were measured under following conditions: Sample concentration, 0.17 mM; Temperature, 9 K; microwave frequency, 9.433 GHz; microwave power, 0.1 mW; modulation amplitude, 16 Gauss; Gain, 2×10^5. The low field region (around $g = 12$) of each spectrum was measured again with a gain of 5×10^6, each signal averaged 16 times. Curves are drawn to guide th eye only.

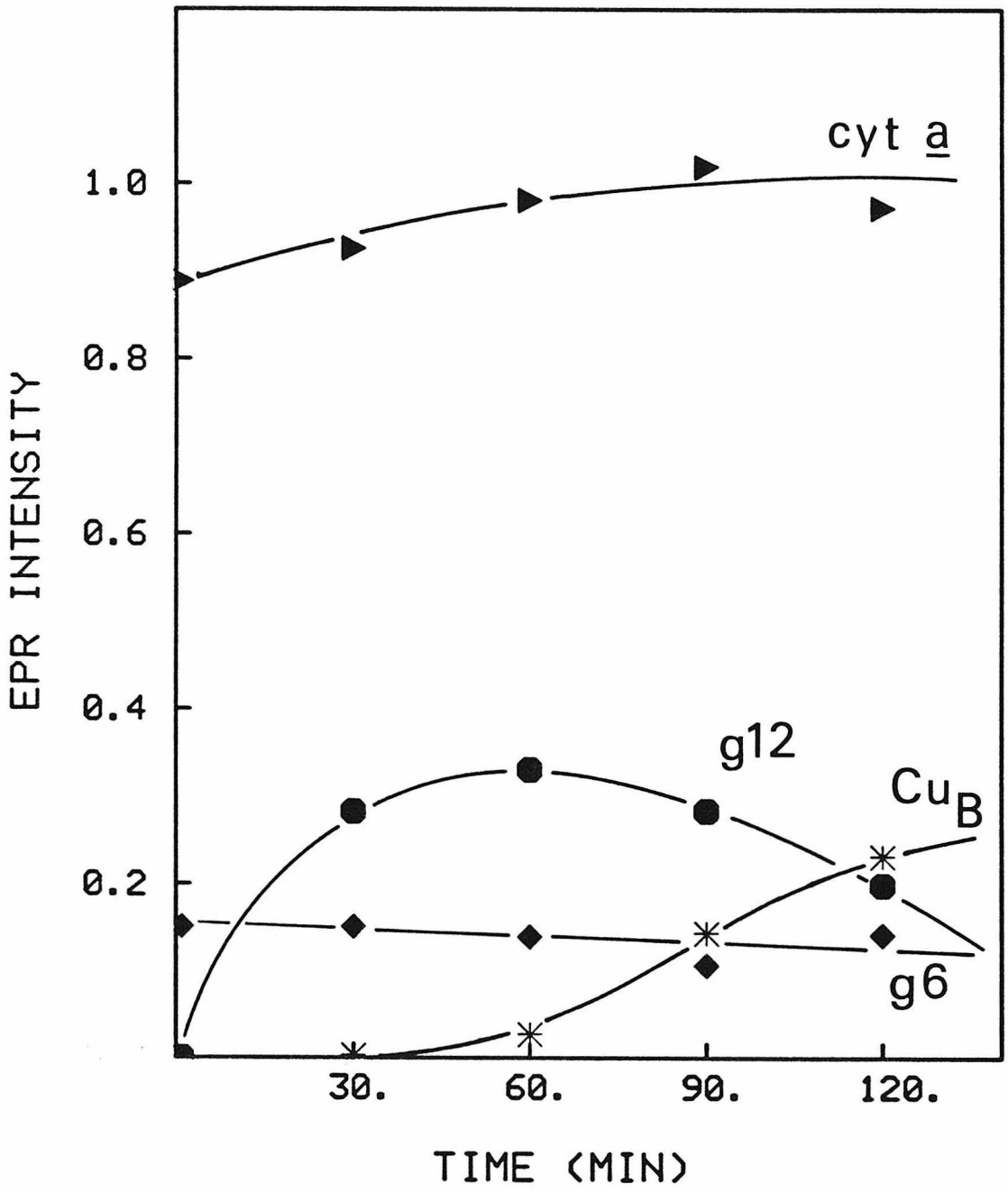
cyt a
1.0
0.8
0.6
0.4
0.2
EPR INTENSITY
g12
Cu B
g6
30.
60.
90.
120.
TIME (MIN)

difference in the fine structure of the resting a_3 site is suggested.

However, the yield of the $g = 12$ signal in yeast cytochrome oxidase is somewhat lower compared to that in the beef heart enzyme. A comparison of peak heights indicates that the yield of this signal in yeast oxidase is roughly 40% of that in the beef heart enzyme. This number is probably an underestimate, as the linewidth observed in the yeast enzyme was greater. The remaining cytochrome a_3 in the sample cannot be explained by the high spin heme signals (which account for 10% of one cytochrome) only. Our reoxidation studies suggest that in the degraded enzyme molecules, cytochrome a_3 exists in a low spin reduced form. This kind of heterogeneity at the a_3 site has not heretofore been suspected.

The existence of reduced materials in the resting oxidized yeast cytochrome oxidase has been pointed out before by Siedow *et al.* (1). However, they attributed the reduced hemes to cytochrome *a* instead. Mössbauer study of the resting oxidized yeast enzyme, which will be presented in the next chapter, shows unequivocally the presence of a low-spin reduced material in the resting yeast enzyme, and demonstrates that the reduced species is derived from cytochrome a_3.

REFERENCES

1. Siedow, J.N., Miller, S., & Palmer, G. (1981). *J. Bioenerg. Biomemb.* **13**, 171-179.
2. Brudvig, G.W., Stevens, T.H., Morse, R.H., & Chan, S.I. (1981). *Biochemistry* **20**, 3912–3921.
3. Brudvig, G.W., Morse, R.H., & Chan, S.I. (1986). *J. Mag. Res.* **67**, 189–201.
4. Hagen, W.R. (1982). *Biochim. Biophys. Acta* **708**, 82-98.
5. Greenaway, F.T., Chan, S.H.P., & Vincow, G. (1977). *Biochim. Biophys. Acta* **490**, 62–78.
6. Antonini, E., Brunori, M., Colosimo, A., Greenwood, C., & Wilson, M.T. (1977). *Proc. Natl. Acad. Sci. USA* **74**, 3128–3132.
7. Falk, K.-E., Vänngård, T., & Ånström, J. (1977). *FEBS Lett.* **75**, 23-27.
8. Tweedle, M.F., Wilson, L.J., Garćia-Iñiguez, L., Babcock, G.T., & Palmer, G. (1978). *J. Biol. Chem.* **253**, 8065–8071.
9. Moss, T.H., Shapiro, E., King, T.E., Beinert, H., & Hartzell, C.R. (1978). *J. Biol. Chem.* **253** 8072–8073.
10. *Difco Manual* (1953). Difco Laboratories, Detroit, p. 251.
11. Tzagoloff, A. (1969). *J. Biol. Chem.* **244**, 5020–5026.
12. Shakespeare, P.G. & Mahler, H.R. (1971). *J. Biol. Chem.* **246**, 7649–7655.
13. George-Nascimento, C. & Poyton, R.O. (1981). *J. Biol. Chem.* **256**, 9363–9370.
14. Stevens, T.H., Martin, C.T., Wang, H., Brudvig, G.W., Scholes, C.P., & Chan, S.I. (1982). *J. Biol. Chem.* **257**, 12106–12113.
15. Ozawa, T., Okumura, M., & Yagi, K. (1975). *Biochem. Biophys. Res. Commun.* **65**, 1102–1107.
16. Godinot, C. & Gautheron, D.C. (1979). *Methods Enzymol.* **55**, 112–124.
17. Stevens, T.H. (1981). Ph.D. Thesis, California Institute of Technology.

18. van Gelder, B.F. (1966). *Biochim. Biophys. Acta* **118**, 36–46.

19. Lowry, O.H., Rosebrough, N.J., Farr, A.L., & Randall, R.J. (1951). *J. Biol. Chem.* **193**, 265-275.

20. Morrison, M. & Horie, S. (1965). *Anal. Biochem.* **12**, 77–82.

21. Power, D.S., Lochrie, M.A., Sevarino, K.A., Patterson, T.E., & Poyton, R.O. (1984). *J. Biol. Chem.* **259**, 6564–6570.

22. Beinert, H., Hansen, R.E., & Hartzell, C.R. (1976). *Biochim. Biophys. Acta* **423**, 339–355.

23. Karlsson, B. & Andréasson, L.-E. (1981). *Biochim. Biophys. Acta* **635**, 73–80.

24. Wikström, M., Krab, K., & Saraste, M. (1981). *Cytochrome Oxidase: A Synthesis*, Academic Press, London.

25. Lemberg, M.R. (1969). *Physiol. Rev.* **49**, 48-121.

26. Vanneste, W.H. (1966). *Biochim. Biophys. Acta* **113**, 175–178.

27. Hartzell, C.R., & Beinert, H. (1974). *Biochim. Biophys. Acta* **368**, 318-338.

28. Aasa, R. & Vänngård, T. (1975). *J. Mag. Res.* **19**, 308–315.

CHAPTER 2

MÖSSBAUER STUDY OF CYTOCHROME OXIDASE FROM BAKER'S YEAST

Saccharomyces cerevisiae

INTRODUCTION

The understanding of the electronic structures of the four metal centers of cytochrome oxidase is essential to its characterization and is prerequisite to understanding the mechanism by which dioxygen is reduced to water at the enzyme's active site. The two heme centers, cytochromes a and a_3, are more accessible to optical studies than are the two copper centers because of the high extinctions of the iron centers in the visible spectrum. However, the interpretation of these studies has generated much confusion. The problem has arisen from overlapping of the spectrum of the two hemes as well as interactions between them that influence their reduction potentials. For a long time there existed two schools of thought regarding the heme structures in cytochrome oxidase, namely, the 'unitarian' and 'dualistic' hypotheses. The former postulated that cytochrome a and a_3 were both low-spin and virtually identical in the oxidized state prior to the addition of ligands. The latter, on the other hand, postulated that they were structurally and functionally different. It was not until the late seventies that the dualistic theory established itself (see reviews by Malmström (1) and by Wikström *et al.* (2)). Several physical methods that probe electronic

structure, such as resonance Raman (3,4), magnetic circular dichroism (MCD*) (5,6), Mössbauer (7) spectroscopies, and magnetic susceptibility measurements (8-10), provided decisive evidence to settle this debate.

In 1974, Lang, Lippard, and Rosén (7) were able to show by Mössbauer spectroscopy that in beef heart cytochrome oxidase there are two different hemes in the oxidized and reduced states. One exhibits a Mössbauer spectrum very similar to that of cytochrome *c*, and the other is very similar to the high-spin component of cytochrome *c* peroxidase in the oxidized state. This study was certainly instrumental in establishing the 'dualistic' theory.

Most of our knowledge about cytochrome oxidase has come from studies on the beef heart enzyme. Unfortunately, it is impractical to enrich the beef heart enzyme with ^{57}Fe, since heme *a* cannot be extracted from the protein and reconstituted. The measurements on the beef heart enzyme had to be performed with the natural abundance of this isotope (2.2%), resulting in spectra with poor signal to noise. This seriously limited the information on the heme electronic structures that could be gained from that study.

The electronic structure of low-spin cytochrome a^{3+} is well understood as a result of numerous EPR studies. The ligand field structure of this ion was predicted from its *g*-values and by comparison with other hemeproteins using Blumberg-Peisach diagrams (11,12). The results suggested that the axial ligands of cytochrome *a* were two histidines. This structure is strongly supported by a recent ENDOR study on isotopically labeled yeast cytochrome oxidase (13).

Information about the electronic structure of cytochrome a_3 is difficult to obtain because of the absence of readily interpretable EPR signals from this site in the resting oxidized enzyme. Van Gelder and Beinert (14) were the first

---

* The abbreviations used are: EPR, electron paramagnetic resonance; MCD, magnetic circular dichroism; ENDOR, electron-nuclear double resonance; EFG electric field gradient.

to propose an antiferromagnetic coupling between high-spin cytochrome $a_3{}^{3+}$ and $Cu_B{}^{2+}$ to account for this 'quenching' of EPR signals. This model quickly captured the interest of the theorists. Within a few years, Griffith (15) showed that in the presence of a strong antiferromagnetic coupling such a system can be viewed as $S = 2$ and is therefore likely to be EPR-silent. Subsequent MCD studies (5,6) indicated that the oxidized enzyme contains a high-spin ferricytochrome a_3 and a low-spin ferricytochrome a. Later, magnetic susceptibility measurements (8-10) indicated that cytochrome a_3 and Cu_B in the oxidized state were best described by one $S = 2$ center, in full agreement with the proposal of van Gelder and Beinert.

In 1980, Seiter and Angelos (16) came up with an alternative to the widely accepted spin coupling model. In their model, Cu_B remains in the cuprous state whether the enzyme is oxidized or reduced, while cytochrome a_3 changes between the ferryl (Fe^{IV}) state and the ferrous state during oxido-reduction. The idea came from the results of copper X-ray edge absorption experiments (17), which showed that one copper center appeared to remain reduced during oxido-reduction. Most researchers attribute this center to the other copper center, Cu_A, because of its unusual spectroscopic properties. The ferryl hypothesis contradicts the results of many physical studies (see review (2)). However, a recent EPR study by Hagen (18) provided some support for the proposal.

Two spectroscopic properties, namely, the optical band at 655 nm and the $g = 12$ signal in the X-band EPR spectrum, have been thought to arise from the Fe_{a_3}/Cu_B center. Beinert *et al.* (19) suggested that the 655 nm band may be due to ferric cytochrome a_3 when it is coupled with Cu_B. This was substantiated by the work of Karlsson and Andréasson (20), who showed that the disappearance of a Cu_B EPR signal was accompanied by the simultaneous appearance of the intensity at 655 nm.

In 1981, Brudvig *et al.* (21) proposed that the '$g = 12$' band observed in

X-band EPR spectra of oxidized cytochrome oxidase arose from the transition between $M_S = \pm 1$ sublevels in the coupled $S = 2$ system. Subsequently, Hagen (18) measured this signal with parallel field X-band EPR. His simulation results indicated that the signal was from an $S = 2$ system, but the transition took place instead among the $M_S = \pm 2$ sublevels. He also reasoned that the measured zero field parameter $D = +1.19$ cm^{-1} was much too small to be consistent with the Griffith model or the modification of it. He therefore argued for the ferryl model. Recently, Brudvig *et al.* (22) simulated the 9 GHz and 15 GHz EPR spectra using both models, and they concluded that the signals were best reproduced by the $\Delta M_S = 2$ transition among $M_S = \pm 1$ sublevels in a coupled $S = 2$ state. Their simulation, however, was not sensitive to the size of D.

Clearly more information is needed in order to understand the electronic structure of this site. We approach this problem by using Mössbauer spectroscopy to study the enzyme from baker's yeast, *Saccharomyces cerevisiae*, grown in ^{57}Fe enriched media. We have presented evidence in Chapter 1 that yeast oxidase exhibits optical and EPR properties similar to those of mammalian oxidase and will present evidence in Chapter 4 that similar reoxidation intermediates have been isolated for both enzymes at low temperature. They are thus structurally and functionally similar. On the other hand, there are dissimilarities also. Siedow *et al.* (23) found a few years ago that a fraction of heme was reduced in the resting state of virtually all known purified yeast enzyme. They indicated that this 'inactive' fraction was present in the submitochondrial particles and was probably present in the intact yeast.

A similar Mössbauer study has been reported by Kent *et al.* (24) on a bacterial cytochrome oxidase (cytochrome c_1aa_3) from *Thermus thermophilus*. The reduced cytochrome a_3 of the bacterial enzyme was high spin. The oxidized a_3, however, was very preparation-dependent. One sample contained cytochrome a_3 whose Mössbauer spectrum was easily broadened by a small field. In an-

other, cytochrome a_3 was virtually diamagnetic in the oxidized enzyme. The spin state of this site was therefore undetermined. They also noted that the spectrum of a_3–CN^- in the oxidized enzyme was broadened by a small magnetic field. Similar broadening was later found for the CN^--derivative of the beef heart enzyme (25). They argued that this broadening indicated that the electronic ground state was a doublet, which implied a ferromagnetic coupling between low spin ferric heme ($S = \frac{1}{2}$) and $Cu_B{}^{2+}$ and a negative D. This interpretation is in agreement with the findings of MCD experiments by Thomson *et al.* (26), but contradicts the magnetic susceptibility measurements by Tweedle *et al.* (9).

In this work we present a Mössbauer study on the resting and the reduced states of yeast cytochrome oxidase. Emphasis is placed on the above-mentioned heterogeneity reported by Siedow *et al.* (23) and the electronic structure of the functioning a_3 site.

MATERIALS AND METHODS

Preparation of the Mössbauer Samples

The enzyme used in the Mössbauer experiments was obtained by growing the wild-type *Saccharomyces cerevisiae* haploid strain D273-10B in an ^{57}Fe-enriched medium in a 350-liter stainless steel fermentor. This medium contained galactose, yeast nitrogen base (Difco formula) components, uracil, adenine, penicillin, streptomycin and ethanol as described in Chapter 1. All the inorganic ingredients used in the yeast growth were of enzyme grade when available. Galactose, amino acids, and vitamins were the highest grade available from Sigma. The iron-56 background from these chemicals was estimated by atomic absorption spectroscopy to be less than 30 μg per liter of the medium. Iron-57 was obtained in the form of iron oxide from Oak Ridge National Laboratory, and the enrichment was 90.24%. The iron oxide was converted into

ferric chloride solution by boiling gently in a dilute hydrochloric acid solution. The hydrochloric acid was ultrapure grade from Alfa. A three-fold excess of iron-57 ferric chloride as required by the Difco formula was employed in the medium. Roughly 75% enrichment in ^{57}Fe in the yeast cell was expected . The enzyme isolation procedure has been described in detail in Chapter 1. Protein concentration in heme *a* was determined by using an extinction difference of 16.5 $mM^{-1}cm^{-1}$ between 600 nm and 630 nm for the reduced enzyme (27).

Four different enzyme samples which were enriched in ^{57}Fe were isolated according to the same purification procedure. Sample 1 was further concentrated by dialyzing 20 minutes against solid Sephadex-200 on an ice bath. Sample 2 was obtained by reprecipitation with ammonium sulfate. Sample 3 was further concentrated to 0.65 mM in heme *a* by dialyzing against 30% (w/v) Aquacide III (from Calbiochem) solution, and the result was quite satisfactory. Sample 4 was 0.59 mM in heme *a* as isolated and no further concentration was necessary. All the preparations were dialyzed against 100 folds tween-20/tris acetate buffer at pH7.4 and centrifuged 20 minutes at 27,000 $\times$ g, to remove insoluble material. The quality of sample 1 and 2 was less satisfactory. The results from these two samples are included because they are helpful in discussion.

The native enzyme was studied as isolated. Due to the nature of this enzyme, the reduction requires strict anaerobicity. Therefore, a special glassware, shown in Figure 1, was designed for this purpose. In it the enzyme was degassed and purged with argon 5-6 times. A tenfold excess of reduced β-nicotinamide adenine dinucleotide(NADH) and 0.26 μmole phenazine methyl sulfonate(PMS) were degassed and then introduced through the septum with a Hamilton gas-tight syringe. The reduction was allowed to take place for at least 1 hour at room temperature. The completion of the reaction was monitored via the α band, using a 1 mm pathlength optical cell.

Figure 1. Glassware designed for the anaerobic operations of Mössbauer samples.

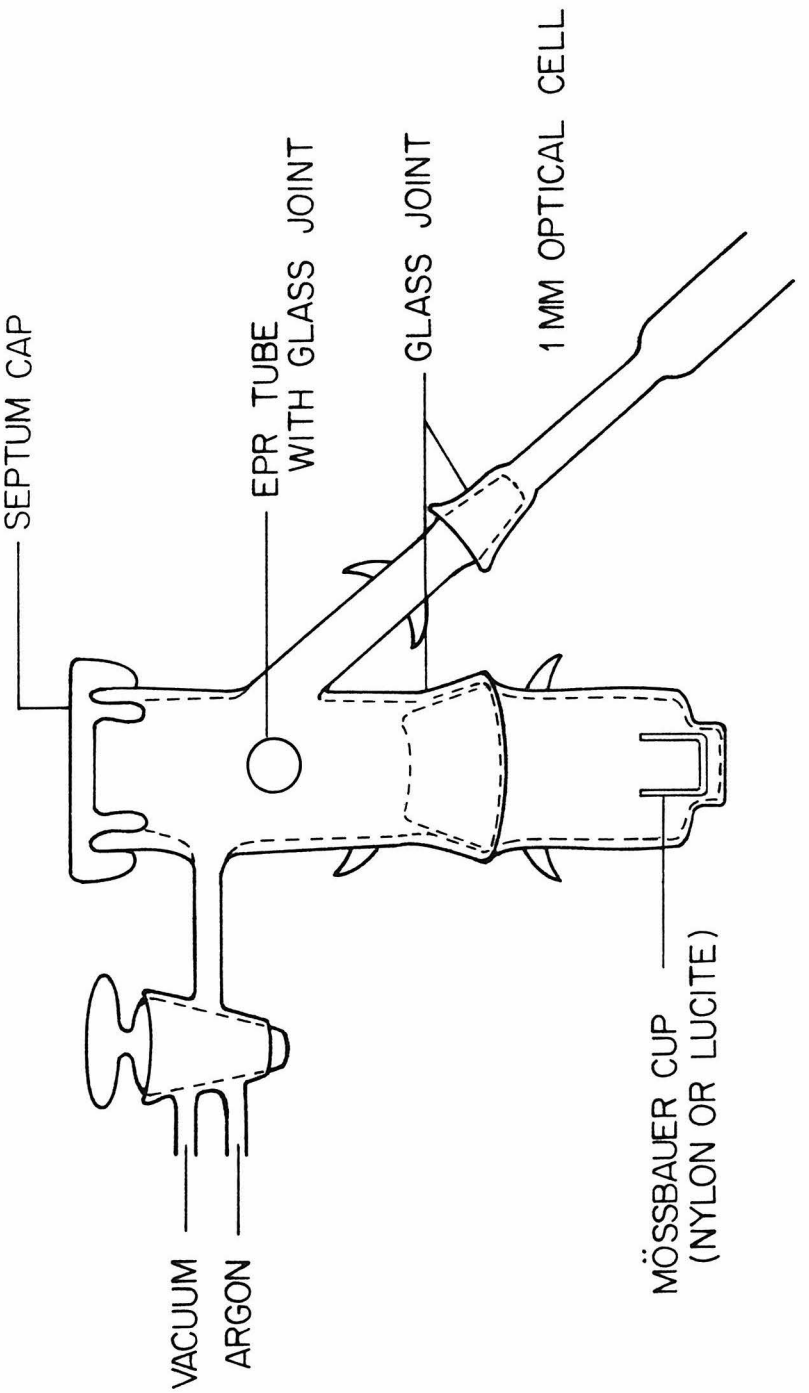
SEPTUM CAP
EPR TUBE
WITH GLASS JOINT
GLASS JOINT
1 MM OPTICAL CELL
VACUUM
ARGON
MÖSSBAUER CUP
(NYLON OR LUCITE)

Mössbauer Spectroscopy

The Mössbauer measurements were recorded in the laboratory of Professor Peter Debrunner at the University of Illinois at Champaign-Urbana. Two spectrometers were used in this study. The low field instrument was equipped with a Janis Research company cryostat. A permanent magnet can be placed either perpendicular or parallel to the propagation direction of the γ ray. The high field measurement was recorded in a cryostat/superconducting magnet system. It allowed a field of up to 4 tesla, which was always parallel to the γ ray. Both instruments were designed and constructed in Debrunner's laboratory. They have been described in detail elsewhere (28,29).

Both instruments were of constant acceleration type. The source was 40 mCi ^{57}Co in Rhodium and was purchased from Amersham, England. The velocity scale was calibrated against an iron foil at room temperature. The linewidth of the iron foil spectrum was typically 0.28 mm/sec. Spectra were measured from 4.2 K to 230 K. Sample temperatures were measured with calibrated carbon resistors and thermistors.

Other Spectroscopic Methods

Absorbance spectra were monitored at room temperature with either a Cary 219 or a Beckman Acta CIII spectrophotometer. EPR spectra were recorded on either a Bruker ER200 X-band spectrometer or a Varian E-line Century Series X-band spectrometer. The Bruker instrument was equipped with an Oxford Instruments helium flow cryostat. This cryostat maintains a set sensor temperature within 0.1 K. The Varian spectrometer was equipped with an Air Products Heli-Tran cryostat. The temperature at the sample position was measured before and after spectra were acquired, using a gold-chromel thermocouple in a glycerol-filled EPR tube. The spectra were obtained at approximately 10 K. The Atomic absorption spectrometer used was Model 151 from Instrumentation

Laboratory.

THEORETICAL BASIS

Biological applications of Mössbauer spectroscopy have been reviewed extensively. Especially relevant to this study are those on hemeproteins written by Lang (30), Debrunner (31), and Münck (32). The Mössbauer transition is a nuclear transition between the ground state ($I = 1/2$) and the excited state ($I = 3/2$) of the iron-57 nucleus. The spectrum reveals the nuclear fine structure of ^{57}Fe. This nuclear fine structure, however, is linked with the electronic structure through hyperfine interaction. The electronic structure and the Mössbauer behavior of the four common iron ions, namely, the high-spin and low-spin forms of ferric and ferrous ions, have been discussed in great detail in the above-mentioned reviews. Cytochrome a_3 in the resting state, however, is a special case. Many studies on the enzyme isolated from beef heart suggest that it is a high-spin ferric heme (2). On the other hand, if the proposed strong antiferromagnetic coupling with Cu_B does exist, this site would behave in many ways like an $S = 2$ ion, similar to that of a high-spin ferrous ion. No other similar system has ever been measured by Mössbauer spectroscopy. A theoretical basis for Mössbauer measurements in general is outlined below, and is extended to enable discussion of cytochrome oxidase.

The Mössbauer data on the yeast oxidase display considerable inhomogeneity in both cytochromes. Therefore a proper deconvolution of the spectra and an accurate assignment of various spectral features are required. When the fluctuation rate between electronic states is much faster than the nuclear precession frequency, the magnetic hyperfine structures collapse and the transitions of cytochrome a and a_3 are satisfactorily identified. The isomer shift and the quadrupole splitting of each component can be precisely determined by a least-squares line fit program that fits the observed spectrum to a sum of Lorentzians.

These parameters often reflect the valencies and spin state of the iron. Figure 2 shows a correlation of spectral parameters with spin and oxidation state for various hemeproteins and porphyrin complexes. In general, however, the spectrum displays rather complicated magnetic hyperfine structures. A wealth of information hidden in these structures can be extracted by applying spin Hamiltonian models.

A specific spin Hamiltonian model that has been sufficient for hemeproteins (31,32) and which has been used in this study can be expressed as follows:

$$\mathcal{H} = \mathcal{H}_e + \mathcal{H}_n, \tag{1a}$$

where

$$\mathcal{H}_e = D\{S_z^2 - \frac{1}{3}S(S+1) + \frac{E}{D}(S_x^2 - S_y^2)\} + \beta \mathbf{S}\cdot\mathbf{g}\cdot\mathbf{H} \tag{1b}$$

$$\mathcal{H}_n = \mathcal{H}_{hf} + \mathcal{H}_{nZ} + \mathcal{H}_Q, \tag{1c}$$

and

$$\mathcal{H}_{hf} = \mathbf{S}\cdot\mathbf{A}\cdot\mathbf{I} \tag{1d}$$

$$\mathcal{H}_{nZ} = -g_n\beta_n \mathbf{I}\cdot\mathbf{H} \tag{1e}$$

$$\mathcal{H}_Q = \frac{eQV_{zz}}{4I(2I-1)}[3I_z^2 - I(I+1) + \eta(I_x^2 - I_y^2)]_{\mathrm{EFG}} \tag{1f}$$

$$\eta = \frac{(V_{xx} - V_{yy})}{V_{zz}}.$$

The electronic Hamiltonian $\mathcal{H}_e$ depends on the electronic variables only. The first term describes the zero field splittings of the iron spin sublevels, where D and E are second-order zero field splitting parameters, also known as the axial and rhombic coefficients, respectively. In this model the fourth-order parameters a and F are not considered. For high-spin ferric ($S = 5/2$) or ferrous ($S = 2$) hemes, D is normally the preponderant term of the electronic Hamiltonian, leading to splittings with energy of order 10 cm^{-1}. The second term describes

Figure 2. Trends of Mössbauer parameters in hemeproteins and iron porphyrin complexes with various valencies and spin states. The squares represent ferrous ions, the triangles, ferric ions, and the diamonds, ferryl ions. For ferrous and ferric ions high spin is designated by open symbols and low spin by solid symbols. All reported ferryl ions have intermediate ($S = 1$) spin states.

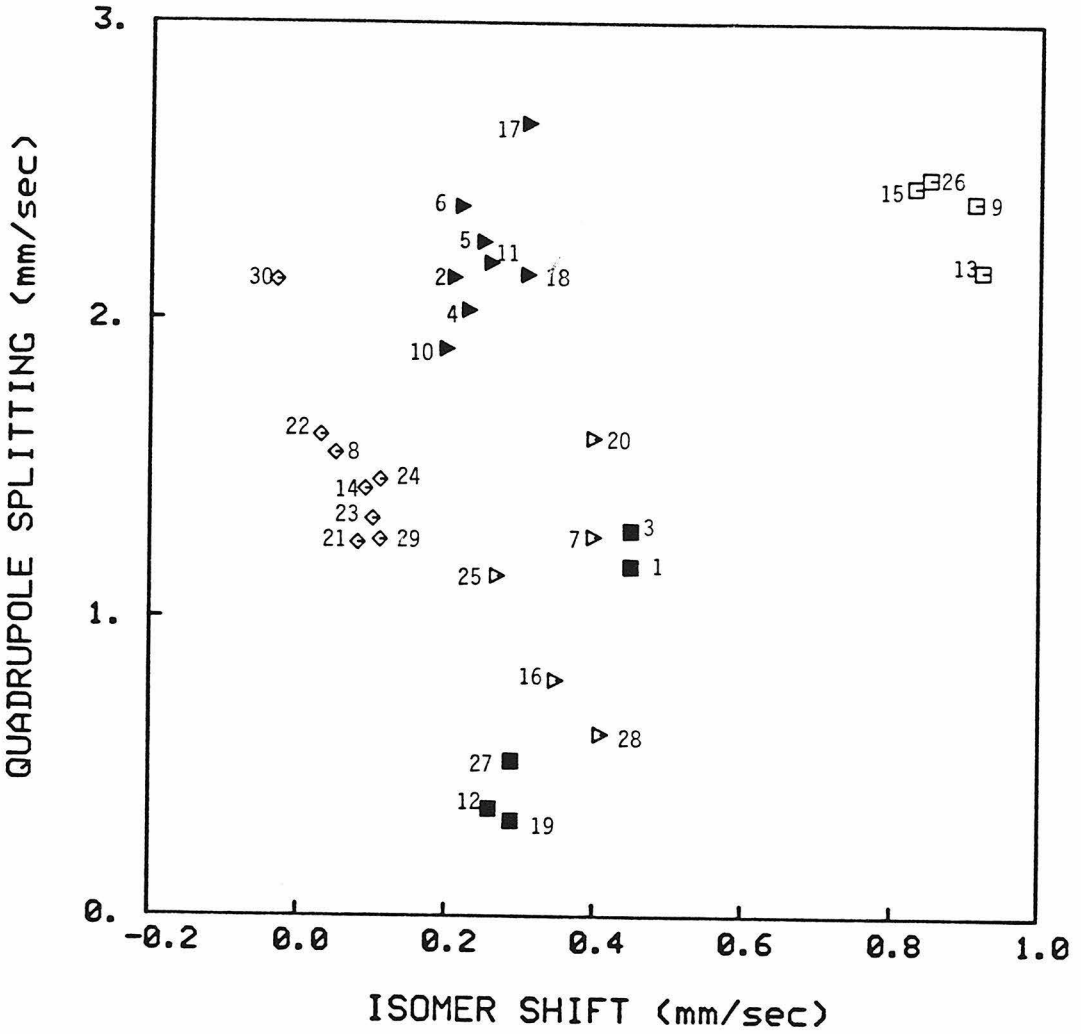
QUADRUPOLE SPLITTING (mm/sec)
ISOMER SHIFT (mm/sec)
3.
2.
1.
0.
-0.2
0.0
0.2
0.4
0.6
0.8
1.0
17
6
5
11
30
2
18
4
10
15
26
9
13
22
8
20
14
24
23
21
29
7
3
1
25
16
28
27
12
19

Figure 2 notes:

	δ(mm/s)	ΔE_Q(mm/s)	Reference
1. ferrocytochrome *c*	0.45	1.17	(48)
2. ferricytochrome *c*	0.21	2.14	(48)
3. ferrocytochrome c_{551}	0.45	1.29	(64)
4. ferricytochrome c_{551}	0.23	2.03	(64)
5. ferricytochrome c_2	0.25	2.26	(63)
6. cytochrome *c* peroxidase, low spin	0.22	2.38	(71)
7. cytochrome *c* peroxidase, high spin	0.40	1.27	(71)
8. cytochrome *c* peroxidase, ES	0.05	1.55	(72)
9. hemoglobin, deoxy	0.91	2.40	(35)
10. met-hemoglobin	0.20	1.90	(35)
11. hemoglobin, oxy	0.26	2.19	(35)
12. hemoglobin, CO-bound	0.26	0.36	(35)
13. myoglobin, deoxy	0.92	2.17	(73)
14. myoglobin, [Fe(IV)]	0.09	1.43	(28)
15. P-450 + camphor, reduced	0.83	2.45	(74)
16. P-450 + camphor, oxidized, high spin	0.35	0.79	(74)
17. P-450 + camphor, oxidized, low spin	0.31	2.66	(74)
18. P-450 + camphor, reduced, oxy	0.31	2.15	(74)
19. P-450 + camphor, reduced, CO-	0.29	0.32	(74)
20. horseradish peroxidase	0.40	1.60	(52)
21. horseradish peroxidase, compound I	0.08	1.25	(52)
22. horseradish peroxidase, compound II	0.03	1.61	(52)
23. Japanese radish peroxidase, compound I	0.10	1.33	(75)
24. Japanese radish peroxidase, compound II	0.11	1.46	(75)
25. catalase	0.27	1.14	(76)
26. chloroperoxidase, reduced	0.85	2.48	(77)
27. chloroperoxidase, reduced, CO-bound	0.29	0.52	(77)
28. (TPP)Fe–O–Fe(TPP)	0.41	0.61	(78)
29. Fe(O)(TPP)(1-MeIm)	0.11	1.26	(78)
30. (TMP)FeCl + iodosylbenzene	−0.03	2.13	(79)
31. horseradish peroxidase, compound III	0.23	2.31	(52)
32. Japanese radish peroxidase, compound III	0.29	2.37	(75)
33. (TPP)Fe–OO–Fe(TPP)	0.54	0.81	(78)

the electronic Zeeman interaction, where **H** is the external magnetic field. The Zeeman interaction energy is roughly $0.03\,\mathrm{cm}^{-1}$ in the presence of a 320 gauss field. The nuclear Hamiltonian $\mathcal{H}_n$ contains terms from the hyperfine interaction, the nuclear Zeeman interaction, and the quadrupole interaction. The quadrupole interaction arises from the interaction of the electric quadrupole moment eQ of the excited iron-57 nucleus with the electric field gradient (EFG), (V_{xx}, V_{yy}, V_{zz}), at the nucleus. In the absence of magnetic interactions, the quadrupole splitting

$$\Delta E_Q = \frac{1}{2} eQV_{zz}\sqrt{1+\frac{\eta^2}{3}} \tag{2}$$

is observed. It is typically a few mm/sec. The magnetic hyperfine interaction, if present, is of order several mm/sec, i.e., of order $10^{-3}\,\mathrm{cm}^{-1}$. The nuclear Zeeman interaction, on the other hand, is only of order $10^{-6}\,\mathrm{cm}^{-1}$ in the presence of a small field of several hundred gauss and is therefore unobservable unless the experiment is carried out under a high magnetic field.

The spin operator **S** is fixed by the electronic system since the electronic Hamiltonian is dominant. Therefore, the nuclear Hamiltonian $\left(Eq.(1c)\right)$ can be rewritten as

$$\begin{aligned}\mathcal{H}_n &= \langle \mathbf{S} \rangle \cdot \mathbf{A} \cdot \mathbf{I} - g_n \beta_n \mathbf{H} \cdot \mathbf{I} + \mathcal{H}_Q \\ &= -g_n \beta_n (\mathbf{H}_{int} + \mathbf{H}) \cdot \mathbf{I} + \mathcal{H}_Q, \end{aligned} \tag{3a}$$

where $\langle \mathbf{S} \rangle$ is the expectation value of the electron spin and the quantity

$$\mathbf{H}_{int} = -\left(\langle \mathbf{S} \rangle \cdot \mathbf{A}\right) / g_n \beta_n \tag{3b}$$

is generally called the internal magnetic field at the nucleus. The degeneracy of the nuclear spin states is thus lifted by an effective magnetic field $\mathbf{H}_{eff} = \mathbf{H}_{int} + \mathbf{H}$.

The strength of the internal field depends on the electronic spin state of the iron, the applied field, and the relaxation time of the electron spin. When the

relaxation rate is much faster than the nuclear precession frequency, the nucleus experiences an average field caused by the thermally averaged electronic spin states. The expectation value of the spin is then

$$\langle \mathbf{S} \rangle_{\mathrm{av}} = \frac{\sum_j \langle \mathbf{S} \rangle_j \exp(-E_j/kT)}{\sum_j \exp(-E_j/kT)}, \tag{4}$$

where E_j is the energy of state j, and j sums over the states. In the presence of a small magnetic field such as several hundred gauss, the internal field is therefore negligible if electronic relaxation is rapid. Such is usually the case for the high-spin ferrous ($S = 2$) hemes even at 4.2 K. If this poses any difficulty in making a definitive assignment between a high-spin ferrous ion and a low-spin one, as has happened in the present study, measurements under strong magnetic fields are used to differentiate between the two. On the other hand, when the electron spin relaxes very slowly, the nucleus sees a stationary electronic spin state. A widespread magnetic hyperfine pattern is then observed. Most ferric hemes, high-spin or low-spin, fall into this category at 4.2 K. Typically, the hyperfine interaction of high spin ferric ion is isotropic and that of low-spin ferric ion is not. In this study a computer program (33) was used to simulate the Mössbauer spectrum of an iron ion of any spin state, assuming one or the other of the two relaxation conditions.

Low-spin ferric ions have a ${t_{2g}}^5$ configuration and can be treated as a t_{2g} hole. The theory has been developed by Griffith (34), and was later expanded by Lang (35,36) to include magnetic hyperfine and quadrupole interactions. Following this theory one can calculate the eigenfunctions from EPR g values, from which one can estimate the hyperfine tensor and quadrupole splitting. This theory has been summarized elsewhere (37).

The theory for the cytochrome a_3 site is more complicated. Since it is magnetically coupled to Cu_B, the Hamiltonian for this site should include terms describing the superexchange interactions between the two spins. The most

general form of such interactions is

$$\mathcal{H}_{ex} = \sum_{\alpha,\beta=x,y,z} J_{\alpha\beta} S_{1\alpha} S_{2\beta}; \tag{5}$$

Erdös (38) showed that this can be rearranged into the form

$$\mathcal{H}_{ex} = J\mathbf{S_1} \cdot \mathbf{S_2} + \mathbf{Q} \cdot (\mathbf{S_1} \times \mathbf{S_2}) + \mathbf{S_1} \cdot \mathbf{\Delta} \cdot \mathbf{S_2}. \tag{6}$$

This first term is the isotropic superexchange coupling, where J is the isotropic superexchange constant. The second and third terms are the asymmetric superexchange and the anisotropic superexchange respectively. They were first introduced by Dzyaloshinsky (39) and Moriya (40). Following Buluggiu and Vera (41) we use the notations $\mathbf{Q}$ and $\mathbf{\Delta}$ instead of the original $\mathbf{D}$ and $\mathbf{J}$ to avoid confusion. The magnitude of the asymmetric superexchange coupling Q is of order $J(\Delta g/g)$, and that of anisotropic superexchange coupling Δ is of order $J(\Delta g/g)^2$, where Δg is the difference in g values of the two ions. The latter includes a contribution from dipole-dipole magnetic interactions.

The electronic Hamiltonian and the nuclear Hamiltonian for the a_3 site are therefore

$$\begin{aligned} \mathcal{H}_e = {} & J\mathbf{S_1} \cdot \mathbf{S_2} + \mathbf{Q} \cdot (\mathbf{S_1} \times \mathbf{S_2}) + \mathbf{S_1} \cdot \mathbf{\Delta} \cdot \mathbf{S_2} \\ & + \mathbf{S_1} \cdot \mathbf{D_1} \cdot \mathbf{S_1} + \beta \mathbf{H} \cdot \mathbf{g_1} \cdot \mathbf{S_1} + \beta \mathbf{H} \cdot \mathbf{g_2} \cdot \mathbf{S_2} \end{aligned} \tag{7a}$$

$$\mathcal{H}_n = \mathbf{S_1} \cdot \mathbf{A_1} \cdot \mathbf{I_1} + \mathcal{H}_{nZ} + \mathcal{H}_Q, \tag{7b}$$

where subscripts 1 refer to the high-spin Fe(III) ($S_1 = 5/2$) and subscripts 2 to Cu(II) ($S = 1/2$); the zero-field splitting of the heme is reexpressed here as $\mathbf{S_1} \cdot \mathbf{D_1} \cdot \mathbf{S_1}$. The hyperfine interaction, the nuclear Zeeman interaction, and the quadrupole interaction at the Cu_B nucleus are not included, since they are irrelevant from the viewpoint of Mössbauer spectroscopy.

In the strong exchange limit, Griffith (15) first treated the electronic structure explicitly for cytochrome oxidase, with neglect of contributions from anisotropic superexchange and dipolar interactions. A more thorough treatment was

given by Buluggiu (41,42) for the $Mn^{2+} - Cu^{2+}$ mixed pair, which is an isoelectronic system to the cytochrome a_3–Cu_B site. They noted that there are two natural coupling schemes to describe the system, i.e., the uncoupled representation $|S_1S_2M_1M_2\rangle$ and the coupled representation $|S_1S_2SM\rangle$. The two spins $S_1 = 5/2$ and $S_2 = 1/2$ pair to give two manifolds characterized by a total spin of $S = 2$ or $S = 3$. Their energies are given by the Landé rule

$$E_S = \frac{1}{2}J[S(S+1) - S_1(S_1+1) - S_2(S_2+1)]. \tag{8}$$

With a strong antiferromagnetic coupling, the S=3 manifold lies $3J$ above the S=2 manifold and is not a concern here. The relation between the two representations is given by Condon and Shortley (43). For the S=2 manifold, it is

$$|S_1S_22M\rangle = -\left(\frac{3-M}{6}\right)^{1/2}|S_1S_2M-\frac{1}{2},\frac{1}{2}\rangle + \left(\frac{3+M}{6}\right)^{1/2}|S_1S_2M+\frac{1}{2},-\frac{1}{2}\rangle. \tag{9}$$

In theory, the asymmetric, or the skew-symmetric superexchange interaction

$$\mathcal{H}_{as} = \mathbf{Q}\cdot(\mathbf{S_1}\times\mathbf{S_2}) \tag{10}$$

exists for a system which does not have a center of inversion at the local center of the two ions. Therefore this interaction is expected for the a_3 site of cytochrome oxidase. It can be shown, however, that within the $S = 2$ manifold,

$$\langle S_1S_22M'|\mathcal{H}_{as}|S_1S_22M\rangle = 0 \tag{11}$$

for any M and M'. The nonvanishing terms of this perturbation are thus between two spin manifolds that are separated by $3J$. The contribution from this term to the zero-field parameter D can be derived as $-(Q_x^2 + Q_y^2 - 2Q_z^2)/24J^*$. This quantity is negligible compared to the D's for high-spin hemeproteins.

---

* Schulz, C.E., personal communication.

Ignoring the asymmetric superexchange interaction, we can then re-express the Hamiltonian in terms of the coupled representation,

$$\mathcal{H}_e = \mathbf{S} \cdot \mathbf{D_S} \cdot \mathbf{S} + \beta \mathbf{H} \cdot \mathbf{g_S} \cdot \mathbf{S} \tag{12a}$$

$$\mathcal{H}_n = \mathbf{S} \cdot \mathbf{A_S(1)} \cdot \mathbf{I_1} + \mathcal{H}_{nZ} + \mathcal{H}_Q, \tag{12b}$$

where the subscript **S** denotes the tensors that are pertinent to the coupled state. They are related to the uncoupled representation through

$$\mathbf{g_S} = \alpha_S \mathbf{g_1} + \beta_S \mathbf{g_2} \tag{12c}$$

$$\mathbf{A_S}(1) = \alpha_S \mathbf{A_1} \tag{12d}$$

$$\mathbf{D_S} = \gamma_S \mathbf{D_1} + \epsilon_S \Delta. \tag{12e}$$

The coefficients are given by Buluggiu (42). For coupled cytochrome a_3, the pertinent relations are

$$\mathbf{g}_S = \frac{7}{6}\mathbf{g}_1 - \frac{1}{6}\mathbf{g}_2 \tag{13a}$$

$$\mathbf{A}_S(1) = \frac{7}{6}\mathbf{A}_1 \tag{13b}$$

$$\mathbf{D}_S = \frac{4}{3}\mathbf{D}_1 - \frac{1}{6}\mathbf{\Delta}. \tag{13c}$$

Therefore, in the strong exchange limit, the coupled $S = 2$ state can be examined as if it were a genuine $S = 2$ state, of which the **g**, **A**, and **D** tensors can be calculated from *Eq.* 13. We shall discuss briefly the implications of these equations. The isotropic superexchange constant J was estimated to be larger than $200\,\mathrm{cm}^{-1}$ by magnetic susceptibility measurements for the enzyme purified from beef heart (9). Thus the anisotropic superexchange interaction is expected to be on the order of 0.5 to 2 cm^{-1}. The zero field parameter D is in the range of 5-15 cm^{-1} for high-spin ferric hemeproteins (12). Specific measurements by Hagen (18) on the uncoupled cytochrome a_3 suggest that it is $\sim$8 cm^{-1}. From these esimates the D for the coupled a_3 site is expected to be around 9 cm^{-1}.

Clearly an understanding of the $S = 2$ system is crucial to understanding the coupled a_3 site. We shall illustrate the electronic structure of the $S = 2$ system following the treatment by Abragam and Bleaney (44). The electronic Hamiltonian ($Eq.(1b)$) is re-expressed as

$$\mathcal{H}_e = D\{S_z^2 - \frac{1}{3}S(S+1) + \frac{E}{D}(S_x^2 - S_y^2)\} + g_{\|}\beta H S_z \cos\theta + g_{\perp}\beta H S_x \sin\theta, \quad (14)$$

where θ is the angle between the direction of external field and the principal symmetry axis. The energy levels are shown in Figure 3, with neglect of the second-order terms, which are of the order $(g\beta H)^2/D$. For comparison, the energy diagram for an $S = 2$ state from a $(5/2 - 1/2)$ pair is displayed in Figure 4. For purposes of illustration, the contributions from anisotropic superexchange coupling were not taken into account. From these figures the relation of **g** tensors in the two representations ($Eq.$ 13a) can be visualized in a straightforward fashion.

One of the difficulties in interpreting Mössbauer data on cytochrome oxidase is the sensitivity of the cytochrome a_3 spectrum towards a small field. This is entirely different from the behavior expected for a typical $S = 2$ system. We shall approach this problem from two directions, namely, by calculating the expectation value of the electron spin and by considering the effects of spin relaxation. Since the eigenfunction of each level determines the spin expectation value and therefore the hyperfine interaction, we venture to solve them for the genuine $S = 2$ system by perturbation theory. It is assumed that $g\beta H$, $E \ll D$. The results are tabulated in Table 1. An $S = 2$ ferrous system normally possesses a non-zero orbital angular momentum. The spin relaxation is therefore fast because of the spin-orbit coupling. Cytochrome a_3, however, has a totally symmetric ground state $^6A_{1g}$. Therefore a somewhat slower relaxation behavior is expected. We shall make use of these results to discuss the magnetic broadening of an $S = 2$ system under various conditions.

Figure 3. Energy levels and wavefunctions corresponding to a genuine $S = 2$ system with a positive D. Second-order terms are small and neglected in this diagram. Here θ is the angle between the symmetry axis and the direction of magnetic field, and α's are defined as follows:

$$\tan 2\alpha_1 = \frac{\Delta_1}{2g\beta H \cos\theta}$$
$$\tan 2\alpha_2 = \frac{\Delta_2}{4g\beta H \cos\theta}.$$

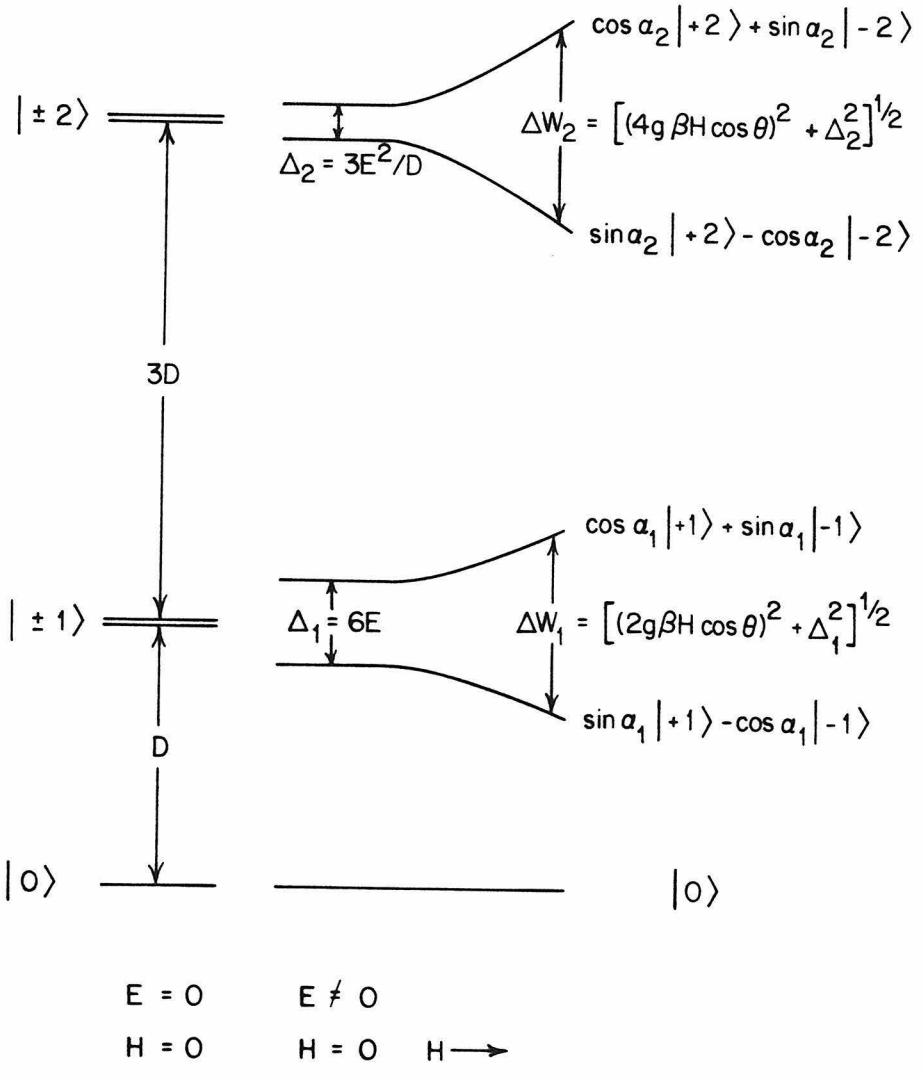
$\cos\alpha_2 |+2\rangle + \sin\alpha_2 |-2\rangle$
$|\pm 2\rangle$
$\Delta W_2 = [(4g\beta H\cos\theta)^2 + \Delta_2^2]^{1/2}$
$\Delta_2 = 3E^2/D$
$\sin\alpha_2 |+2\rangle - \cos\alpha_2 |-2\rangle$
3D
$\cos\alpha_1 |+1\rangle + \sin\alpha_1 |-1\rangle$
$|\pm 1\rangle$
$\Delta_1 = 6E$
$\Delta W_1 = [(2g\beta H\cos\theta)^2 + \Delta_1^2]^{1/2}$
$\sin\alpha_1 |+1\rangle - \cos\alpha_1 |-1\rangle$
D
$|0\rangle$
$|0\rangle$
E = 0
H = 0
E ≠ 0
H = 0
H ⟶

Figure 4. Energy levels and wavefunctions corresponding to an $S = 2$ manifold arising from a strongly antiferromagnetically coupled $(\frac{5}{2} - \frac{1}{2})$ ion pair, with neglect of the anisotropic superexchange (Δ) and second-order terms. ϕ's are wavefunctions expressed in the coupled representation and $|M_1 M_2\rangle$'s in the uncoupled representation, where subscripts 1 and 2 describe $S = \frac{5}{2}$ and $S = \frac{1}{2}$ systems respectively. θ and α's are as defined in the Figure 3 legend, where

$$g = \frac{7}{6} g_1 - \frac{1}{6} g_2.$$

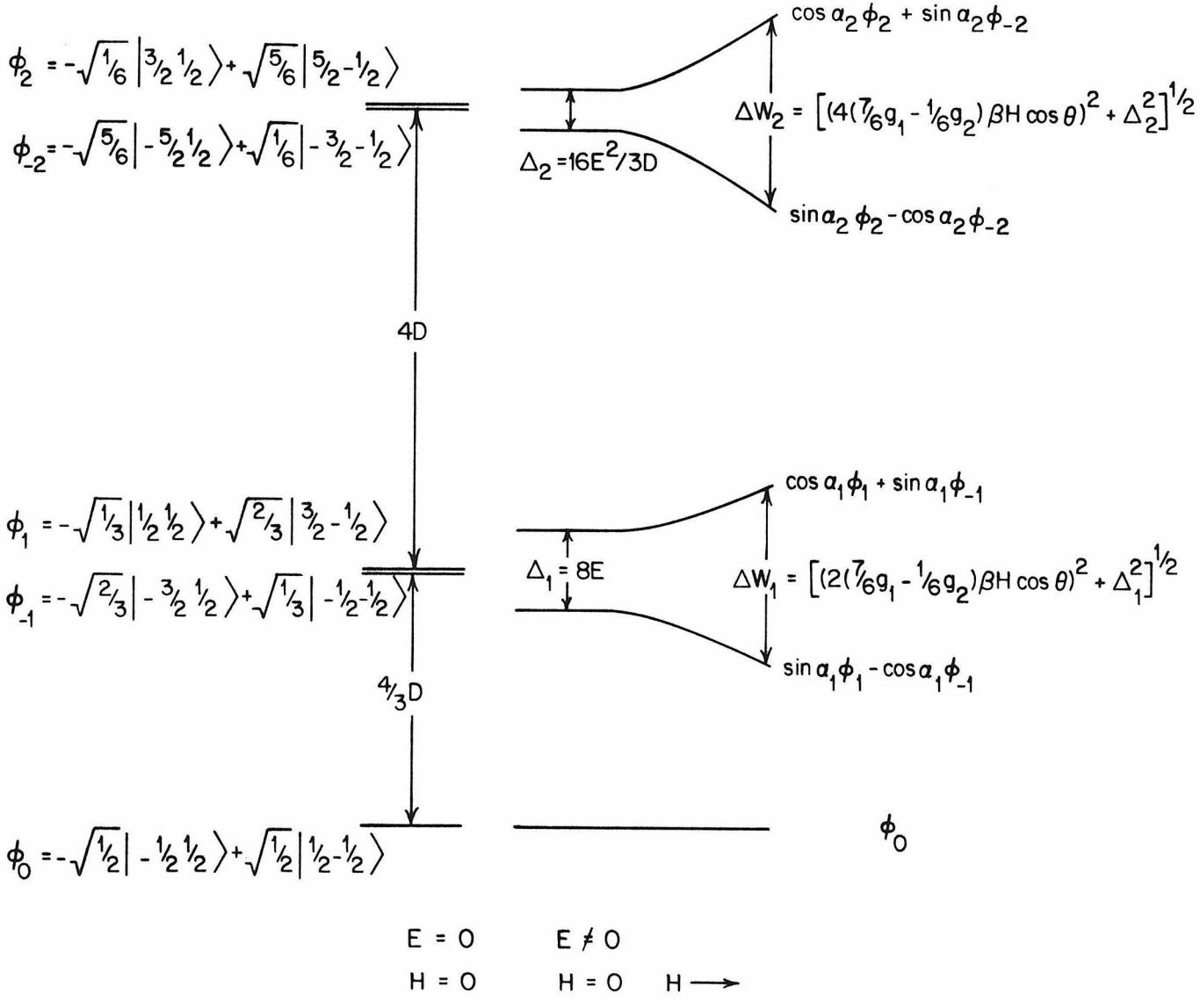
$\phi_2 = -\sqrt{1/6}\,|3/2\ 1/2\rangle + \sqrt{5/6}\,|5/2\ -1/2\rangle$
$\phi_{-2} = -\sqrt{5/6}\,|-5/2\ 1/2\rangle + \sqrt{1/6}\,|-3/2\ -1/2\rangle$
$\cos\alpha_2\phi_2 + \sin\alpha_2\phi_{-2}$
$\Delta W_2 = \left[(4(7/6 g_1 - 1/6 g_2)\beta H\cos\theta)^2 + \Delta_2^2\right]^{1/2}$
$\Delta_2 = 16E^2/3D$
$\sin\alpha_2\phi_2 - \cos\alpha_2\phi_{-2}$
4D
$\phi_1 = -\sqrt{1/3}\,|1/2\ 1/2\rangle + \sqrt{2/3}\,|3/2\ -1/2\rangle$
$\phi_{-1} = -\sqrt{2/3}\,|-3/2\ 1/2\rangle + \sqrt{1/3}\,|-1/2\ -1/2\rangle$
$\cos\alpha_1\phi_1 + \sin\alpha_1\phi_{-1}$
$\Delta_1 = 8E$
$\Delta W_1 = \left[(2(7/6 g_1 - 1/6 g_2)\beta H\cos\theta)^2 + \Delta_1^2\right]^{1/2}$
$\sin\alpha_1\phi_1 - \cos\alpha_1\phi_{-1}$
4/3D
$\phi_0 = -\sqrt{1/2}\,|-1/2\ 1/2\rangle + \sqrt{1/2}\,|1/2\ -1/2\rangle$
ϕ_0
E = 0
E ≠ 0
H = 0
H = 0
H ⟶

Table 1. Wavefunctions and spin Expectation Values of an $S = 2$ System

	Wavefunctions	$\langle S_z \rangle$	$\langle S_x \rangle$
ψ_0	$\|0\rangle - \frac{\sqrt{6}E}{4D}(\|+2\rangle + \|-2\rangle)$ $-\frac{\sqrt{6}g_\perp \beta H \sin\theta}{2D}(\|+1\rangle + \|-1\rangle)$	0	$-\frac{3g_\perp \beta H \sin\theta}{D}$
ψ_{1-}	$\sin\alpha_1\|+1\rangle - \cos\alpha_1\|-1\rangle$ $+\frac{\sqrt{6}g_\perp \beta H \sin\theta}{2D}(\sin\alpha_1 - \cos\alpha_1)\|0\rangle$ $-\frac{g_\perp \beta H \sin\theta}{3D}(\sin\alpha_1\|+2\rangle - \cos\alpha_1\|-2\rangle)$	$-\cos 2\alpha_1$	$\frac{g_\perp \beta H \sin\theta}{2D}(\frac{5}{3} - 3\sin 2\alpha_1)$
ψ_{1+}	$\cos\alpha_1\|+1\rangle + \sin\alpha_1\|-1\rangle$ $+\frac{\sqrt{6}g_\perp \beta H \sin\theta}{2D}(\sin\alpha_1 + \cos\alpha_1)\|0\rangle$ $-\frac{g_\perp \beta H \sin\theta}{3D}(\cos\alpha_1\|+2\rangle + \sin\alpha_1\|-2\rangle)$	$+\cos 2\alpha_1$	$\frac{g_\perp \beta H \sin\theta}{2D}(\frac{5}{3} + 3\sin 2\alpha_1)$
ψ_{2-}	$\sin\alpha_2\|+2\rangle - \cos\alpha_2\|-2\rangle$ $+\frac{\sqrt{6}E}{4D}(\sin\alpha_2 - \cos\alpha_2)\|0\rangle$ $+\frac{g_\perp \beta H \sin\theta}{3D}(\sin\alpha_2\|+1\rangle - \cos\alpha_2\|-1\rangle)$	$-2\cos 2\alpha_2$	$\frac{2g_\perp \beta H \sin\theta}{3D}$
ψ_{2+}	$\cos\alpha_2\|+2\rangle + \sin\alpha_2\|-2\rangle$ $+\frac{\sqrt{6}E}{4D}(\sin\alpha_2 + \cos\alpha_2)\|0\rangle$ $+\frac{g_\perp \beta H \sin\theta}{3D}(\cos\alpha_2\|+1\rangle + \sin\alpha_2\|-1\rangle)$	$+2\cos 2\alpha_2$	$\frac{2g_\perp \beta H \sin\theta}{3D}$

*θ is the angle between the magnetic field direction and the principal symmetry axis; α's are as defined in Figure 4.

(1) $D > 0$. We have shown the energy levels in Figure 3. Table 1 shows that at the lowest level the largest spin expectation value lies in the heme plane; this is caused by the mixing with upper levels. This mixing depends on the strength and direction of the applied field and the magnitude of D. Indeed, simulation shows that under a 320 Gauss field the absorption becomes significantly broadened when D is smaller than 3 cm^{-1}.

(2) $D < 0$. The energy diagram is displayed in Figure 5. The lowest states in this case are the $M_S = \pm 2$ levels. The largest spin density lies along the heme normal. Its magnitude can be calculated as

$$\left|\langle S_z \rangle_{2\pm}\right| = \frac{8 g_{\|} \beta H}{\left[(4 g_{\|} \beta H)^2 + {\Delta_2}^2\right]^{1/2}}. \tag{15}$$

The denominator is the energy spacing between the two levels. When the relaxation becomes fast, the spin average does not depend on the energy difference any more and can be shown to be

$$\langle S_z \rangle_{av} = -\frac{4 g_{\|} \beta H}{kT}. \tag{16}$$

RESULTS

Among the four samples that were used in the present study, Sample 4 exhibited good optical and EPR properties, and its Mössbauer measurements have excellent statistics. We shall concentrate on the data measured on this preparation unless otherwise indicated.

Optical & EPR Properties of the Mössbauer Samples

Optical spectra of sample 4 are displayed in Figure 6. They are very similar to those presented in Figure 2 in Chapter 1. The resting enzyme had a Soret maximum at 420 nm, slightly red-shifted compared with that of beef heart

Figure 5. Energy levels and wavefunctions corresponding to a genuine $S = 2$ system with a negative D. Second-order terms are small and neglected. θ and α's are as defined in the Figure 4 legend.

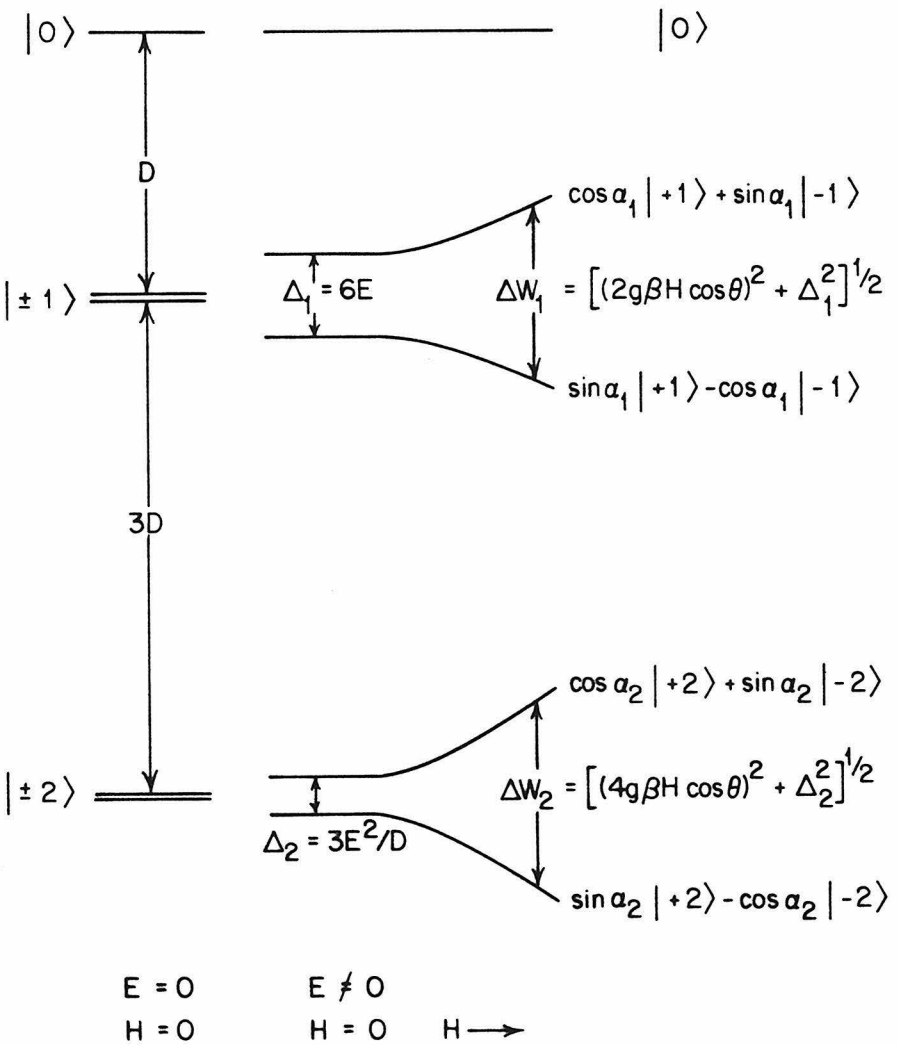
|0⟩
|0⟩
D
|±1⟩
cos α1 |+1⟩ + sin α1 |-1⟩
Δ1 = 6E
ΔW1 = [(2gβH cosθ)² + Δ1²]^1/2
sin α1 |+1⟩ - cos α1 |-1⟩
3D
|±2⟩
cos α2 |+2⟩ + sin α2 |-2⟩
ΔW2 = [(4gβH cosθ)² + Δ2²]^1/2
Δ2 = 3E²/D
sin α2 |+2⟩ - cos α2 |-2⟩
E = 0
H = 0
E ≠ 0
H = 0
H →

enzyme. The α band (at 598 nm) had a higher intensity than the β band (around 540 nm), which is not expected from the totally oxidized enzyme. These phenomena are common for the isolated yeast cytochrome oxidase (23) and are signs of partial reduction. The ratio of A_{598}/A_{540} was 1.21, which suggests that roughly 20 % of one cytochrome was reduced. A prominent shoulder can be discerned at 655 nm. This band is very similar in wavelength and extinction to that of 655 nm band found in beef heart oxidase, which has been proposed to originate from the coupled cytochrome a_3–Cu_B site (19). The dithionite-reduced enzyme showed a minor contamination of cytochrome b at 562 nm. Using the method developed by Vanneste (45), we estimated it to be 4% of the total heme.

The EPR spectrum of resting oxidized sample 4 is displayed in Figure 7. The spectral features are very similar to those presented in Figure 3 of Chapter 1. As mentioned in Chapter 1, the low field signal in yeast cytochrome oxidase centered around $g = 13.5$ rather than $g = 12$. However, we shall use the term $g = 12$ throughout this chapter since $g = 12$ is a familiar term to the researchers in this field. Although Hagen (18) felt that the term $g = 12$ signal should be abolished, it is clear to us that it would be premature to do so, since the detailed origin of this signal has not been settled (22). The expanded $g = 12$ region shows that the intensity of this signal when quantitated against the intensity of the low-spin signal at $g = 3$ is roughly half of that of Chapter 1 sample. We should remark, however, that these two spectra were measured on different EPR instruments. When both samples were measured on the same instrument (Varian E-line) and under identical conditions, the unexpanded spectra showed that they were almost identical in every signal (including the $g = 3, 2.2$ signals of cytochrome a, $g = 2.18, 2.0$ signals of Cu_A, high-spin heme signals around $g = 6$, and the $g = 12$ signal, which were proposed to be associated with the coupled a_3 site). Therefore the difference at $g = 12$ in these two samples may be smaller than 50%. The amount of high-spin material was estimated by the

Figure 6. Optical spectra of the ^{57}Fe enriched yeast cytochrome oxidase (sample 4) at room temperature. The solid line refers to the resting state and the dashed line refers to the reduced state. The enzyme was reduced with a pinch of sodium dithionite.

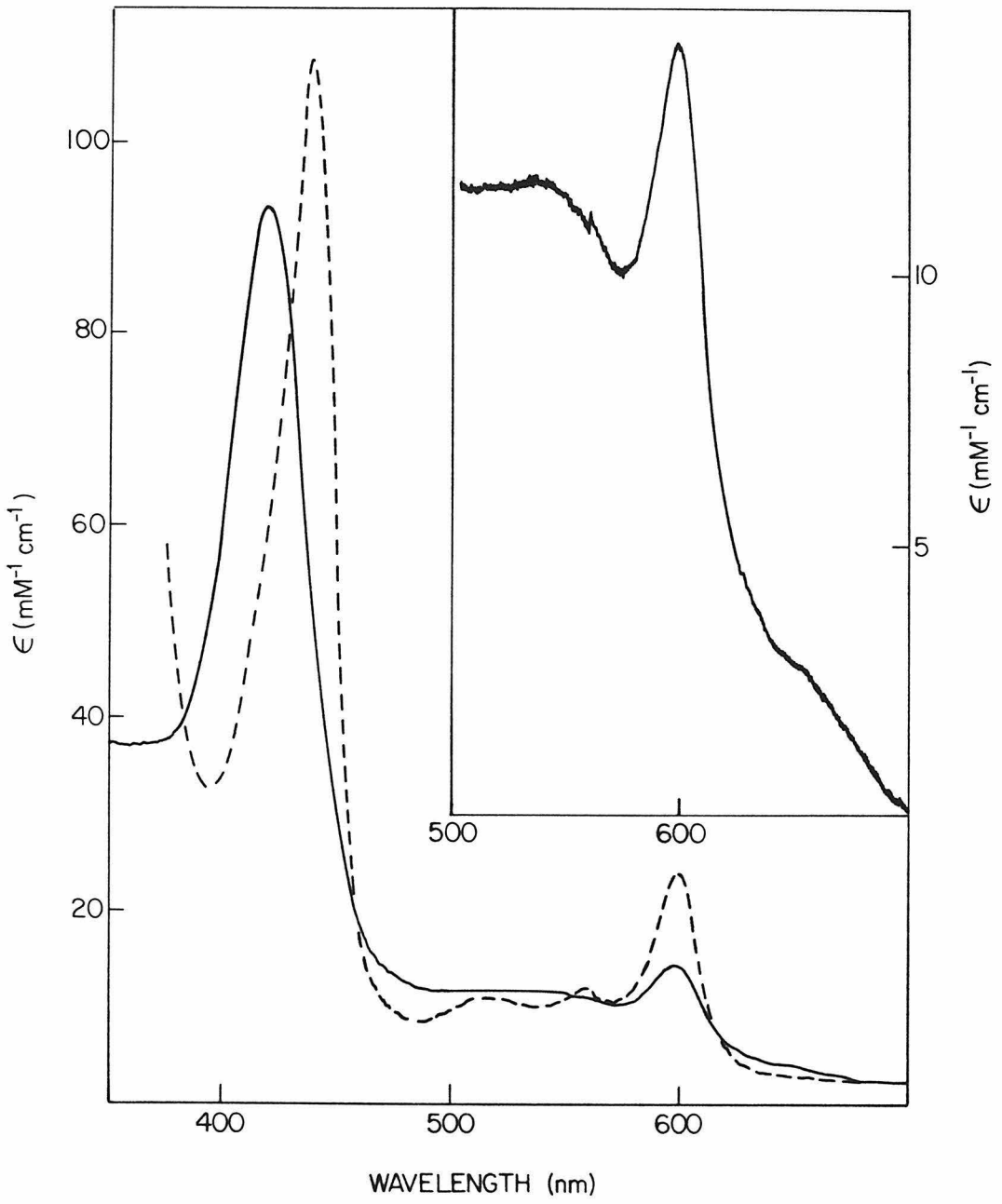
100
80
60
40
20
ε (mM⁻¹ cm⁻¹)
400
500
600
WAVELENGTH (nm)
10
5
ε (mM⁻¹ cm⁻¹)
500
600

method of Aasa and Vänngård (46,47) to be 11% of that of cytochrome a^{3+}.

Sample 3 had optical properties very similar to sample 4. The ratio of A_{598}/A_{540} was 1.15, suggesting that it is slightly less reduced than sample 4. Sample 1 had a A_{598}/A_{540} ratio of 1.34, and appeared to be substantially reduced. The 655 nm band of sample 1 and sample 2 was quite diminished. The EPR spectrum of sample 1 (not shown) showed that the $g = 3$ signal was broadened, a prominent axial high-spin signal at $g = 6$ (*ca.* 20% compared to the $g = 3$ signal), and no detectable $g = 12$ signal.

Reduced Yeast Oxidase

Mössbauer parameters of sample 4, determined by least-squares fits to sums of Lorentzian lines, are summarized in Table 2. The Mössbauer spectrum of the reduced sample 4 at 4.2 K is shown in Figure 8a. No magnetic hyperfine structure was present and the spectrum was composed of two quadrupolar doublets. Component A with $\delta = 0.451$ mm/sec and $\Delta E_Q = 1.018$ mm/sec is typical of a low-spin ferrous heme. In fact, these parameters are very similar to those of ferrocytochrome *c* (48). Component B had a larger linewidth (Table 2), which suggests that it is inhomogeneous. Its Mössbauer parameters ($\delta = 0.91$ mm/sec and $\Delta E_Q = 2.00$ mm/sec) are very close to those of hemoglobin(35). Therefore these components can be readily assigned to be ferrocytochrome *a* and ferrocytochrome a_3 respectively. These assignments agree very well with those reported for cytochrome oxidase from beef heart (7,25) and from *Thermus thermophilus* (24).

However, the ratio of the area under these two doublets was 2:1 in favor of the low-spin species. Since the parameters of component A are also in the region for high-spin ferric species, one might suspect an incomplete reduction in the enzyme. Optical spectra of the α band region showed, however, an A_{600}/A_{575} ratio of 2.6. This is clearly an indication of full reduction. Furthermore, the

Figure 7. EPR spectrum of the ^{57}Fe enriched yeast cytochrome oxidase (sample 4) in the resting oxidized state. Conditions for obtaining the EPR spectrum are: sample concentration, 0.3 mM; temperature, 9 K; microwave power, 0.1 mW; gain, 5×10^3. The expansion of the low field region was measured with a gain of 2×10^4.

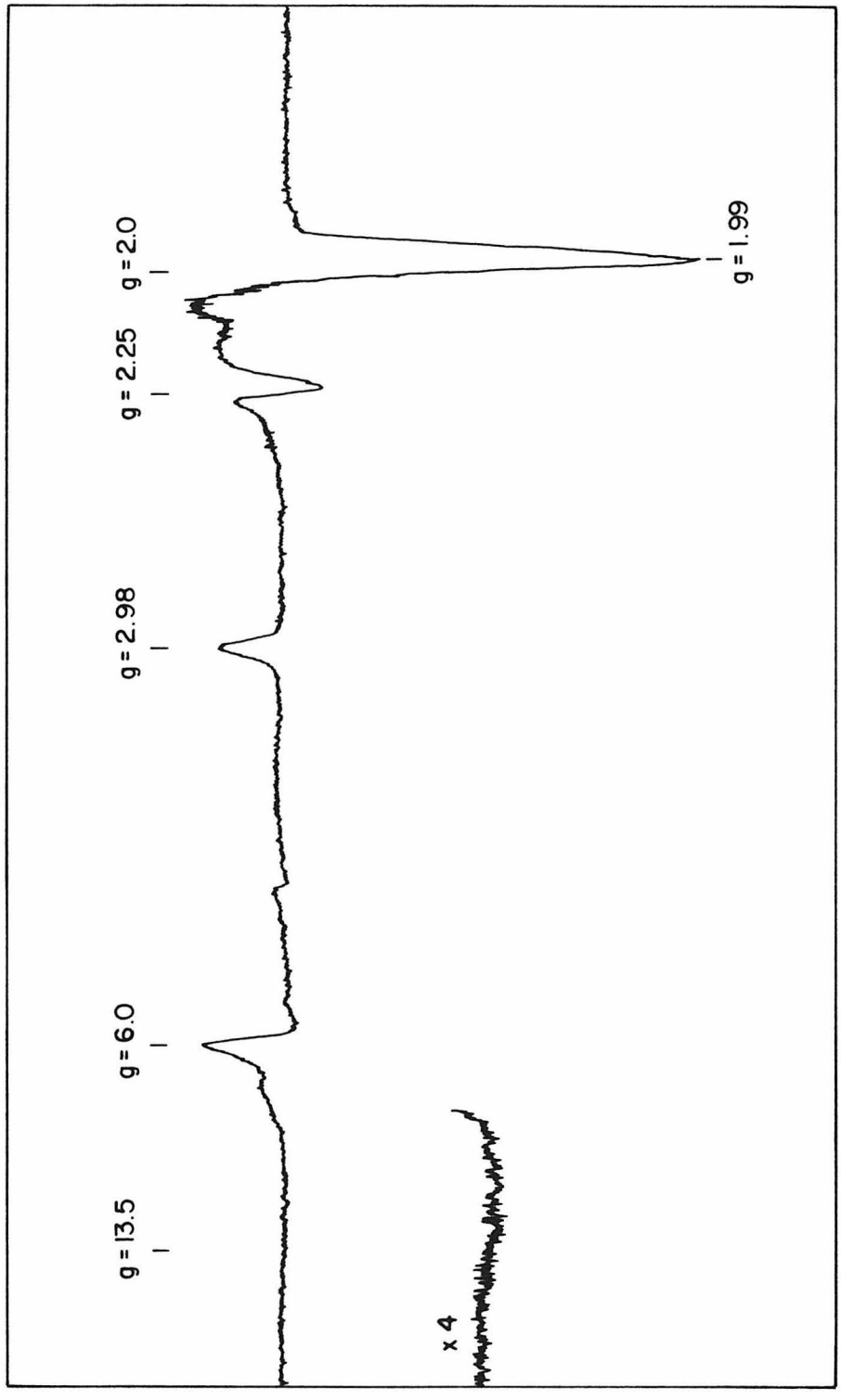
g = 13.5
g = 6.0
g = 2.98
g = 2.25
g = 2.0
g = 1.99
x 4

Table 2. Mössbauer Parameters of Yeast Cytochrome Oxidase obtained from least-square Lorentzian fit

Species	Temp °K	Field Gauss	δ mm/sec	ΔE_Q mm/sec	Linewidth mm/sec
Resting					
Cytochrome a	200	0	0.23 ± 0.02	1.99 ± 0.02	0.38, 0.52
Cytochrome a_3	200	0	0.34 ± 0.04	1.07 ± 0.04	0.49, 0.51
	4.2	0	0.41 ± 0.01	1.15 ± 0.01	0.53, 0.58
	4.2	320$\parallel$	0.44 ± 0.02	0.98 ± 0.02	0.44, 0.29
	4.2	320$\perp$	0.43 ± 0.03	1.04 ± 0.03	0.59, 0.38
Reduced					
low spin	4.2	320$\perp$	0.451 ± 0.005	1.018 ± 0.005	0.29
high spin	4.2	320$\perp$	0.91 ± 0.02	2.00 ± 0.02	0.38

Figure 8. Mössbauer spectra of the NADH-reduced yeast cytochrome oxidase enriched in ^{57}Fe: (a) Sample 4 (b) Sample 1. The spectra were measured at 4.2 K.

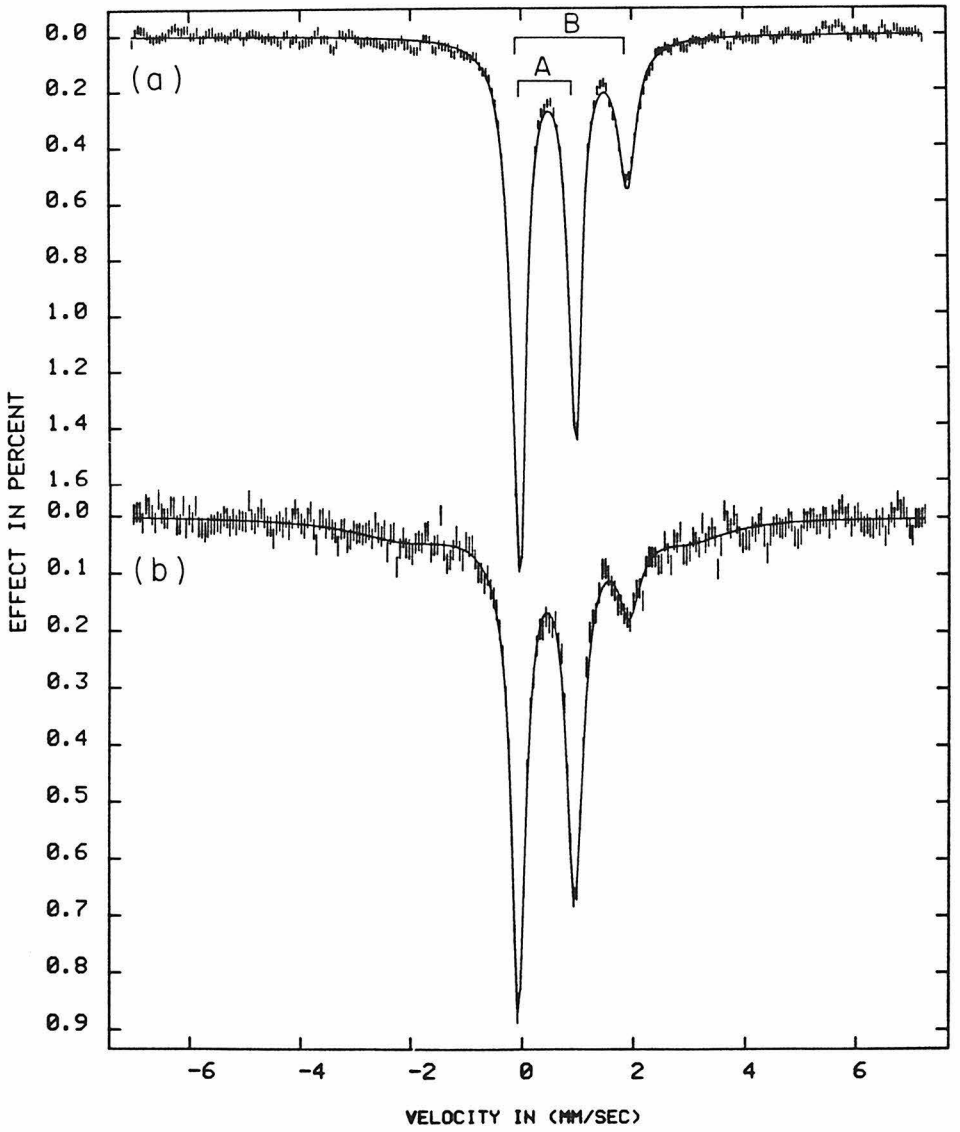
B
A
(a)
(b)
0.0
0.2
0.4
0.6
0.8
1.0
1.2
1.4
1.6
0.0
0.1
0.2
0.3
0.4
0.5
0.6
0.7
0.8
0.9
EFFECT IN PERCENT
-6
-4
-2
0
2
4
6
VELOCITY IN (MM/SEC)

content of the low-spin component increased when more reductant was added and longer incubation time was used (*cf.* Table 3). The linewidth of this doublet was quite narrow; we thus expect two indistinguishable components. Assuming that all the high-spin components are from a_3, we estimate that about one-third of a_3 is in the low-spin form.

The amount of low-spin ferrous cytochrome a_3 is very much preparation-dependent. The spectrum of reduced sample 1 is shown in Figure 8b, and the ratio of low-spin heme to high-spin heme is 3.6. The spectrum does show a small amount of oxidized material, noticeably in the region around -2 and $+3$ mm/sec. This iron center with a low redox potential is also detected in the spectroelectrochemical study of the CO-inhibited yeast cytochrome oxidase (Chapter 5). It is thus likely to be from cytochrome *a* rather than cytochrome a_3. In both preparations part of cytochrome a_3 appeared to have experienced spin transformation. We will show that low-spin cytochrome a_3^{2+} was detected in the resting enzyme, and its fraction increases during the process of reduction. This effect is much more pronounced for sample 1, probably due to the relatively harsh treatment during the concentration procedure.

Mössbauer spectra of the reduced sample 4 were recorded at a range of temperatures to investigate the possibility of spin transition at higher temperatures. The data were analyzed by least-squares Lorentzian fit and the results are summarized in Table 3. Within experimental uncertainty, the amount of either spin state remains the same between 4.2 and 230 K. Therefore spin crossover did not occur. While the quadrupole splitting of the low-spin component does not show much temperature dependence, that of high-spin component decreases drastically at elevated temperatures. The temperature dependence is steeper than that reported for deoxyhemoglobin (49).

Resting Yeast Oxidase

Table 3. Mössbauer Parameters of Reduced
Yeast Cytochrome Oxidase at Various Temperatures

species	temp °K	δ mm/sec	ΔE_Q mm/sec	area %
high spin	4.2*	0.91 ± 0.02	2.00 ± 0.02	33 ± 1
	4.2	0.92 ± 0.03	2.02 ± 0.03	29 ± 2
	115	0.89 ± 0.02	1.61 ± 0.02	26 ± 2
	230	0.85 ± 0.03	1.42 ± 0.03	26 ± 3
low spin	4.2*	0.451 ± 0.005	1.018 ± 0.005	67 ± 1
	4.2	0.45 ± 0.01	1.01 ± 0.01	71 ± 1
	115	0.427 ± 0.005	1.058 ± 0.005	74 ± 1
	230	0.40 ± 0.01	1.08 ± 0.01	74 ± 2

* Mössbauer spectra were all measured on sample 4. For the first measurement at 4.2 K, the sample was reduced with 1-fold excess of NADH at room temperature. After the first measurement, the sample was thawed in a strictly inert atmosphere (which had been exchanged with high-purity argon at least 6 times), reacted with 10-fold more NADH and incubated at room temperature for additional 3 hours. During these processes, the optical spectra were monitored at α band region and no significant change was detected. This sample was then used in all the rest of the measurements.

Mössbauer spectra of the resting yeast cytochrome oxidase are displayed in Figure 9. At 200 K, the magnetic structure was completely collapsed so that two quadrupole doublets could be resolved. This spectrum is displayed in Figure 9a. Component A ($\delta = 0.23$ mm/sec, $\Delta E_Q = 1.99$ mm/sec) is typical of a low-spin ferric ion and is assigned to ferricytochrome *a*. Component B was quite broad and its parameters suggest a high-spin ferric center, namely, cytochrome a_3. Thus the molecular picture of the yeast oxidase emerging from Mössbauer measurements is similar to that derived for beef heart oxidase by MCD(5,6) and magnetic susceptibility (8-10). However, as mentioned before, the parameters of component B fall also in the range of a low-spin ferrous ion. This ambiguity as well as the broadness of the peaks will be discussed in greater detail later.

At 4.2 K, the spin relaxation time of the low-spin ferric heme ($S = 1/2$) becomes long compared with the nuclear precession frequency, $A/\hbar$. Cytochrome *a* displayed an anisotropic magnetic structure (Figure 9b). We will tentatively attribute the central doublet, whch was largely insensitive to a small applied field, to the high-spin cytochrome a_3. This assignment will be discussed at length later. The lack of magnetic structure (Figure 9b) is not inconsistent with the model in which cytochrome a_3 is coupled with Cu_B antiferromagnetically to form an $S = 2$ state.

The use of a small magnetic field, 320 gauss in this study, caused the electron spin to align along the field, and distinctive magnetic hyperfine patterns appeared for cytochrome *a* (Figure 9c,d). Careful examination of the central doublet in these figures revealed that it consisted of two components. Component 1 was not affected by the small field, while component 2 displayed a slight, yet distinctive, broadening. The broadening pattern appeared to depend on the direction of the field. There were other signs of heterogeneity in the central doublet. Table 2 showed a discrepancy in the Mössbauer parameters of the sharp components of the central doublet obtained in the presence and absence

Figure 9. Mössbauer spectra of the resting yeast cytochrome oxidase enriched in ^{57}Fe (Sample 4): (a) at 200 K, the solid line is the least-squares Lorentzian fit of 4 lines; (b) at 4.2 K without external magnetic field; (c) at 4.2 K in the presence a 320 Gauss magnetic field parallel to the γ ray; (d) at 4.2 K in the presence of a 320 Gauss perpendicular field.

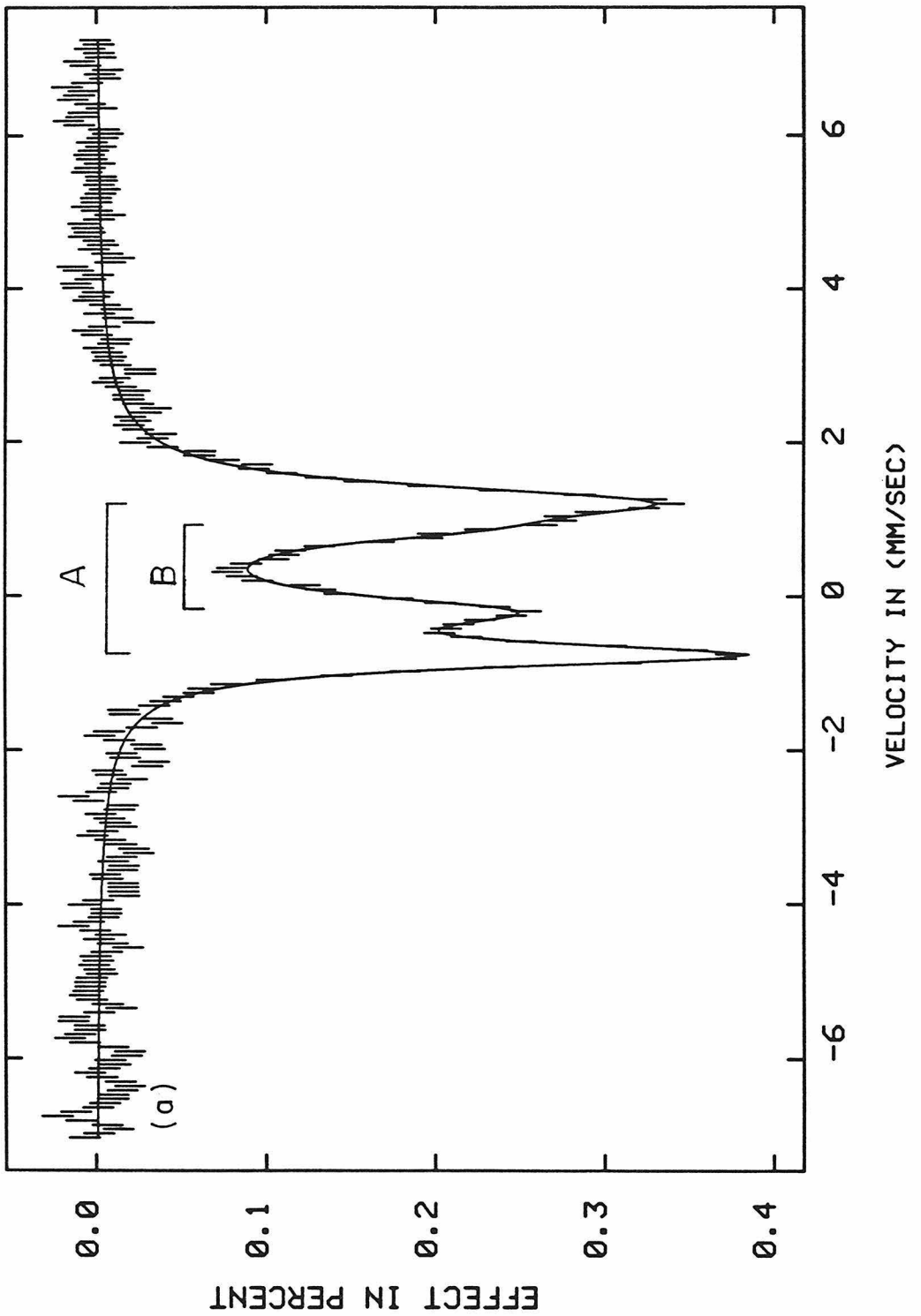
EFFECT IN PERCENT
0.0
0.1
0.2
0.3
0.4
VELOCITY IN (MM/SEC)
-6
-4
-2
0
2
4
6
A
B
(a)

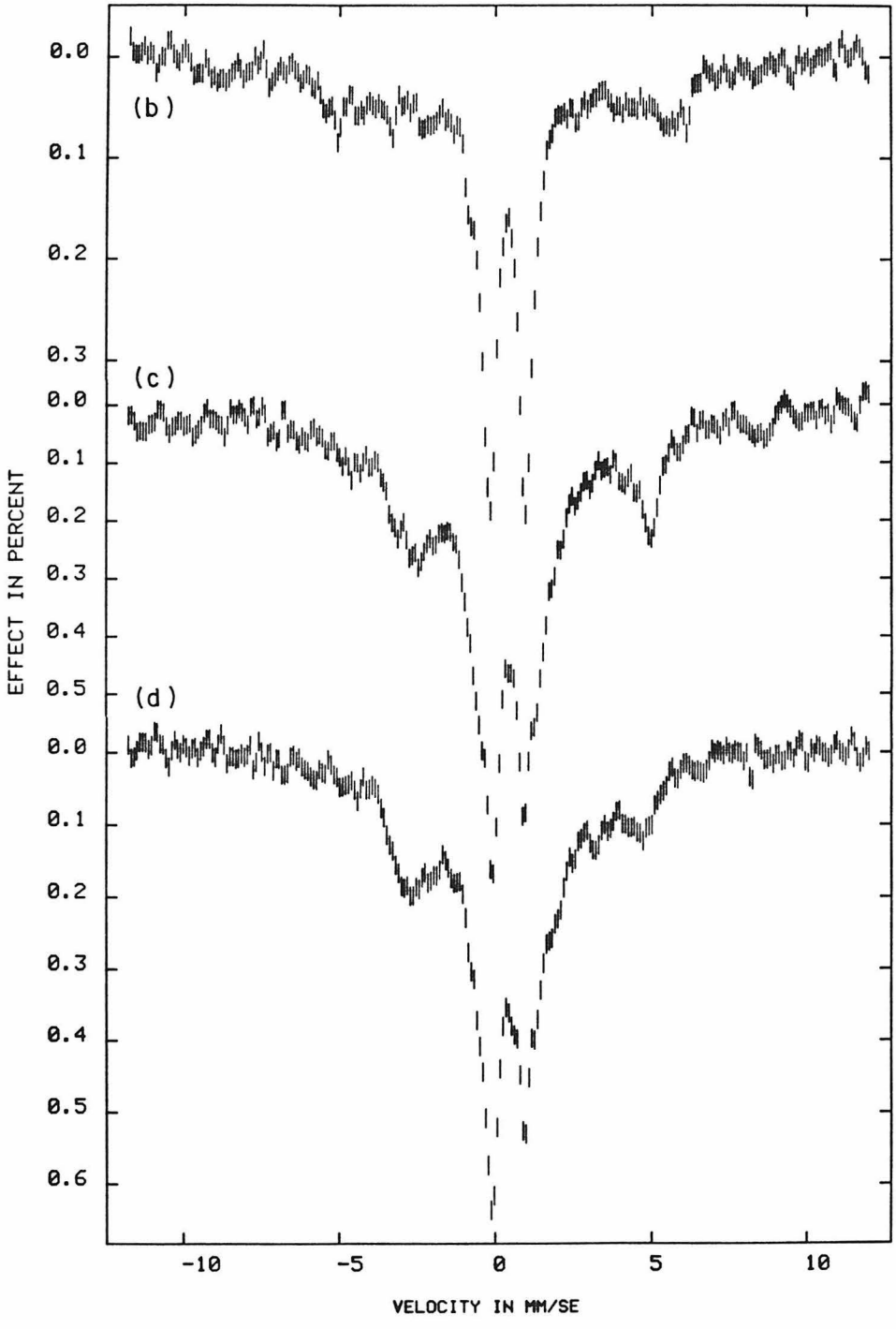
(b)
(c)
(d)
0.0
0.1
0.2
0.3
0.0
0.1
0.2
0.3
0.4
0.5
0.0
0.1
0.2
0.3
0.4
0.5
0.6
EFFECT IN PERCENT
-10
-5
0
5
10
VELOCITY IN MM/SE

of the field. In the absence of the small field, the isomer shift is noticeably lower and the quadrupole splitting is substantially larger than those observed in the presence of the field. This discrepancy is most easily understood by fitting the central doublet in Figure 9b with two pairs of Lorentzian lines, as is shown in Figure 10a. The nature of these two components will be discussed later.

First we shall tackle the hyperfine pattern of cytochrome *a*. Following the electronic theory of the low-spin ferric ion, we were able to estimate the hyperfine tensors as well as the quadrupole parameters from *g*-values obtained in EPR experiments. The calculated parameters are $A_{xx} = -465$ kGauss, $A_{yy} = 212$ kGauss, $A_{zz} = 615$ kGauss, $\Delta E_Q = 3.11$ mm/sec, and $\eta = -1.7$ mm/sec. The quadrupole splitting was clearly overestimated by this calculation, and the experimental value at 200K was used instead. The other values served as a starting point for the simulation with a computer program (33). After many iterations, reasonable fits were obtained for the spectrum measured with either a perpendicular or a parallel field with a single set of parameters. In this simulation, the **g** tensor and **A** tensor were assumed to be coaxial. However, best results were obtained when a set of small Euler angles was adopted between EFG and **A** tensors. The simulation results are reproduced in Figure 10b,c and the parameters used in these simulations are listed in Table 4. The low-spin ferric heme signal represent roughly 50% of the total ion. Included in Figure 10b,c and Table 4 respectively are the simulations and simulation parameters of other components as well.

Normally cytochrome a_3 is EPR silent. However, in most yeast oxidase preparations, high-spin ferric heme signals were observed by EPR (*cf.* Figure 7). At least part of these signals is due to the uncoupled cytochrome a_3^{3+}. The amount of the high-spin material was estimated by the method of Aasa and Vänngård (46,47) to be typically around 10% compared to the intensity of low-spin cytochrome *a*. There are, in fact, at least two sets of high-spin EPR signals.

Figure 10. Simulation of the Mössbauer spectra of resting yeast cytochrome oxidase enriched in ^{57}Fe (Sample 4). The spectra were measured (a) without external field, (b) with a 320 Gauss parallel field and (c) with a 320 Gauss perpendicular field. They are exactly the same as those in Figure 9b,c,d. The spectra are described by 4 components with appropriate percentages of the total absorption: low spin cytochrome a^{3+} ($-\cdot-\cdot-$), 48%; uncoupled high spin cytochrome $a_3{}^{3+}$ ($\cdots\cdots$), 4%; low spin cytochrome a_3^{2+}, which is referred to in the text as component 1 of the central doublet, (- - - - -), 12%; and the coupled cytochrome a_3, or component 2, ($- - --$), 27%. Simulations of the Mössbauer spectra of a few other minor components such as rhombic high spin ferrihemes and contaminating cytochrome *b* are not attempted, as the structural information on these metal centers and the statistics of the experimental data are both inadequate to justify such efforts.

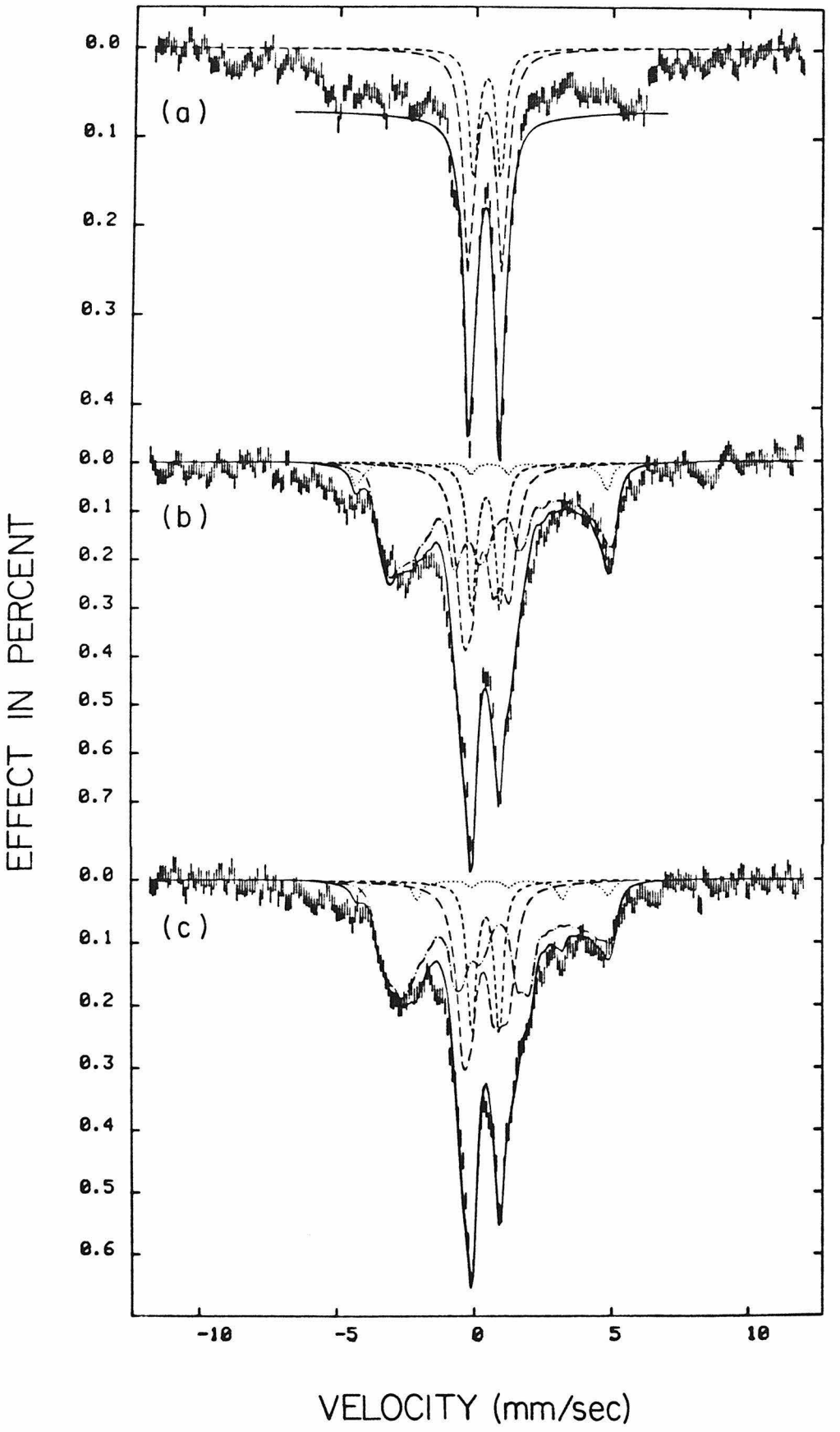
(a)
(b)
(c)
0.0
0.1
0.2
0.3
0.4
0.5
0.6
0.7
-10
-5
0
5
10
EFFECT IN PERCENT
VELOCITY (mm/sec)

Table 4. Parameters Used to Calculate Mössbauer Spectra of Resting Yeast Cytochrome Oxidase at 4.2°K

Species	Spin assumed	δ (mm/sec)	ΔE_Q (mm/sec)	η (mm/sec)	(A_{xx}, A_{yy}, A_{zz}) (kGauss)	(g_x, g_y, g_z)	width (mm/sec)	relaxation limit
Cytochrome a*	$S = \frac{1}{2}$	0.324	+2.00	−1.7	(−290, +170, +505)	(1.49, 2.26, 2.98)	0.35	slow
Cytochrome a_3 Uncoupled,	$S' = \frac{1}{2}$	0.434	+0.51	–	(−573, −573, −191)	(6, 6, 2)	0.35	slow
Coupled†, (Component 2)	$S' = \frac{1}{2}$	0.384	−1.20	–	(−51.5, −51.6, −17.2)	(6, 6, 2)	0.55	slow
Reduced, (Component 1)	$S = 0$	0.437	+1.02	–	–	–	0.35	–

* D frame is rotated by $(0°, 10°, 0°)$ into EFG frame.

† This is a phenomenological fit, and does not have a physical basis. See text.

One is axial at $g = 6.0$; the other is fairly rhombic and only the low field signal g_y was identified at 6.70. The rhombic signal in the yeast oxidase is more asymmetric than the rhombic signal generated in beef heart during partial reduction of the enzyme (50) and is inert to ligand binding. On the other hand, reacting the enzyme with cyanide diminishes the axial signal. Thus the axial signal probably comes from the disrupted oxygen binding site. Typically, a high spin ferric ion has a relatively long relaxation time due to the lack of the orbital momentum from the totally symmetric ${}^6A_{1g}$ ground state (31). Therefore, it is expected that the Mössbauer resonance of these hemes would be broadened by a magnetic field. Indeed, the spectral features around -5, -2, and $+3$ mm/sec (Figure 10b,c) cannot be ascribed to the low-spin ferric ion. We simulated the spectra of an axial high-spin ferric ion to match these features. This iron center was treated as an effective $S' = 1/2$ system assuming that

$$\frac{g_x}{A_x} = \frac{g_y}{A_y} = \frac{g_z}{A_z} = \frac{g_0}{A_0} \tag{17}$$

as suggested by Wickman *et al.* (51). The results are displayed in Figure 10b,c, and the parameters are included in Table 4. The intrinsic field of this species is expected to be isotropic and is estimated to be 192 kGauss. This is fairly close to those found for other high-spin hemeproteins (32,52). This species accounts for only a very small amount (<5%) of the total iron detected by Mössbauer spectroscopy. The assignment may not be definite because of the poor signal-to-noise at certain regions. It does provide a clue as to the magnitude of the hyperfine interaction at the coupled cytochrome a_3–Cu_B site. The latter can be estimated through *Eq.*(13*b*). The small features at either side of the spectra, namely, around 6 mm/sec and -5 mm/sec (Figure 10b,c), are probably due to other species such as rhombic high-spin ferric ions or low spin cytochrome b_{562}. The EPR signal of cytochrome b_{562} is more anisotropic than that of cytochrome *a* (53). Its Mössbauer spectrum is therefore expected to be more anisotropic as well.

Component 1 of the central doublet has an isomer shift and a quadrupole splitting that are suggestive of either a high-spin ferric iron or a low-spin ferrous iron. On the other hand, the lack of magnetic structure at 4.2 K under a small field is most consistent with either an $S = 2$ or an $S = 0$ center. It seems that the strongly superexchange-coupled cytochrome a_3, a ferric iron with a coupled $S = 2$ state, fits nicely into one of the two possibilities. (The other possibility is a low-spin ferrous ion.) As mentioned before, it is possible to distinguish between the two cases with a high field Mössbauer measurement. From Table 1 we see that at high field the internal field of an $S = 2$ system can be substantial. A 35 kGauss measurement on sample 2 is displayed in Figure 11 along with its 320 Gauss measurement. The deconvolution of the low field spectrum showed that component 1 represented roughly 20% of the total iron, i.e., 40% of one cytochrome. The high field spectrum of this component displayed a nuclear Zeeman interaction with no intrinsic field at all. The optical spectrum of this sample showed a diminished 655 nm, suggesting that the content of the coupled cytochrome $a_3 - Cu_B$ was decreased. The ratio of A_{598}/A_{540} was difficult to estimate accurately due to the poor baseline of the spectrum. However, the Soret had a more red-shifted maximum at 422 nm than sample 4. All these observations point to an assignment of component 1 as a reduced low spin heme. Its parameters are identical to those for the low-spin component in the reduced enzyme within the experimental uncertainty. From the simulation fit of the Mössbauer spectra of sample 4, 12% of the total iron, namely, 24% of one cytochrome, was reduced in sample 4. This conclusion is in good agreement with the estimate from optical spectroscopy.

These assignments leave the EPR-'silent' a_3 site to be the only candidate for component 2. Spectroscopic properties that have been proposed for that site are: the 655 nm band and the EPR '$g = 12$' signal. Among the four samples we studied with Mössbauer spectroscopy, sample 3 and sample 4 had a pronounced

Figure 11. Mössbauer spectra of the resting yeast cytochrome oxidase enriched in ^{57}Fe (Sample 2) at 4.2 K: with an (a) 320 Gauss, (b) 35 kGauss magnetic field parallel to the γ ray. Overlaid on top of (b) are simulations for low spin cytochrome a^{3+} ($- \cdot - \cdot -$), 40% and low spin cytochrome $a_3{}^{2+}$ (- - - - -), 20%. The content of each constituent was determined by a simulation of (a) (not shown).

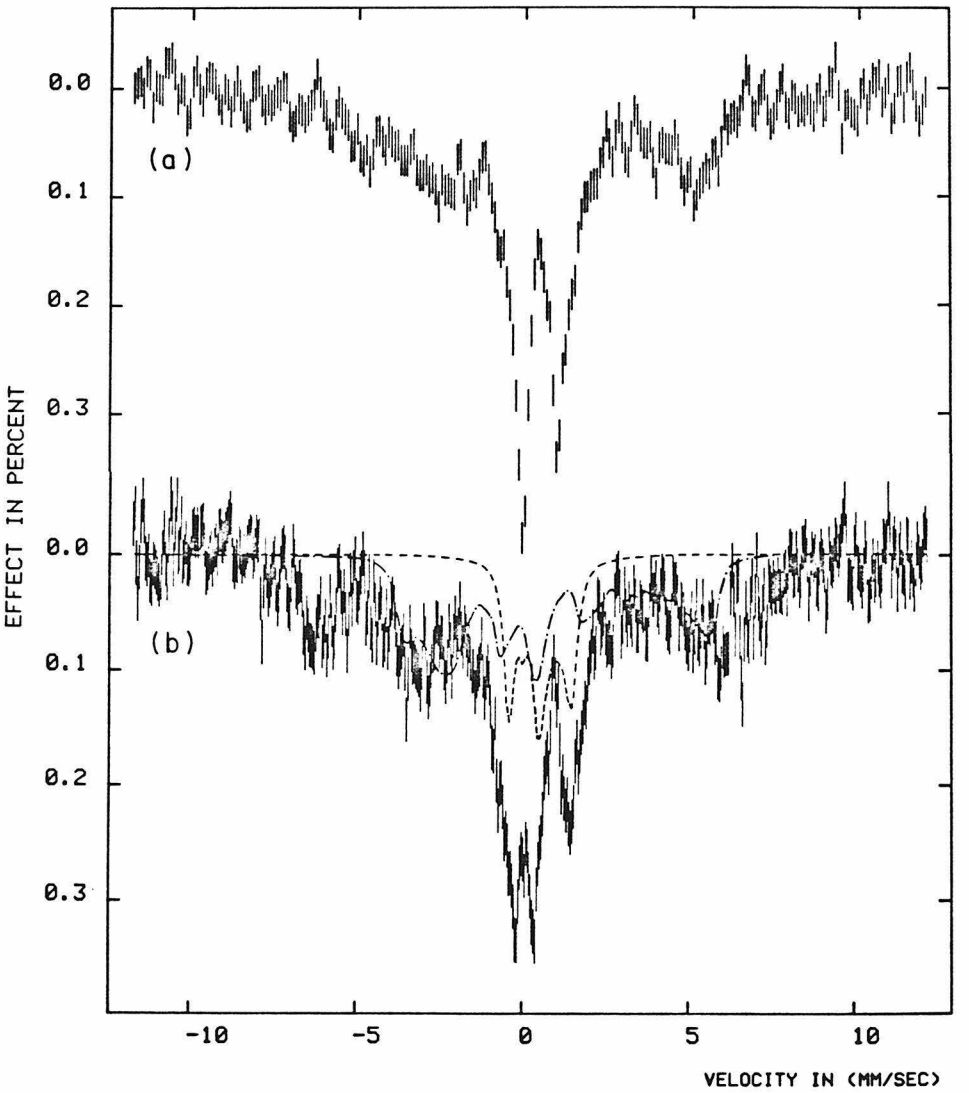
0.0
0.1
0.2
0.3
(a)
0.0
0.1
0.2
0.3
(b)
EFFECT IN PERCENT
-10
-5
0
5
10
VELOCITY IN (MM/SEC)

655 nm band, while sample 1 and sample 2 had diminished intensity. Comparing the available EPR measurements, we found that sample 4 exhibited a reasonable intensity at $g = 12$, and no such signal can be detected in sample 1. We will show that there are indeed correlations between the amount of the component 2 and the intensity of the 655 nm band and the intensity of $g = 12$ signal.

The broadening of the component 2 at a small field is puzzling. If the antiferromagnetic exchange coupling is strong, the component 2 or the a_3 site could be treated as if it were a genuine $S = 2$ system. We shall present simulation results on the Mössbauer spectrum of the a_3 site using appropriate A tensor and g-values, and three different magnitudes of the zero-field parameter D assuming the a_3 site is an $S = 2$ system: (1) D predicted by theory (34,42) from the corresponding D_1 of the uncoupled cytochrome a_3; (2) a small D (< 2 cm^{-1}); and (3) a negative D. As no satisfactory fit resulted from these approaches, a phenomenological fit is provided for the purpose of quantitation. The possibility of having a weak exchange coupling between cytochrome a_3 and Cu_B instead of a strong one has been suggested by Kent *et al.* (24). We shall consider this alternative in the 'discussion' section.

The zero field parameter D_1 of the uncoupled cytochrome a_3 has been investigated previously. Brudvig *et al.* (54) noted that the coupling between cytochrome a_3 and Cu_B was disrupted when the enzyme reacts with NO. As a result, a rhombic high-spin ferric signal was observed by EPR. The temperature dependence study of this signal (21) indicates that the zero-field parameter D of this uncoupled cytochrome a_3 is similar to that of myoglobin (55), namely, 9 cm^{-1}. (They also indicated that the D drops to 6 cm^{-1} when F^- is bound to cytochrome a_3, similar to that found in myoglobin–F^-. The implication of this decrease in D upon ligand binding will be discussed later.) Hagen (18) determined the D to be $\sim$8 cm^{-1} for the high-spin EPR signals, which were prepared by partial reduction, by EPR depopulation experiments. His other

measurements using frequency-dependent g-values confirmed that D is at least 4.6 cm^{-1}. Therefore the results from the two groups are in good agrrement.

Theoretically, the anisotropic superexchange depends on $J(\Delta g/g)^2$, whereas the magnitude of J was suggested to be $\geq$ 200 cm^{-1} (9) and not precisely determined. We therefore expect the contribution of the anisotropic exchange to the zero field splitting to be small (*cf.* *Eq.* 13c) and D for the coupled system to be around 10 cm^{-1}. Judging from the hyperfine tensor found for the uncoupled state, we estimate A for the coupled state to be around 225 kGauss. Reinhammar *et al.* (56) have determined the g-values of the EPR signal from uncoupled Cu_B, which was produced during partial reoxidation. Assuming the **g** tensor for the iron to be isotropic, we thus deduce that the g-values for the coupled state are 1.99, 1.98, and 1.95. As has been pointed out before, the two metal centers might not have the same symmetry axes. The above g-values may not represent the real g-values, but they are essentially isotropic and the Mössbauer spectrum is not very sensitive to them.

Using these parameters, we were not able to reproduce the broadening assuming either fast or slow relaxation conditions. Indeed, from Table 1 it is clear that at 320 Gauss with D between $5 - 10$ cm^{-1} one cannot expect enough spin expectation value in the ground state from mixing. The simulated lines are broadened when a small D ($\leq$ 3 cm^{-1}) is assumed. This is because of the increased mixing of upper levels with the $M_S = 0$ level as well as the population of $M_S = \pm 1$ level. Especially when D is between $1 - 2cm^{-1}$, the right amount of broadening seemed to be achieved. However, the lineshape predicted under these assumptions cannot be fit very well with the experimental data.

Physically, the spin relaxation of cytochrome a_3 is expected to be not very fast, because it has an $^6A_{1g}$ ground state, nor very slow, because it is next to a paramagnetic center, Cu_B. Recently, a relaxation theory and computer program appropriate to this case have been developed by Schulz *et al.* (57). We applied

this program to the small D case, and the best fit so far is presented in Figure 12 along with the simulations of the other components. The parameters used to generate these spectra are provided in the figure legend. The region between $-1.$ and 0. mm/sec fit remarkably well in both field directions. The right-hand side of the central doublet in the perpendicular field spectrum (Figure 12b), however, was not well represented. A weakness that may be hard to reconcile is the intensity at the middle of the central doublet ($\sim$ 0.5 mm/sec), especially in the parallel field spectrum. It cannot be said at this moment whether an acceptable fit can be obtained through this approach. Analytical analysis of the likelihood is not possible. Obviously, quite a bit of fiddling with the parameters is required and it involves the adjustment in the simulation of other components as well. It is beyond the limit of this work and should be pursued later.

A similar broadening has been observed with the CN^- bound *T. Thermophilus* cytochrome oxidase (24). It was argued that a negative D, which agrees with an MCD study of the CN^- derivative (26), with an energy splitting of $0.3cm^{-1}$ or less among $M_S = \pm 1$ levels, will suffice to explain such a broadening. To explore the possibility of negative D in the resting yeast oxidase, we refer to Table 1. The energy diagram of such a system was displayed in Figure 5. The lowest states are the $M_S = \pm 2$ levels. The maximum spin expectation value, therefore the maximum internal field, lies along the heme normal. Taking the example of axial symmetry, in which the asymmetry parameter is 0, we find that the maximum broadening (58) is

$$\frac{1}{2}\Delta_{\max} = (3g_n^{ex} + g_n^{gnd})\beta_n H_z^{eff}\langle S_z\rangle, \tag{18}$$

where g_n^{ex} and g_n^{gnd} are the g-values for the excited state ($I = 3/2$) and the ground state ($I = 1/2$), -0.103 and 0.180, respectively. From Figure 9d we estimate the broadened halfwidth is roughly 0.6–0.7 mm/sec, from which $\langle S_z\rangle$ can be shown to be $\sim$ 0.1. In the fast relaxation limit, $\langle S_z\rangle_{av}$ is given by Eq. 16, and the maximum spin polarization will be 0.04, too small to cause the observed

Figure 12. Simulations of the Mössbauer spectra of the resting yeast cytochrome oxidase using a small zero field parameter D and an intermediate spin relaxation rate for the oxidized cytochrome a_3. The spectra presented in (a) and (b) are exactly the same as those in Figure 10c and 10d; namely, they are the spectra of sample 4 with a parallel and perpendicular external field of 320 Gauss, repectively. The spectra are described by 4 constituents with appropriate percentages of the total absorption: low spin cytochrome a^{3+} ($-\cdot-\cdot-$), 48%; uncoupled high spin cytochrome ${a_3}^{3+}$ ($\cdots\cdots$), 4%; low spin cytochrome a_3^{2+}, which is referred in the text as the component 1 of the central doublet, (- - - - -), 12%; and the coupled cytochrome a_3, the component 2, ($- - --$), 30%. Simulation parameters are the same as those in Figure 10 for all components except for the coupled cytochrome a_3. The latter is assumed to be an $S = 2$ state and is simulated with an intermediate electronic spin relaxation rate using a computer program by Schulz*. The parameters are: δ=0.38 mm/sec; ΔE_Q=1.2 mm/sec; η=0; g=(2, 2, 2); A=256 kGauss, isotropic; D=1.38 cm^{-1}; E=0.055cm^{-1}; linewidth 0.3 mm/sec and relaxation parameter W=0.0001 rad sec^{-1} K^{-3}. The relaxation parameter is as defined in Schulz *et al.* (55).

*I wish to thank Dr. Schulz for providing the program and the simulation.

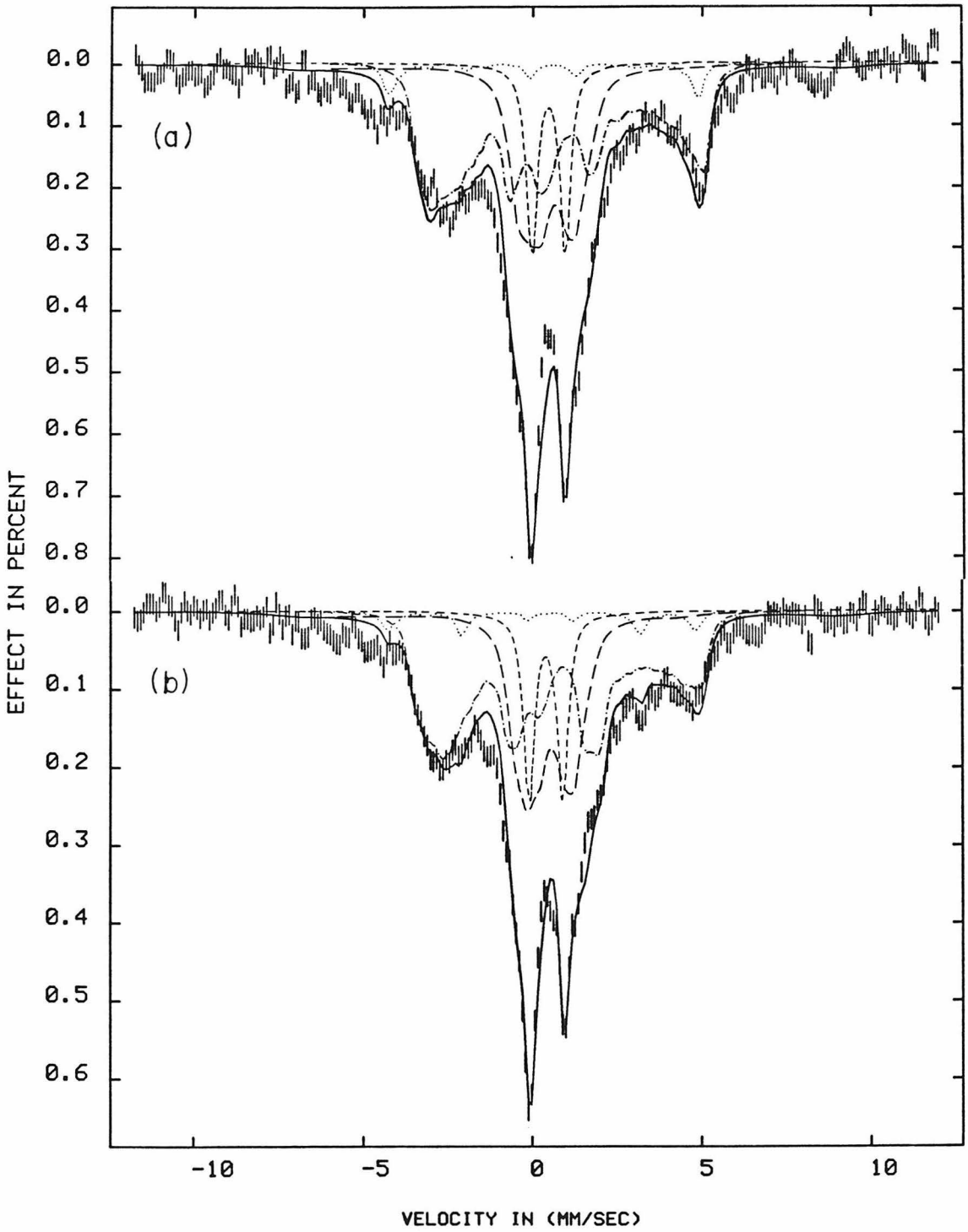
0.0
0.1
0.2
0.3
0.4
0.5
0.6
0.7
0.8
(a)
(b)
EFFECT IN PERCENT
-10
-5
0
5
10
VELOCITY IN (MM/SEC)

broadening. When the relaxation is slow, we estimate that the energy splitting of the $M_S = \pm 2$ levels would have to be around 2.4cm^{-1} to cause a 0.7 mm/sec broadening. For $D = -9$ cm^{-1}, this implies that $E = 2.7\text{cm}^{-1}$. Results from computer simulation are in good agreement with this analysis. The lineshape thus obtained is acceptable. However, besides the novelty of a negative D, such a rhombicity has never been seen among hemeproteins.

Since no satisfactory physical interpretation is available for component 2, the spectrum is described phenomenologically as follows. Assuming that the iron was in the high-spin ferric state with a positive D, using a hyperfine tensor roughly 1/11 of that for the uncoupled ion, we were able to fit the data in the slow relaxation limit quite well. The parameters are listed in Table 4. The simulation results on sample 4 are presented in Figure 10b,c along with the other components and their sum. With one set of parameters, the two spectra of component 2 measured under two different field directions can be described quite well.

In the same figures, it is also shown that the Mössbauer spectra of sample 4 can be fit with the above mentioned 4 components satisfactorily. There might be other minor components, such as other types of high-spin ferric species and cytochrome *b*, the assignments of which are not possible at this stage. In Figure 13, we see that the spectra of other samples can be described reasonably well with these four major components. The universality of these simulated spectra indicates that the deconvolution of the experimental data is likely to be correct. The contribution of each component to the spectrum is given in the figure legends. The concentration of the coupled cytochrome a_3, or component 2, in 3 samples (*cf.* Figures 10,13) correlates well with the intensity of the optical band at 655 nm and the EPR signal around $g = 12$. Thus Mössbauer studies provide support for the original proposals by Beinert *et al.* (19) and Brudvig *et al.* (21) about the origins of these two physical properties.

Figure 13. Mössbauer spectra of resting yeast cytochrome oxidase enriched in ^{57}Fe at 4.2 K: (a) Sample 3 with a 320 Gauss perpendicular field; (b) Sample 1 with a 320 Gauss parallel field; and (c) Sample 1 with a 320 Gauss perpendicular field. Each spectrum is fitted using the 4 constituents whose Mössbauer parameters were determined from Sample 4. The contents of these constituents in Sample 3 are: low spin cytochrome a^{3+} ($- \cdot - \cdot -$), 48%; the uncoupled high spin cytochrome ${a_3}^{3+}$ ($\cdots\cdots$), 6%; low spin cytochrome a_3^{2+} (- - - - -), 9%; and the coupled cytochrome a_3 ($- - --$), 24 %. The content of these constituents in Sample 1 are: low spin cytochrome a^{3+} ($- \cdot - \cdot -$), 48%; the uncoupled high spin cytochrome ${a_3}^{3+}$ ($\cdots\cdots$), 6%; low spin cytochrome a_3^{2+} (- - - - -), 26%; and the coupled cytochrome a_3 ($- - --$), 10%. Simulations of the Mössbauer spectra of a few other minor components such as rhombic high spin ferrihemes and contaminating cytochrome *b* are not attempted as the structural information on these centers and the statistics of the experimental data are both inadequate to justify such efforts.

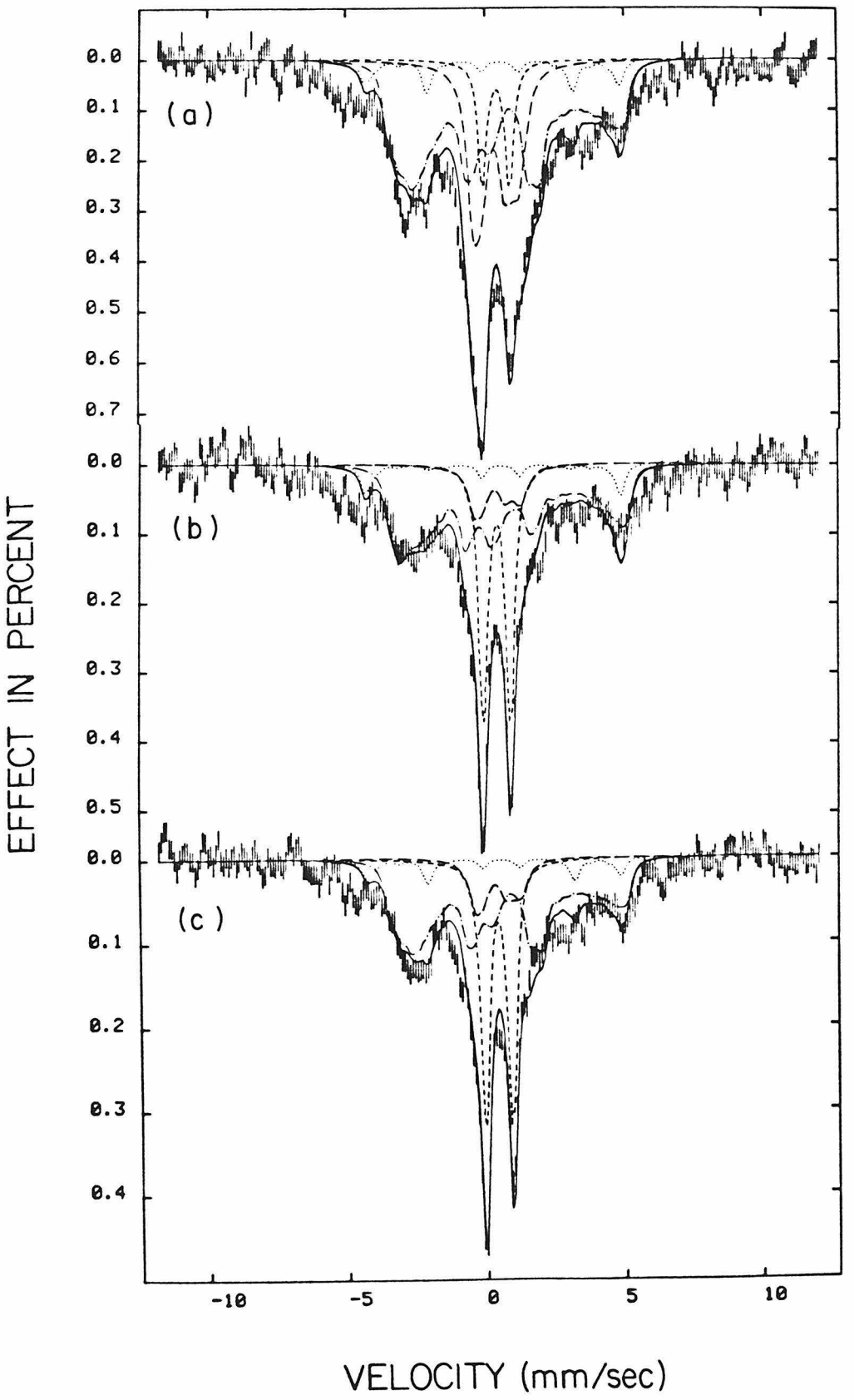
(a)
(b)
(c)
0.0
0.1
0.2
0.3
0.4
0.5
0.6
0.7
0.0
0.1
0.2
0.3
0.4
0.5
0.0
0.1
0.2
0.3
0.4
-10
-5
0
5
10
EFFECT IN PERCENT
VELOCITY (mm/sec)

DISCUSSION

The Reduced Material in The Resting Oxidized Enzyme

The Mössbauer spectra presented here demonstrate the existence of a diamagnetic heme in the resting cytochrome oxidase from baker's yeast. The Mössbauer parameters δ and ΔE_Q of this component were virtually identical to those of reduced cytochrome *a*. This result supports the finding of Siedow *et al.* (23) that in the purified yeast oxidase there is an 'inactive' fraction that contains reduced low spin heme. However, we do not agree with their assignment of the origin of this reduction. Based on an EPR study of cytochrome *a* intensity changes upon reaction with ferricyanide, they suggested that part of the cytochrome *a* developed an inactive conformation with an increased reduction potential. We do not see such changes in EPR intensity in our samples. (We should point out, however, that such changes do not discriminate against our assignment, since the ferricyanide-oxidized low-spin cytochrome a_3 is likely to contribute an EPR signal around the $g = 3$ region.) From Figures 10 and 13 we saw that the content of the diamagnetic material varied from 9% to 26% of the total absorption among different samples, and that that of the low spin ferric ion changed very little. This indicates that the reduced low-spin heme was that of cytochrome a_3 rather than cytochrome *a* as Siedow *et al.* suggested. Furthermore, the spectrum of the NADH-reduced sample (same sample) showed that a substantial amount of the reduced cytochrome a_3 was low-spin. Therefore the diamagnetic material is most likely due to a high- to low-spin transition and autoreduction of cytochrome a_3.

One might still invoke a complicated scheme to suggest otherwise. The Mössbauer data could also be explained by assuming that both cytochrome *a* and a_3 adopt different conformations at the same time, therefore causing *a* to become reduced and a_3 low-spin. It would be desirable to have a direct measurement of

the reduction potential of each center, but understandably the system would be too complicated to yield unambiguous assignments. We thus measured the redox potential of CO-inhibited yeast cytochrome oxidase by spectroelectrochemistry. The detailed results will be presented in Chapter 5, but the relevant findings will be discussed here. The redox potential of cytochrome *a* in yeast is indeed higher than that in beef heart by roughly 45 mV. The interaction potential with Cu_A (i.e.,the potential change at cytochrome *a* which accompanies the reduction of Cu_A (59)) is roughly the same as that observed in the beef heart enzyme. No fraction of cytochrome *a* with an especially high redox potential was observed. On the contrary, after a few cycles of oxidation-reduction, a low redox potential center developed. EPR measurement showed that the intensity of the cytochrome *a* signal at $g = 3$ decreased as a new broad peak developed at $g = 2.9$. This is consistent with the presence of non-reducible material in sample 1 as revealed by the Mössbauer spectrum of NADH-reduced sample 1 (Figure 8b). To summarize, Mössbauer spectra and spectroelectrochemistry results both indicate that the reduced material is from the a_3 site.

The reduction as well as the spin transition of cytochrome a_3 suggests a sizable conformation change at that site. Photolysis experiments, the results of which will be presented in the next chapter, showed that Cu_B in this conformation no longer binds the flashed-off CO molecules as it does in the other conformation and in the native beef heart enzyme (60). Very likely the two metal centers have moved apart. Either Cu_B is reduced as well, or one should expect an EPR signal. The 'adventitious' copper signal at $g = 2.30$ (*cf.* Chapter 1), which is accessible to cyanide and accounts for roughly 20% of the total copper signal in a typical preparation, probably arises from the disrupted Cu_B.

Functionally, the oxygen-binding ability of cytochrome a_3 may be diminished, because the geometry of this site is likely to change into 6-coordinated, as most low-spin hemes are 6-coordinated (61). Also, the spin change at this

site does not favor the reaction with triplet dioxygen. From the EPR studies by Stevens and Chan (62) on yeast cytochrome oxidase enriched with isotopically labeled amino acid, it is established that histidine is the fifth ligand of cytochrome a_3. The Mössbauer spectrum of the reduced enzyme showed that the linewidth (*cf.* Table 2) of low-spin doublet is very close to that of the iron foil, although it consists of both cytochromes. This sharpness suggests that the environment of the low-spin cytochrome a_3 is very similar to that of cytochrome *a*. Although the isomer shift of reduced cytochrome *a* is very close to that of reduced *c* type cytochromes (63,64), the quadrupole splittings of the *c* type cytochromes have higher values (1.14-1.29 mm/sec). Therefore we might be able to distinguish the structures of the low-spin cytochrome *a* or a_3 from the methionine-liganded *c* type cytochromes. The axial ligands of cytochrome *a* were first suggested to be two histidines by Blumberg-Peisach diagrams (11); this assignment was later supported by ENDOR experiments by Martin *et al.* (13). Therefore the sixth ligand of the reduced low-spin cytochrome a_3 is likely to be histidine as well.

It seems that we have a case very similar to the cytochrome oxidase isolated from *T. thermophilus* (24): at least two kinds of a_3 were found in the purified enzyme; one was totally diamagnetic and the other could be broadened by a small magnetic field. For the enzyme from either organism, the spectrum of a_3 was preparation-dependent. In the case of yeast oxidase, both components were present in all samples. The content of the diamagnetic material seems to increase upon harsh treatment. As mentioned before, we found that in the reduced enzyme the content of low-spin heme increased noticeably upon standing at room temperature for a few hours. For the bacterial oxidase, the reported high temperature (230 K) data showed that only one component was discernible in any specific preparation. In fact, no transition was observed between the two components even when the sample was subjected to freeze-thaw-heat treatment.

Both components were considered conformations of the oxidized state in the bacterial oxidase. It seems that *T. thermophilus* cytochrome oxidase is more stable, possibly because it was evolved in a high-temperature environment. However, this does not exclude the possibility that the diamagnetic material in the bacterial oxidase is the same as that seen in yeast oxidase. The autoreduction at the a_3 site was dismissed in their report because a high- to low-spin transition was not anticipated.

Cytochrome a

The anisotropic hyperfine structure of the low-spin cytochrome a^{3+} has been described reasonably well by the simulation of the spectra of 3 different enzyme preparations under different field directions using a single set of parameters . This indicates that the simulation is quite accurate. We were thus able to resolve this component from the rest of the spectrum and can make a rough estimate of the concentration of this center. In all of the 3 samples for which the Mössbauer spectra were presented in Figures 10 and 13, this center accounted for close to half of the total iron, while the concentrations of the various species for the other center varied over a wide range.

While the perpendicular field spectrum of sample 4 (Figure 10c) was well represented by the low-spin cytochrome a^{3+} simulation, inspection of the parallel field spectrum (Figure 10b) reveals some notable discrepancies between the experimental data and the simulated spectrum, especially in the range between -2 and -3 mm/sec. The simulation tends to exaggerate the intensity of outer rims. Similar discrepancies were found for other samples (Figure 13), although the magnitude of the discrepancy varied from sample to sample. Similar problems have been encountered previously in the analysis of hemeproteins. Huynh *et al.* (63) suggested that the inadequacy of the simulation is due to an intrinsic heterogeneity of the protein, namely, each molecule's having a different g-tensor

and hyperfine interaction. Dwivedi *et al.* (64) first applied this concept by using a g-strain model and successfully simulated the spectrum of cytochrome c_{551}. In this model, g-values are parameterized by a Gaussian distribution of crystal-field splitting through which the **g**, **A**, and EFG tensors are calculated by the methods of Griffith (34) and Lang (35,36). This distribution of crystal-field splitting is thought to be due either to a freezing artifact that reflects the response of the protein to the external stress, or to a frozen-in distribution of conformation states (64). Judging from the complexity in the a_3 site shown by the Mössbauer spectra and from the results of the spectroelectrochemical studies on the CO-inhibited yeast cytochrome oxidase (Chapter 5), we see that cytochrome a is likely to be quite heterogeneous as well. A slightly different magnetic structure in the Mössbauer spectrum probably reflects not only a different g-strain but also a different kind of conformation distribution in each sample.

The Coupled Cytochrome a_3

Due to the presence of the reduced cytochrome a_3 in the resting yeast cytochrome oxidase, the spectrum of the coupled a_3 site can be obtained only indirectly from curve subtraction. However, it is possible to show that the spectrum of this site is sensitive to a magnetic field, in a manner similar to that observed for the enzyme from beef heart (7) and from the thermophilic bacterium *T. thermophilus* (24). The only published Mössbauer spectrum of cytochrome oxidase under a small field is the work on beef heart oxidase by Lang *et al.* (7). Understandably, the signal-to-noise was poor even after a week's accumulation. Nonetheless, while the magnetic structure of cytochrome a was smeared beyond recognition, the breadth of the coupled cytochrome a_3 spectrum stood out between -0.8 and 1.3 mm/sec. It is similar to what we see from the component 2 in the yeast oxidase. Further evidence of the structural similarity between this component and cytochrome a_3 in beef heart comes from the correlation with the intensity of the 655 nm band and the '$g = 12$' signal.

Thus there is little doublt that this component is the functional cytochrome a_3.

As we have pointed out, the slight broadening of this component by a weak applied magnetic field has been a mystery to investigators in this field. There is not yet a suitable model to interpret the data. Aside from the origin of the broadening, there is another difficulty: the intrinsic heterogeneity of this site. It has been shown that the oxidized cytochrome oxidase can have many different conformations (21). If more than one conformer is present in the yeast oxidase sample, we are confident that their Mössbauer spectra are all broadened to a similar extent under a small field. It is possible that the zero field structure varies slightly among conformers, and a fine tuning is necessary to improve the simulation of the mixture.

Several approaches have been used to interpret the spectrum of the coupled cytochrome a_3 in the resting state. The model with strong antiferromagnetic coupling between Fe_{a_3} and Cu_B predicts an $S = 2$ state with an isotropic hyperfine interaction of 225 kGauss, a nearly isotropic **g** tensor, and a zero field paramerter D around 9 cm^{-1}. The latter value was estimated from Hagen's measurement (18) on the zero field splitting of the uncoupled cytochrome ${a_3}^{3+}$ and an estimate of anisotropic superexchange coupling Δ assuming an isotropic superexchange of 200 cm^{-1}. Based on this model, we were not able to describe the broadening of the spectrum under any kind of electronic relaxation condition. Theoretically, the spin expectation value in the heme plane in the $M_S = 0$ level will increase as D decreases. Adopting the lowest limit ($D_1 = 4.6 cm^{-1}$) for the uncoupled state (18), we were still not able to produce enough broadening in the simulated spectrum.

It was found, however, by lowering D below 2 cm^{-1}, a sizable broadening was obtained with the $S = 2$ model. Improvement was achieved by using an intermediate relaxation rate. The best result so far using this approach was generated by a D of 1.38 cm^{-1}, which is very close to the value of 1.19 cm that

was reported by Hagen (18) from EPR simulation studies of the $g = 12$ signal of the beef heart enzyme, and an E of 0.055 cm^{-1}, which is close to the best value determined by Brudvig *et al.* (22), also from EPR simulation studies of beef heart enzyme $g = 12$ signal. As Brudvig *et al.* pointed out, their simulation is not sensitive to D; thus the small D suggested by this approach does not contradict either EPR study. We should stress, however, that there are serious imperfections with this simulation, and at this moment we do not know whether it can be improved. Nevertheless, it should be useful to discuss whether the small positive D can be derived from the coupled model and whether there is any alternative model to explain the Mössbauer spectra of cytochrome a_3. Using *Eq.* 13*c*, assuming an anisotropic superexchange $\Delta = 0.01J$, a $J \sim 2400 cm^{-1}$ is required, when lowest D_1 4.6 cm^{-1} is used, where D_1 is the zero-field parameter for the uncoupled state, to derive a $D = 1.38$ cm^{-1} for the coupled state. Such magnitude of superexchange has never been reported and is unlikely between an asymmetric ion pair. Obviously the situation can be improved if D_1 is as low as 1–2 cm^{-1}.

The fact that a small D cannot be derived from the current spin-couple model seems to put cytochrome a_3 into a genuine $S = 2$ system–such as a ferryl ion, as Hagen (18) suggested a few years ago in accordance with the model proposed by Seiter & Angelos (16). However, this idea is inconsistent with the Mössbauer parameters. All the reported ferryl complexes are $S = 1$ systems with isomer shift in the range from −0.1 to 0.1 mm/sec and quadrupole splitting around 1.5 mm/sec (Figure 2). The isomer shift of the coupled cytochrome a_3, 0.38 mm/sec, is much too high. One could argue that an $S = 2$ ferryl could have a higher isomer shift, as such trends have been observed in ferric and ferrous ions (*cf.* Figure 2). However, an $S = 2$ system would have an asymmetric electric field gradient and a larger quadrupole splitting such as ~2 mm/sec is expected. Therefore we agree with Kent *et al.* (24) that the assignment cytochrome a_3 to

a ferryl species in the native state is unlikely.

Another possibility that has been considered is a negative D for the coupled site. The computer simulation shows that the energy splitting between the $M_S = \pm 2$ levels is required to be $\geq 2\text{cm}^{-1}$ for this approach to yield an acceptable lineshape. This restriction sets the rhombicity (E/D) at 0.3 when $D = -9\text{cm}^{-1}$, and it increases as the magnitude of D decreases. The rhombicity measured for hemeproteins is generally below 0.05 (12). Therefore this proposal is highly unlikely also.

It is clear from the above analysis that the current theory (34,42) for the strongly superexchange-coupled a_3 site is not adequate to explain the Mössbauer results. Evidences seem to suggest that the system may indeed have a small zero field parameter D. A serious flaw of the theory is that it has not considered the chemical effect of the the bridging ligand on the zero-field structure of the a_3 site. The finding of Brudvig *et al.* (21) that F^--bound cytochrome a_3 has a smaller D than the uncoupled cytochrome a_3 suggests that the 6th, or the bridging, ligand can exert a significant influence on the zero-field structure. Indeed, Yim *et al.* (65) demonstrated that a small D can be resolved in the high-spin system when the iron atom is pulled toward the porphyrin plane by a 6th ligand. This point can be understood by considering that D is related to crystal-field splittings and spin-orbit coupling through the relationship (66):

$$D = \frac{\lambda^2}{5}\left(\frac{1}{\Delta_{\|}} - \frac{1}{\Delta_{\perp}}\right), \tag{19}$$

where λ is the spin-orbit coupling constant and $\Delta_{\|}$ and $\Delta_{\perp}$ are crystal-field splittings as illustrated in Figure 14. Therefore a more cubic symmetry can reduce the magnitude of D. The spin-orbit coupling constant decreases as the covalent character of the ligand increases. Therefore it may be an important factor to bring D down to 1–2 cm^{-1}.

The possibility of having a weak exchange coupling instead of a strong one between cytochrome ${a_3}^{3+}$ and Cu_B^{2+} has been suggested (24). This kind of sys-

Figure 14. The crystal-field splitting diagram of a high-spin ferric ion under tetragonal distortion of an octahedral field.

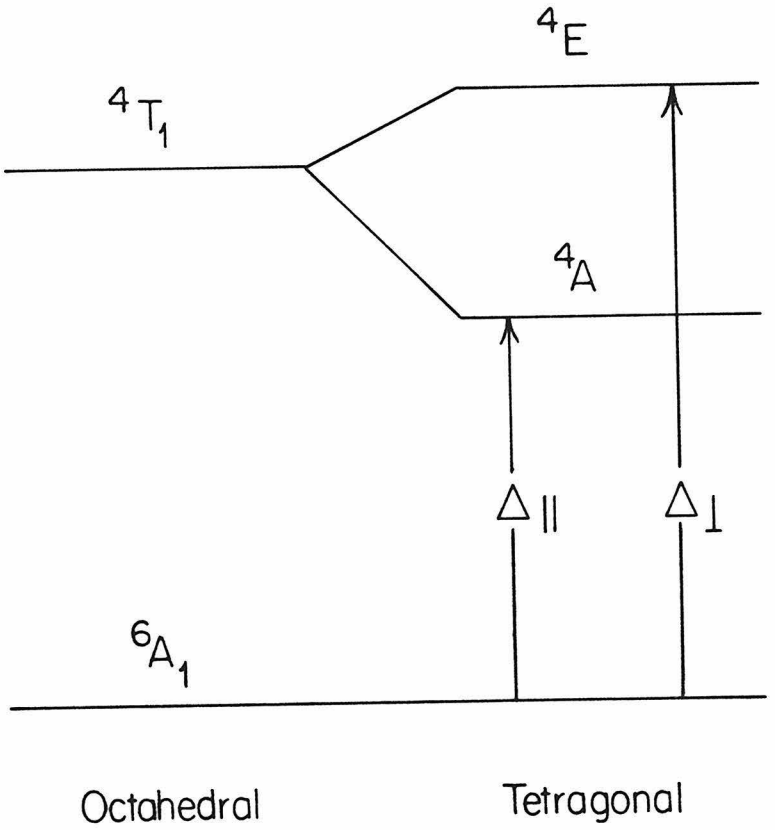
^4E
$^4T_1$
^4A
$\Delta_{\parallel}$
$\Delta_{\perp}$
$^6A_1$
Octahedral
Tetragonal

tem is extremely complex, since the two metal centers can adopt two different coordinate systems, which increase the obstacle for theoretical treatments immensely, and there are other types of interaction, such as dipolar interaction, to consider as well. To demonstrate the potential of utilizing such kind of interaction scheme to explain the Mössbauer behavior of cytochrome a_3, we present in Figure 15 the energy diagram of a much simplified case. In this system, the coordinate systems are assumed colinear, the exchange coupling is treated as a perturbation to the zero field splittings, and no other perturbation is considered except for the isotropic superexchange J. From the viewpoint of the perturbation theory, it is conceivable that a significant internal field can be induced by a small field in such a system. The broadening effect on the Mössbauer spectrum in such a small J system is similar to the case of small D. One appealing feature of the small J system is that after slight modifications of energy levels of $\phi_{\pm 1}$ states, for example, by dipolar interaction and/or coordination changes, the EPR $g = 12$ signal can be explained just as well as with a coupled $S = 2$ system. However, this model can be shown to be valid only by testing it numerically. Given the extra degrees of freedom this model demands and the signal-to-noise of the experimental data, we did not undertake this adventure.

At this stage we present the data with a phenomenological description. The model assumes an $S = 5/2$ spin system with a diminished **A** tensor. On the surface, it suggests a noncoupled high-spin ferric ion with a diminished spin expectation value in the lowest Kramers doublet. The diminished spin expectation value could be conceivably achieved by an intermediate electronic spin fluctuation rate caused by the neighboring copper. However, this may not be the case. Blume (67) showed that in the case of an intermediate fluctuation rate, the averaging effect is different for each member of the doublet. Therefore, in general, the transition to $M_I = \pm\frac{3}{2}$ is much broader than the transition to $M_I = \pm\frac{1}{2}$. This is verified through application of the relaxation program of

Figure 15. Lowest energy levels and wavefunctions generated by a much simplified model which describes a weak exchange-coupled $(\frac{5}{2} - \frac{1}{2})$ ion pair. In this system, the coordinate systems of the two ions are assumed to be colinear and the isotropic exchange interaction is treated as a perturbation to the zero field splittings. The basis functions are expressed in the form of $|M_1 M_2\rangle$, where subscripts 1 and 2 describe $S = \frac{5}{2}$ and $S = \frac{1}{2}$ systems respectively. ΔW_0, ΔW_1, and α are defined as follows:

$$\Delta W_0 = [(3J)^2 + (\Delta g_{||} \beta H \cos\theta)^2]^{1/2}$$

$$\Delta W_1 = \Sigma g_{||} \beta H \cos\theta$$

$$\tan 2\alpha = \frac{3J}{\Delta g_{||} \beta H \cos\theta}$$

where θ is the angle between the direction of external magnetic field and the principal symmetry axis, and

$$\Sigma g_{||} = g_{||}(1) + g_{||}(2)$$

$$\Delta g_{||} = g_{||}(1) - g_{||}(2).$$

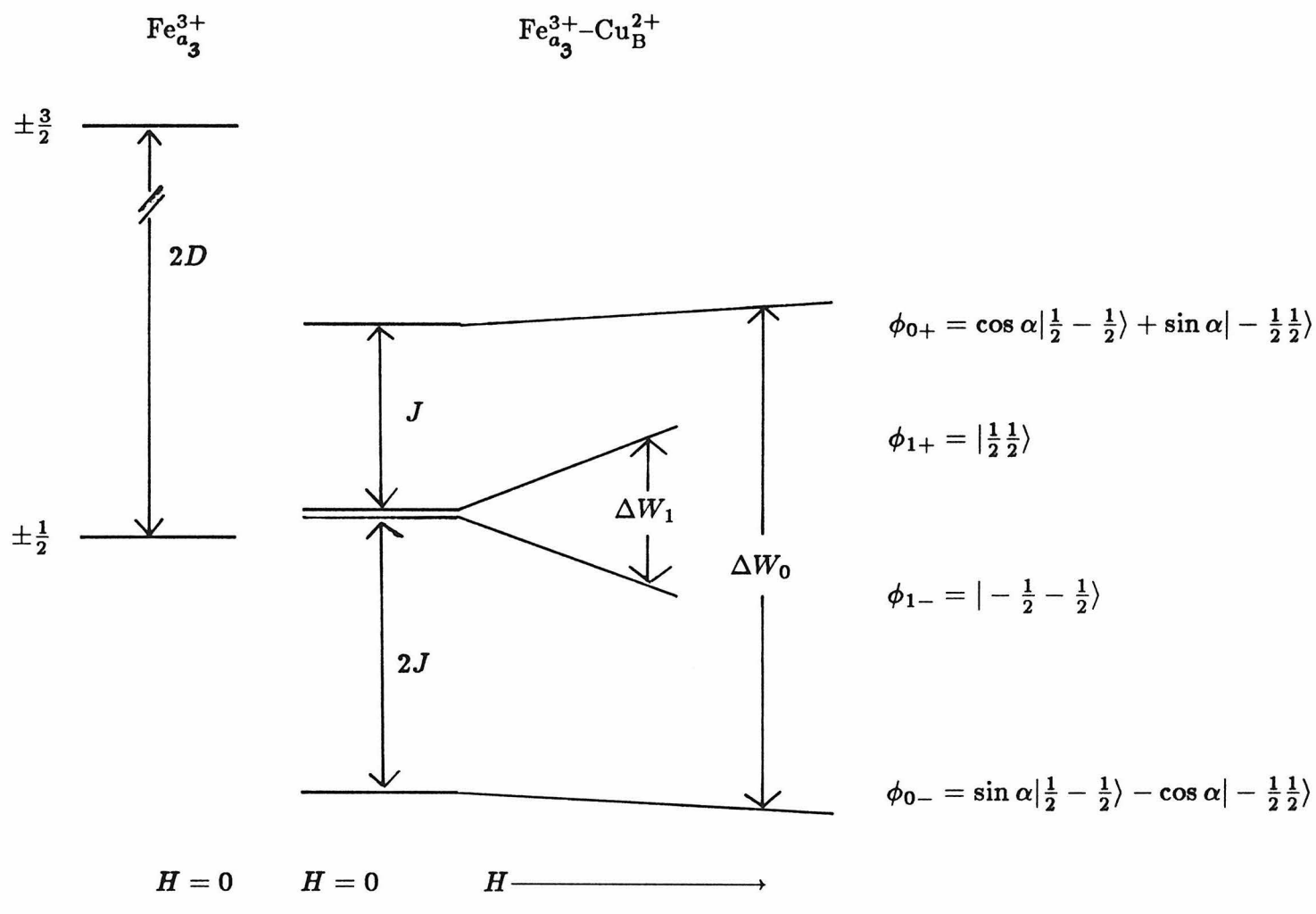
$Fe^{3+}_{a_3}$
$Fe^{3+}_{a_3}$–Cu^{2+}_{B}
$\pm\frac{3}{2}$
$2D$
$\pm\frac{1}{2}$
J
ΔW_1
ΔW_0
$2J$
$\phi_{0+} = \cos\alpha|\frac{1}{2}-\frac{1}{2}\rangle + \sin\alpha|-\frac{1}{2}\frac{1}{2}\rangle$
$\phi_{1+} = |\frac{1}{2}\frac{1}{2}\rangle$
$\phi_{1-} = |-\frac{1}{2}-\frac{1}{2}\rangle$
$\phi_{0-} = \sin\alpha|\frac{1}{2}-\frac{1}{2}\rangle - \cos\alpha|-\frac{1}{2}\frac{1}{2}\rangle$
$H=0$
$H=0$
H

Schulz *et al.* (57). The fit does serve a good purpose in enabling us to quantitate each component fairly accurately. The true description of the electronic structure awaits a better spin Hamiltonian and more iteration work on the computer. These will be pursued later on. Clearly, more high-field measurements at various temperatures are needed to pin down this evidently complicated structure.

Baker's Yeast Cytochrome Oxidase

In terms of spectral properties, our preparation contains very little contamination from other metalloproteins as judged by optical, EPR, and Mössbauer spectroscopies. The activity of the enzyme in general is comparable to what has been reported in the literature. However, we have seen severe inhomogeneity in all samples, some apparently due to the harsh treatment that the sample endures. This leads to questions about the quality of our samples. Even the best ones have about 20% inactive, reduced cytochromes. As Siedow *et al.* (23) pointed out, not only is this phenomenon universal for all known soluble preparations, it is seen in submitochondrial particles as well. Therefore it involves the intrinsic material in yeast cells. Baker's yeast is able to metabolize anaerobically by fermentation and aerobically by respiration. Perhaps the machinary for respiration is not as highly perfected since it always has an alternative way to generate energy. This imperfection may affect the lifetime and turnover rate of the enzyme. The lifetime of cytochrome oxidase in rat liver was estimated to be longer than 190 hours (68). At present no such study on yeast oxidase is available.

Employing microorganisms to study similar enzymes in higher organisms has become a popular trend. The structures of these enzymes are highly conserved. This method enables researchers to use isotopes to facilitate physical observation. The present work shows by Mössbauer spectroscopy that most of the yeast oxidase is very similar to the enzyme from beef heart, but that there is a substantial population of inactive material in the yeast enzyme. It is highly

probable that this form of oxidase is related to the occasionally reported 'inactive' form in beef heart oxidase (69). Caution thus should be taken when using the yeast system: While the study by a specific probe is likely to be valid, the study of bulk properties could be misleading. For example, the EPR and ENDOR study of isotopically labeled yeast oxidase by Chan and coworkers results in valuable ligation information of cytochrome a_3 (62), cytochrome a (13) and Cu_A (70), which would otherwise be difficult to obtain. On the other hand, if the measurement of magnetic susceptibility were to be carried out on yeast oxidase, a coupled study by other physical methods on the same sample would be necessary.

REFERENCES

1. Malmström, B.G. (1974). *Quart. Rev. Biophys.* **6**, 389–431.
2. Wikström, M., Krab, K., & Saraste, M. (1981). *Cytochrome Oxidase: A Synthesis*, Academic Press, London.
3. Salmeen, I., Rimai, L., Gill, D., Yamamoto, T., Palmer, G., Hartzell, C.R., & Beinert, H. (1973). *Biochem. Biophys. Res. Commun.* **52**, 1100–1107.
4. Babcock, G.T., Callahan, P.M., Ondrias, M.R., & Salmeen, I. (1981). *Biochemistry* **20**, 959–966.
5. Babcock, G.T., Vickery, L.E., & Palmer, G. (1976). *J. Biol. Chem.* **251**, 7907–7919.
6. Thomson, A.J., Brittain, T., Greenwood, C., & Springall, J. (1976). *FEBS Lett.* **67**, 94–98.
7. Lang, G., Lippard, S.J., & Rosén S. (1973). *Biochim. Biophys. Acta* **336**, 6–14.
8. Falk, K.-E., Vänngård, T., & Ånström, J. (1977). *FEBS Lett.* **75**, 23–27.
9. Tweedle, M.F., Wilson, L.J., Garćia-Iñiguez, L., Babcock, G.T., & Palmer, G. (1978). *J. Biol. Chem.* **253**, 8065–8071.
10. Moss, T.H., Shapiro, E., King, T.E., Beinert, H., & Hartzell, C.R. (1978). *J. Biol. Chem.* **253** 8072–8073.
11. Blumberg, W.E., & Peisach, J. (1971). In *Probes of Structure and Function of Macromolecules and Membranes* (B. Chance, T. Yonetani, & A.S. Midvan, eds.), Vol. 2, Academic Press, New York, pp. 215–229.
12. Palmer, G. (1983). In *Iron Porphyrins* (A.B.P. Lever & H.B. Gray, eds.), Part II, Addison-Wesley, Reading, Massachusets, pp.43-88.
13. Martin, C.T., Scholes, C.P., & Chan, S.I. (1985). *J. Biol. Chem.* **260**, 2857–2861.
14. van Gelder & Beinert, H. (1969). *Biochim. Biophys. Acta* **189**, 1–24.
15. Griffith, J.S. (1971). *Mol. Phys.* **21**, 141–143.

16. Seiter, C.H.A. & Angelos, S.G. (1980). *Proc. Nat. Acad. Sci., U.S.A.* **77**, 1806–1808.

17. Hu, V., Chan, S.I., & Brown, G. (1977). *Proc. Nat. Acad. Sci., U.S.A.* **74**, 3821–3825.

18. Hagen, W.R. (1982). *Biochim. Biophys. Acta* **708**, 82-98.

19. Beinert, H., Hansen, R.E., & Hartzell, C.R. (1976). *Biochim. Biophys. Acta* **423**, 339–355.

20. Karlsson, B. & Andréasson, L.-E. (1981). *Biochim. Biophys. Acta* **635**, 73–80.

21. Brudvig, G.W., Stevens, T.H., Morse, R.H., & Chan, S.I. (1981). *Biochemistry* **20**, 3912–3921.

22. Brudvig, G.W., Morse, R.H., & Chan, S.I. (1986). *J. Mag. Res.* **67**, 189–201.

23. Siedow, J.N., Miller, S., & Palmer, G. (1981). *J. Bioenerg. Biomemb.* **13**, 171-179.

24. Kent, T.A., Münck, E., Dunham, W.R., Filter, W.F., Findling, K.L., Yoshida, T., & Fee, J.A. (1982). *J. Biol. Chem.* **257**, 12489–12492.

25. Kent, T.A., Young, L.J., Palmer, G., Fee, J.A., & Münck, E. (1983). *J. Biol. Chem.* **258**, 8543–8546.

26. Thomson, A.J., Johnson, M.K., Greenwood, C., & Gooding, P.E. (1981). *Biochem. J.* **193**, 687–697.

27. van Gelder, B.F. (1966). *Biochim. Biophys. Acta* **118**, 36–46.

28. Schulz, C.E. (1979). Ph.D. Thesis, University of Illinois at Champaign-Urbana.

29. Boso, B. (1982). Ph.D. Thesis, University of Illinois at Champaign-Urbana.

30. Lang, G. (1970). *Quart. Res. Biophys.* **3**, 1–60.

31. Debrunner, P.G. (1970). In *Spectroscopic Approaches to Biomolecular Conformations* (D.W. Urry, ed.), American Medical Association, pp. 209–262.

32. Münck, E. (1979). In *The Porphyrins* (ed. D. Dolphin), Vol. IV, Academic Press, New York, pp. 379–423.

33. Münck, E., Groves, J.L., Tumolillo, T.A., & Debrunner, P.G. (1973). *Comp.*

Phys. Commun. **5**, 225–238.

34. Griffith, J.S. (1957). *Nature, Lond.* **180**, 30–31.
35. Lang, G. & Marshall, W. (1966). *Proc. Phys. Soc.* **87**, 3–34.
36. Oosterhuis, W.T. & Lang, G. (1969). *Phys. Rev.* **178**, 439–456.
37. Sharrock, M.P. (1973). Ph.D. Thesis, University of Illinois at Champaign-Urbana.
38. Erdös, P. (1966). *J. Phys. Chem. Solids* **27**, 1705–1720.
39. Dzyaloshinsky, I. (1958). *J. Phys. Chem. Solids* **4**, 241.
40. Moriya, T. (1960). *Phys. Rev.* **120**, 91–98.
41. Buluggiu, E. & Vera, A. (1976). *Z. Naturforsch.* **31a**, 911–914.
42. Buluggiu, E. (1980). *J. Phys. Chem. Solids* **41**, 43–45.
43. Condon, E.U. & Shortley, G.H. (1963). *The Theory of Atomic Spectra*, Cambridge Univ. Press, Cambridge.
44. Abragam, A. & Bleaney, B. (1970). *Electron Paramagnetic Resonance of Transition Ions*, Oxford Univ. Press (Clarendon), Oxford.
45. Vanneste, W.H. (1966). *Biochim. Biophys. Acta* **113**, 175–178.
46. Aasa, R. & Vänngård, T. (1975). *J. Mag. Res.* **19**, 308–315.
47. Aasa, R., Albracht, S.P.J., Falk, K.-E., Lanne, B., & Vänngård, T. (1976). *Biochim. Biophys. Acta* **422**, 260–272.
48. Lang, G., Herbert, D., & Yonetani, T. (1968). *J. Chem. Phys.* **49**, 944–950.
49. Huynh, B.H., Papaefthymiou, G.C., Yen, C.S., Groves, J.L., & Wu, C.S. (1974). *J. Chem. Phys.* **61**, 3750–3758.
50. Beinert, H. & Shaw, R.W. (1977). *Biochim. Biophys. Acta* **462**, 121–130.
51. Wickman, H.H., Klein, M.P., & Shirley, D.A. (1966). *Phys. Rev.* **152**, 345–357.
52. Schulz, C.E., Rutter, R., Sage, J.T., Debrunner, P.G., & Hager, L.P. (1984). *Biochemistry* **23**, 4743–4754.
53. Siedow, J.N., Power, S., de la Rosa, F.F., & Palmer, G. (1978). *J. Biol. Chem.* **253**, 2392–2399.

54. Brudvig, G.W., Stevens, T.H., & Chan, S.I. (1980). *Biochemistry* **19**, 5275–5285.

55. Scholes, C. P., Isacson, R.A., & Feher, G. (1971). *Biochim. Biophys. Acta* **244**, 206–210.

56. Reinhammar, B., Malkin, R., Jensen, P., Karlsson, B., Andréasson, L.-E., Aasa, R., Vänngård, T., & Malmström, B.G. (1980). *J. Biol. Chem.* **255**, 5000–5003.

57. Schulz, C.E., Nyman, P., & Debrunner, P.G., in preparation.

58. Champion, P.M. (1975). *Thesis*, University of Illinois at Champaign-Urbana.

59. Wang, H., Blair, D.F., Ellis, W.R., Jr., Gray, H.B., & Chan, S.I. (1986). *Biochemistry* **25**, 167-171.

60. Fiamingo, F.G., Altschuld, R.A., Moh, P.P., & Alben, J.O. (1982). *J. Biol. Chem.* **257**, 1639–1650.

61. Scheidt, W.R. & Gouterman, M. (1983). In *Iron Porphyrins* (A.B.P. Lever and H.B. Gray, eds.), Part I, Addison-Wesley, Reading, Massachusetts, pp.89–134.

62. Stevens, T.H. & Chan, S.I. (1981). *J. Biol. Chem.* **256**, 1069–1071.

63. Huynh, B.H., Emptage, M.H., & Münck, E. (1978). *Biochim. Biophys. Acta* **534**, 295–306.

64. Dwivedi, A., Toscano, W.A., Jr., & Debrunner, P.G. (1979). *Biochim. Biophys. Acta* **576**, 502–508.

65. Yim, M.B., Kuo, L.C., & Makinen, M.W. (1982). *J. Mag. Res.* **46**, 247–256.

66. Kotani, M. (1968). *Advan. Quant. Chem.* **4**, 227.

67. Blume, M. (1965). *Phys. Rev. Lett.* **14**, 96–98.

68. Russel, S.M., Burgess, R.J., & Mayer, R.J. (1980). *Biochem. J.* **192**, 321.

69. Vanneste, W.H., Ysebaert-Vanneste, M., & Mason, H.S. (1974). *J. Biol. Chem.* **249**, 7390–7401.

70. Stevens, T.H., Martin, C.T., Wang, H., Brudvig, G.W., Scholes, C.P., & Chan, S.I. (1982). *J. Biol. Chem.* **257**, 12106–12113.

71. Lang, G., Asakura, T., & Yonetani, T. (1969). *J. Phys. C (Solid St. Phys.), ser 2*, **2**, 2246–2261.

72. Lang, G., Spartalian, K., & Yonetani, T. (1976). *Biochim. Biophys. Acta* **451**, 250–258.

73. Kent, T., Spartalian, K., Lang, G., & Yonetani, T. (1977). *Biochim. Biophys. Acta* **490**, 331–340.

74. Sharrock, M., Münck, E., Debrunner, P.G., Marshall, V., Lipscomb, J.D., & Gunsalus, I.C. (1973). *Biochemistry* **12**, 258–265.

75. Maeda, Y. & Morita, Y. (1967). *Biochem. Biophys. Res. Commun.* **29**, 680–685.

76. Parak, F., Bade, D., & Marie, A.L. (1979). *J. Physique* **40**, C2, 528–530.

77. Champion, P.M., Münck, E., Debrunner, P.G., Hollenberg, P.F., & Hager, L.P. (1973). *Biochemistry* **12**, 426–432.

78. Simonneaux, G., Schloz, W.F., Reed, C.A., & Lang, G. (1982). *Biochim. Biophys. Acta* **716**, 1–7.

79. Groves, J.T., Quinn, R., McMurry, T.J., Nakamura, M., Lang, G., & Boso, B. (1985). *J. Amer. Chem. Soc.* **107**, 354–360.

CHAPTER 3

MÖSSBAUER & FLASH PHOTOLYSIS STUDIES OF CARBON MONOXIDE-INHIBITED YEAST CYTOCHROME OXIDASE

INTRODUCTION

Carbon monoxide (CO) inhibited cytochrome oxidase has played a unique and important role in our understanding of the function and mechanism of cytochrome oxidase. Between 1926 and 1933, Warburg and coworkers realized (*cf.* review by Wikström *et al.* (1)) that CO inhibited a heme-containing enzyme, which is responsible for cellular respiration. Furthermore, they also knew that the CO inhibition is very photosensitive, and measured the 'photochemical action spectrum' of the CO-inhibited enzyme. This enzyme, however, was not identified as cytochrome oxidase which Keilin had reported earlier until Chance (2) produced identical 'photochemical action spectra' in the Soret region in heart muscle and baker's yeast in 1953. The α region 'photochemical action spectrum' in baker's yeast was reported soon after (3).

Subsequently it was found that the photolyzed CO displayed a unique recombination behavior in cytochrome oxidase. In 1965, Chance *et al.* (4) reported that in pigeon-heart mitochondria, the photodissociated CO practically does not return to cytochrome a_3 below 160 K. This is unlike many other hemeproteins, in which the CO recombination takes place rapidly, i.e., of the

order of msec or less, even at 50 K (5). In 1972, Erecińska & Chance (6) found that the CO-recombination follows simple Arrhenius behavior with an activation energy of 13 kJ/mole in the liquid solution and 35 kJ/mole in the frozen state above 120 K. Comprehensive studies utilizing modern flash photolysis techniques and detergent-solubilized beef heart cytochrome oxidase were reported by Sharrock & Yonetani in 1976 & 1977 (7,8). The salient points of these studies are: Only one intermediate state is found between the photodissocated CO and cytochrome a_3, as opposed to at least 3 in myoglobin (9,10); this intermediate state is always occupied by CO in the frozen state and is mostly occupied in liquid solution under a high concentration of CO; and the activation energy between this intermediate and cytochrome a_3 is 35 kJ/mol above the freezing point and 43 kJ/mol in the frozen state. The magnitude of the activation barrier is considerably larger than that found in myoglobin (10 kJ/mol, *cf.* Ref.(10)).

These observations became perfectly understandable after Fiamingo *et al.* (11) reported their CO-photodissociation study of beef heart mitochondria using FTIR. They showed the formation of a chemical bond between CO and Cu_B when CO was flashed off cytochrome a_3. The recombination kinetics between 140 K and 180 K was described by a power law (which will be described briefly in the 'Theoretical Basis' section), and the peak activation energy for CO to return from Cu_B to cytochrome a_3 was determined to be 40.3 kJ/mol.

Taking advantage of the unusual recombination behavior of CO in cytochrome oxidase, Chance *et al.* (12) introduced the 'triple-trapping' technique in 1975, which opened up a new direction of active research on the reoxidation of cytochrome oxidase by dioxygen. Many optical and EPR studies utilizing this method contribute to shape the current understanding of the reoxidation mechanism. They will be summarized in Chapter 4.

The disadvantage of the optical studies is that rarely do they provide

by themselves direct evidence of the spin state or the oxidation state of cytochrome a_3 in the reoxidation intermediate states. As for EPR spectroscopy, most intermediates do not display any EPR signals (*cf.* Chapter 4). For the few intermediates that do, especially in the early stage of reoxidation, the EPR signals often arise from Cu_B. Therefore EPR is not very helpful in the direct assessment of the spin and oxidation state of cytochrome a_3 in the intermediate states.

It is therefore highly desirable to use Mössbauer spectroscopy to study the reoxidation intermediates of cytochrome oxidase, since there is no 'inactive' iron from the viewpoint of Mössbauer spectroscopy. As we have mentioned before, the measurements have to be made on the enzyme purified from ^{57}Fe -enriched microorganism, such as baker's yeast. The CO-inhibited enzyme is the starting point of all the low temperature kinetics studies and has to be understood first. A special concern about yeast oxidase arises from the finding by Mössbauer spectroscopy that both high-spin and low-spin cytochrome a_3 exist in the reduced enzyme (*cf.* Chapter 2). (The concentration of the latter species increases when the sample is subjected to the 'thaw-freeze' procedure, which suggests that it may be in a denatured conformation. Siedow *et al.* (13) reported the presence of partial reduction in yeast mitochondria. Therefore this reduced low-spin cytochrome a_3 may be intrinsic to yeast cells.) It is therefore important to investigate the reaction of CO with these two forms of cytochrome a_3.

In this chapter, we present a Mössbauer study of the reaction of CO with reduced yeast cytochrome oxidase. Both the high-spin and low-spin forms of cytochrome a_3 are found to bind CO. Also included in this chapter is a CO-recombination study in yeast cytochrome oxidase between 90 K and 270 K using the flash photolysis technique. The photolysis study confirms the existence of two different CO-bound complexes with the yeast oxidase. The CO-

recombination behavior is drastically different for these two complexes, however. A complete understanding of these two types of recombination behavior requires a more comprehensive investigation and is beyond the goal of this study. Nevertheless, the activation energies for the two processes are estimated. The implications of these results to the study of reoxidation of yeast cytochrome oxidase are also discussed.

MATERIALS AND METHODS

Preparation of the Mössbauer Samples

The sample used in the Mössbauer measurement of the CO-inhibited yeast cytochrome oxidase is derived from sample 4 used in the previous study on the resting oxidized and NADH-reduced enzyme, for which the purification procedure and enzyme characterization have been described in Chapter 2. Special glassware that has been described in Figure 1 of Chapter 2 was used to carry out the reduction of the enzyme and its reaction with CO. The sample containing 0.17 μmol ^{57}Fe -enriched yeast cytochrome oxidase was reduced with 10-fold excess NADH and 2 nmol PMS. After the reduced sample was measured by Mössbauer spectroscopy, it was thawed in an atmosphere that was thoroughly purged with argon. The sample was purged with CO for 15 minutes and incubated on ice for 3 hours. It was then frozen for Mössbauer measurements. The reduction of the sample and its reaction with CO were monitored with optical spectra which were obtained on a Cary 219 spectrophotometer at room temperature.

Preparation of the Flash Photolysis Sample

Yeast cytochrome oxidase that was used in the photolysis experiments had been purified according to the procedure described in Chapter 1. The enzyme (17 nmol) in a 0.5% tween-20, 50 mM tris, pH 7.4 buffer was degassed

thoroughly and reduced with 200-fold excess NADH in the presence of 2 nmol PMS. The sample was then introduced into a 75% glycerol solution, which was also thoroughly degassed. The final concentration in glycerol was roughly 65%. The use of such a high percentage of glycerol in the solution was to ensure a good transparency of the sample from room temperature to 4.2 K. The completion of the reduction in the glycerol solution was monitored by the UV-visible absorption spectrum obtained on a Cary 219 spectrophotometer at room temperature. The sample was purged with CO for 10 minutes and incubated on ice for several hours before being transferred to the plastic cuvette used in the photolysis experiments. The plastic cuvette was first sealed with silicon rubber and purged thoroughly with CO through a syringe needle. After the sample was introduced into the cuvette with a gas-tight syringe, the cuvette was sealed again with melted paraffin to ensure the anaerobicity. The sample thus made produced a transparent glass when frozen and is suitable for photolysis experiments.

Mössbauer spectroscopy

The Mössbauer measurements were recorded in the laboratory of Professor Peter Debrunner at the University of Illinois at Champaign-Urbana. A spectrometer which was equipped with a Janis Research company cryostat was used. This spectrometer has been described in the previous chapter. Spectra were measured at 4.2 K either with or without a 320 Gauss magnetic field.

Flash Photolysis

The flash photolysis experiments were done in the laboratory of Professor Hans Frauenfelder at the University of Illinois at Champaign-Urbana. The instrumentation arrangement is illustrated in Figure 1. A Neodymium glass laser at 1060 nm was frequency-doubled to photodissociate CO from cytochrome a_3 via absorbance in the β band region of the heme spectrum. The laser pulse

duration was 30 μsec, and the typical output was 0.2 J. A tungsten lamp was used to monitor the recombination of CO. Unlike what Sharrock & Yonetani observed in beef heart cytochrome oxidase, in the present case, the tungsten lamp causes observable photodissociation of CO from cytochrome a_3 and affects the results at the high-temperature range (between 160 K and 270 K). A 450 nm interference filter was therefore inserted between the lamp and the sample to reduce the photodissociation caused by the monitor light. The problem is not completely eliminated by this precaution. Accordingly an alternative method to obtain accurate measurements of rate constants is provided in the 'theoretical basis' section and was applied successfully. The fast rebinding process observed at low temperatures (between 90 K and 130 K) was found to be insensitive to the tungsten light, and the interference filter was not used in these experiments. The recombination process was monitored at 448 nm for the high-temperature experiments and at 444 nm for the low temperature experiments with a monochromator. The transmitted intensity measured by the photomultiplier was fed to a transient recording system, which enabled us to observe absorbance changes over a dynamic range of 3 decades and a time span of 8 decades, from μseconds to 100 seconds. In the present report, the data obtained below 10 μsec were not presented because they were generally noisy. The transient recording system has been reported in detail by Austin *et al.* (14).

THEORETICAL BASIS FOR PHOTOLYSIS DATA TREATMENT

Basics

To illustrate the principle of flash photolysis, the Soret region absorbance spectra of a typical purified preparation of yeast cytochrome oxidase in the resting oxidized, dithionite-reduced, and CO-inhibited reduced states are displayed in Figure 2. The arrow depicts the absorbance change accompanying the

Figure 1. Experimental setup for flash photolysis studies.

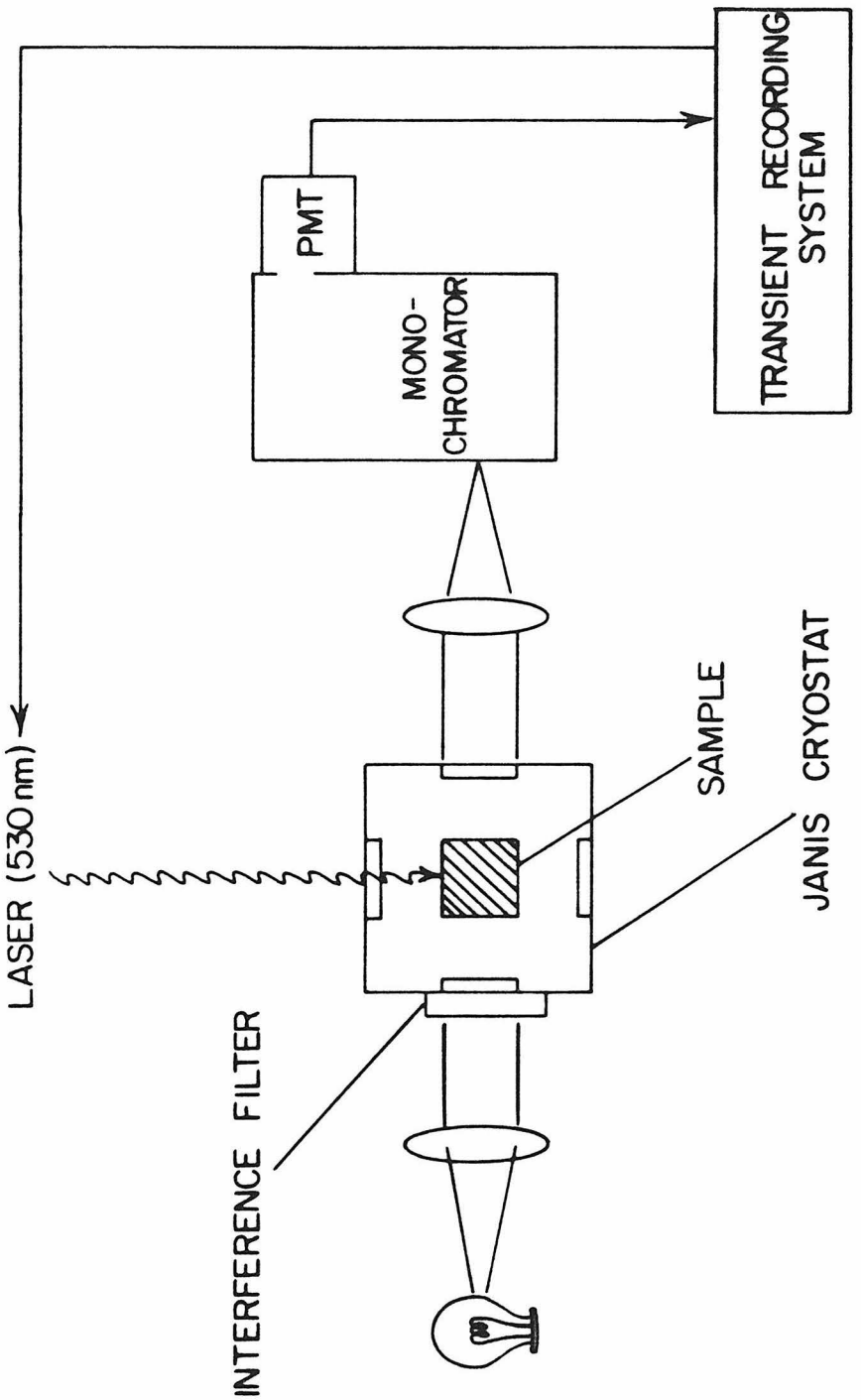
TRANSIENT RECORDING SYSTEM
PMT
MONO-CHROMATOR
LASER (530 nm)
SAMPLE
JANIS CRYOSTAT
INTERFERENCE FILTER

photodissociation. The absorbance of CO-inhibited yeast cytochrome oxidase is defined as

$$A_{\mathrm{CO}} = \log \frac{I_0}{I_b} \tag{1}$$

where I_b is the intensity of the transmitted light before photolysis, which is referred to as baseline intensity, and I_0 is the intensity of the incident light. Upon photolysis, the absorbance increases at the monitored wavelength. Therefore the absorbance of the totally CO-dissociated, or the reduced yeast cytochrome oxidase is

$$A_{dis} = \log \frac{I_0}{I_{\mathrm{min}}} \tag{2}$$

where I_{min} is the mininum intensity observed immediately after photodissociation. The total absorbance difference ΔA_{total} accompanying the photolysis is therefore

$$\Delta A_{total} = \log \frac{I_b}{I_{\mathrm{min}}}, \tag{3}$$

and the absorbance difference between the CO-inhibited enzyme and the partially inhibited enzyme at time t is given by

$$\Delta A(t) = \log \frac{I_b}{I(t)}, \tag{4}$$

where $I(t)$ is the intensity of the transmitted light at time t. The fraction of photodissociated CO that is not yet rebound to cytochrome a_3, $N(t)$, is then

$$N(t) = \Delta A(t)/\Delta A_{total}. \tag{5}$$

Basis for the Slow Rebinding Process Data Treatment

At high temperatures (270–160 K) the CO-recombination follows a nearly single exponential behavior, very similar to that observed in the beef heart enzyme by Sharrock & Yonetani (7,8). On the other hand, the CO-bound yeast enzyme is found to be sensitive to the monitor light. The chemical processes

Figure 2. Absorbance spectra in the Soret region of a typical purified preparation of yeast cytochrome oxidase in the resting oxidized (– – ––), dithionite reduced (——), and CO-inhibited reduced (–·––·–) states. The arrow denotes the absorbance difference accompanying the photodissociation of cytochrome a_3^{2+}–CO at 444 nm.

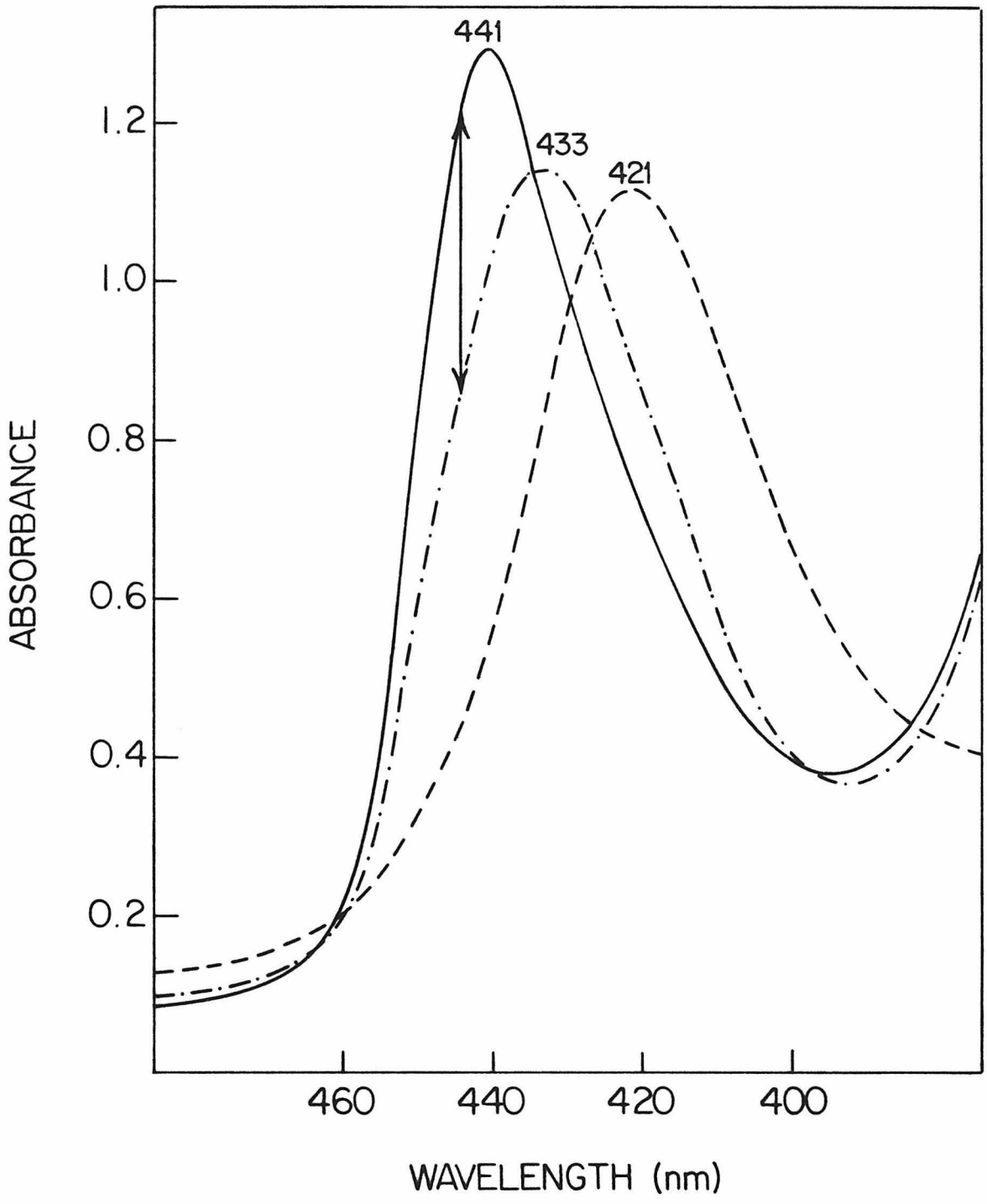
441
433
421
1.2
1.0
0.8
0.6
0.4
0.2
ABSORBANCE
460
440
420
400
WAVELENGTH (nm)

under observation are adequately represented by the following chemical equation,

$$\text{CO} + \text{cytochrome } a_3^{2+} \underset{k_l}{\overset{k_r}{}} \text{cytochrome } a_3^{2+} - \text{CO}, \tag{6}$$

where k_r is the pseudo-first-order rate constant of the CO-recombination, and k_l is the rate constant of the continuing photodissociation caused by the monitor light. The kinetics is thus described by

$$-\frac{dN}{dt} = k_r N - k_l(1 - N). \tag{7}$$

It is straightforward to show that the recombination behavior after the first photodissociation of CO is described by

$$N(t) = N_b^{\infty} e^{-(k_r + k_l)t} + N_u^{\infty} \tag{8a}$$

where

$$N_b^{\infty} = \frac{k_r}{k_r + k_l} \tag{8b}$$

$$N_u^{\infty} = \frac{k_l}{k_r + k_l}. \tag{8c}$$

N_b^{∞} and N_u^{∞} respectively denote the CO-bound and unbound fractions of cytochrome a_3 in the photostationary state. They are measured at a sufficient delay after the photodissociation.

It is desirable to remove the nonexponential term in *Eq.*8*a* artificially in order for a straight-forward analysis. In the present study, this was achieved by monitoring the CO-recombination behavior with a second photodissociation after the first one without warming up the sample. In fact, photodissociations can be repeated many times after the second one to achieve better signal-to-noise by signal averaging. One should be careful, however, to ensure that the steady state is achieved before each photolysis. In the present study, sufficient delays had been used and the same baseline was verified before each photolysis. The results were generally reproducible.

Under such circumstances, the absorbance difference $\Delta A_2(t)$ accompanying the subsequent photolyses does not reflect the total fraction $N(t)$ of the CO-unbound cytochrome a_3. Rather, it represents the following,

$$\frac{\Delta A_2(t)}{\Delta A_{total}} = N(t) - N_u^{\infty}$$
$$= N_b^{\infty} e^{-k_{obs}t}, \tag{9a}$$

where k_{obs} is the apparent recombination rate constant, and

$$k_{obs} = k_r + k_l, \tag{9b}$$

and ΔA_{total} is the total absorbance difference that accompanies the first photodissociation.

Because the data are presented in double-logarithmic scales, it is straightforward to estimate N_b^{∞} according to *Eq.9a*. The apparent rate constant k_{obs} is obtained through

$$k_{obs} = \frac{1}{\tau_{obs}}, \tag{10}$$

where τ_{obs} is the apparent recombination time and is defined in the following expression,

$$\frac{\Delta A_2(\tau_{obs})}{\Delta A_{total}} = \frac{1}{e} N_b^{\infty}. \tag{11}$$

Combining *Eq.8b* and *Eq.9b*, we derive the expression for the rate constant of CO-recombination,

$$k_r = k_{obs} N_b^{\infty}. \tag{12}$$

Basis for the Low Temperature Data Treatment

In our low temperature (90–130 K) experiments, the sample was photolyzed repeatedly without warming up to a higher temperature. The CO that is flashed off the slow-rebinding site never returns in our time scales of observation at these temperatures. Under such circumstances, we discovered a fast recombination process. This fast-returning process is represented in the following expression,

$$N(t) = \frac{\Delta A_2(t)}{\Delta A_{total}(2)}; \tag{13}$$

ΔA_2 and $\Delta A_{total}(2)$ are used in this expression to emphasize that they are obtained during repeated photodissociations. In fact, $\Delta A_{total}(2)$ denotes the maximum absorbance difference due to this fast process and was not precisely determined in this study because the process is too fast; however, this number is estimated through computer simulations.

Unlike the slow-rebinding process, the fast-returning process cannot be described with a single exponential recombination behavior. It is well-established through the work of Frauenfelder and co-workers (9,10,15) that description of photolysis data in the low-temperature regime often requires a spectrum of activation energies for the recombination process. If the function $g(E_a)$ denotes the probability of having an unbound metal center with activation energy for CO recombination between E_a and $E_a + dE_a$, then $N(t)$ is given by

$$N(t) = \int_0^\infty g(E_a) e^{-k(E_a)t} dE_a, \tag{14}$$

where the CO-recombination constant $k(E_a)$ is related to the activation energy E_a and the frequency parameter A by the Arrhenius equation,

$$k(E_a) = Ae^{-E_a/RT}. \tag{15}$$

Austin *et al.* (16) found that the low-temperature CO-recombination kinetics often follows a power law:

$$N(t) = (1 + t/t_0)^{-n}, \tag{16}$$

where t_0 and n are parameters that depend on the temperature. The physics behind a power law kinetics predicts a distribution of activation energy $g(E_a)$ for the recombination process (11) as follows:

$$g(E_a) = \frac{n^n}{RT\Gamma(n)} \exp^{-n[(E_a - E_{a,p})/RT + e^{-(E_a - E_{a,p})/RT}]}, \tag{17}$$

where $E_{a,p}$ is the activation energy at the maximum value of $g(E_a)$, referred to in this study as the peak activation energy, and $\Gamma(n)$ is the gamma function.

Some of our data are not readily explained by the power law. The fast CO-recombination process is therefore approximated instead by a Gausssian distribution of activation energy

$$g(E_a) = \exp[-\frac{(\ln 2)(E_a - E_{a,p})^2}{\Gamma^2}], \tag{18}$$

where Γ is the half-width at the half peak activation energies. The details will be discussed in the results section.

RESULTS

Mössbauer Study of CO-inhibited Yeast Cytochrome Oxidase

The optical control of Mössbauer experiments is obtained by monitoring absorbance spectra of the sample in the α band region. The Soret absorption is too intense to be monitored by the spectrophotometer with a 1 mm path-length optical cell. The absorbance spectra between 700 and 480 nm of the reduced and CO-inhibited reduced enzyme are displayed in Figure 3. The A_{600}/A_{575} ratio, $\sim$ 2.6, in the reduced spectrum demonstrates that the reduction was complete. Upon reaction with CO, the β band shifted from 560 nm to 546 nm, while the α band maximum shifted very little. The only observable difference in the α band between the reduced and CO-inhibited reduced yeast cytochrome oxidase is a slight broadening in the blue side of the peak. These observations are commonly encountered in the CO-inhibited reduced yeast enzyme. The small change in the α band is unlike the CO-inhibited beef heart enzyme. The latter typically displays a prominent shoulder around 590 nm. The difference in the α band region between the yeast and beef heart enzyme is, at least in part, due to wavelength shifts of the absorption maxima in both the reduced and the CO-bound yeast cytochrome oxidase. The 'photochemical action spectrum' measured by Castor & Chance (3) showed that the peak of the CO-inhibited

yeast cytochrome a_3^{2+} was at $\sim$ 592 nm, slightly shifted to the red ($\sim$ 3 nm) compared to that found in the heart muscle. The peak of the α band of the reduced enzyme in beef heart oxidase is typically at 604 nm, while that in yeast oxidase is typically at 601 nm.

The Mössbauer spectrum of the CO-inhibited reduced yeast cytochrome oxidase is shown in Figure 4. Three pairs of Lorentzian lines were determined through the use of a least-squares computer fit program. Their Mössbauer parameters and areas are listed in Table 1 along with those of the reduced enzyme measured prior to the reaction with CO. The sample was also measured with a wider scale, thus less resolution, under the same condition. The Lorentzian lines and their areas determined in these two spectra are, within uncertainties, identical. Component A has identical Mössbauer parameters as the low-spin ferrous cytochrome a in the reduced enzyme. Component C with δ = 0.279 mm/sec and ΔE_Q = 0.316 mm/sec is typical of CO-bound hemeproteins (17,18). Curiously, the concentration of this component accounts for roughly 50% of the total iron. We have shown in the previous chapter that roughly 20% of reduced low-spin cytochrome a_3 is routinely observed in the purified yeast cytochrome oxidase. Therefore the Mössbauer spectrum of component C indicates that both the high-spin and low-spin cytochrome a_3^{2+} react with CO. The two forms of CO-complexes, however, cannot be distinguished by Mössbauer spectroscopy: each of the three components has one peak near 0 mm/sec, and the linewidth of component C, which is determined by the least-squares Lorentzian linefit, is very narrow (0.29 mm/sec, compared to 0.28 mm/sec for the iron foil calibration spectrum).

Component B is a high-spin ferrous heme; its isomer shift and quadrupole splitting (δ=0.95 and ΔE_Q = 2.20 mm/sec) are both slightly higher than those found in the reduced enzyme (*cf.* Table 1). The concentration of this CO-inactive high-spin ferrous component is quite substantial ($\sim$15% of the total

Figure 3. Absorbance spectra of the ^{57}Fe enriched yeast cytochrome oxidase in the NADH-reduced (solid line) and CO-inhibited reduced enzyme (dashed line) between 700 and 480 nm. The absorbance in the Soret region is too intense to be monitored by the spectrophotometer with a 1 mm path-length optical cell.

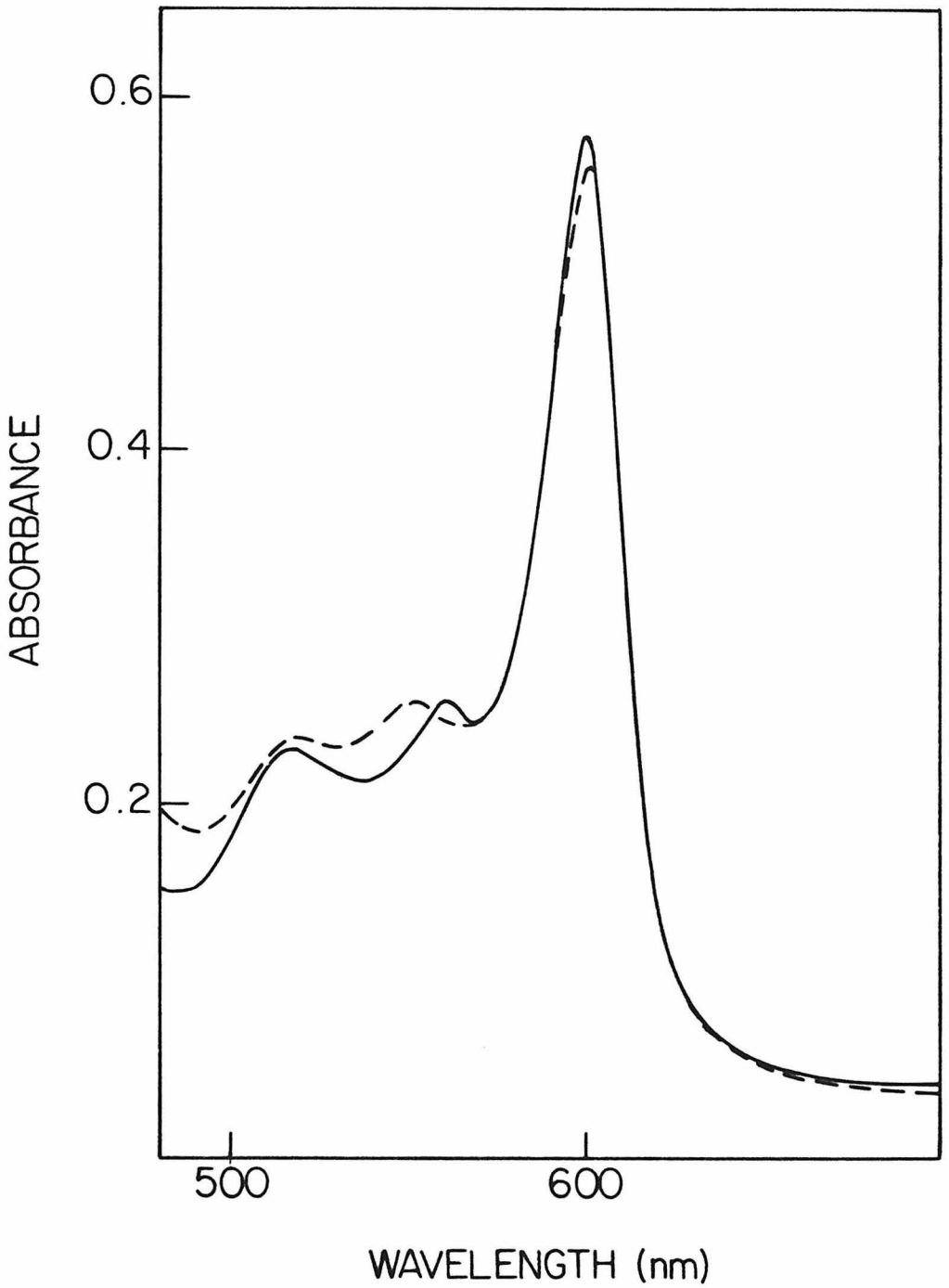
0.6
0.4
0.2
ABSORBANCE
500
600
WAVELENGTH (nm)

Figure 4. Mössbauer spectrum of the CO-inhibited reduced yeast cytochrome oxidase. The solid curve is the sum of 3 pairs of Lorentzian lines which were determined by a least-squares computer fit program.

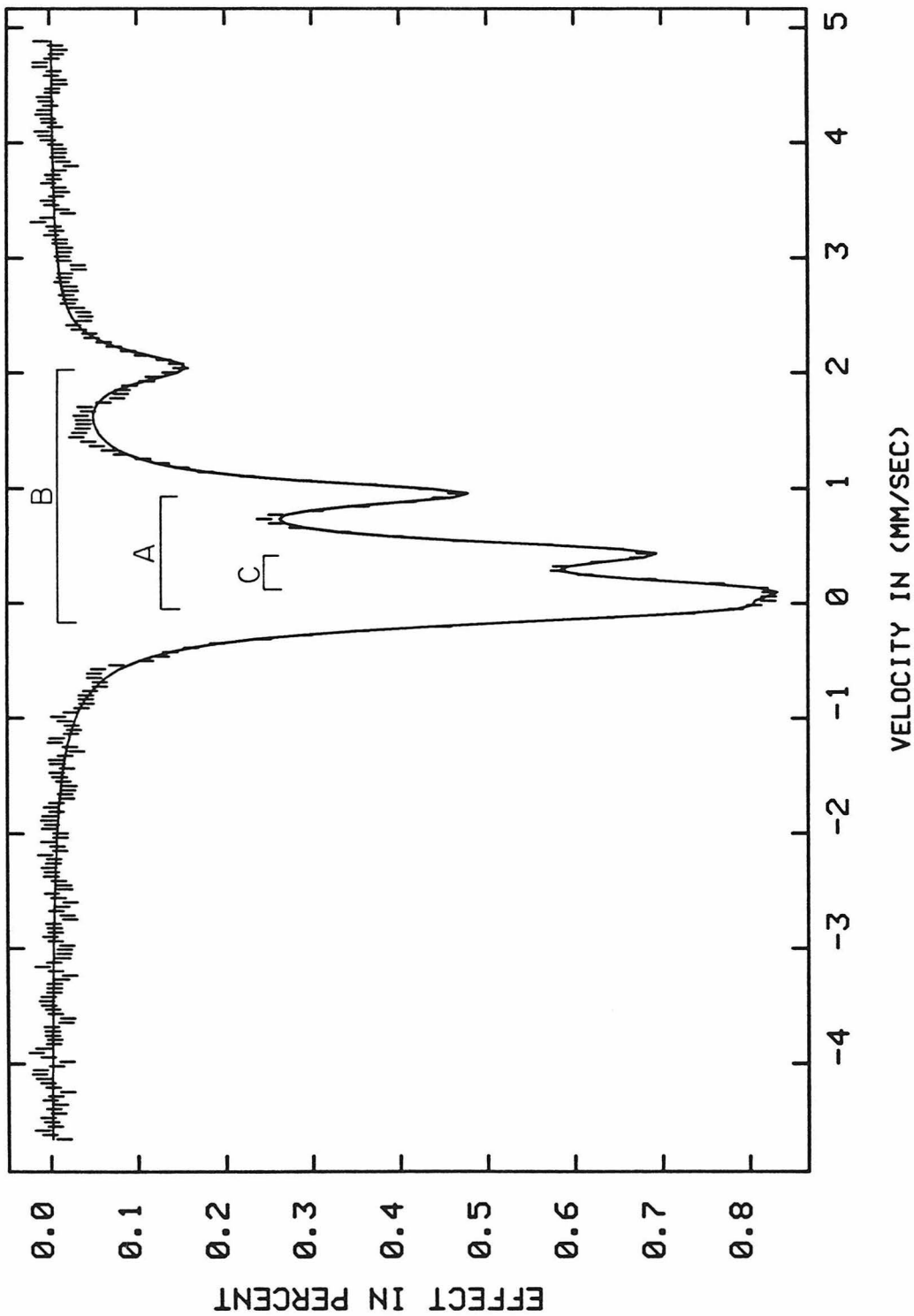
EFFECT IN PERCENT
0.0
0.1
0.2
0.3
0.4
0.5
0.6
0.7
0.8
A
B
C
-4
-3
-2
-1
0
1
2
3
4
5
VELOCITY IN (MM/SEC)

Table 1. Mössbauer Parameters of Reduced and CO-inhibited Reduced Yeast Cytochrome Oxidase at 4.2K

	species	δ mm/sec	ΔE_Q mm/sec	linewidth mm/sec	area %	assignment
	Reduced					
	low spin	0.45 ± 0.01	1.01 ± 0.01	0.30	71 ± 1	a, a_3
	high spin	0.92 ± 0.03	2.02 ± 0.03	0.38	29 ± 2	a_3
	Reduced + CO					
A	low spin	0.449 ± 0.004	1.009 ± 0.004	0.27	35.0 ± 0.8	a
B	high spin	0.95 ± 0.01	2.20 ± 0.01	0.32	14.6 ± 0.7	?
C	CO-complex	0.279 ± 0.003	0.316 ± 0.003	0.29	50.4 ± 0.7	a_3

iron). The EPR spectrum of this same sample in the resting oxidized state (Figure 7 of chapter 2) showed the presence of high-spin ferric heme signals which are estimated to be 11% compared with the low-spin $g = 3$ signal, i.e., roughly 5.5% of the total iron. The EPR result is consistent with the Mössbauer spectra of the same sample in the same oxidation state. An EPR spectrum of CO-inhibited yeast cytochrome oxidase which had been poised at 430 mV vs. NHE for several hours before the spectrum was measured, shown in the Figure 13 of Chapter 5, indicates that these high-spin cytochromes are not stabilized in the ferrous state by CO since the high-spin ferric EPR signal remains. It is conceivable that these hemes might contribute to the high-spin ferrous heme signals observed in the Mössbauer spectrum of the CO-bound reduced yeast oxidase.

This possibility can probably be ruled out. We have undertaken numerous EPR studies of the reoxidation studies of yeast oxidase in this laboratory, in which the first step was always the reduction of the enzyme by NADH. In none of these studies have we observed by EPR the reduction of these high-spin hemes. It is thus quite possible these high-spin hemes remained oxidized throughout our Mössbauer studies. Mössbauer spectra of such high-spin ferric hemes are typically spread out because of the magnetic hyperfine coupling (*cf.* Chapter 2). Therefore Mössbauer signals due to these species at a concentration of 5% are most likely hidden in the baseline of the Mössbauer spectrum of both the reduced enzyme and the CO-bound reduced enzyme.

Furthermore, the right hand side peak of component B is at a significantly higher velocity than the corresponding peak in the reduced enzyme (*cf.* Table 1). In fact, the former is not completely covered by the latter if the two spectra are superimposed (*cf.* Figure 8 of Chapter 2). Thus it is possible that when the enzyme reacts with CO, a fraction of low-spin ferrous hemes undergo a low- to high-spin transformation. We shall discuss this point at length later.

CO-recombination Processes

The slow CO-recombination process that has been previously observed in beef heart cytochrome oxidase is not the only process observed in yeast cytochrome oxidase. This is demonstrated by absorbance spectra monitored when the sample was incubated for at least 10 minutes at different temperatures after repeated photolyses (Figure 5). At 250 K, the recombination is relatively fast and the spectrum of the CO-bound enzyme with a peak around 436 nm was obtained. At 110 K and 180 K, most of the CO-recombination is sufficiently slow so that a spectrum corresponding to the mostly reduced enzyme was measured as evidenced by the peak absorption at 440 nm with substantial intensity around 435 nm. This suggests that there is a very fast CO-rebinding process at these temperatures. Indeed, only at 4 K is this process sufficiently slowed down so that a totally reduced spectrum could be obtained.

Flash Photolysis Studies of the Slow CO-recombination Process

The first noticeable property of the slow-rebinding yeast cytochrome a_3^{2+}–CO site is that it is very sensitive to light. Even the monitor light whose intensity was reduced with an interference filter caused a substantial decrease in transmittance readings, indicating photodissociation of CO (*cf.* Figure 2), until the photodissociation and recombination reached equilibrium. Therefore special care has been taken to ensure correct measurements: When the sample was measured below 200 K, it was warmed up to 270 K first to ensure the complete recombination of CO and then cooled down to the desired temperature in the dark; above 200 K, the sample was warmed up to the desired temperature in the dark and equilibrated for at least 20 minutes. The monitor light was blocked during this time. The block was removed only immediately prior to the photodissociation. The recombination curves measured under such 'first shot' conditions at temperatures between 180 K and 270 K are displayed in

Figure 5. Absorbance spectra of yeast cytochrome oxidase–CO at a sufficient delay after repeated photolyses at various temperatures. The temperatures are denoted as follows: ▲, 4–5 K; ●, 110–117 K; ×, 180 K; and ■, 250 K. The spectra were obtained by manually scanning the monochromator through the Soret region. Curves are drawn to guide the eye.

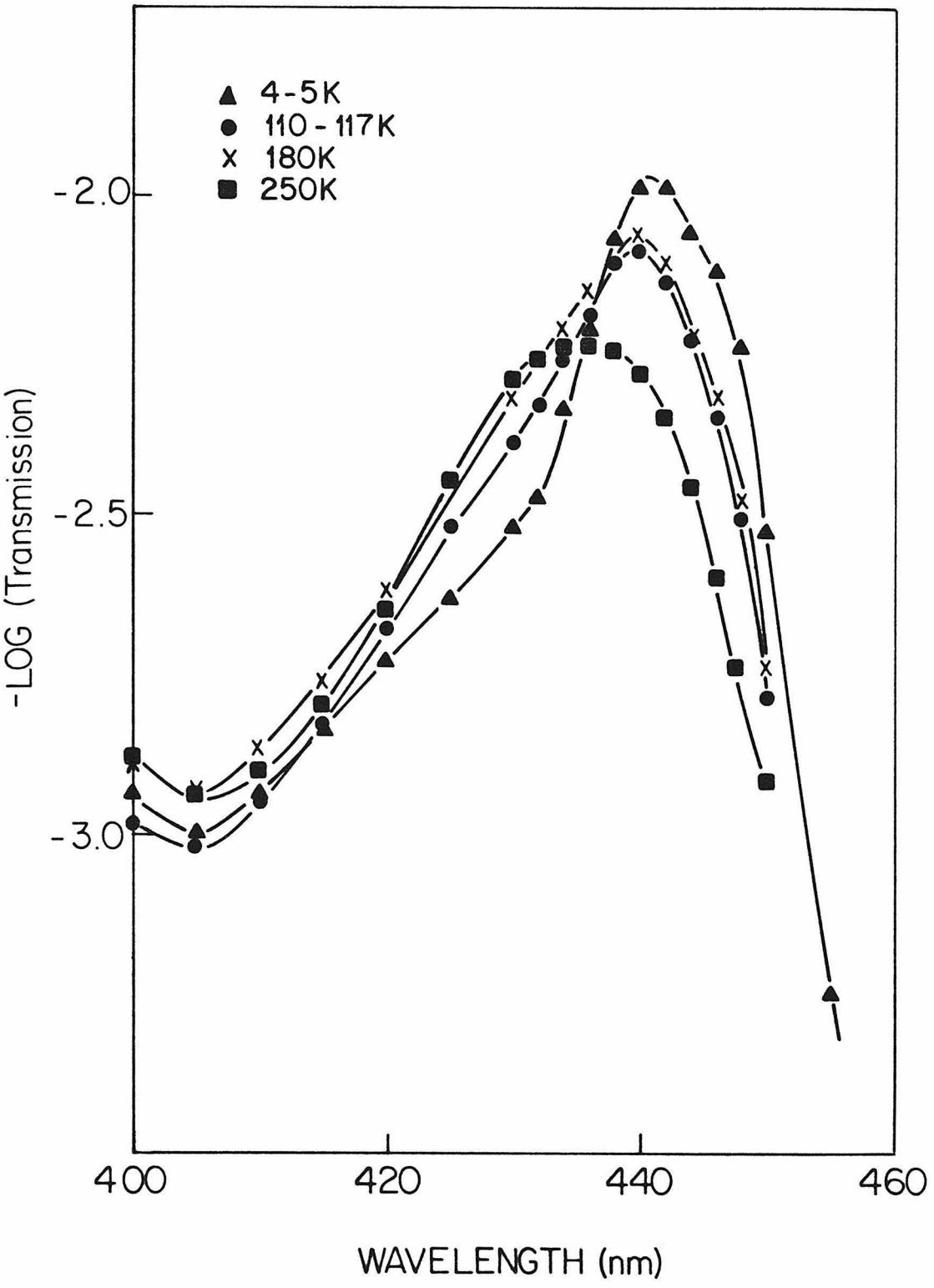
4-5K
110-117K
180K
250K
-2.0
-2.5
-3.0
-LOG (Transmission)
400
420
440
460
WAVELENGTH (nm)

Figure 6. At high temperatures (270–240 K), the CO-recombination follows quite closely, although not exactly, single-exponential behavior. At 180 K, the photodissociated CO does not show signs of returning in 100 seconds.

However, Figure 6 does not reflect the true recombination behavior of CO. Rather, it reflects the net results of the recombination and ongoing photodissociation as described by *Eq.*8. The simulation of the experimental results with *Eq.*8 was not attempted, as it is clear to us that the true CO-recombination does not follow single-exponential behavior exactly, as revealed in the 270–240 K data. To simulate the experimental data with two processes which are not exactly known in detail would be unrealistic.

As has been described in the 'theoretical basis' section, the nonexponential term in *Eq.*8*a* is dropped when the recombination is measured with 'subsequent shots' at each temperature. After each photolysis, the sample was left equilibrating with the monitor light on until a stable transmittance baseline was achieved. Typically, this process takes 10 minutes or slightly longer. The dependability of this method is verified by the fact that the same baseline can be achieved repeatedly. The ratio $\Delta A_2(t)/\Delta A_{total}$, instead of $N(t)$, thus obtained from 270 K to 160 K are plotted versus time and the results are displayed in Figure 7. All the recombination data, with the exception of the tail end of 210 K data, can be described quite well by single-exponential traces as predicted by *Eq.*9. (The deviation observed in the 210 K trace may be due to the enhanced scattering in the sample that undergoes a phase transition). The apparent recombination time τ_{obs} and the quantity N_b^{∞} are determined as described previously, and the rate constant of CO-recombination is calculated through *Eqs.*10 and 12. These parameters are tabulated in Table 2. The kinetics of recombination of yeast cytochrome a_3–CO follows a simple Arrhenius behavior from 270 K to 160 K, as is shown in Figure 8. The activation energy for this process thus determined is 33.1 kJ/mol.

Figure 6. The slow rebinding of yeast cytochrome a_3 with photolyzed CO measured in the 'first shot' experiments between 270 K and 180 K. A single-exponential rebinding curve is drawn in a thin line for comparison. The fraction of photolyzed CO that is not yet rebound to yeast cytochrome a_3 is plotted versus time on a log-log scale. The manner in which the experiments were carried out is described in the text.

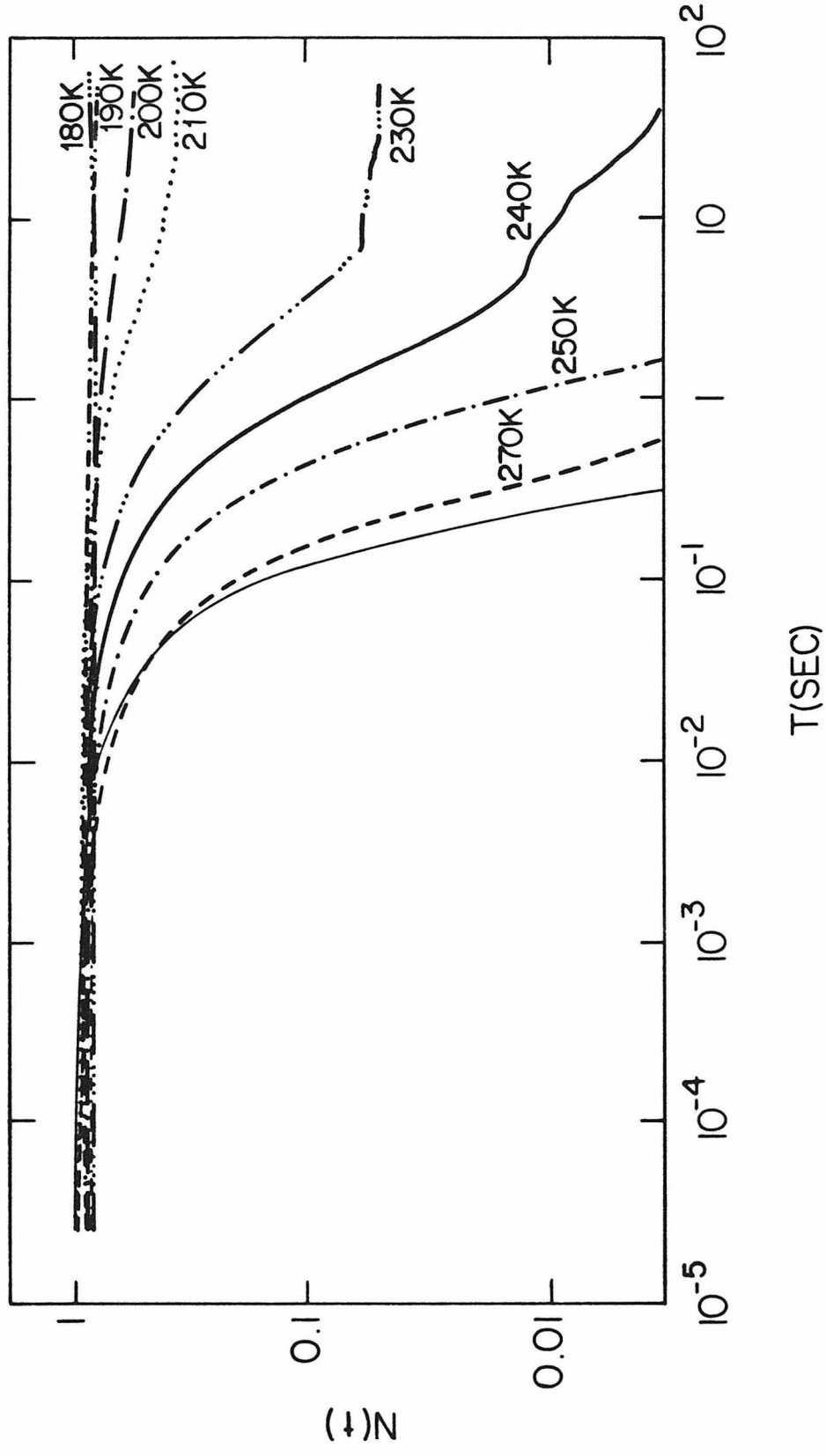
180K
190K
200K
210K
230K
240K
250K
270K
1
0.1
0.01
N(t)
10^{-5}
10^{-4}
10^{-3}
10^{-2}
10^{-1}
1
10
10^{2}
T(SEC)

Figure 7. The slow rebinding of yeast cytochrome a_3 with the photolyzed CO measured in the 'subsequent shots' experiments monitored at 448 nm between 270 K and 160 K. A single-exponential rebinding curve is drawn in a thin line for comparison. The absorbance difference accompanied the 'subsequent' photodissociation without having the sample warmed up to higher temperature is normalized against the total absorbance difference detected at 270 K. This quantity is plotted versus time on a log-log scale. The advantage of such a presentation and the manner in which the experiments were carried out are described in the text.

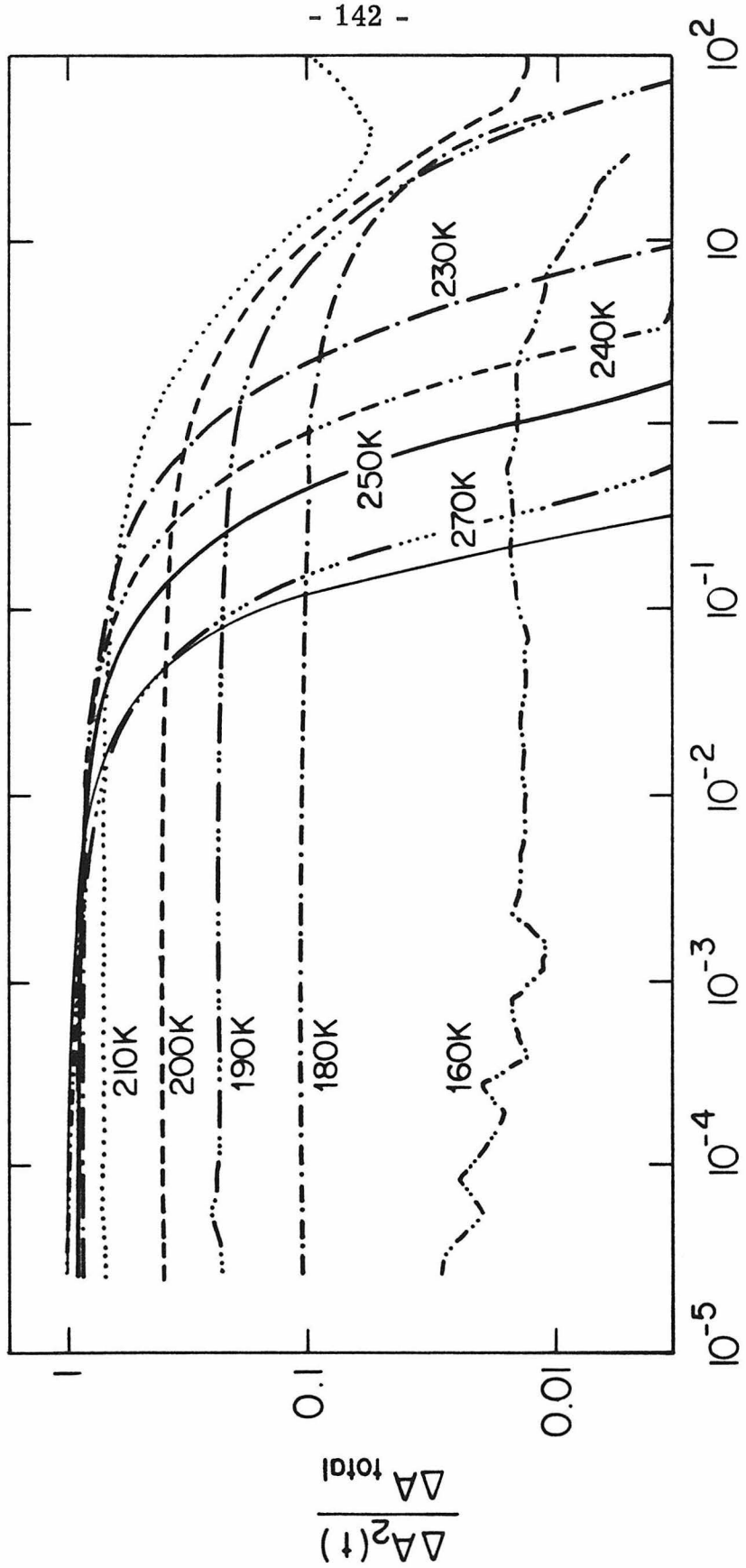
$\frac{\Delta A_2(t)}{\Delta A_{total}}$
1
0.1
0.01
10^{-5}
10^{-4}
10^{-3}
10^{-2}
10^{-1}
1
10
10^2
T(SEC)
210K
200K
190K
180K
160K
250K
270K
230K
240K

Table 2. Rate Constants of the Slow CO-Recombination Process in Yeast Cytochrome Oxidase at Various Temperatures

Temp K	N_b^{∞}	τ_{obs} sec	k_r sec^{-1}
270	1.	0.058	17.25
250	1.	0.18	5.56
240	1.	0.35	2.86
230	1.	0.70	1.43
210	0.84	3.3	0.254
200	0.48	5.0	0.096
190	0.29	7.9	0.037
180	0.14	18.	0.008
160	0.017	21.	0.0008

Notations:

1 . k_r is the rate constant for the recombination of CO.

2 . k_l is the rate constant for continuing CO photolysis by the monitor light.

3 . $N_b^{\infty} = k_r/(k_r + k_l)$.

4 . τ_{obs} is the apparent recombination time and is defined in the text.

Figure 8. Arrhenius plot of the slow CO-recombination process measured in yeast cytochrome oxidase between 270 K and 160 K. The activation energy thus obtained is 33.1 kJ/mol.

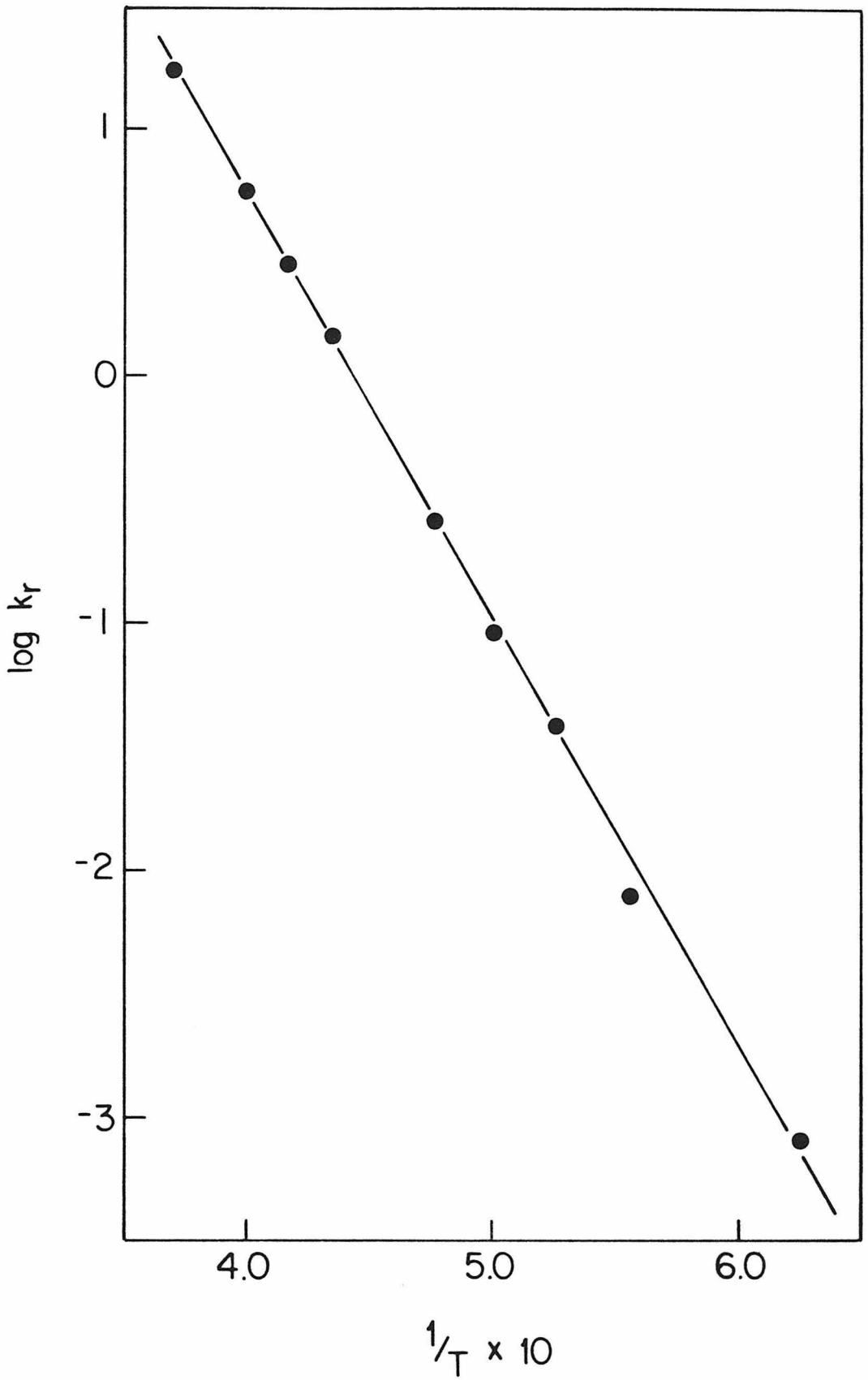
1
0
-1
-2
-3
log k_r
4.0
5.0
6.0
$1/T \times 10$

Flash Photolysis Studies of the Fast CO-Recombination Process

At 160 K, the CO-recombination rate constant of the slow process is 8×10^{-4} sec^{-1} (*cf.* Table 2). Therefore, if the sample is repeatedly photolyzed below 160 K without warming up, the slow process will not be observed on a time scale of minutes. Under such circumstances, a very fast recombination process is found in the temperature range between 130 K and 90 K. The data were normalized against the total absorbance difference observed at 270 K and displayed in Figure 9. The total absorbance difference observed at 90 K in the fast process is roughly 20% of that observed in the slow process. The quantitation of these two sites is not possible at this stage because the difference extinction coefficients at the monitored wavelength are not known.

The fast CO-recombination behavior is not readily explained by the power law, especially that observed at 90 K and 100 K. In Figure 10a, the same sets of data are renormalized by an optimal ΔA_{total}, which allows the recombination behavior at five different temperatures to be described by the same frequency factor A and a Gaussian distribution of activation energy. The frequency factor A thus determined is 1.0×10^{10}. The Gaussian distribution function $g(E_a)$ of the activation energy is shown in Figure 10b. The peak activation energy is 13 kJ/mol and the half-width at the half-peak energies is 2.9 kJ/mol.

It is quite clear from Figure 10a that the lower temperature data obtained at 90 K and 100 K cannot be described satisfactorily with the same set of parameters. At present, this discrepany is not understood. A thorough understanding of the recombination process would require a comprehensive study that covers a wider temperature range and includes measurements of the CO concentration dependence. Substantial deviation is also observed between the simulated curve and experimental data at 130 K. This deviation is quite clearly due to the presence of the slow recombination process that is observed at the higher temperature.

Figure 9. The fast CO-recombination of yeast cytochrome a_3 after photodissociation, monitored at 444 nm between 90 K and 130 K. At each temperature the sample was photolyzed repeatedly without warming up and the results are averaged. The absorbance difference accompanied the photodissociation is compared to the total absorbance difference monitored at 444 nm and at 270 K. The latter represents the complete photodissociation of the slow-rebinding site. No interference filter was used in these experiments, as the intensity of the tungsten lamp was not sufficient to cause appreciable changes in the measured kinetics. Curves are drawn to guide the eye only.

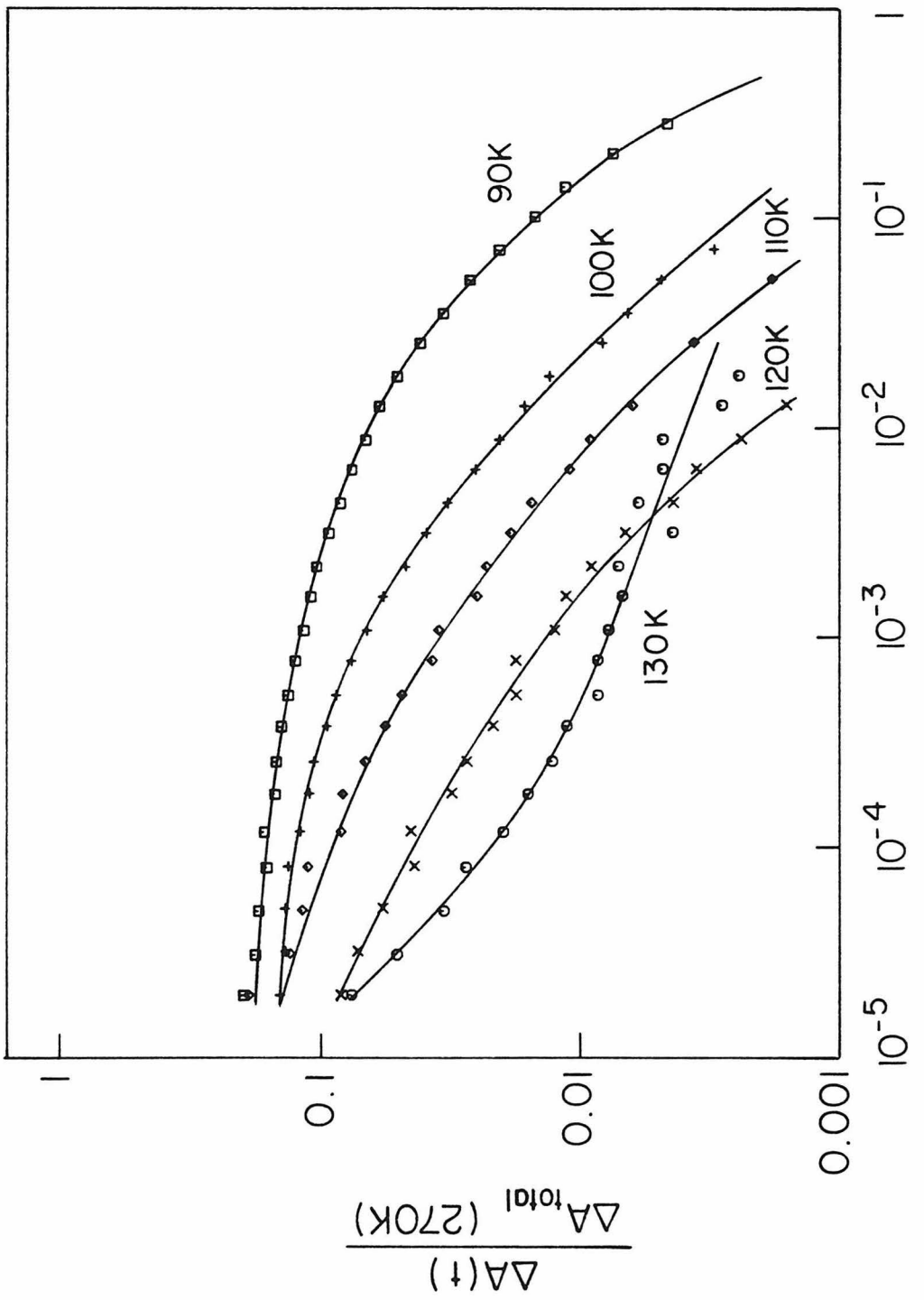
90K
100K
110K
120K
130K
1
0.1
0.01
0.001
10^{-5}
10^{-4}
10^{-3}
10^{-2}
10^{-1}
1
T(SEC)
$\frac{\Delta A(t)}{\Delta A_{total}\ (270K)}$

Figure 10. (a) The fast CO-recombination measured in yeast cytochrome oxidase between 90 K and 130 K. Curves are optimal results produced by a model that assumes a Gaussian distribution of activation energy for the recombination reaction under investigation. (b) The corresponding Gaussian distribution function with a peak activation energy of 13.0 kJ/mol and a half-width at the half-peak energies of 2.9 kJ/mol. The optimal frequency factor is 1.0×10^{10}.

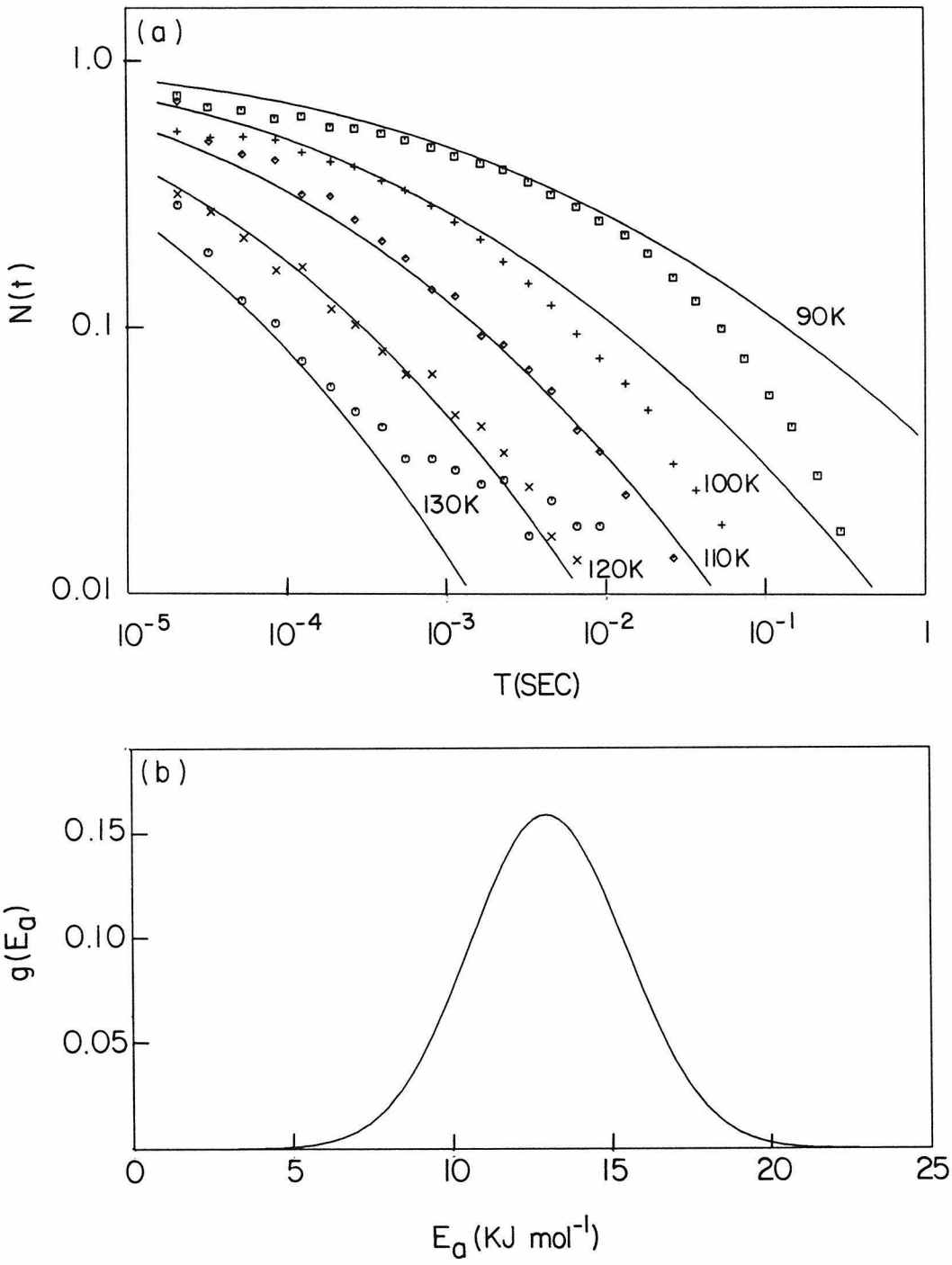
(a)
1.0
0.1
0.01
N(t)
90K
100K
110K
120K
130K
10^{-5}
10^{-4}
10^{-3}
10^{-2}
10^{-1}
1
T(SEC)
(b)
0.15
0.10
0.05
$g(E_a)$
0
5
10
15
20
25
E_a (KJ mol^{-1})

DISCUSSION

A Tale of Two Cytochrome a_3's

In Chapter 2, we showed by Mössbauer spectroscopy that in typical purified preparations of yeast cytochrome oxidase, roughly 10% of the total iron is in the low-spin reduced ferrous state. As has been pointed out by Siedow *et al.* (13), the reduced material exists in the thoroughly washed mitochondrial particles and therefore is probably an intrinsic component in yeast cells. The Mössbauer spectrum of the reduced enzyme showed that low-spin hemes account for more than 60% of the total iron. This indicates that a fraction of yeast cytochrome a_3 is in the low-spin ferrous state. In fact, continuing spin state change was evident during the 'freeze-thaw' process (*cf.* Chapter 1 & 2). In the present study, a reduced enzyme sample containing 29% high-spin ferrous heme ended up with 50% of CO-complex when reacted with CO. It is totally consistent with the view that there are two types of cytochrome a_3 in the sample: one in the high-spin state, which is probably functional, and has strong exchange coupling with nearby Cu_B when oxidized; the other in the low-spin state, which exists in the reduced state unless reacted with a strong oxidant such as ferricyanide, and is probably a product of degradation.

Although the CO-adducts of these two types of cytochrome a_3 are not distinguishable by Mössbauer spectroscopy, they are clearly demonstrated by the photolysis experiments. Two types of cytochrome a_3 with drastically different CO recombination behavior were detected. They shall be discussed subsequently. There remains one puzzle, however, in the Mössbauer spectrum of CO-bound reduced yeast cytochrome oxidase. A sizable fraction (15%) of the hemes is found to be in the high-spin ferrous state and is unable to react with CO. Although Cytochrome a_3 in the functional molecules is known to adopt at least 3 different conformations (19), the presence of approximately

50% CO-bound hemes in the Mössbauer spectrum precludes it as the origin of the high-spin ferrous heme signal observed in the spectrum of the CO-bound reduced enzyme. We have also shown that this signal does not arise from the high-spin ferric hemes that were present in the resting oxidized enzyme. The presence of such a signal seems to suggest the presence of heme-heme interaction that accompanies the ligation of cytochrome a_3 with CO. We shall come back to this point.

The Slow CO-Rebinding Cytochrome a_3

The slow CO-recombination behavior found in yeast cytochrome oxidase (*cf.* Figure 6) is very similar to that observed previously in the heart enzymes (4-8). The activation energy for this process in yeast is 33.1 kJ/mol, calculated from the temperature dependence of the rate constant through the temperature range between 270 K and 160 K. It is very similar to that determined in the liquid phase (35 kJ/mol) in beef heart cytochrome oxidase by Sharrock & Yonetani (8), but smaller than that determined in the frozen state in beef heart enzyme by Sharrock & Yonetani (8), 43 kJ/mol, or by Fiamingo *et al.* (11), 40.3 kJ/mol. From the ample examples of photodissociation and recombination of CO among hemeproteins, one should that the recombination behavior to be different in liquid and frozen phases. The freezing point of the glycerol solution (~65%) employed in the current study is roughly 210 K. Therefore the observed single Arrhenius behavior through the wide temperature range came as a surprise. Sharrock & Yonetani (7,8) observed a curvature in the Arrhenius plot in the temperature range where phase transition took place. This curvature disappeared, however, when a high concentration of CO was present in the solution. They concluded that there must be one intermediate state in the pathway of CO-recombination with cytochrome a_3. At low CO concentrations, the photolyzed CO could diffuse out of the heme pocket, but this intermediate

should be mostly occupied when CO concentration is high. This hypothesis is consistent with the results of the FTIR study by Fiamingo *et al.* (11). They showed that this intermediate state is Cu_B^+–CO. The present study employed a high concentration of CO (1 atm); therefore the photolyzed CO is expected to stay with Cu_B. If the return of the photolyzed CO from Cu_B to cytochrome a_3 is the primary event under investigation, then the observed single Arrhenius behavior through the temperature range between 270 K and 160 K is not surprising.

The differences between the results of this and previous studies can be resolved if the monitor light was not as 'harmless' as assumed previously. At higher temperatures, the recombination rate is fast compared to the photodissociation by the monitor light. Therefore the result is little affected. However, the photodissociation will slow down the recombination more and more as the temperature decreases (*cf.* Figure 6). The activation energy thus obtained can be overestimated.

The Fast CO-rebinding Cytochrome a_3

In addition to the slow CO-rebinding process observed at higher temperatures, a rebinding process with a prefactor rate of order 10^{10} sec^{-1} is located between 130 K and 90 K. The presence of two different CO-rebinding sites is consistent with the Mössbauer results, that two types of cytochrome a_3 exist in yeast oxidase preparations. The high-spin cytochrome a_3 is the functional site. The fact that this cytochrome a_3 has Cu_B sitting nearby or in the same pocket presumably causes the slow CO-rebinding process. The low-spin cytochrome a_3, on the other hand, is likely to be 6-coordinated. Cu_B might have moved away. The Mössbauer parameters of this site in the reduced state, however, cannot be distinguished from those of cytochrome a^{2+} (*cf.* Chapter 2). It is thus concluded that the coordination environment of this site is probably

very similar to that of cytochrome *a*, namely, with two axial histidine ligands (20, 21). In order for this site to bind CO, one histidine has to move away slightly. Thus the ligand environment of this CO-heme complex is probably very similar to myoglobin–CO. The CO-recombination behavior of this site is not completely resolved in this study as the behavior at 90 K and 100 K is not totally understood by either a power law or a Gaussian distribution of activation energy. However, the bulk activation energy estimated in this study (13 kJ/mol at the peak) is of the same order as that reported for myoglobin. The fast CO-recombination is consistent with the hypothesis that, in this conformation, cytochrome a_3 and Cu_B have moved away from each other.

The presence of this fast CO-rebinding, low-spin cytochrome a_3 casts a shadow on the use of yeast cytochrome oxidase to study the reoxidation mechanism of this enzyme. Most likely, this low-spin site does not react with the dioxygen due to the mismatch of the spin states and the six-coordinate nature of the low-spin cytochrome a_3. Even if it does, the CO-recombination is so fast that the dioxygen cannot compete with it. In the next chapter, we shall describe the reoxidation study of yeast cytochrome oxidase by EPR and Mössbauer spectroscopies. It proved to be difficult.

A Heme-Heme Interaction in the Degraded Enzyme

The high-spin signal which accounts for 15% of the total iron is so far not explained, while at the same time, 15% intensity of low-spin cytochrome a^{2+} is missing. On the other hand, nearly 50% intensity is found for the low-spin cytochrome a^{3+} in the Mössbauer spectrum of the resting oxidized enzyme (*cf.* Chapter 2). The indication is obvious enough. Is there any heme-heme interaction between cytochrome *a* and a_3 that results in a spin state change at cytochrome *a* when cytochrome a_3 reacts with CO?

The cytochrome oxidase literature is full of interaction schemes (*cf.* Chap-

ter 5 for potential interactions). One of the most famous examples concerning the spin state interaction was reported by Leigh *et al.* (22) in 1974. They found that the photodissociation of CO from the mixed-valence cytochrome oxidase (which is a term that is generally used to describe an exactly half-reduced enzyme sample) induced an increase of the $g = 6$ signal intensity and a decrease at $g = 3$. Most astonishingly, this event took place even at 5 K. It was interpreted by postulating that CO binding induced a spin state change of cytochrome *a* from high spin to low spin. As Wikström *et al.* (1) pointed out, the weakness of these results is that the spectroscopic changes account for only a small fraction of the enzyme molecule present in the sample. Therefore, the event may not take place generally.

Our finding of the high-spin component in the Mössbauer spectrum of CO-bound reduced yeast cytochrome oxidase can be explained quite simply in this light. As discussed before, the low-spin cytochrome a_3 is likely to be 6-coordinated. The detection of the CO-complex formation at this site by Mössbauer and photolysis studies indicates that the 6th ligand, possibly a histidine, has moved away. An adjustment in the protein backbone is likely to induce a change in the chemical environment at cytochrome *a* of that molecule, which results in a spin state change at that site. The concentration of the reduced low-spin cytochrome a_3 was 12% of the total iron in the resting oxidized sample. It is most likely to increase during the reduction and CO reaction. The presence of 15% high-spin ferrous heme can thus be explained quite reasonably.

The majority of the cytochrome *a* is in the low-spin state when CO is bound to cytochrome a_3. Furthermore, its Mössbauer parameters do not change upon CO binding. Therefore, Mössbauer studies indicate that the heme-heme interaction regarding the CO-binding of cytochrome a_3 is not present in the normal, functional molecules of cytochrome oxidase.

REFERENCES

1. Wikström, M., Krab, K., and Saraste, M. (1981). *Cytochrome Oxidase: A Synthesis*, Academic Press, London.
2. Chance, B. (1953). *J. Biol. Chem.* **202**, 397–406.
3. Castor, L.N. & Chance, B. (1955). *J. Biol. Chem.* **217**, 453–465.
4. Chance, B., Schroener, B., & Yonetani, T. (1965). In *Oxidases and Related Systems I* (T.E. King, H.S. Mason, & M. Morrison, eds.) Vol. **2**, Wiley & Sons, New York, pp. 609–614.
5. Yonetani, T., Iizuka, T., Yamamoto, H., & Chance, B. (1973). In *Oxidases and Related Systems II* (T.E. King, H.S. Mason, & M. Morrison, eds.) Vol. **1**, University Park Press, Baltimore, pp. 401–405.
6. Erecińska, M. & Chance, B. (1972). *Arch. Biochem. Biophys.* **151**, 304–315.
7. Sharrock, M. & Yonetani, T. (1976). *Biochim. Biophys. Acta* **434**, 333–344.
8. Sharrock, M. & Yonetani, T. (1977). *Biochim. Biophys. Acta* **462**, 718–730.
9. Austin, R.H., Beeson, K.W., Eisenstein, L., Frauenfelder, H., & Gunsalus, I.C. (1975). *Biochemistry* **14**, 5355–5373.
10. Alberding, N., Austin, R.H., Chan, S.S., Eisenstein, L., Frauenfelder, H., Gunsalus, I.C., & Nordlund, T.M. (1976). *J. Chem. Phys.* **65**, 4701–4711.
11. Fiamingo, F.G., Altschuld, R.A., Moh, P.P., & Alben, J.O. (1982). *J. Biol. Chem.* **257**, 1639–1650.
12. Chance, B., Saronio, C., & Leigh, J.S., Jr. (1975). *J. Biol. Chem.* **250**, 9226–9237.
13. Siedow, J.N., Miller, S., and Palmer, G. (1981). *J. Bioenerg. Biomemb.* **13** 171-179.
14. Austin, R.H., Beeson, K.W., Chan, S.S., Debrunner, P.G., Downing, R.,

Eisenstein, L., Frauenfelder, H., & Nordlund, T.M. (1975). *Rev. Sci. Instrum.* **47**, 445–447.

15. Young, R.D. & Bowne, S.F. (1984). *J. Chem. Phys.* **81**, 3730–3737.
16. Austin, R.H., Beeson, K.W., Eisenstein, L., Frauenfelder, H., Gunsalus, I.C., & Marshall, V.P. (1974). *Phys. Rev. Lett.* **32**, 403–405.
17. Lang, G. & Marshall, W. (1966). *Proc. Phys. Soc.* **87**, 3–34.
18. Sharrock, M., Münck, E., Debrunner, P.G., Marshall, V., Lipscomb, J.D., & Gunsalus, I.C. (1973). *Biochemistry* **12**, 258–265.
19. Brudvig, G.W., Stevens, T.H., Morse, R.H., and Chan, S.I. (1981). *Biochemistry* **20**, 3912–3921.
20. Blumberg, W.E., & Peisach, J. (1971). In *Probes of Structure and Function of Macromolecules and Membranes* (B. Chance, T. Yonetani, & A.S. Midvan, eds.), Vol. 2, Academic Press, New York, pp. 215–229.
21. Martin, C.T., Scholes, C.P., & Chan, S.I. (1985). *J. Biol. Chem.* **260**, 2857–2861.
22. Leigh, J.S., Jr., Wilson, D.F., Owen, C.S. & King, T.E. (1974). *Arch. Biochem. Biophys.* **160**, 476–486.

CHAPTER 4

EPR & MÖSSBAUER STUDIES OF LOW-TEMPERATURE INTERMEDIATES FORMED DURING THE REOXIDATION OF FULLY REDUCED YEAST CYTOCHROME OXIDASE BY DIOXYGEN

INTRODUCTION

The reaction mechanism for the catalytic reduction of dioxygen by cytochrome oxidase is one of the most fascinating questions from the bioenergetics point of view. This enzyme is responsible for more than 90% of the O_2 consumed by cellular respiration (1). The reduction of O_2 is very efficient, and no toxic substances such as superoxide and peroxide are released to the cell environment during the reaction (2). Therefore the search for reaction intermediates and kinetic studies of this reaction have been vigorously pursued. These efforts have been recently reviewed by Wikström *et al.* (1), Malmström (3), and Blair *et al.* (4), among others.

As is obvious from the discussions in previous chapters, direct access to the structural state of cytochrome a_3, such as by Mössbauer spectroscopy, is highly desirable due to the shortcomings of optical and EPR studies. In this chapter, we shall present a study of the reoxidation of fully reduced yeast cytochrome oxidase by EPR and Mössbauer spectroscopies. However, the extensive knowl-

edge that has been gained on this subject from the intensive studies of beef heart cytochrome oxidase is essential in understanding our results. The above-mentioned reviews, although only a few years old, did not cover the most recent advances that have furthered our understanding of the reaction mechanism. Therefore an effort will be made in this chapter to present a concise review on the reoxidation of the reduced beef heart cytochrome oxidase. Emphasis will be on the EPR evidence, since it is most complementary to Mössbauer results.

The detection of the intermediates at room temperature is very difficult due to the fast reaction rate. (Turnover rate as high as 400 electrons per second has been reported (5)). A few intermediates at the later stage of the reaction, however, have been detected at room temperature. High-spin heme signals around $g = 6$ (6,7) and a low-spin heme signal at $g = 2.59$, 2.16, & 1.86 (7) have long been known to exist in partially reduced or partially reoxidized samples. They have been proven to arise from cytochrome a_3. It is quite clear that in such cases, Cu_B is reduced. The high-spin cytochrome a_3 is likely to be liganded by a water molecule and the low-spin cytochrome a_3 is likely to be liganded by a hydroxyl group. An opposite case, namely, a copper signal, has been reported at $g = 2.28$, 2.11, & 2.05 by Reinhammar *et al.* (8) and confirmed later (9) to be from Cu_B. A rather small copper hyperfine coupling (102 Gauss) was found for $g_{||}$ component towards lower field. In this state, cytochrome a_3 is both reduced and low-spin, judging from the lack of any relaxation effect or static dipolar splitting of the Cu_B signal. The iron was thought to be liganded by dioxygen as in oxymyoglobin (4) because of the unusual requirement of bubbling oxygen through the sample during the reoxidation of the reduced enzyme. Curiously though, this signal has not been reported in the absence of CO. Finally, another EPR signal at $g = 5$, 1.78, 1.69 has been reported by Shaw *et al.* (10). It was thought to arise from a coupled a_3 site (11) and was found to correlate optically very well with the so-called 'pulsed' enzyme (12).

The latter is a form of cytochrome oxidase reported by Brunori *et al.* (13) that is generated freshly after the reoxidation of stoichiometrically reduced enzyme and has a higher activity than the resting enzyme.

In 1975, Chance *et al.* (14) designed the 'triple-trapping' technique and the study of reoxidation intermediates at the early stages became possible. This method makes use of CO inhibition to enable mixing of the enzyme with dioxygen without the reoxidation of the enzyme at $-20°C$ in the dark. It then takes advantage of the unusually slow CO-recombination (which has been described in detail in the previous chapter) to free cytochrome a_3 of CO by photolyzing the sample at liquid-nitrogen temperature. The reoxidation of cytochrome oxidase is initiated and studied at $\sim$173 K by spectroscopic, mostly optical and EPR, methods. An ethylene glycol/water mixture is used as the solvent in order to achieve $-20°C$ temperature without freezing the sample. When frozen, this solution also forms a glass that is suitable for photodissociation.

For a long time no EPR signal from the oxygen-binding site was detected at the early stage of reoxidation. The only signals observed were from the oxidations of cytochrome *a* and Cu_A. Clore *et al.* (15) studied the reaction kinetics at 173 K and described their results using a mechanism with four intermediates for the reoxidation of the enzyme at this temperature. Intermediate I is formed when O_2 binds at the a_3 site, with the *a* sites (cytochrome *a* & Cu_A) remaining reduced. This is then converted to either intermediate IIA, with cytochrome *a* oxidized, or intermediate IIB, with Cu_A oxidized. The intermediate IIB is a stable product at 173 K, while intermediate IIA is converted to Intermediate III, in which both of the *a* sites are oxidized. Since the *a* sites are not oxidized in the intermediate I, only two electrons, namely, from cytochrome a_3 and Cu_B, are available for the reaction with dioxygen at this stage. Intermediate II's are produced when a third electron is transferred from either cytochrome *a* or Cu_A to the a_3 site. Intermediate III forms when the fourth electron is transferred

from Cu_A. Intermediate I and III were found to be identical to the compound A_1 and B reported earlier by Chance *et al.* (14,16).

Although Brudvig *et al.* (17) predicted a ferryl (Fe^{IV}) species at cytochrome a_3 when the third electron is transferred to the oxygen binding site, no evidence suggestive of such nature at the intermediate II level had been reported until Karlsson *et al.* (18) discovered an unusual copper EPR signal at $g = 2.25$ at a sufficiently high level of microwave power that nearly saturates every other signal in the spectrum. The inability to saturate this copper signal was attributed to the enhanced electron spin relaxation at Cu_B by a nearby, rapidly relaxing species such as a ferryl cytochrome a_3. This assignment turns out to be incorrect, as revealed by the detailed low-temperature kinetic study by Blair *et al.* (19), which monitored this 'unusual' copper signal as well as the signals from the *a* sites. The latter work, to which the present study is a preliminary, parallel study on the yeast cytochrome oxidase, is outlined in detail below.

Blair *et al.* (19) confirmed the three-level, four-intermediate mechanism that was observed by Clore *et al.* (15) as illustrated in Scheme 1. A 30% and 70% branching was observed for the third electron to come from cytochrome *a* and Cu_A respectively. Both processes generate an identical '$3e^-$-reduced' intermediate at the a_3 site, which exhibits the 'unusual' Cu_B signal. An 80% maximum Cu_B intensity was observed after incubation at 180 K. The rate of the following reaction, i.e., the reduction of the dioxygen by the fourth electron, depends on the source of the electron. The electron transfer from cytochrome *a* at this stage, namely, the further reduction of IIB at the a_3–O_2 site, is found to be a highly activated process and slow at these temperatures (see below). On the other hand, the conversion of IIA to III, i.e., the transfer of the fourth electron from Cu_A to the a_3 site, is relatively fast. Therefore about 30% of the dioxygen becomes reduced to the formal oxidation level of water quickly, while

the rest remains in the 'three-electron-reduced' level for a substantial amount of time at 180–190 K. We shall come back to this point later.

The identity of the intermediate I (compound A) at the a_3 site has become clear through the last few years. Although it has been suggested that it contains a peroxo-bridge between cytochrome a_3 and Cu_B (3), the original assignment by Chance *et al.* (14) that compound A is an O_2 adduct, bound to cytochrome a_3 only, is likely to be more correct. This 'oxy' geometry for intermediate I is consistent with the results of Blair *et al.* (19). They found that the formation of intermediate II, judged by the intensity of the 'unusual' Cu_B signal, was a highly activated process (E_a= 13.2 kcal mol^{-1}). If this were just the activation barrier of the electron transfer from a sites to the a_3 site, the high turnover rates would imply intersite distances shorter than those estimated by magnetic studies. However, it is known that CO becomes attached to Cu_B after being photodissociated from cytochrome a_3 (20). The activation energy for CO to return from Cu_B to cytochrome a_3 is roughly 10 kcal mol^{-1} (20,21). If ~10 kcal mol^{-1} out of the 13.2 kcal mol^{-1} is required to remove CO from Cu_B, then the high activation barrier for the production of intermediate II can be understood. This process is illustrated in Scheme 2. A peroxo-bridged intermediate is predicted after CO is removed from Cu_B. This view is supported by the recent Resonance Raman study of Babcock *et al.* (22). They found that an O_2 adduct is formed within 20 μsec after the photodissociation of CO at room temperature. Only after 50–75 μsec is the dioxygen anchored between the two metal centers. The former intermediate is labile towards photolysis, while the latter is stable.

We should bear in mind, however, that the long lifetime of compound A (or intermediate I), as has been pointed out before by other researchers (*cf.* review(1)), may be an artifact due to the employment of CO in the study of the reoxidation of cytochrome oxidase. Under physiological conditions, the peroxo-

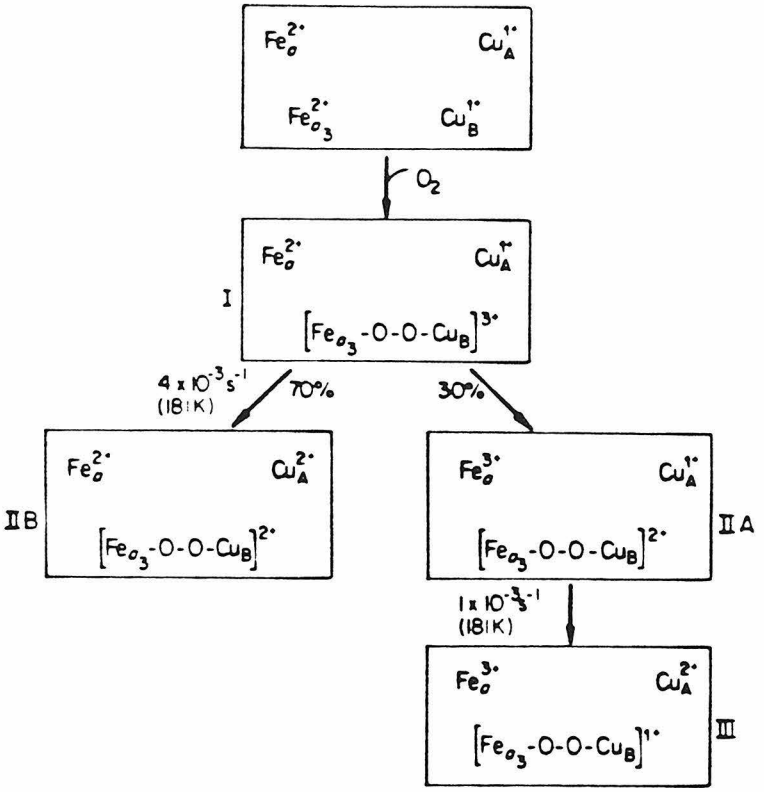

Scheme 1

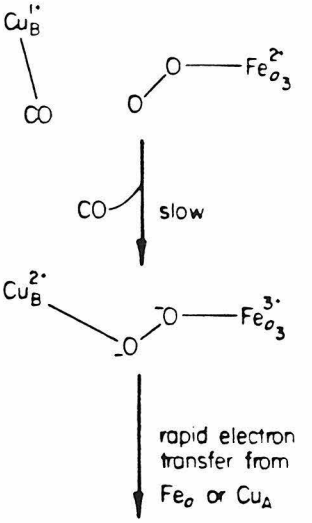

Scheme 2

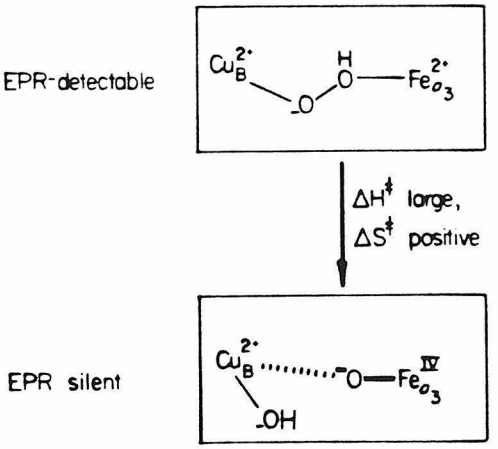

Scheme 3

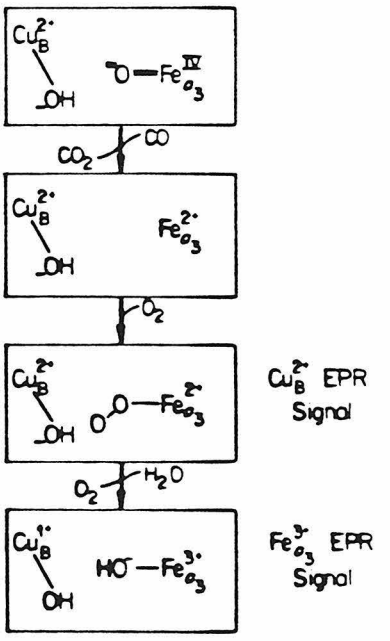

Scheme 4

bridged intermediate most likely will form very shortly after the dioxygen is anchored on cytochrome a_3, as Malmström (3) indicated. The intermediates detected after compound A using the 'triple-trapping' technique should be relevant to the physiological reaction mechanism, since CO is excluded from the reaction (see below, however, for possible exceptions).

The peroxo-bridged intermediate does not accumulate in the reoxidation of the fully reduced enzyme, since the transfer of the third electron is relatively fast. This intermediate can be detected if the third electron is not available. It can be found in the oxidation of half-reduced (or mixed-valence) cytochrome oxidase in the presence of CO at ~173 K (16,23). This state has a distinctive optical band peaked at 607 nm and was denoted compound C by Chance *et al.* (16).

An 'unusual' copper signal is found at the 'three-electron-reduced' level. Because of the presence of odd numbers of electrons, this level is also the only level for which EPR signals are predicted. The original suggestion as to the identity of the a_3 site that exhibits the 'unusual' copper signal is a ferryl cytochrome a_3. However, Blair *et al.* (19) found that the disappearance of this signal at ~190 K could not be accounted for by the relatively small concomitant increase in the EPR intensities of cytochrome *a* and Cu_A. This result indicated that there is a second '$3e^-$-reduced' intermediate. The activation enthalpy for the conversion from the first to the second intermediate was found to be quite large and the activation entropy positive, suggestive of a bond-breaking process. Blair *et al.* (19) proposed the structures of these two intermediates as are shown in Scheme 3. The first intermediate contained a peroxo-bridge between reduced cytochrome a_3 and oxidized Cu_B. The fast relaxation of the 'unusual' Cu_B signal demands that the ferrous cytochrome a_3 be in either the high-spin state ($S = 2$) or the intermediate spin state ($S = 1$). During the formation of the second intermediate, the oxygen-oxygen bond is thought to be disrupted.

A ferryl species is thus predicted. Theoretically, the Cu_B in this state should exhibit an EPR signal. It has not been located, however, presumably because of extremely fast spin relaxation due to the ferryl center, which is normally seen in the intermediate state (*cf.* Chapter 2).

The reaction that follows the second '$3e^-$-reduced' intermediate does not take place until the sample is incubated at 211 K. This reaction does not involve further electron transfer from cytochrome *a*. Interestingly, a rhombic copper signal (at $g = 2.32$ with A=102 Gauss) and a low-spin heme signal(at g= 2.63 & 1.89) developed at this temperature. They are identical to the signals observed at room temperature and have been discussed before. A reaction mechanism that involves the oxidation of CO by the ferryl group was proposed (19) and is illustrated in Scheme 4. Interestingly, this mechanism suggests that CO is partially responsible for the formation of the rhombic copper. As has been mentioned before, the rhombic signal has not been reported in the absence of CO. Therefore, there is some likelihood that this rhombic copper signal is also an artifact resulting from the use of CO.

To summarize, the low-temperature kinetic study of beef heart cytochrome oxidase by Blair *et al.* (19) showed that a large fraction (~70%) of the enzyme goes through two '$3e^-$-reduced' intermediates when reoxidized from the fully reduced state. They suggested that the second intermediate contains a ferryl group. The rest (~30%) of the enzyme reduced the dioxygen in a more concerted way; i.e., the successive transfer of the third and the fourth electrons is relatively fast. Therefore the reaction may not go through the ferryl intermediate (or the ferryl species may be very short-lived). A proposed mechanism for the steady-state reaction of cytochrome oxidase is reproduced from Ref. (4) in Scheme 5 with minor modifications.

The shortcomings of EPR studies of the reaction intermediates of cytochrome oxidase are quite obvious: Few EPR signals from the oxygen-binding

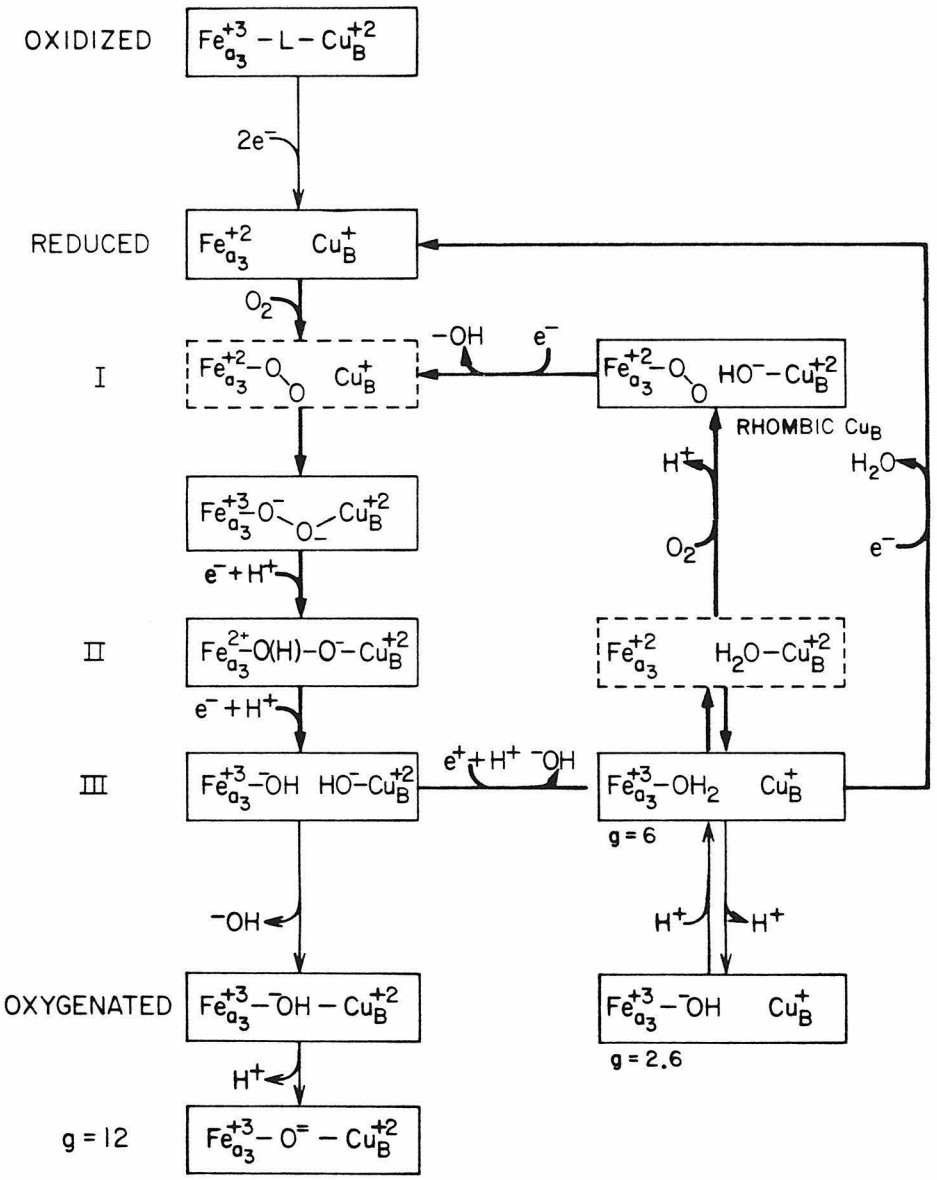
OXIDIZED
$Fe^{+3}_{a_3} - L - Cu^{+2}_B$
$2e^-$
REDUCED
$Fe^{+2}_{a_3}$ Cu^+_B
O_2
I
$Fe^{+2}_{a_3}-O_2$ Cu^+_B
$-OH$ e^-
$Fe^{+2}_{a_3}-O_2$ $HO^- - Cu^{+2}_B$
RHOMBIC Cu_B
H^+
O_2
H_2O
e^-
$Fe^{+3}_{a_3}-O^-_2-Cu^{+2}_B$
$e^- + H^+$
II
$Fe^{2+}_{a_3}-O(H)-O^- - Cu^{+2}_B$
$Fe^{+2}_{a_3}$ $H_2O - Cu^{+2}_B$
$e^- + H^+$
III
$Fe^{+3}_{a_3}-\bar{O}H$ $HO^- - Cu^{+2}_B$
$e^- + H^+$ ^-OH
$Fe^{+3}_{a_3}-OH_2$ Cu^+_B
g = 6
$-OH$
H^+
H^+
OXYGENATED
$Fe^{+3}_{a_3} - \bar{O}H - Cu^{+2}_B$
$Fe^{+3}_{a_3}-\bar{O}H$ Cu^+_B
g = 2.6
H^+
g = 12
$Fe^{+3}_{a_3} - O^= - Cu^{+2}_B$

Scheme 5

site are observed, and in most cases the signals arise from Cu_B. The structural state of cytochrome a_3 is inferred from the signal from Cu_B and the kinetic parameters. A direct access to the structural information about cytochrome a_3 is necessary to test the proposed mechanisms.

In this chapter, a parallel EPR study and a preliminary Mössbauer study of the reoxidation of the fully reduced yeast cytochrome oxidase, using the 'triple-trapping' technique, are presented. Because extensive EPR studies of the beef heart enzyme are available, our task is to discern the reaction intermediates of the yeast enzyme by EPR and correlate them with the Mössbauer results. A few identical intermediates are discovered, indicating that the reaction mechanism may be very similar to that in beef heart oxidase. Differences, however, are also observed. The development of the EPR signals of cytochrome a, Cu_A, and the 'unusual' Cu_B are followed and discussed. Efforts have also been made to observe the reaction intermediates in yeast cytochrome oxidase at room temperature by the method of Beinert & Coworkers (10). Although the results indicate that the $g = 12$ signal does not recover to a maximum intensity until $\sim$ 1 h after the reoxidation of the stoichiometrically reduced enzyme, as would be expected from the transition of the enzyme from the 'pulsed' state to the resting state, the attempts to locate the '$g = 5$' signal have not been fruitful so far. Therefore these results will not be presented here.

MATERIALS AND METHODS

EPR Experiments

Yeast cytochrome oxidase was prepared by the method that has been described in Chapter 1. The enzyme was dissolved in 0.5% Tween-20, 50 mM tris, pH7.4. It was dialyzed against the same buffer containing 2 mM EDTA first to remove the ammonium sulfate and adventitious metal ions, and then dialyzed again to remove EDTA. Samples were stored at $-80°C$. The heme a concen-

tration was determined by using an extinction difference of 16.5 mM^{-1} cm^{-1} between 600 nm and 630 nm for the reduced sample (24). The enzyme solutions used for EPR experiments were typically 0.25–0.3 mM in cytochrome oxidase, i.e., 0.5–0.6 mM in heme *a*.

EPR samples for low-temperature reoxidation studies were prepared in 5 mm o.d. (3.4 mm i.d.) quartz tubes. They were degassed by six cycles of evacuation and purging with argon, which had been scrubbed of oxygen by passage through 0.1 M vanadous ion in 2 N HCl followed by passage through 0.02 M NaOH. A small excess (*ca.* 1.5 equiv) of NADH (β-nicotinamide adenine dinucleotide) (Sigma) and 0.01 equiv of PMS (phenazine methosulfate, also from Sigma) were added to the samples under an argon atmosphere, causing complete reduction of the oxidase within 30 min at room temperature. An equal volume of glycerol, which had been degassed thoroughly, was mixed with the reduced enzyme solutions at 4°C. The argon atmosphere was then exchanged for one atmosphere of CO (Matheson 99.99%). The sample was cooled to −20°C and evacuated. One atmosphere of oxygen was admitted to the samples in the dark, and the samples were vigorously agitated for 1 min and frozen in liquid nitrogen. The frozen solution formed an optically transparent glass.

The samples were then photolyzed in a finger dewar at 77 K by irradiation with a 200-W Hg-Xe arc-lamp (Oriel Corp.) for 30 min in order to remove CO from cytochrome a_3, with frequent rotation of the sample so that all sides were equally exposed to the light. Following photolysis, samples were stored in liquid nitrogen. The reaction with dioxygen was allowed to take place at the desired temperature by immersing the sample tubes in methanol/ethanol solutions cooled by the addition of liquid nitrogen. The bath was constantly stirred to ensure thermal equilibrium. The reaction was quenched by returning the samples to liquid nitrogen.

EPR spectra were recorded on a Varian E-line Century series X-band

spectrometer equipped with an Air Products Heli-Tran temperature controller. They have been described in Chapter 2. The modulation amplitude used in these experiments was 16 Gauss and the modulation frequency 100 kHz. Spectra were measured at 10 ± 0.5 K. EPR intensities were measured as peak heights at $g = 3$ (cytochrome *a*), or peak-to-trough distances (Cu_A), or the average peak heights of the first two of the four copper hyperfine peaks observed at $g = 2.25$ (the 'unusual' Cu_B).

Mössbauer Experiments

The ^{57}Fe-enriched yeast cytochrome oxidase sample used in the Mössbauer experiments was sample 3 used in Chapter 2. Sample preparation and characterization have been described previously. 0.4 ml of yeast oxidase (0.65 mM in heme *a*) was placed in a transparent Mössbauer cup (0.5 in o.d., made of lucite), degassed, and purged with argon (which had been scrubbed of oxygen by vanadous ion solution) 6 times. The sample solution was then reduced by a 2-fold excess of NADH in the presence of 0.01 equiv of PMS. After complete reduction, an equal volume of glycerol, also thoroughly degassed and purged with argon, was added and mixed well. The sample was briefly evacuated and a 50%/50% mixture of CO and scrubbed argon was admitted. The sample was incubated under such an atmosphere for 15 min and then frozen in liquid nitrogen. All the anaerobic operations were performed in the glassware that has been described in Figure 1 of Chapter 2. The sample mixing and degassing were aided by a small magnetic stir bar, which was removed from the sample prior to freezing.

The frozen sample was placed in an argon atmosphere, brought to a $-20°C$ cold room, and thawed in the dark. Oxygen was blown gently at the surface of the sample for 1 min while the sample was stirred with a glass rod. Again this was done in the dark. The sample was then frozen in liquid nitrogen.

The sample was immersed in liquid nitrogen in a dewar and photolyzed by a 1000 W arc lamp (Schoeffel Instruments Co.) for 3 h. The sample was rotated frequently in order to achieve a thorough and even photolysis. After being monitored by Mössbauer spectroscopy, the sample was incubated at the desired temperatures by being placed in a long vial which had been pre-equilibrated and immersed in the methanol/ethanol bath that has been described before.

Mössbauer spectra were recorded on a Janis cryostat-equipped spectrometer. The spectrometer has been described in Chapter 2. A 320 Gauss magnetic field that was perpendicular to the propagation direction of the γ rays was used in all the experiments. Spectra were measured at either 100 K or 4.2 K.

RESULTS

EPR Study of the Reoxidation of Yeast Cytochrome Oxidase

The reaction between dioxygen and the fully reduced yeast oxidase was initiated by incubating the photolyzed samples around 173 K. The 'unusual' Cu_B EPR signal was immediately observable afterwards. The EPR spectrum that contained the maximum intensity of Cu_B signal is shown in Figure 1. The signal of cytochrome *a*, at $g = 2.98$ & 2.25, and Cu_A, around $g = 2$, are mostly removed by the power saturation. The unsaturated copper signal, at $g = 2.25$ with a hyperfine coupling of 135 Gauss, is identical to that reported by Karlsson *et al.* (18) in the beef heart enzyme within experimental uncertainties. The maximum yield of this signal, quantitated by the intensity of the lowest-field peak, is found to be ~60% of that observed in the beef heart enzyme*. The maximum yield of the Cu_B signal in beef heart oxidase was estimated to be roughly 80% (19). Considering that in typical preparations of yeast cytochrome oxidase, roughly 20% of cytochrome a_3 is in a degraded, low-spin form which does not participate in the reaction (*cf.* Chapter 2), the yield is reasonable.

* Witt, S.N., personal communication.

Figure 1. EPR spectra observed after incubation of a yeast cytochrome oxidase sample for 30 min at 183 K. The reoxidation of the fully reduced yeast enzyme was initiated at 175 K. The signals of cytochrome a^{3+} and Cu_A were recorded with 0.2 mW microwave power. The 'unusual' Cu_B spectrum was recorded with 20 mW microwave power. The same gain was used in recording both spectra. Other conditions: temperature, 10 K; modulation amplitude, 16 Gauss; microwave frequency, 9.18 GHz.

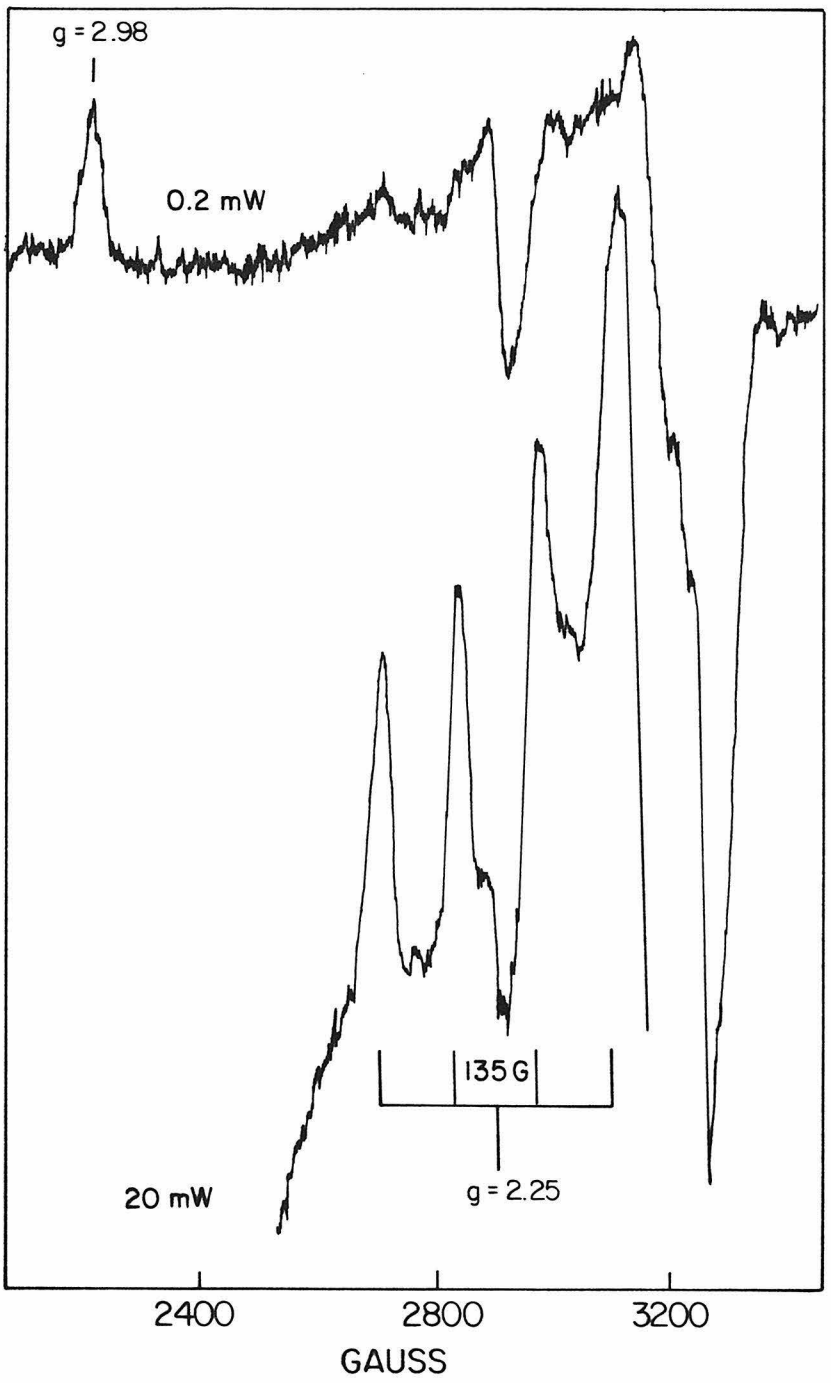
g = 2.98
0.2 mW
135 G
g = 2.25
20 mW
2400
2800
3200
GAUSS

We should note, however, that the solvent used in the experiments concerning yeast cytochrome oxidase is a 50%/50% glycerol/aqueous detergent solution rather than an ethylene glycol/detergent solution that is normally used in the beef heart enzyme experiments. (Blair *et al.* (19) reported that with the beef heart enzyme, the yields of the 'unusual' Cu_B signal in glycerol and ethylene glycol are similar.) Attempts to locate the 'unusual' copper signal of yeast in the latter solvent were not successful.

The development of the EPR intensities of cytochrome *a*, Cu_A, and the 'unusual' Cu_B signals in a typical sample during incubations at various temperatures is plotted in Figure 2. A substantial amount of Cu_B signal, accompanied by the reoxidation of cytochrome *a* and Cu_A, is produced right after the reaction is initiated. While cytochrome *a* and Cu_A become reoxidized steadily at 183 K and 193 K, the amount of the 'unusual' Cu_B signal is kept at roughly the same level. This indicates that the EPR-unsaturable Cu_B is produced and consumed at the same time. As has been discussed before, there are two ways in which this Cu_B can be consumed: either it is further reduced by the fourth electron, thus causing both cytochrome *a* and Cu_A of that molecule to be oxidized, or it is converted to the second, EPR-silent '$3e^-$-reduced' intermediate. A sharp decrease in the Cu_B intensity is found at 206 K without a parallel increase in either cytochrome *a* or Cu_A intensities. The reaction at this stage does not involve further electron transfer from the *a* sites. Therefore the conversion of most of the first '$3e^-$-reduced' intermediate into the second one does not occur until the temperature reaches 206 K or above. The near-steady state of the 'unusual' Cu_B at 183 K and 193 K, on the other hand, indicates that the intermediate III is produced at these temperatures via consumption of the intermediate II.

In fact, two intermediates, IIA & IIB, are found at the 'three-electron-reduced' level at temperatures between 175 K and 193 K, in a manner very

Figure 2. Intensities of the EPR signals due to Cu_B (◆), Cu_A (●), and cytochrome *a* (▶) during incubation of a yeast cytochrome oxidase sample at various temperatures. Microwave power: the 'unusual' Cu_B, 20 mW; Cu_A and cytochrome *a*, 0.2 mW (the first 5 points) and 0.02 mW (the last 7 points). For cytochrome *a* and Cu_A, the 6th data point was measured with both 0.02 mW and 0.2 mW power. The saturation factors observed at 0.2 mW for these two metal centers were then applied to all the earlier points. The oxidation of cytochrome *a* and Cu_A during the sample preparation has been subtracted. The curves are drawn to guide the eye.

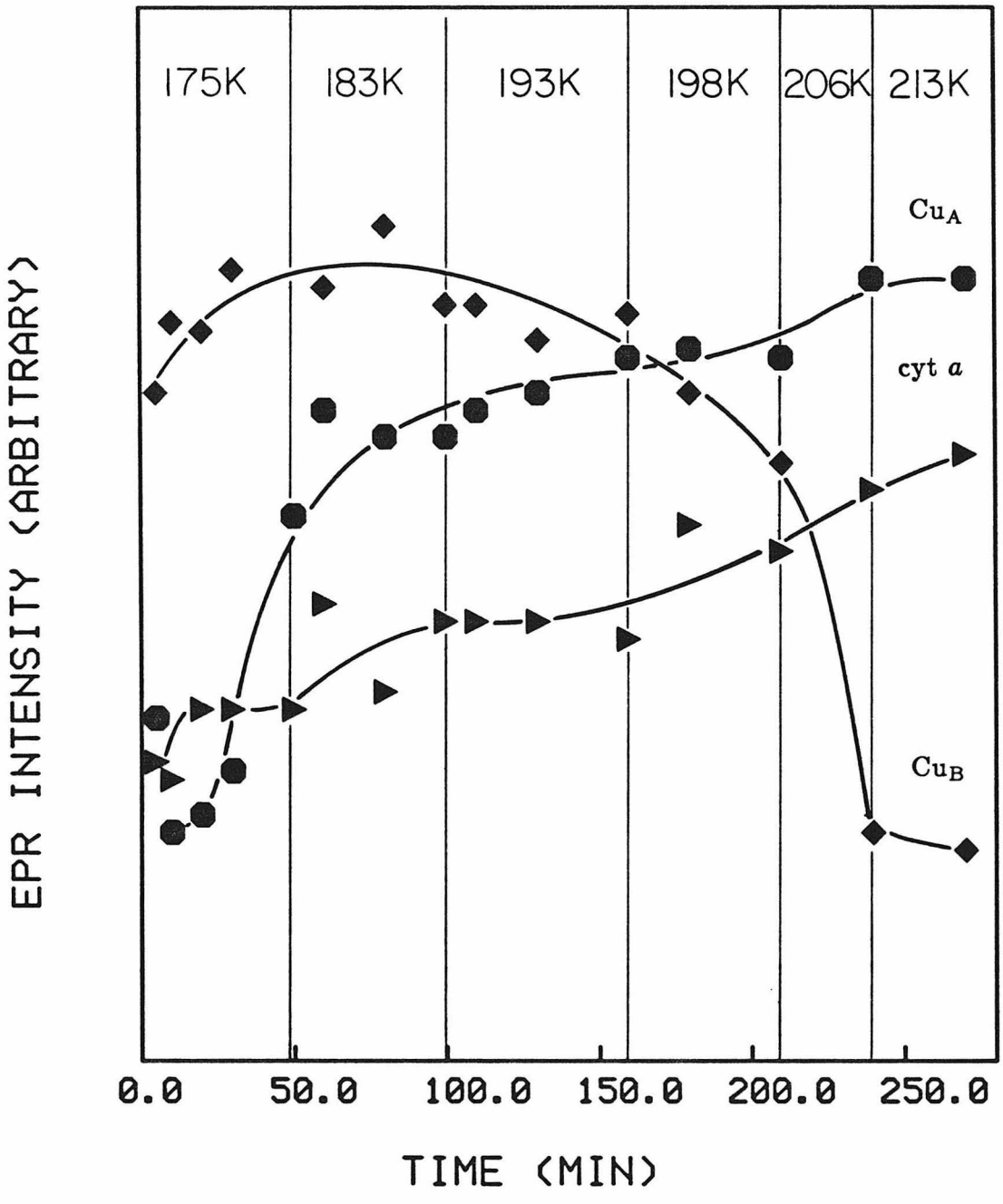
175K
183K
193K
198K
206K
213K
Cu$_A$
cyt *a*
Cu$_B$
EPR INTENSITY (ARBITRARY)
0.0
50.0
100.0
150.0
200.0
250.0
TIME (MIN)

similar to that observed in the study of beef heart enzyme (15,19). In Figure 2, we see that the initial growth of the cytochrome *a* EPR signal is greater than that of the Cu_A signal. However, the Cu_A EPR signal increases rapidly at higher temperatures and surpasses that of cytochrome *a*. This indicates that in the molecules that had the third electron transferred from cytochrome *a* (producing intermediate IIA), the further reduction of the oxygen binding site (to become intermediate III) by the fourth electron from Cu_A is relatively fast; on the other hand, in the molecules that had the third electron transferred from Cu_A (producing intermediate IIB), the further electron transfer from cytochrome *a* is very slow (*cf.* Scheme 1).

The properties of intermediates IIA and IIB are illustrated in Figure 3. In this figure, the relative concentrations of the three intermediates (IIA, IIB, & III) in the yeast oxidase studies were calculated from the EPR intensities of the Cu_A, Cu_B, and cytochrome *a* signals between 175 K and 193 K. The intensity of Cu_B signal is assumed to represent the sum of IIA and IIB, which should be valid below 193 K. (The intensities of cytochrome *a* and Cu_A, respectively, have been normalized according to the total intensities developed at 253 K. The maximum development of the Cu_B signal is assumed to be 50%, which is equivalent to assuming a $\sim$ 7% growth of intermediate III after 10 min incubation at 175 K. This assumption is probably not far off, judging from the report by Clore *et al.* (15), that more than 15% of intermediate III was produced under similar conditions in the beef heart enzyme and also from the sluggishness of the reoxidation in yeast cytochrome oxidase.) The figure indicates that while the increase in the concentration of intermediate III is accompanied by a loss in that of intermediate IIA, the concentration of intermediate IIB increases steadily with the incubation. Exactly the same properties for the intermediate IIA & IIB have been derived in the study of the beef heart enzyme (15,19). The initial growth in the concentrations of the three intermediates (IIA, IIB, & III)

in the yeast enzyme suggests that the branching of the electron transfer takes place as follows:

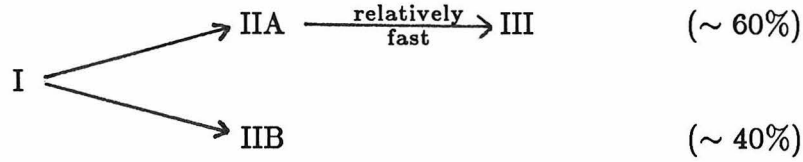

The percentage of the enzyme molecules that becomes oxidized via intermediate IIB should decrease if the initial formation of intermediate III is higher than what we have estimated.

As has been noted before, the large drop in the intensity of the 'unusual' Cu_B signal at 206 K indicates the conversion from one '$3e^-$-reduced' intermediate to a second one. Indeed, the reoxidation level of cytochrome a increases rather steeply between 223 K and 235 K (data not shown), totally consistent with this picture. (This process was also found to be slow in the beef heart enzyme when a glycerol/detergent solution was used (19). The temperature at which the process became fast was also found to be around 206 K. It was approximately 100 times faster when ethylene glycol was used.) Since intermediate IIA has been mostly converted to intermediate III by this stage, the second '$3e^-$-reduced' intermediate is derived from intermediate IIB. Therefore the maximum yield of the second '$3e^-$-reduced' intermediate is estimated to be roughly 40%.

One should then expect the detection of the rhombic Cu_B signal or the low spin cytochrome a_3 signal at a slightly higher temperature, as suggested by Scheme 4. However, the rhombic Cu_B signal has not been seen in yeast cytochrome oxidase. On the other hand, a low-spin heme signal appears at 235 K. Its intensity grows substantially at 253 K, and the spectrum is displayed in Figure 4. (The features between $g = 2.57$ and $g = 2.25$ are probably not due to the rhombic Cu_B, because the latter displays a distinctively small hyperfine coupling (~100 Gauss).) Its g-values (2.57, 2.16, & 1.86) are almost identical

Figure 3. Relative concentrations of intermediates IIA, IIB, & III during incubation of a yeast cytochrome oxidase sample between 175 K and 193 K, deduced from the EPR intensity data shown in Figure 2. The conversion of the first, EPR-detectable '$3e^-$-reduced' intermediate into the second, EPR-silent one was assumed not to occur at these temperatures. EPR intensities of cytochrome *a* and Cu_A respectively had been normalized according to the full intensities developed at 253 K. This plot assumes a maximum development of 50% for the 'unusual' Cu_B signal. Species: intermediate IIA, (◆); intermediate IIB, (▶); and intermediate III, (●). The curves are drawn to guide the eye.

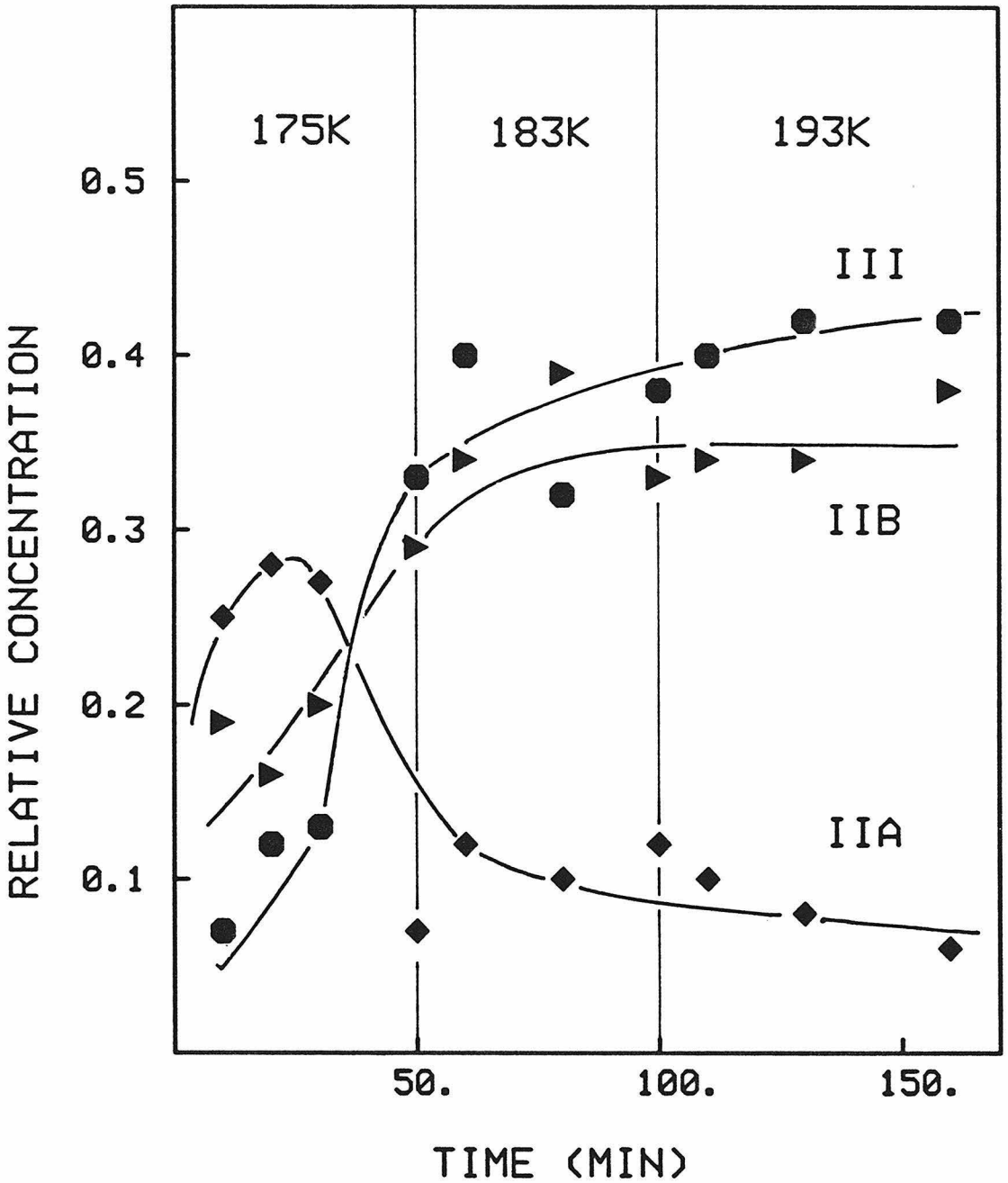
175K
183K
193K
III
IIB
IIA
0.5
0.4
0.3
0.2
0.1
RELATIVE CONCENTRATION
50.
100.
150.
TIME (MIN)

to those reported in the beef heart enzyme (7,19) by other researchers. The quantitation of the $g = 2.57$ absorption peak using the method of Aasa & Vänngård (25) shows that it accounts for 26% of the hemes when compared with the oxidized cytochrome *a* (quantitated by the $g = 2.98$ peak presented in the same spectrum). To our knowledge, this is the biggest yield of the low-spin hemes in cytochrome oxidase ever reported. The fact that this signal appears after the steep rise of the cytochrome *a* signal (between 223 K and 235 K) indicates that it is probably produced after a full cycle of reduction and reoxidation. The formation of this species suggests that the enzyme is further reduced by the excess of reductant in the solution, consistent with Scheme 5.

Mössbauer Study of the Reoxidation of Yeast Cytochrome Oxidase

The reoxidation intermediates of the fully reduced yeast oxidase were studied under similar conditions using Mössbauer spectroscopy. Two Mössbauer spectra that show the progress of reoxidation in the ^{57}Fe -enriched yeast cytochrome oxidase are displayed in Figure 5. These spectra were measured at 4.2 K. In Figure 5a, the CO-bound reduced sample that had been mixed with O_2 at $-20°C$ was photolyzed at 77 K. Figure 5b shows the spectrum of the same sample after initiating the reoxidation at 177 K for 10 min and then incubating the sample at 183 K for 1 h. The most noticeable difference in these spectra is the formation of a new doublet, which is indicated by the arrows. The difference spectrum (Figure 5c) indicates that the formation of the new component (component O) is accompanied by the loss of the high-spin ferrous cytochrome a_3 (component B). An intensity loss of the low-spin ferrous cytochrome *a* (component A) is also detected in the subtracted spectrum, indicating the partial reoxidation of cytochrome *a* at 183 K. The Mössbauer spectrum of the oxidized cytochrome *a* exhibits an anisotropic magnetic hyperfine structure at 4.2 K (*cf.* Chapter 2). Therefore it is smeared into the background and cannot be

Figure 4. EPR spectrum of a yeast cytochrome oxidase sample of which the reoxidation was initiated at 175 K and successively incubated at various temperatures between 183 K and 253 K. The final incubation was 10 min at 253 K. Conditions for EPR spectroscopy: microwave power, 0.02 mW; others, as in Figure 1.

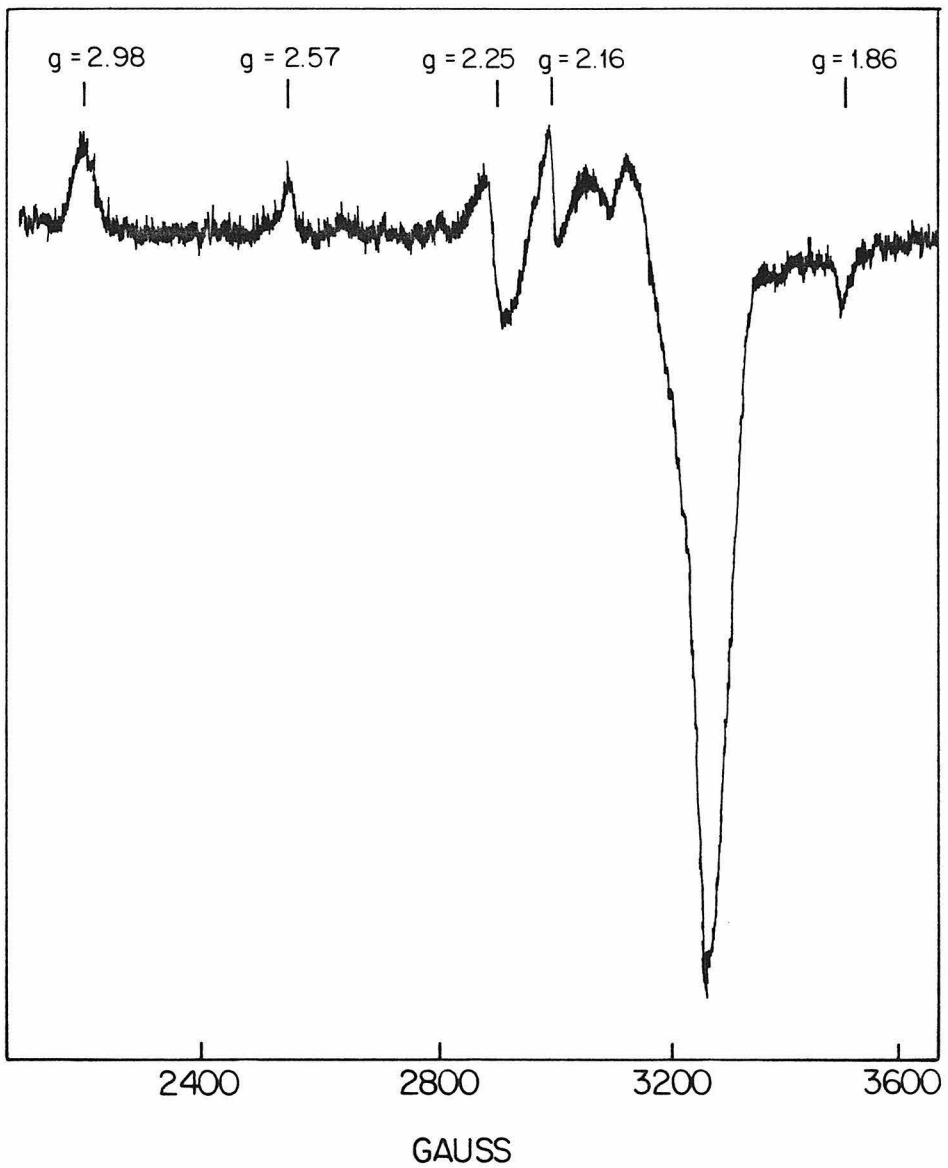
g = 2.98
g = 2.57
g = 2.25
g = 2.16
g = 1.86
2400
2800
3200
3600
GAUSS

distinguished in Figure 5.

The Mössbauer parameters of the component O ($\delta = 0.31$ mm/sec, $\Delta E_Q = 2.02$ mm/sec) are very similar to those of the compound III of cytochrome P-450 ($\delta = 0.31$ mm/sec, $\Delta E_Q = -2.15$ mm/sec), and other oxy-adducts of hemeproteins (26,27). It is therefore assigned to the intermediate I (or compound A), the O_2-adduct of ferrous cytochrome a_3. The stability of this intermediate at 183 K is probably due to the presence of CO, as has been discussed before.

Close examination of the high-spin ferrous component (B) in these two spectra shows that after incubation at 177 K and 183 K, the right-hand side peak seems to shift to the lower velocity. A concern thus arises about whether a high-spin ferrous intermediate could be generated during the reoxidation, whose Mössbauer parameters would be expected to be in the same region. Comparison of the high-spin ferrous component in the spectra measured after successive incubations at 177 K (spectrum not shown) and 183 K shows that the intensity decreases steadily. The right-hand side peak also shifts to lower velocity steadily. Therefore it can be most logically explained by the inhomogeneity of this component rather than by the formation of a new species.

In Figure 6, we compare two spectra measured at 100 K: One shows the effect of initiating the reaction with dioxygen at 177 K for 10 min, the other the effect of the following incubation at 183 K for 1 h. At 100 K, the electronic spin relaxation rate is fast enough to collapse the magnetic hyperfine structure of the low-spin cytochrome a^{3+} into a quadrupolar doublet. The position of this doublet, $\delta = 0.23$ mm/sec, $\Delta E_Q = 1.99$ mm/sec (*cf.* Chapter 2), is marked as D in Figure 6. It should be pointed out that the pair of sharp peaks that appears near the doublet D is actually the oxy-adduct of cytochrome a_3 (component O), with slightly different Mössbauer parameters (δ=0.31 mm/sec, ΔE_Q=2.02 mm/sec). The difference in the amount of oxidized cytochrome a between Figure 6a and 6b is difficult to assess due to the presence of the

Figure 5. 4.2 K Mössbauer spectra of an ^{57}Fe enriched yeast cytochrome oxidase sample of which the reoxidation reaction with dioxygen was studied by the 'triple-trapping' technique: (a) after photolysis at 77 K; (b) after 1 hr incubation at 183 K (the reaction was initiated and incubated for 10 min at -175 K); (c) the subtraction of (a) from (b). A 320 Gauss perpendicular field was used in the measurements. Three doublets that are marked are the spectrum of: A, the reduced low-spin cytochrome; B, the reduced high-spin cytochrome; C, the cytochrome a_3^{2+}–CO complex. The parameters of these three doublets are obtained from Chapter 3.

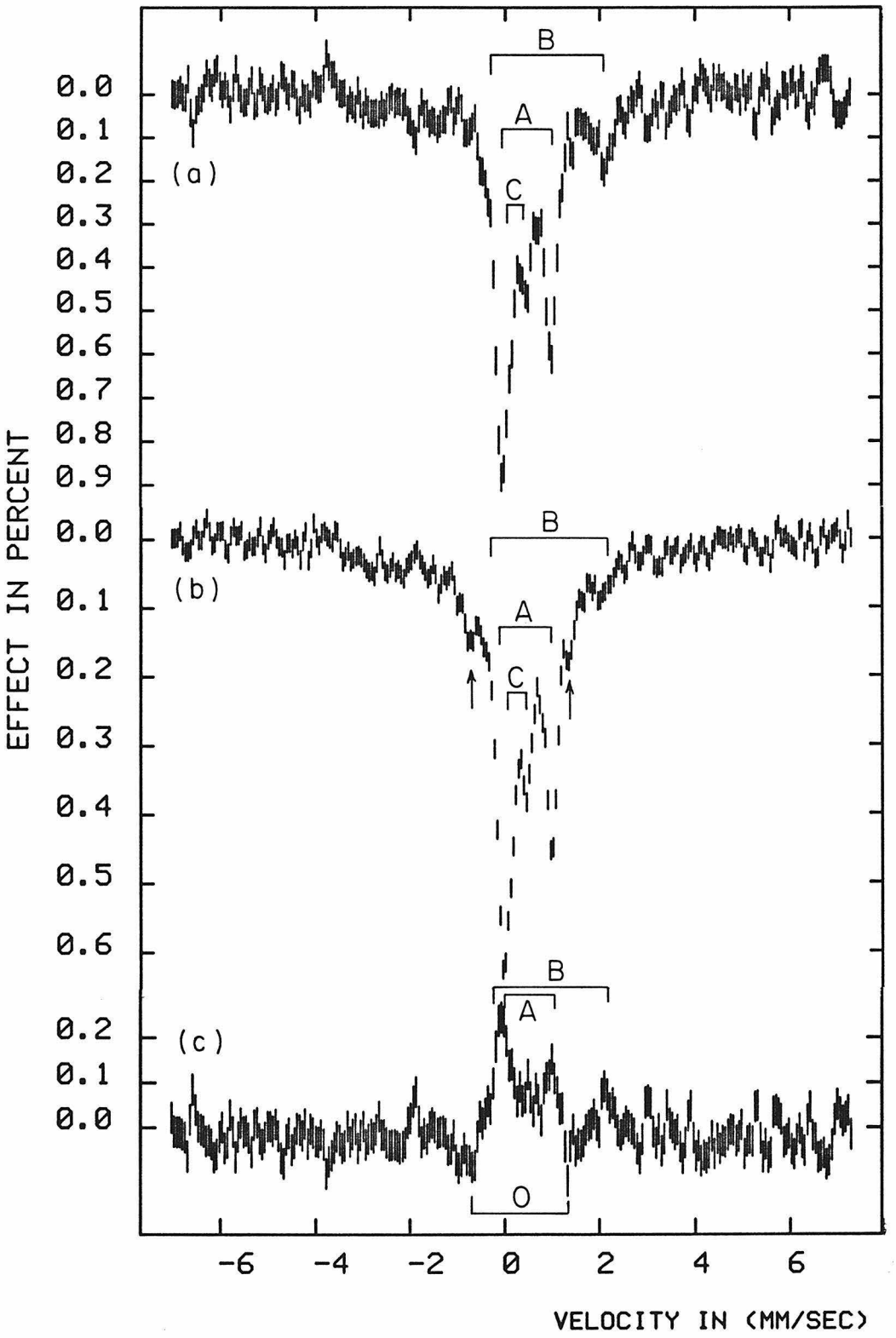
B
A
C
(a)
0.0
0.1
0.2
0.3
0.4
0.5
0.6
0.7
0.8
0.9
B
A
C
(b)
0.0
0.1
0.2
0.3
0.4
0.5
0.6
B
A
(c)
0.2
0.1
0.0
O
EFFECT IN PERCENT
-6
-4
-2
0
2
4
6
VELOCITY IN (MM/SEC)

oxy-adduct. Interestingly, there seems to be a peak around −1.3 mm/sec in Figure 6b (marked by an arrow). At present, we cannot rule out the possibility that this is an artifact due to the poor statistics of the data. However, if this peak is a true signal, given a reasonable limit for the quadrupole splitting such as 2 mm/sec, it suggests the presence of an iron species with an isomer shift between 0 and −1 mm/sec. This region of isomer shift is found only for the ferryl Fe^{IV} ions (*cf.* Figure 2 of Chapter 2).

Such a potential signal should be very interesting to watch. If it is confirmed to be a ferryl intermediate, it would be very useful in testing the model of two '$3e^-$-reduced' intermediates proposed by Blair *et al.* (19). Unfortunately, the statistics of our data were poor. Given the valuable information about the mechanism of dioxygen reduction that cannot be gained by other methods, the experiments should be pursued further.

DISCUSSION

The detection of the 'unusual' Cu_B^{2+} and the low-spin cytochrome a_3^{3+} by EPR spectroscopy demonstrates that the oxygen binding site of the yeast cytochrome oxidase follows a very similar mechanism to that of beef heart cytochrome oxidase when reoxidized with dioxygen. Indeed, the correlation of the intensities of three EPR signals, namely, the 'unusual' Cu_B, Cu_A, and cytochrome *a* signals, between 177 K and 183 K, can be explained quite successfully by the 3-level, 4-intermediate mechanism (*cf.* Scheme 1) that has been previously observed in the beef heart enzyme by Clore *et al.* (15) and Blair *et al.* (19). The current study also agrees with them that the oxidation of Cu_A following that of cytochrome *a* is fast and that the oxidation of cytochrome *a* following that of Cu_A is rather slow. This result suggests that when the third electron is transferred from Cu_A to the a_3 site, the enzyme is changed into a conformation that makes the transfer of the fourth electron from cytochrome *a*

Figure 6. 100 K Mössbauer spectra of an ^{57}Fe enriched yeast cytochrome oxidase sample of which the reoxidation reaction with dioxygen was studied by the 'triple-trapping' technique: (a) after the reaction initiation and incubation for 10 min at 177 K; (b) after 1 hr incubation at 183 K after (a). A 320 Gauss perpendicular field was used in the measurements. Doublets that are marked are the spectrum of: A, the reduced low-spin cytochrome; B, the reduced high-spin cytochrome; C, the cytochrome a_3^{2+}–CO complex; D, the oxidized cytochrome a (measured at 200 K). The parameters of these doublets are obtained from Chapters 2 and 3.

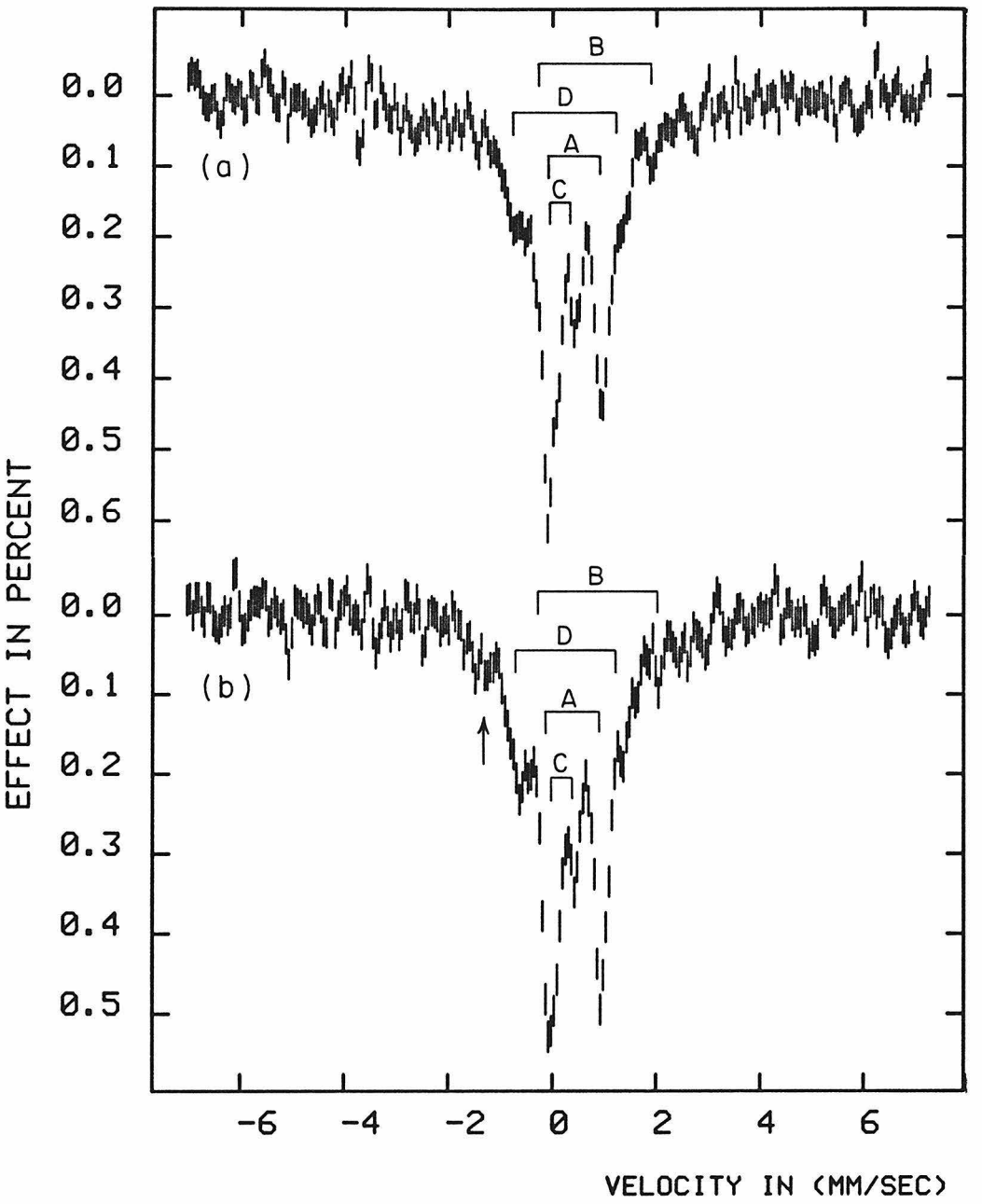
B
D
A
C
(a)
0.0
0.1
0.2
0.3
0.4
0.5
0.6
B
D
A
C
(b)
0.0
0.1
0.2
0.3
0.4
0.5
EFFECT IN PERCENT
-6
-4
-2
0
2
4
6
VELOCITY IN (MM/SEC)

more difficult. Furthermore, this study agrees with the observation of Blair *et al.* that in such a molecule, a '$3e^-$-reduced' intermediate at the a_3 site converts itself into a second intermediate without further reduction by electrons from the other sites. This process is significantly slowed down in 50% glycerol solution relative to that in 40% ethylene glycol solution (19), consistent with the notion that it is linked with a conformational change.

The branching ratio for the transfer of the third electron to the a_3 site is different in this study from the previous studies of the beef heart enzyme. Roughly 60% of the yeast enzyme molecules are estimated to go through intermediate IIA (with cytochrome *a* oxidized) and 40% through IIB (with Cu_A oxidized), compared to 30% and 70%, respectively, in beef heart; as a result, only ~40% of the enzyme molecules are expected to go through the second '$3e^-$-reduced' intermediate.

Structures for the two '$3e^-$-reduced' intermediates have been proposed by Blair *et al.* (19). It would be most interesting if this model could be tested by Mössbauer spectroscopy. The proposed structures have been shown in Scheme 3. First, EPR-detectable intermediate, cytochrome a_3 is proposed to be a ferrous ion liganded by a peroxo-bridge (to Cu_B). Due to the unusual saturation properties of Cu_B signal, the iron is required to be in either an $S = 2$ or an $S = 1$ spin state. We did observe a high-spin ferrous ion in the Mössbauer spectrum. However, its concentration decreases after the incubation at 183 K, rather than increases as expected from the EPR results (*cf.* Figure 2). Therefore it is probably due to the inhomogeneity of reduced high-spin cytochrome a_3. On the other hand, the Mössbauer parameters of the intermediate spin ferrous ion has not been reported in proteins. However, a few $S = 1$ inorganic porphyrin ferrous complexes have been studied (28). At 4.2 K, their isomer shifts ranged from 0.48 to 0.59 mm/sec and quadrupole splitting from 1.51 to 2.70 mm/sec. The only new, distinguishable signal that appeared upon

the sample incubation at 183 K was component O (δ= 0.31 mm/sec, ΔE_Q= 2.02 mm/sec) in Figure 5, which has been assigned to the oxy-adduct of cytochrome a_3 (intermediate I). The isomer shift of component O may be low for the proposed '$3e^-$-reduced' ferrous hydroperoxide intermediate (*cf.* Figure 2 of Chapter 2). However, since the isomer shifts observed in proteins are generally lower than those in inorganic complexes, the possibility that component O is the '$3e^-$-reduced' ferrous hydroperoxide intermediate cannot be ruled out.

The proposed structure for the second '$3e^-$-reduced' intermediate involves a ferryl ion. It is predicted from EPR results to exist in substantial quantity only above 206 K. Therefore the suspected presence of ferryl ions at 183 K (Figure 6b) is surprising. However, it is not possible to derive a decisive conclusion on this matter at present since the statistics of the data are quite limited.

In this study, we have shown the potential of using Mössbauer spectroscopy to complement the EPR studies of the reoxidation mechanism of cytochrome oxidase. Mössbauer spectroscopy would be most useful in the identification of the two '$3e^-$-reduced' intermediates. Although the yields of these intermediates are somewhat limited in yeast cytochrome oxidase, their production trends at different temperatures are well predicted by EPR results. The special range of Mössbauer parameters that is generally observed for the ferryl ions is especially convenient for the Mössbauer measurements at a temperature around 100 K.

REFERENCES

1. Wikström, M., Krab, K., and Saraste, M. (1981). *Cytochrome Oxidase: A Synthesis*, Academic Press, London.
2. Malmström, B.G. (1974). *Quart. Rev. Biophys.* **6**, 389–431.
3. Malmström, B.G. (1982). *Ann. Rev. Biochem.* **51**, 21–59.
4. Blair, D.F., Martin, C.T., Gelles, J., Wang, H., Brudvig, G.W., Stevens, T.H., and Chan, S.I. (1983). *Chemica Scripta* **21**, 43-53.
5. Vik, S.B. & Capaldi, R.A. (1980). *Biochem. Biophys. Res. Commun.* **94**, 348–354.
6. Beinert, H. & Shaw, R.W. (1977). *Biochim. Biophys. Acta* **462**, 121–130.
7. Aasa, R., Albracht, S.P.J., Falk, K.-E., Lanne, B., & Vänngård, T. (1976). *Biochim. Biophys. Acta* **422**, 260–272.
8. Reinhammar, B., Malkin, R., Jensen, P., Karlsson, B., Andréasson, L.-E., Aasa, R., Vänngård, T., & Malmström, B.G. (1980). *J. Biol. Chem.* **255**, 5000–5003.
9. Karlsson, B. & Andréasson, L.-E. (1981). *Biochim. Biophys. Acta* **635**, 73–80.
10. Shaw, R.W., Hansen, R.E., & Beinert, H. (1978). *J. Biol. Chem.* **253**, 6637–6640.
11. Dunham, W.R., Sands, R.H., Shaw, R.W., & Beinert, H. (1983). *Biochim. Biophys. Acta* **748**, 73–85.
12. Armstrong, F., Shaw, R.W., and Beinert, H. (1983). *Biochim. Biophys. Acta* **722**, 61–71.
13. Brunori, M., Colosimo, A., Rainoni, G., Wilson, M.T., & Antonini, E. (1979). *J. Biol. Chem.* **254**, 10769–10775.
14. Chance, B., Saronio, C., & Leigh, J.S., Jr. (1975). *J. Biol. Chem.* **250**, 9226–9237.
15. Clore, G.M., Andreasson, L.E., Karlsson, B., Aasa, R., & Malmstrom, B.G.

(1980). *Biochem. J.* **185**, 139–154.

16. Chance, B., Saronio, C., Leigh, J.S., Jr., Ingeldew, W.J., & King, T.E. (1978). *Biochem. J.* **171**, 787–798.
17. Brudvig, G.W., Stevens, T.H., & Chan, S.I. (1980). *Biochemistry* **19**, 5275–5285.
18. Karlsson, B., Aasa, R., Vänngård, T., & Malmstöm, B.G. (1981). *FEBS Lett.* **131**, 186–188.
19. Blair, D.F., Witt, S.N., & Chan, S.I. (1985). *J. Amer. Chem. Soc.* **107**, 7389–7399.
20. Fiamingo, F.G., Altschuld, R.A., Moh, P.P., & Alben, J.O. (1982). *J. Biol. Chem.* **257**, 1639–1650.
21. Sharrock, M. & Yonetani, T. (1977). *Biochim. Biophys. Acta* **462**, 718–730.
22. Babcock, G.T., Jean, J.M., Johnston, L.N., & Woodruff, W.H. (1985). *J. Bioinorg. Chem.* **23**, 243–251.
23. Clore, G.M., Andreasson, L.E., Karlsson, B., Aasa, R., & Malmstrom, B.G. (1980). *Biochem. J.* **185**, 155–167.
24. van Gelder, B.F. (1966). *Biochim. Biophys. Acta* **118**, 36–46.
25. Aasa, R. & Vänngård, T. (1975). *J. Mag. Res.* **19**, 308–315.
26. Sharrock, M., Münck, E., Debrunner, P.G., Marshall, V., Lipscomb, J.D., & Gunsalus, I.C. (1973). *Biochemistry* **12**, 258–265.
27. Schulz, C.E., Rutter, R., Sage, J.T., Debrunner, P.G., & Hager, L.P. (1984). *Biochemistry* **23**, 4743–4754.
28. Dolphin, D., Sams, J.R., Tsin, T.B., & Wong, K.L. (1976). *J. Amer. Chem. Soc.* **98**, 6970–6975.

CHAPTER 5

SPECTROELECTROCHEMICAL STUDY OF CO-INHIBITED CYTOCHROME OXIDASE FROM BEEF HEART AND BAKER'S YEAST

INTRODUCTION

The redox properties of cytochrome oxidase have been actively studied in the last 20 years (1–12), the reason being that the thermodynamic properties of the four metal centers are likely to shed significant insights into how electrons are transferred within the enzyme and hence the mechanism of the reduction of dioxygen to water. In spite of a great number of investigations, the present picture of the redox thermodynamics of the oxidase remains confused or incomplete. One source of confusion arises from anticooperative interactions among the metal centers within the enzyme. As far back as 1965, Minnaert (1) measured the midpoint potential of cytochrome *a* to be 278 mV vs. NHE*. However, the titration behavior of cytochrome *a* was not that expected for a Nernstian $n = 1$ (one-electron acceptor) site; the observed Nernst slope was close to $n = 0.5$. It was subsequently realized that cytochrome *a* and a_3 interact anticooperatively (11,13,14). A similar interaction between cytochrome *a* and Cu_B was reported recently (12). In such a situation, a departure from simple Nernstian behavior is predicted (13,14).

* The abbreviations used are: NHE, normal hydrogen electrode; SCE, saturated calomel electrode; EPR, electron paramagnetic resonance.

We (Chan and Gray laboratories in Caltech) undertook an extensive study of cytochrome oxidase, mostly of the beef heart enzyme, by spectroelectrochemical methods. We studied the redox properties of cytochrome *a* (15) and Cu_A (16) first by employing CO to inhibit the a_3 site (cytochrome a_3 and Cu_B), thereby eliminating many possibe intersite interactions. (Theoretically, as many as 11 different interaction terms could in principle be required to parameterize all of the possible thermodynamic interactions among 4 sites.) By computer fits of the data to a two-site interaction model, we located a previously unsuspected interaction between cytochrome *a* and Cu_A. We then proceeded to examine the cytochromes in the more complicated native enzyme (17) by the deconvolution method developed by Blair *et al.* (18). Both the studies on the CO-inhibited and the native enzyme were carried out under a wide range of temperature, pH, and ionic strength. The results of these studies are relevant to questions such as whether the site under observation undergoes significant conformation change during oxidoreduction, whether the site, especially cytochrome *a* or Cu_A, is involved in proton pumping, and whether the site is accessible to solvent. Obviously these questions are very important in understanding the biological function of the enzyme. This thesis, however, will restrict itself to the topics that are related to the findings on yeast cytochrome oxidase. Readers interested in other aspects of the investigation are referred to the papers (15–17) as well as theses by Blair (19) and Ellis (20).

Topics that will be presented in this chapter are as follows: a two-site interaction model, which is the basis of the data treatment; the verification of such an interaction between cytochrome *a* and Cu_A in the beef heart enzyme; the comparison of the redox bahavior of yeast and beef heart cytochrome *a*; and a proposed process that describes the inactivation of both beef heart and yeast cytochrome oxidase. One important consequence of the interaction model is that the conventionally defined midpoint potential does not reflect the intrinsic

properties of the monitored site (17). The higher asymptotic potential determined via computer fits, which pertains when the interaction partner(s) are oxidized, is reported instead throughout this work. CO is employed in the work on yeast enzyme, not only because this method simplifies the intersite interaction but also because it is prerequisite to the understanding of the native enzyme.

As we have demonstrated by Mössbauer spectroscopy in the previous chapters, yeast oxidase is very inhomogeneous. A reliable analysis thus can not be obtained until the properties of the constituents are understood. Mössbauer studies on the native enzyme (Chapter 2), in either the resting oxidized or the reduced form, indicate that an intrinsic fraction of cytochrome a_3 is in a reduced low-spin state. Evidence shows that this may be a denatured conformation of cytochrome a_3. In Chapter 3, it is established that CO reacts with both the reduced high-spin cytochrome a_3 and the reduced low-spin cytochrome a_3. Therefore by monitoring the visible spectrum of the CO-inhibited enzyme, we are examining cytochrome a only. However, the Mössbauer spectrum of the CO-bound reduced enzyme (*cf.* Chapter 3) also indicates the presence of a high-spin ferrous ion that is not bound to CO. This species is likely to be the cytochrome a of degraded enzyme molecules of which the cytochrome a_3 assumes a low-spin state, as has been described above. It is therefore important to isolate this species from our measurements on the low spin cytochrome a. It turns out that this species has rather different spectral properties and a much lower reduction potential. By selecting the monitoring wavelength and the observation potential range judiciously, we were able to obtain accurate measurements on yeast cytochrome a in a fresh sample. A few other minor contaminants were also detected in the low-potential range. They are well-separated in potential from the normal functioning yeast cytochrome a, so the accuracy of the present analysis of cytochrome a is not affected.

MATERIALS AND METHODS

Enzyme Preparations

Beef heart cytochrome oxidase was purified from mitochondria by the method of Hartzell & Beinert (21). Yeast cytochrome oxidase was purified as described in Chapter 1. Both enzymes were stored frozen at −80 °C. Protein concentration was determined by the method of Lowry *et al.* (22). The heme *a* concentration of the beef heart oxidase was determined by the reduced-minus-oxidized extinction of the uninhibited enzyme at 604 nm using an extinction coefficient of 12 mM^{-1} cm^{-1} (23). The heme *a* concentration of yeast oxidase was determined by using an extinction difference of 16.5 mM^{-1} cm^{-1} between 600 nm and 630 nm for the uninhibited reduced enzyme (24). Just prior to use, the enzyme was thawed and dialyzed into potassium phosphate buffer at pH 7.0 (ionic strength 0.245 M) containing 0.5%Tween-20. Phosphate buffer was used because the pH of phosphate is relatively insensitive to temperature. Following dialysis, samples were centrifuged at 27,000×*g* for 20 minutes to remove insoluble material. Enzyme concentrations were typically 0.10–0.15 mM for thin-layer experiments and 40 μM for 2-cm path-length experiments.

All buffer solutions were prepared with glass-distilled water and research-grade reagents. The following redox mediators were added: hexaammineruthenium trichloride, obtained from Alfa and purified by the method of Pladziewicz *et al.* (25); pentaammine(pyridine)ruthenium perchlorate, prepared as described previously by Cummins & Gray (26); (hydroxymethyl)ferrocene, obtained from Strem Chemicals; 1,1'-bis(hydroxymethyl)ferrocene, obtained from Research Organic/Inorganic Chemical Corp. The above mediators (see Table 1) were selected because they have a negligible absorbance in the 400–900 nm region at the concentration used and have reduction potentials that allow the solution potential to be poised from −50 to 550 mV vs. NHE. Equilibrium

dialysis experiments indicate that these mediators do not bind strongly to the enzyme.

Spectroelectrochemistry Apparatus

Two types of electrode cells were employed in the study of cytochrome oxidase: (1) a thin-layer cell (path-length *ca.* 0.47 mm), for the investigation of the visible and Soret regions; (2) a long-path cell (path-length 2 cm), for the near infrared (NIR) region. They were machined from lucite and employed quartz windows. A Sargent-Welch S-30080-17 miniature saturated calomel reference electrode (SCE) was used along with a platinum wire counter electrode. For the thin-layer cell, the working electrode consisted of two pieces of 500 lines/in. electroformed gold mesh (Buckbee-Mears Co., Minneapolis MN) soldered to 18-gauge copper wire. For the long-path cell, the working electrode was a thin gold foil that lined the bottom and the sides of the cell, and the sample was stirred by a magnetic stirring bar. The cell assembly was contained in a gas-tight stainless steel shroud in order to maintain strict anaerobicity. By assaying the stability of nitrogenase and chromous ion, which are both extremely sensitive to reaction with dioxygen, it was verified that oxygen leakage into the sample chamber was negligible (below the limit of detection) for a period of at least one week. Sample temperatures were varied with a Forma Model 2095 constant temperature bath and measured directly ($\pm 2°C$) with a miniature copper-constantan thermocouple (Omega) placed in the protein solution in close proximity to the cavity of the cell. After 3–4 hours of equilibration, the long-path cell became an isothermal cell (27); i.e., the sample solution and the reference electrode were thermostated at the same temperature; the reference electrode of the thin-layer cell was partially thermostated, so that it was neither an isothermal nor a nonisothermal cell. Detailed design of the cell assemblies is described in Ref. (20).

Table 1. Redox Mediators Employed in the Study of Cytochrome Oxidase

mediator	$E^{\circ\prime}$(mV vs. NHE)	no. of equiv. A	B
$[Ru(NH_3)_6]Cl_3$	51	1.0	5.0
$[Ru(NH_3)_5py](ClO_4)_3$	260	1.0	5.0
(hydroxymethyl)ferrocene	405	0.5	2.5
1,1′-bis(hydroxymethyl)ferrocene	465	0.5	2.5

[A] Thin-layer experiments.

[B] Long-path experiments.

A Princeton Applied Research Model 174A potentiostat was used to control the potentials applied across the protein solutions, which were measured (±0.1 mV) with a Keithley Model 177 microvolt digital multimeter. Absorption spectra in the visible and NIR region were obtained with a Cary 219 spectrophotometer (0.55 nm spectral bandwidth) interfaced to a Spex Industries SCAMP SC-31 data processor.

EPR Spectroscopy

EPR spectra were recorded on a Varian E-line Century Series X-band spectrometer operating in the absorption mode. The modulation amplitude was 16 Gauss and the modulation frequency 100 kHz. Sample temperature was controlled with an Air Products Heli-Tran cryostat. The temperature at the sample position was measured before and after spectra were acquired, using a gold-chromel thermocouple in a glycerol-filled EPR tube. Other conditions will be stated in the figure legend.

Methods

After the addition of redox mediators, enzyme and buffer solutions were thoroughly degassed on a vacuum-line and subsequently allowed to stir under one atmosphere of CO (99.99%, Matheson) for at least 30 minutes. The CO-saturated solution, cell, electrodes, and shroud were then transferred into an inert atmosphere box where the cell was loaded, fitted with the reference and auxiliary electrodes, and placed into the shroud. A specially constructed aluminum mount was used to support the shroud in the spectrophotometer sample compartment.

Enzyme/mediator solutions were poised at −200 mV vs. SCE until no further change occurred in the absorbance at either 443 nm (thin-layer experiments) or at 604 nm (long-path experiments). Titrations were then carried out by sequentially increasing the potential at a series of intervals to the highest po-

tential and rereduction in a staggered series of intervals. The highest potential for the titration of beef heart oxidase was 140 mV and for that of yeast oxidase was 190 mV (both are vs. SCE) to avoid oxidation of the Fe_{a_3}/Cu_B site. The higher limit was used for yeast oxidase because yeast cytochrome *a* has a reduction potential roughly 50 mV higher than that of beef heart. Slow oxidation of CO and the a_3 site in yeast oxidase did not take place at this potential, as judged by the temporal behavior of the absorbance at 443 nm. Each potential was maintained, typically for 1 hour in the thin-layer experiments and more than 2 hours in the long-path experiments, until electrolysis ceased (verified by cessation of spectral change at the monitoring wavelength). Assuming that equilibrium is established at each potential, the ratio of concentrations of oxidized to reduced forms (ox/red) of all redox couples in solution is then defined by the Nernst equation as follows:

$$E_{app} = E^{\circ\prime} + [2.303RT/n\mathcal{F}] \log (\text{ox/red}) \qquad (1)$$

where $E^{\circ\prime}$ is the reduction potential of the redox couple (the prime signifies that the present measurements were made near neutral pH). The total absorbance change accompanying oxidation was used in calculating log (ox/red) for the oxidative titration, and the total absorbance change accompanying rereduction was used in calculating log (ox/red) for the rereductive titration, thus partially compensating for irreversibility in the absorbance changes.

In order to avoid oxidation of the a_3 site, potentials above the above-mentioned limits were not applied to the sample solutions. Oxidation of the Fe_a and Cu_A was thus not complete at the highest potential used. A correction for this incomplete oxidation was applied in the following manner: The values for $E^{\circ\prime}$ that were estimated from the initial computer fits (*cf.* next section) were used to calculate the fraction of Fe_a or Cu_A that remained reduced at the highest potentials used. The corresponding absorbance difference was then added to the observed absorbance changes, to obtain a corrected fully oxidized end point.

By use of the corrected absorbance differences, new values of log (ox/red) were calculated, and new estimates of $E^{\circ\prime}$ were obtained from computer fits.

The calculated reduction potential is referenced to the normal hydrogen electrode (NHE) through the temperature dependence of the SCE (28):

$$E^{\circ}_{SCE}(T) = 244.4 - 0.66(T - 25), \qquad (2)$$

where T is temperature of the reference electrode in degrees Centigrade and $E^{\circ}_{SCE}(T)$ is the potential in millivolts of the SCE vs. NHE at T. At each potential, the absorbance spectrum, between 700 and 350 nm for thin-layer experiments or between 900 and 500 nm for long-path experiments, was recorded and stored on a magnetic diskette. Difference spectra were obtained by computer subtraction.

A Two-Site Interaction Model

The Nernst plots obtained from titrations of either chromophore, i.e., cytochrome *a* or Cu_A, of the CO-inhibited beef heart cytochrome oxidase, or cytochrome *a*, in the oxidase from baker's yeast, did not exhibit the slope expected for a one-electron acceptor. Malmström (13) and Cornish-Bowden & Koshland (29) have shown that this kind of behavior may be due to modulation of the reduction potential of the redox center under observation by interaction with one or more other sites in the enzyme. In the case of CO-inhibited cytochrome oxidase, the interaction is likely to occur between cytochrome *a* and Cu_A. Indeed, the behaviors of both Fe_a and Cu_A were well accounted for by postulating an anticooperative interaction between these sites that causes the reduction potential for one to decrease somewhat (by a quantity which shall be termed the interaction potential) upon the reduction of the other. We shall present evidence of the mutual interaction of Fe_a and Cu_A in the 'Results' section. Figure 1 shows the reaction scheme appropriate to the situation of Fe_a and Cu_A as well as a generalized two-site interaction model. In this model, $E_1^{\circ\prime}$

and $E_2^{\circ\prime}$ are the reduction potentials of site **1** and site **2** when their respective interaction partner(s) are oxidized, and ΔE is an interaction potential that measures the decrease in reduction potential of one site which accompanies the reduction of the other site.

The spectral quantitation of the oxidized and reduced forms of site **1** is therefore given by

$$\frac{\mathbf{1}^{\mathrm{ox}}}{\mathbf{1}^{\mathrm{red}}} = \frac{\mathbf{1}^{\mathrm{ox}}\mathbf{2}^{\mathrm{ox}} + \mathbf{1}^{\mathrm{ox}}\mathbf{2}^{\mathrm{red}}}{\mathbf{1}^{\mathrm{red}}\mathbf{2}^{\mathrm{ox}} + \mathbf{1}^{\mathrm{red}}\mathbf{2}^{\mathrm{red}}} \tag{3}$$

and similarly for site **2**. Implicitly assumed in this expression is that the extinction of one site in a specific oxidation state does not depend on the oxidation state of the other. In short, they are assumed not to be optically interactive. (No such interaction between Fe_a and Cu_A has been reported.) The relative concentrations of the four species involved are defined by the Nernst equations of the four subreactions. The equation that describes site **1** at an applied potential E in the interactive system can then be derived:

$$\begin{aligned}\log_{10}\frac{\mathbf{1}^{\mathrm{ox}}}{\mathbf{1}^{\mathrm{red}}} = {} & \frac{\mathcal{F}}{2.303RT}(E - E_1) + \log_{10}\bigl(1 + \exp[\frac{\mathcal{F}}{RT}(E_2 - E)]\bigr) \\ & - \log_{10}\bigl(1 + \exp[\frac{\mathcal{F}}{RT}(E_2 - E' - E)]\bigr).\end{aligned} \tag{4}$$

In this work, Eq.(4) was used in a nonlinear least-squares fitting program to calculate the best-fit values for the reduction potential of the chromophore under observation (Fe_a or Cu_A), that of its interaction partner, and ΔE. As will be shown in several figures, the Nernst plots of interacting sites approach $n = 1$ behavior at sufficiently high or low potentials. The higher asymptote defines the reduction potential when the partner is oxidized and the lower asymptote when the partner is reduced. The conventionally defined midpoint potential is

Figure 1. Two-site interaction schemes. (a) Proposed interaction scheme between cytochrome *a* and Cu_A in redox titrations of CO-inhibited cytochrome oxidase. (b) A generalized two-site interaction scheme.

(a)

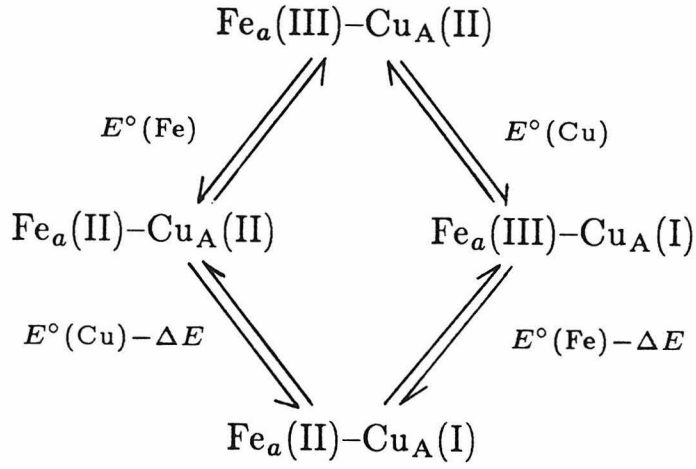
$Fe_a(III)$–$Cu_A(II)$
$E°(Fe)$
$E°(Cu)$
$Fe_a(II)$–$Cu_A(II)$
$Fe_a(III)$–$Cu_A(I)$
$E°(Cu)-\Delta E$
$E°(Fe)-\Delta E$
$Fe_a(II)$–$Cu_A(I)$

(b)

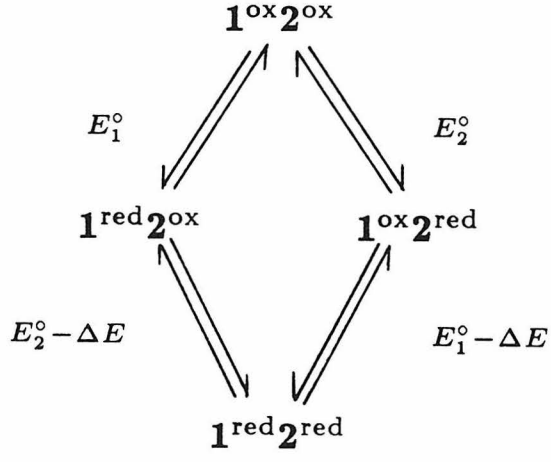
$\mathbf{1}^{ox}\mathbf{2}^{ox}$
E_1°
E_2°
$\mathbf{1}^{red}\mathbf{2}^{ox}$
$\mathbf{1}^{ox}\mathbf{2}^{red}$
$E_2^\circ-\Delta E$
$E_1^\circ-\Delta E$
$\mathbf{1}^{red}\mathbf{2}^{red}$

no longer useful as a measure of the intrinsic properties of the site, because the midpoint potential is sensitive not only to the properties of this site but to the potential of its interaction partner as well as the strength of the interaction (17). The two reduction potentials determined from the asymptotes, on the other hand, represent the well-defined physical situations. Due to the manner in which the experiments were carried out, i.e., oxidation followed by rereduction, the higher asymptotes are in general more accurately determined through computer fits and are presented here.

RESULTS

Thin-Layer Spectroelectrochemistry of Beef Heart Cytochrome a

Overlay difference spectra obtained in a typical experiment at 9.8°C are displayed in Figure 2. A linear relation between ΔA_{605} and ΔA_{443}, with a slope consistent with measurements of the reduced minus oxidized spectrum of cytochrome *a* (18,30) was observed (plot not shown), indicating that only cytochrome *a* is titrated at the potentials used. A Nernst plot of the spectral data is shown in Figure 3. Equilibration at each applied potential was determined from the absorbance change at 443 nm. The plot is not like that expected for a simple $n = 1$ Nernstian process (which, from Eq. 1, is a straight line with a slope of 56 mV/decade at 9.8°C). It is well described by the two-site anticooperative interaction model. The curve through the data points is the least-squares fit of Eq. 4. From this fit, cytochrome *a* has a reduction potential of 290 mV and is found to participate in an anticooperative interaction of magnitude 24 mV with another site. The redox potentials of cytochrome *a* and of its interaction partner determined from this experiment are listed in Table 2. We should note, however, that the interaction potential varied between *ca.* 20 and 40 mV in different batches.

Figure 2. Representative set of absorbance difference spectra of beef heart cytochrome *a* at different applied potentials in a thin-layer spectroelectrochemical titration of CO-inhibited cytochrome oxidase. Conditions: sample temperature 9.8°C, SCE temperature 16°C (because of partial thermostating, *cf.* Materials and Methods), pH 7.0, ionic strength 0.245 M. Applied potentials (mV vs. SCE): (A) −220, (B) −100, (C) −70, (D) −40, (E) −25, (F) −10, (G) 5, (H) 20, (I) 35, (J) 50, (K) 65, (L) 80,(M) 95, (N) 110, and (O) 140. The most oxidized spectrum (measured at 140 mV vs. SCE) has been subtracted from the spectra recorded at each potential to yield the difference spectra shown.

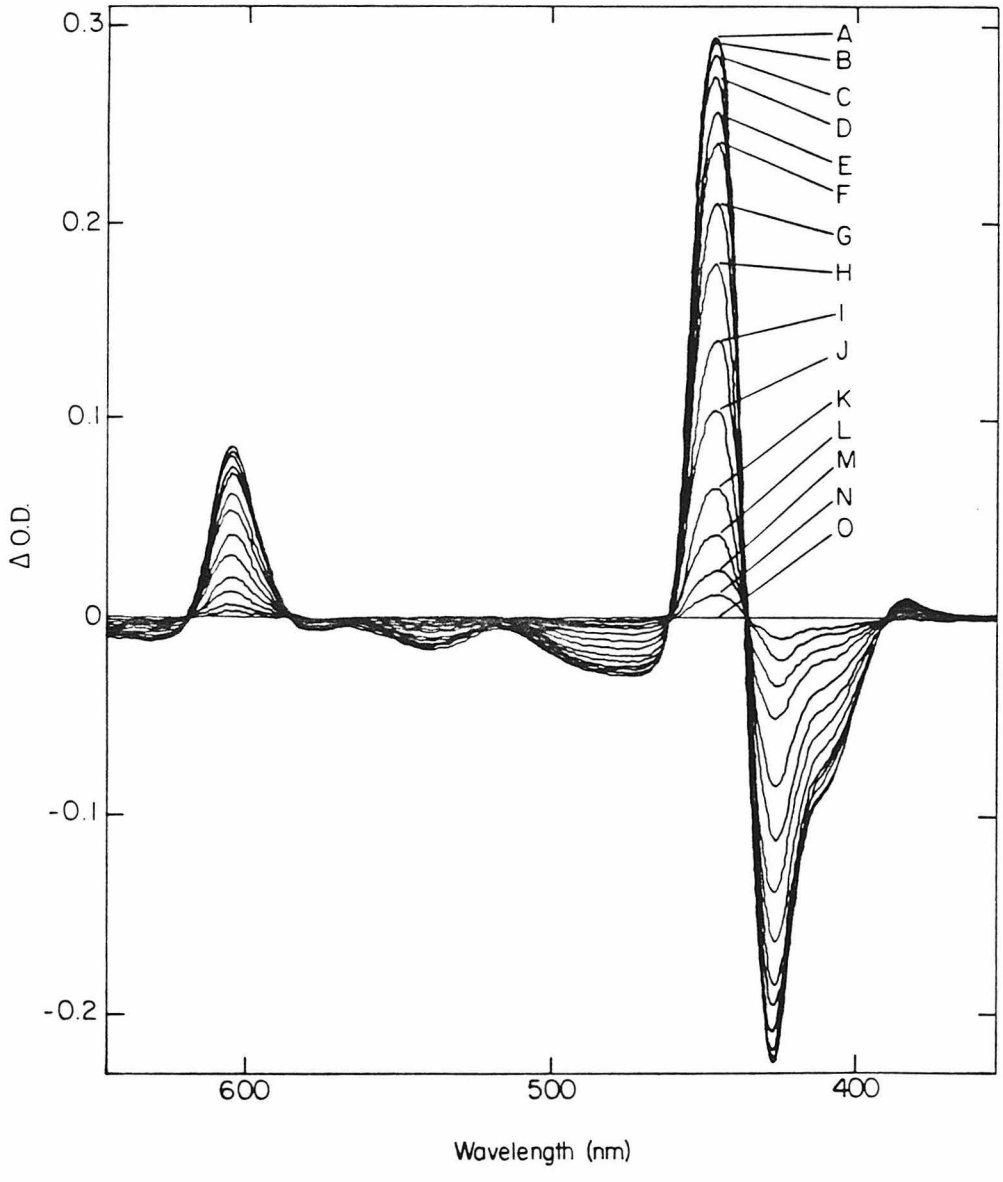
0.3
0.2
0.1
0
-0.1
-0.2
ΔO.D.
600
500
400
Wavelength (nm)
A
B
C
D
E
F
G
H
I
J
K
L
M
N
O

Figure 3. Nernst Plot Calculated from the spectra shown in Figure 2 by using ΔA_{443}. The solid line is the computer-generated best fit to a model described in the text. Solid squares and open squares correspond to spectra obtained during the oxidation and rereduction respectively.

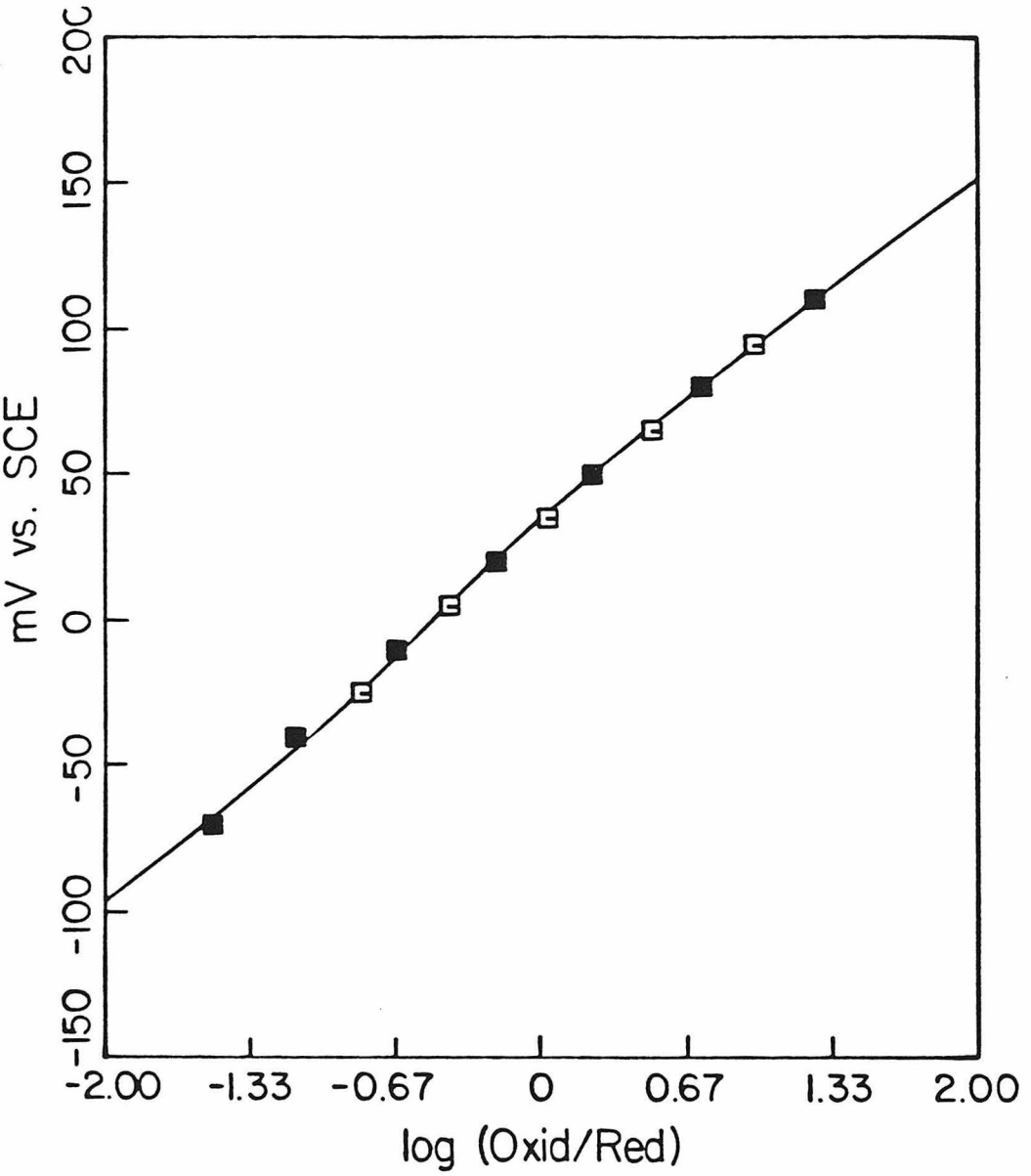
mV vs. SCE
200
150
100
50
0
-50
-100
-150
-2.00
-1.33
-0.67
0
0.67
1.33
2.00
log (Oxid/Red)

Table 2. Representative Non-Linear Least-Square Fits of Spectroelectrochemistry Data of CO-inhibited Cytochrome Oxidase[†,‡]

Species	Cell*	Temp °C	Wavelength nm	$E_1^{\circ\prime}$ mV	$E_2^{\circ\prime}$ mV	ΔE mV
Beef Heart						
Cyt *a*	TL	9.8	443	290 ± 1	262 ± 7	24 ± 2
Cyt *a*	LP	6.0	604	321 ± 2	312 ± 6	39 ± 2
Cu_A	LP	6.0	830	319 ± 2	321[§]	41 ± 3
Baker's Yeast						
Cyt *a*	TL	10.0	602	336 ± 2	344 ± 7	42 ± 2

† Potentials are referenced to NHE. pH 7.0, ionic strength 0.245 M.

‡ $E^{\circ\prime}$ refers to the upper asymptotic potential obtained from the fits to the Nernst plots, which is the potential that pertains when the partner is oxidized.

* TL: thin-layer; LP: long-path.

§ Determined from the cytochrome *a* fit in the same experiment.

Long-Path Spectroelectrochemistry of Beef Heart Cytochrome a and Cu_A

In long-path experiments, spectra between 900 and 500 nm were recorded. Thus we obtained the difference spectrum that covered the α band at ~600 nm of the cytochrome *a* and the broad 830 nm band of Cu_A. This method provided a unique opportunity to investigate both metal centers at the same time. It enabled us to test the model of interaction between Fe_a and Cu_A and to avoid any confusion arising from batch and sample differences.

Displayed in Figure 4 are overlay difference spectra in the α band region obtained in a typical titration at 6°C. Equilibration at each applied potential was determined from the absorbance change at 604 nm, and the Nernst plot is shown in Figure 5. The data certainly do not follow $n = 1$ behavior. They were fitted to Eq. 4 by the least-squares method with $E_1^{\circ\prime}$, $E_2^{\circ\prime}$, and ΔE floating freely. The best fit determined the reduction potential of cytochrome *a* to be 321 mV vs.NHE and the interaction potential with its partner to be 39 mV.

Corresponding absorbance difference spectra in the NIR region are displayed in Figure 6. The spectra indicate that the titration is very nearly reversible except for minor base-line drift. The redox state of Cu_A was monitored by the intensity of the absorption band centered at 830 nm. The bulk of available evidence indicates that this band is due almost entirely to Cu_A (31,32). The intensity was measured as the area under the curves and above a straight line connecting the data points at 900 and 740 nm; this method compensates for changes in base-line slope and offset.The difference spectrum obtained during the high-potential half of the titration (140 to 35 mV) was not significantly different from that obtained during the low-potential half of the titration (35 to −200 mV) (spectra not shown), indicating that the properties of the chromophore did not change during the course of the titration. A change in the shape of the spectrum would be expected, for example, if reduction of cytochrome *a*, whose reduction potential is close to that of Cu_A under these

Figure 4. Absorbance difference spectra in the α band region obtained during a long-pathlength spectroelectrochemical titration of CO-inhibited beef heart cytochrome oxidase at 6°C. pH was at 7.0 and ionic strength 0.245 M. The indicated potentials are relative to SCE; all spectra are referenced to the spectrum of the fully reduced enzyme obtained at a potential of −200 mV.

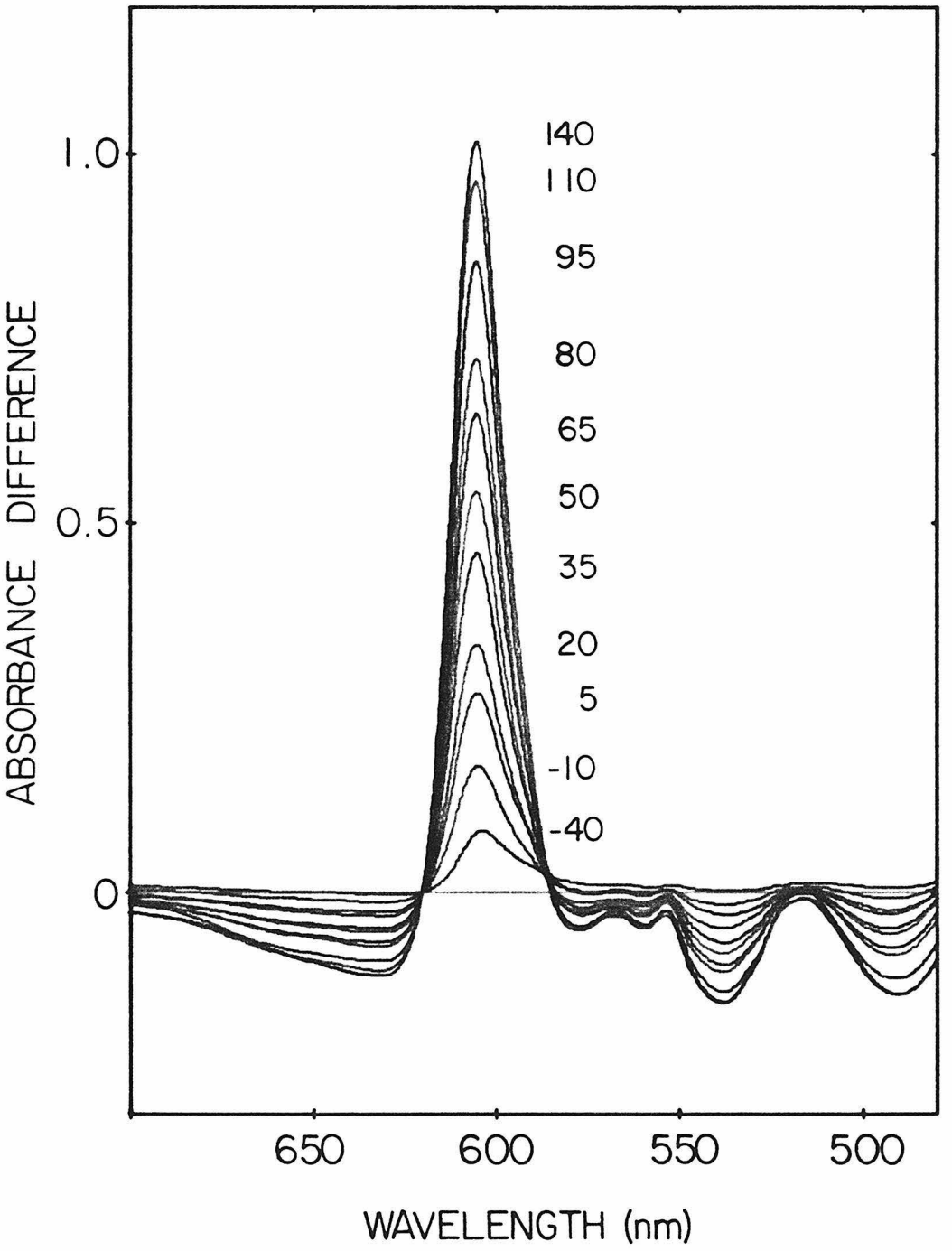
1.0
0.5
0
ABSORBANCE DIFFERENCE
140
110
95
80
65
50
35
20
5
-10
-40
650
600
550
500
WAVELENGTH (nm)

Figure 5. Nernst Plot Calculated from the spectra shown in Figure 4 by using ΔA_{604}. The solid line is the computer-generated best fit to a model described in the text. Solid squares and open squares correspond to spectra obtained during the oxidation and rereduction respectively.

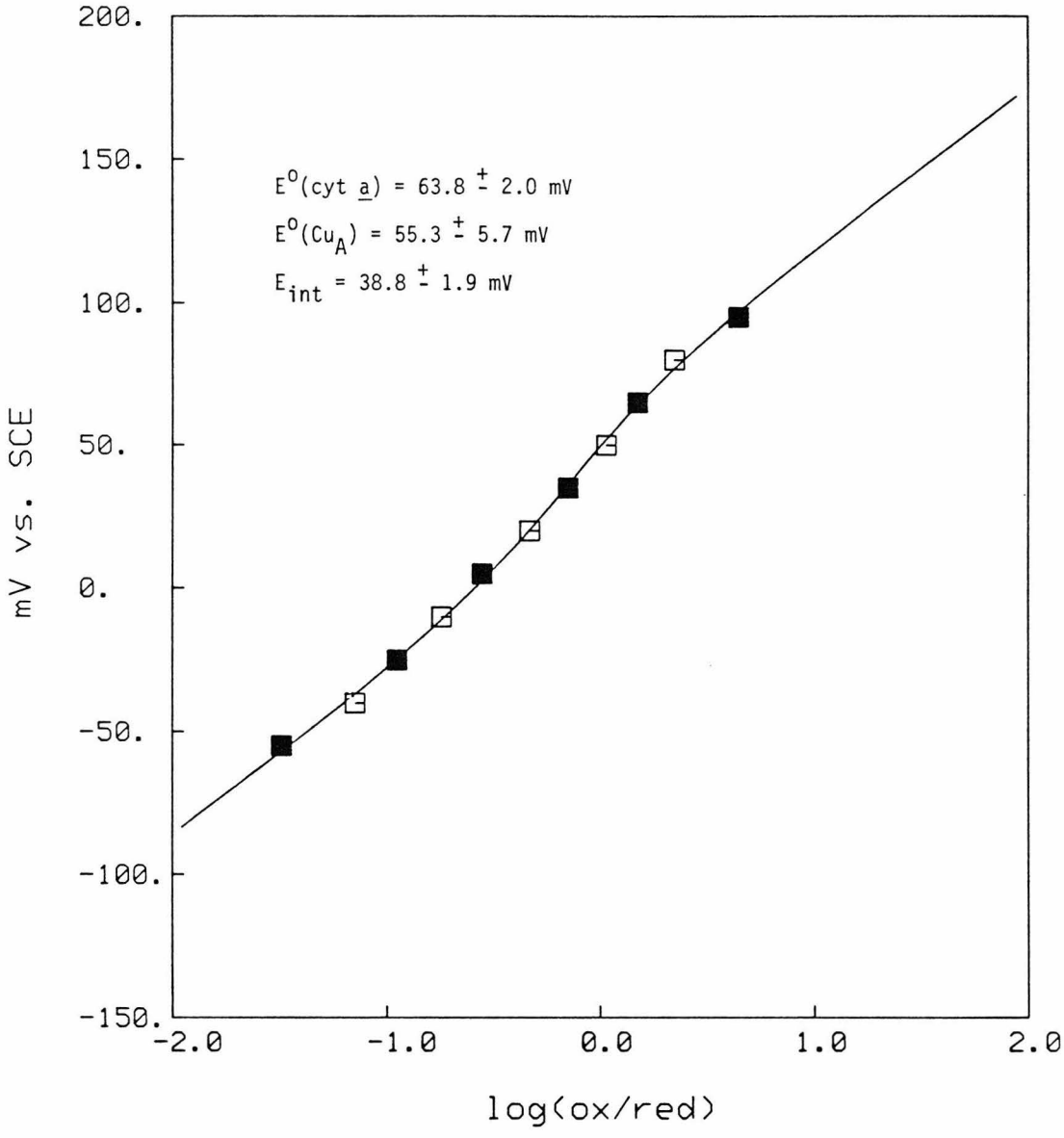
200.
150.
100.
50.
0.
-50.
-100.
-150.
mV vs. SCE
-2.0
-1.0
0.0
1.0
2.0
log(ox/red)
E°(cyt a) = 63.8 ± 2.0 mV
E°(Cu_A) = 55.3 ± 5.7 mV
E_int = 38.8 ± 1.9 mV

conditions (*cf.* Table 2), caused a large change in the structure of the Cu_A site.

A Nernst plot of the absorbance differences measured in the above Cu_A titration is shown in Figure 7. As expected, the plot did not follow $n = 1$ behavior. In addition, by inputting as $E_2^{\circ\prime}$ the reduction potential of cytochrome *a*, which was determined from the α band Nernst plot, the computer fit resolved an interaction potential of 41 mV and a Cu_A reduction potential of 319 mV vs. NHE, both in excellent agreement with the findings from the fit, in the α band region (*cf.*Table 2). Thus the investigation with a long-path cell provides solid evidence that cytochrome *a* and Cu_A interact with each other anticooperatively. Specifically, the reduction potential for one is lowered by approximately 40 mV upon the reduction of the other.

Thin-Layer Spectroelectrochemistry of Yeast Cytochrome a

Titration of CO-inhibited yeast cytochrome oxidase was carried out at 10°C between −250 and 190 mV vs. SCE. The absorption spectra were recorded in the 700–350 nm range, covering both the Soret and the α bands. However, the spectra measured between −250 and −80 mV turned out to be unsuitable for the study of cytochrome *a*. The difference spectra (reduced minus oxidized) of the absorption at succesive potentials in this range are displayed in Figure 8. Although these spectra are not well understood at this moment, they show quite clearly several species in the Soret region. At −200 mV vs. SCE (Figure 8a), the peak at 428 nm and the prominent trough at 416 nm are identified as associated with the low potential cytochrome *b*, for which the reduction potential was reported to be 30 mV vs. NHE at 25°C (33). Another peak at ~424 nm developed above −80 mV (Figure 8e,f), and its contribution to the titration at 441 nm is quite small. This band appeared to be a degraded form of cytochrome *a* and will be discussed in more detail later. The Soret band of

Figure 6. Near-infrared absorbance difference spectra obtained during a long-pathlength spectroelectrochemical titration of CO-inhibited beef heart cytochrome oxidase at 6°C. The indicated potentials are relative to SCE; all spectra are referenced to the spectrum of the fully reduced enzyme obtained at a potential of −200 mV. Sample conditions are as in Figure 4.

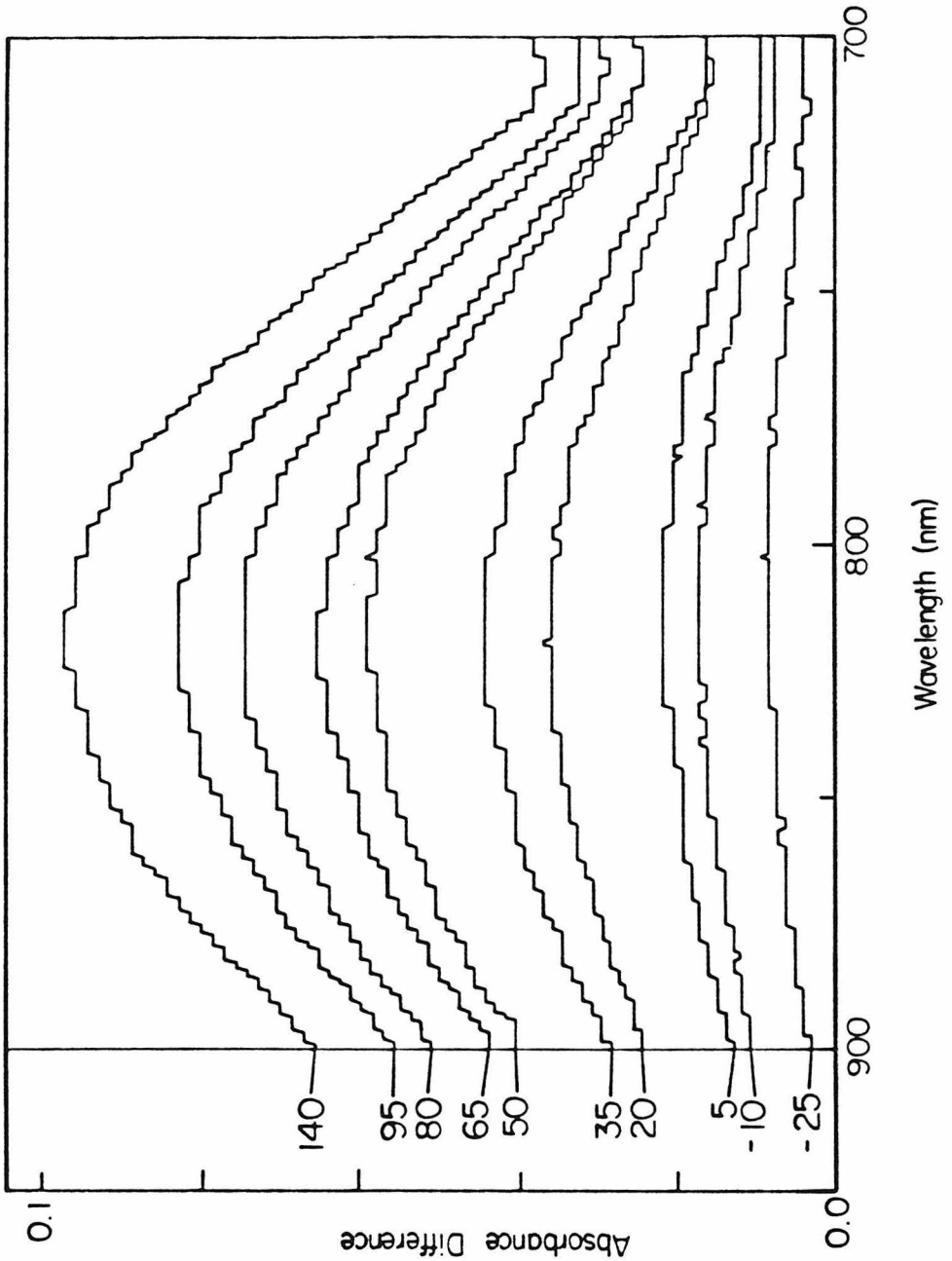
0.1
0.0
Absorbance Difference
140
95
80
65
50
35
20
5
-10
-25
900
800
700
Wavelength (nm)

Figure 7. Nernst plot calculated from the spectra shown in Figure 6. The intensity at 830 nm is quantitated according to the text. The solid line is the computer-generated best fit to the two-site interaction model. Solid squares and open squares correspond to spectra obtained during the oxidation and rereduction respectively.

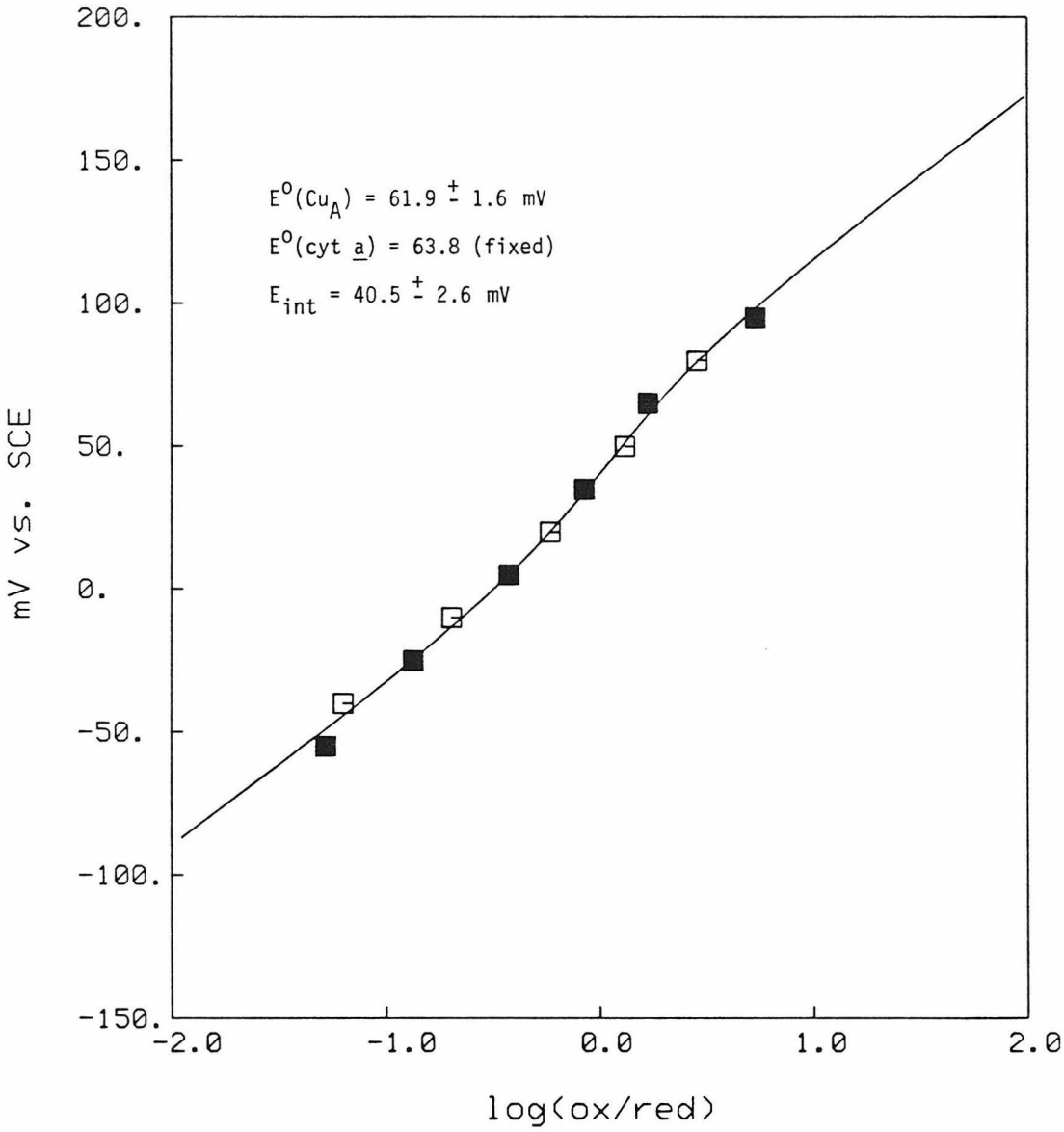
200.
150.
100.
50.
0.
-50.
-100.
-150.
-2.0
-1.0
0.0
1.0
2.0
mV vs. SCE
log(ox/red)
$E^o(Cu_A)$ = 61.9 ± 1.6 mV
E^o(cyt a) = 63.8 (fixed)
E_{int} = 40.5 ± 2.6 mV

the difference spectrum of beef heart cytochrome *a* peaks at 443 nm; in yeast it is normally around 441 nm. However, a band around 450 nm developed at −200 mV and went away above −80 mV. The α band associated with this Soret change is too small for it to be due to cytochrome *a*. The absorbance difference at 450 nm is roughly 5.5% of the total titrated difference at 441 nm. Most likely it is due to one of the high spin hemes usually observed in yeast oxidase preparations. EPR measurements show that it is 5–10% of the low-spin heme in typical enzyme preparations and cannot be reduced by β-nicotinamide adenine dinucleotide (NADH) and phenazine methosulfate (PMS) in 30 minutes at room temperature (spectra not shown).

Therefore the spectra recorded between −80 and 190 mV vs. SCE were used to investigate the redox properties of cytochrome *a*. The reduction at −80 mV turned out to be nearly complete because yeast cytochrome *a* has a reduction potential roughly 45 mV higher than that of beef heart cytochrome *a*. Linear relations between ΔA_{441} and ΔA_{602}, with a slope of 4.2 for the oxidative titration and 4.1 for the rereductive titration, were observed. They are not very different from measurements of the reduced minus oxidized spectrum of beef heart cytochrome *a*. The difference spectra obtained during the low-potential half and those during the high-potential half are displayed in Figure 9 for comparison. The high-potential half difference spectra showed a typical difference spectrum of cytochrome *a*, with a peak at 441.5 nm and a trough at 422.5 nm in the Soret region. The low-potential half, however, did not show any trough at all. On the other hand, the lineshape of the α band in both halves is very similar. The lineshape distortion in the Soret region is at least in part related to the ~424 cm^{-1} peak that was shown in Figure 8e,f. The cause of this band will become clear later on when we discuss the spectral features of the denatured enzyme after extended measurements. We should note, however, that the absorption of this species in the α band region is negligible. Details will be

Figure 8. Absorbance difference spectra at low potentials obtained during a thin-layer spectroelectrochemical titration of CO-inhibited yeast cytochrome oxidase. Sample conditions: pH 7.0, ionic strength 0.245 M, and temperature 10°C (SCE 10°C). Difference spectra were measured and calculated at succesive potentials: (a) −250 mV minus −200 mV, (b) −200 mV minus −160 mV, (c) −160 mV minus −120 mV, (d) −120 mV minus −80 mV, (e) −80 mV minus −50 mV, and (f) −50 mV minus −20 mV. All potentials are relative to SCE.

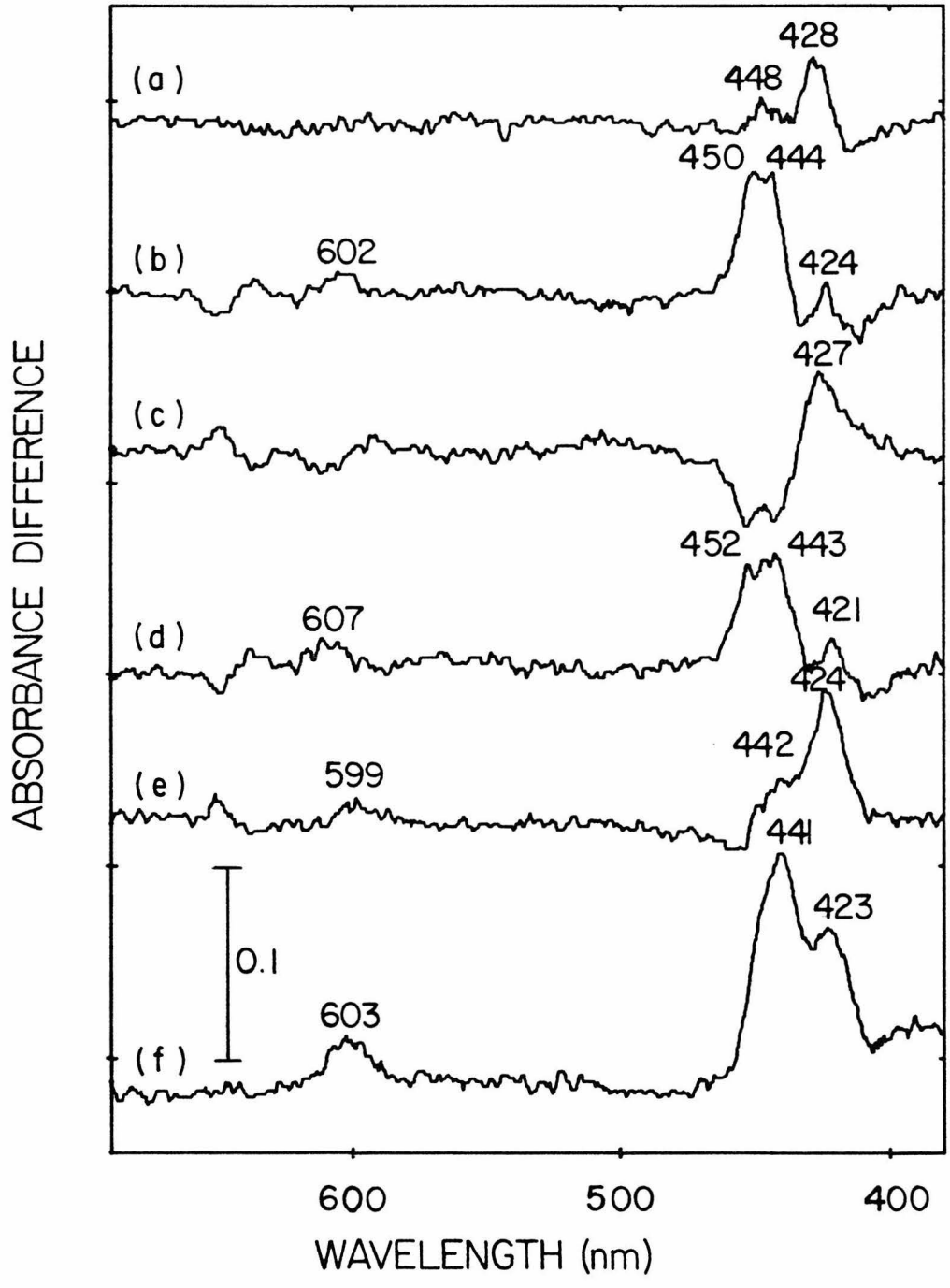
428
448
(a)
450
444
(b)
602
424
427
(c)
452
443
421
(d)
607
424
442
(e)
599
441
423
0.1
603
(f)
600
500
400
WAVELENGTH (nm)
ABSORBANCE DIFFERENCE

given later.

Because of the complication in the Soret region, the α band intensities at 602 nm were used. Overlay difference spectra are displayed in Figure 10; the oxidative and the rereductive titrations are plotted separately due to roughly 8% loss in the total absorbance after one cycle of oxido-reduction. The corresponding Nernst plot is displayed in Figure 11. Despite the loss in intensity, the titration was reasonably reversible. Once again, the data were well described by the two-site interaction model. The interaction potential determined from the fit was 42 mV, very similar to what is observed in the corresponding study of the beef heart enzyme. The reduction potential of cytochrome *a*, however, was roughly 45 mV higher than that in the beef heart enzyme at 10°C. Interestingly, the yeast Cu_A reduction potential, which was inferred from the computer fit, was very close to the cytochrome *a* reduction potential. Essentially equal reduction potentials for cytochrome *a* and Cu_A were also observed in the CO-inhibited beef heart enzyme.

An attempt was made to use the same sample for a few more experiments at various temperatures in order to measure the temperature dependence of the reduction potential of yeast cytochrome *a*. It was realized later that the structure of this metal center underwent significant changes and the data were disregarded for that purpose. The degraded material had a much lower reduction potential than cytochrome *a*, and no other new species were detected at the high-potential range. After a few cycles of oxido-reduction, the difference spectrum of the degraded material can be subtracted out from the absorption spectra measured at low potentials. It is shown in Figure 12. Its Soret band peaked at 428 nm and its α band was unrecognizable. From heme *a* model compound studies (34,35), it is known that the high-spin complexes have much smaller extinction coefficients at the α band than the low spin ones. This indicates that the denatured heme detected in spectroelectrochemistry is, in

Figure 9. Absorbance difference spectra that describe the low (a) and high (b) potential portions of spectroelectrochemical titrations of CO-inhibited yeast cytochrome oxidase. (a) Sample poised at −80 mV (versus SCE) minus sample poised at +70 mV; (b) Sample poised at +70 mV minus sample poised at +190 mV. Sample conditions: pH 7.0, ionic strength 0.245 M, temperature 10°C (SCE temperature 16°C).

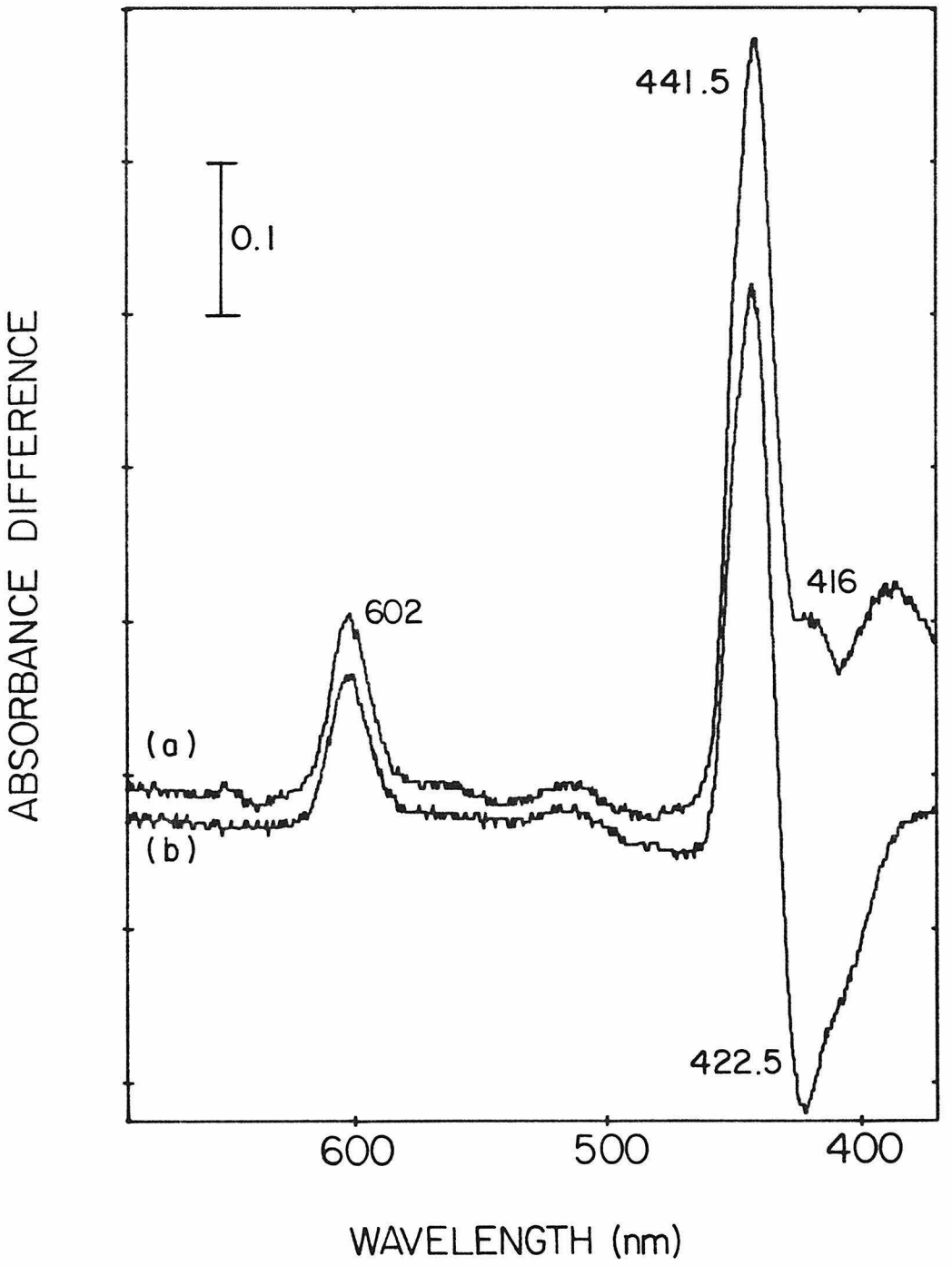
441.5
0.1
602
416
(a)
(b)
422.5
600
500
400
ABSORBANCE DIFFERENCE
WAVELENGTH (nm)

Figure 10. Absorbance difference spectra in the α band region obtained during a thin-layer spectroelectrochemical titration of carbon monoxide inhibited yeast cytochrome oxidase. (a) and (b) are spectra obtained during oxidation and rereduction respectively. The indicated potentials are relative to SCE; all spectra are referenced to the spectrum of the fully oxidized enzyme obtained at a potential of +190 mV. Sample conditions: pH 7.0, ionic strength 0.245 M, temperature 10°C (SCE temperature 16°C).

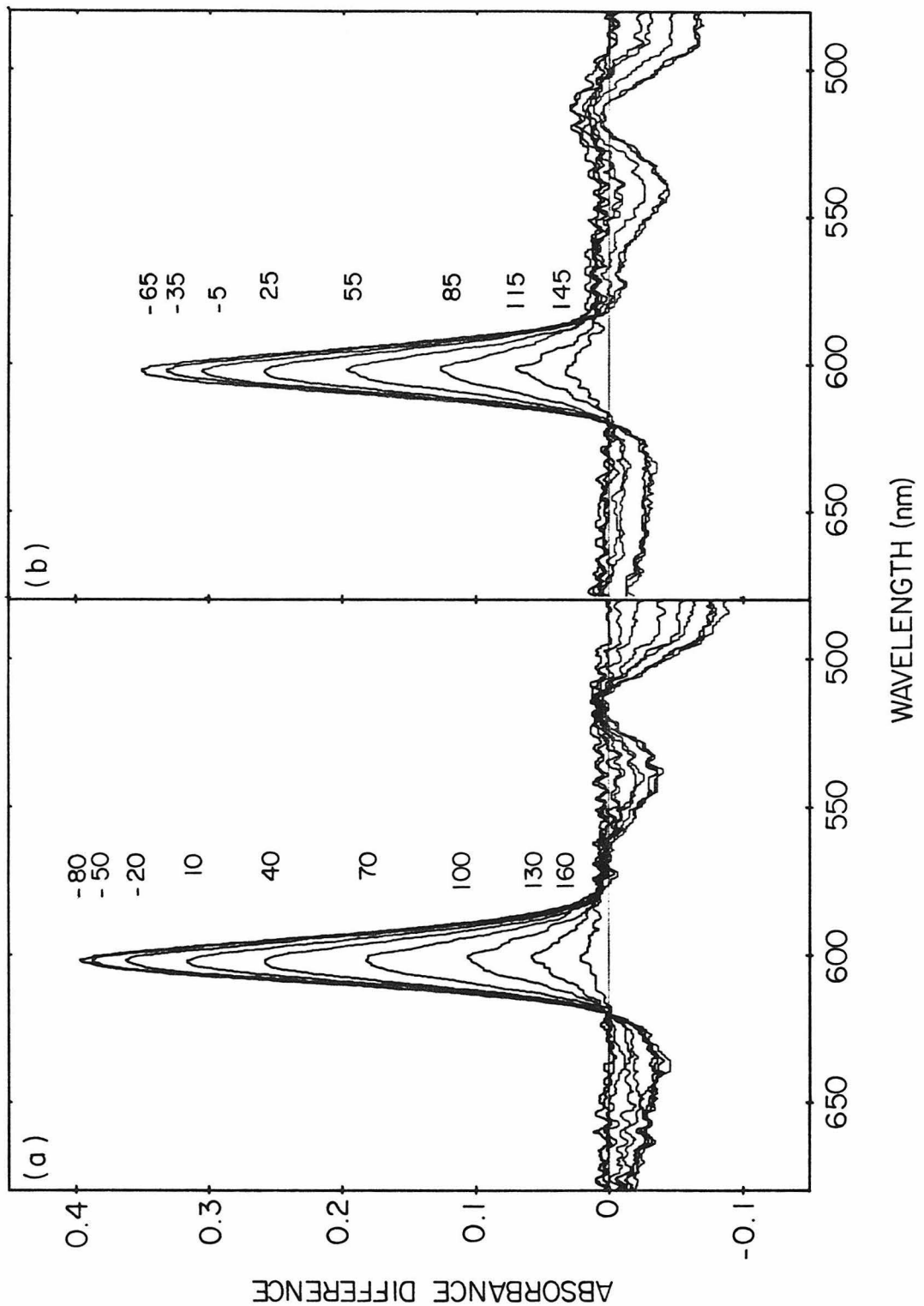
(a)
(b)
-80
-50
-20
10
40
70
100
130
160
-65
-35
-5
25
55
85
115
145
0.4
0.3
0.2
0.1
0
-0.1
500
550
600
650
ABSORBANCE DIFFERENCE
WAVELENGTH (nm)

Figure 11. Nernst plot calculated from the spectra shown in Figure 10 by using ΔA_{602}. The solid line is the computer-generated best fit to a model described in the text. Open squares and solid squares correspond to spectra obtained during the oxidation and rereduction respectively.

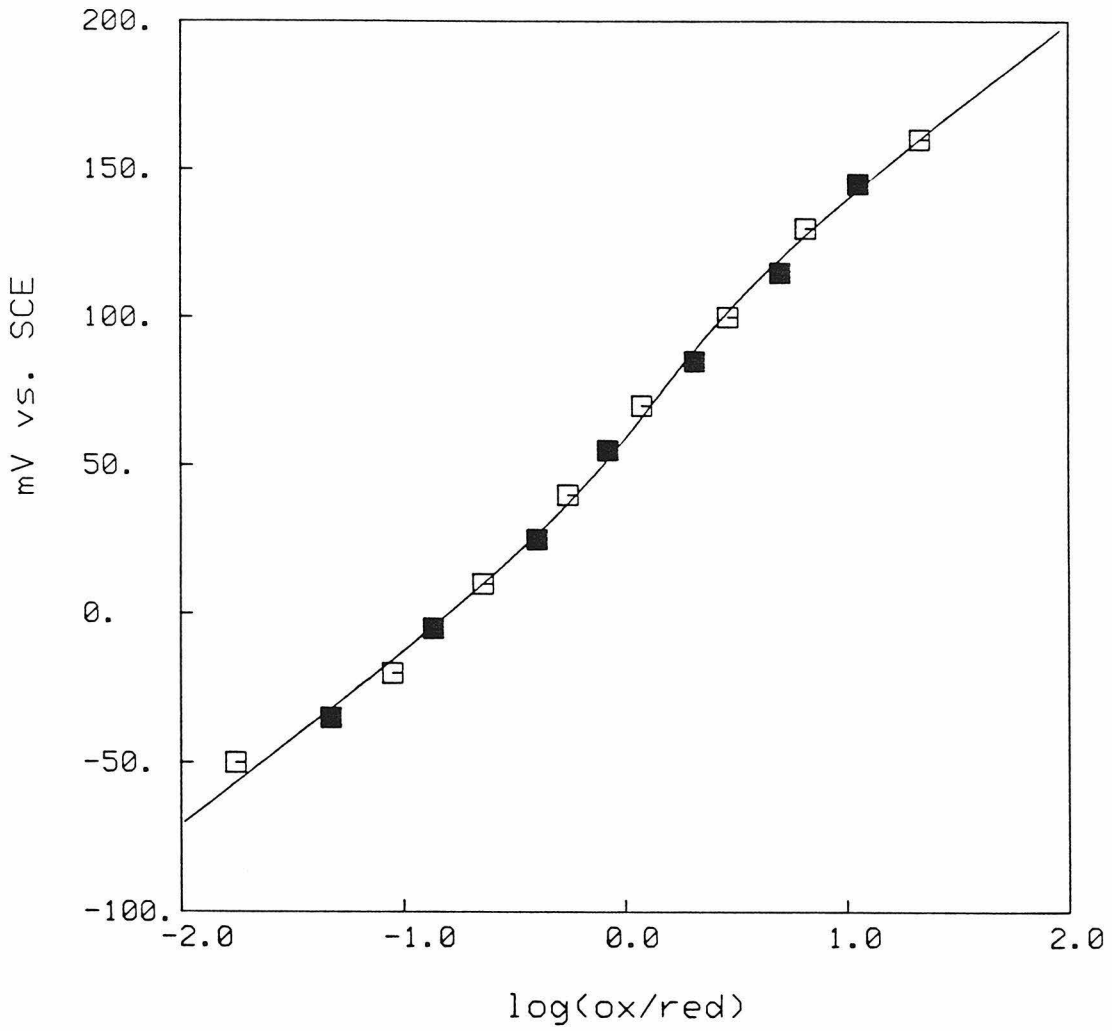
200.
150.
100.
50.
0.
-50.
-100.
mV vs. SCE
-2.0
-1.0
0.0
1.0
2.0
log(ox/red)

fact, a high-spin heme, which is a result totally consistent with the detection of high-spin ferrous ions in CO-bound reduced enzyme by Mössbauer spectroscopy (*cf.* Chapter 3). It also explains the absence of a trough at 422.5 nm in the low-potential half difference spectrum (Figure 9a). In the first cycle of the experiment, however, its contribution to the intensity at 602 nm would be negligible since the amount of this material is small. Therefore, this finding does not affect the reduction potential determination of yeast cytochrome *a*.

After the 5th day of experiments, the sample was poised at 190 mV for several hours and was taken out of the thin-layer cell to be measured by EPR spectroscopy. The EPR spectrum is displayed in Figure 13 along with a spectrum of a fresh, oxidized sample. Since the optical spectra suggested that the denatured heme in its reduced state is high spin, we expected a high-spin EPR signal when it is oxidized. Surprisingly, the $g = 6$ signal is quite small. The low-spin cytochrome a^{3+} signal at $g = 3$ was diminished and a broad low-spin signal appeared at $g = 2.9$. Therefore we must conclude that the denatured cytochrome *a* was in the low-spin state when oxidized but became high-spin when reduced. Much of the Cu_A also disintegrated into a tetragonal structure, as indicated by the axial signal at $g = 2.3$ and a hyperfine coupling of 140 Gauss that is typical of inorganic copper. This signal is identical to the so called 'adventitious' copper (*cf.* Chapter 1). Possibly part of this signal was contributed from the disintegrated Cu_B as well. These observations suggest that there is a global change on the structure of every metal center in the enzyme and that it may be the result of variation in the tertiary structure of the protein.

DISCUSSION

The Anticooperative Interaction between Cytochrome a and Cu_A

In the CO-inhibited cytochrome oxidase used in this study, only two of the four metal sites in the enzyme undergo oxidoreduction, so long as very highly

Figure 12. Absorbance difference spectrum of a degraded form of yeast cytochrome *a* at 10°C. Sample was as in Figure 10 but in its 4th cycle of oxidoreduction. Sample poised at −120 mV (versus SCE) was substracted from sample poised at −250 mV.

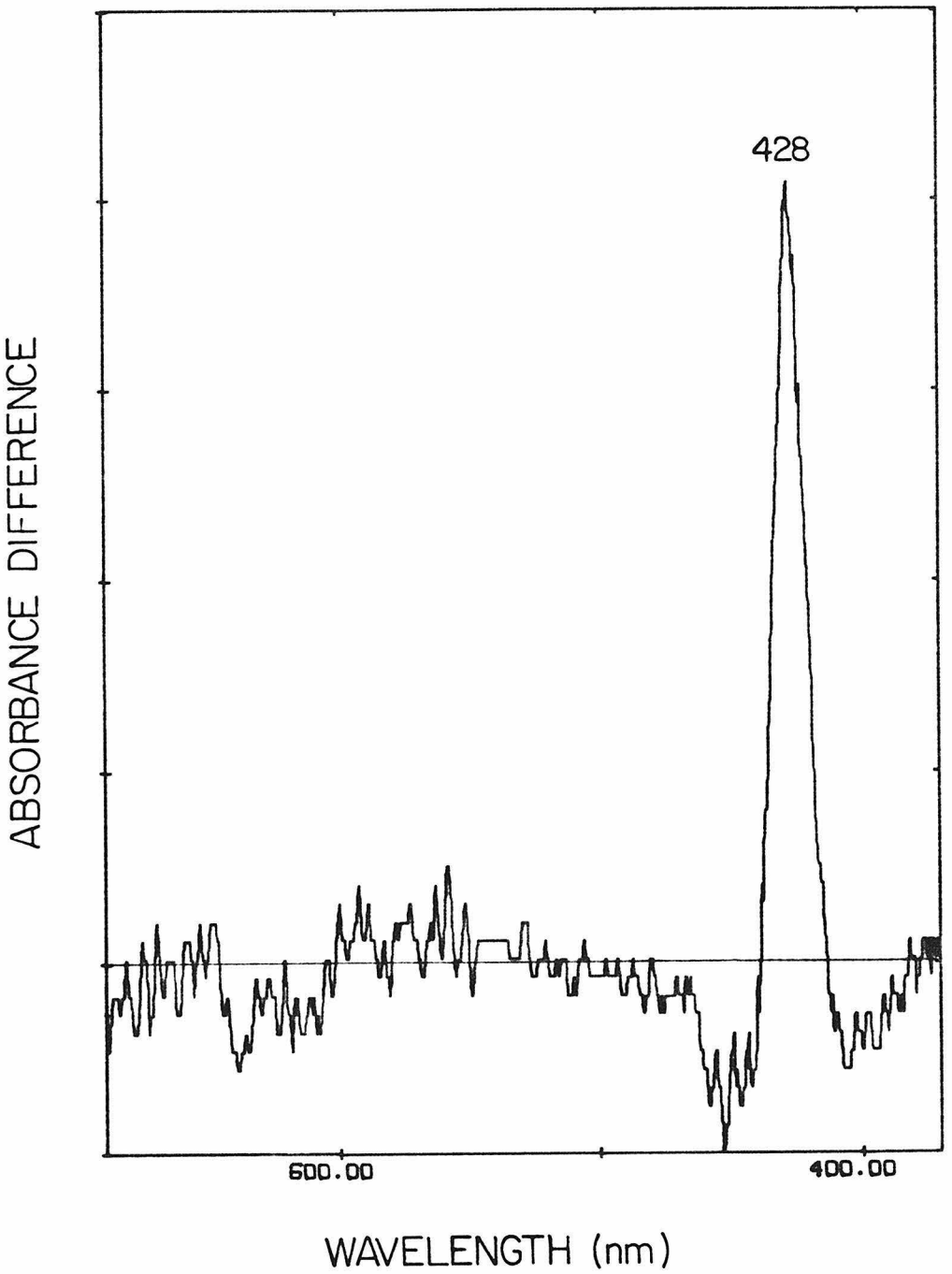
428
ABSORBANCE DIFFERENCE
600.00
400.00
WAVELENGTH (nm)

Figure 13. EPR spectrum of CO-inhibited yeast cytochrome oxidase after 4 cycles of spectroelectrochemical titration. The sample was poised at 190 mV for several hours before it was measured by EPR. Conditions for obtaining EPR spectrum were: temperature, 11 K; microwave power, 0.2 mW; gain, 8×10^3. The expanded inset around $g = 3$ was measured at 11 K, microwave power 5.0 mW and gain 5×10^3. The spectrum of a fresh sample is displayed in the dashed line. Conditions: temperature, 11 K; microwave power, 0.8 mW; gain, 6.3×10^3.

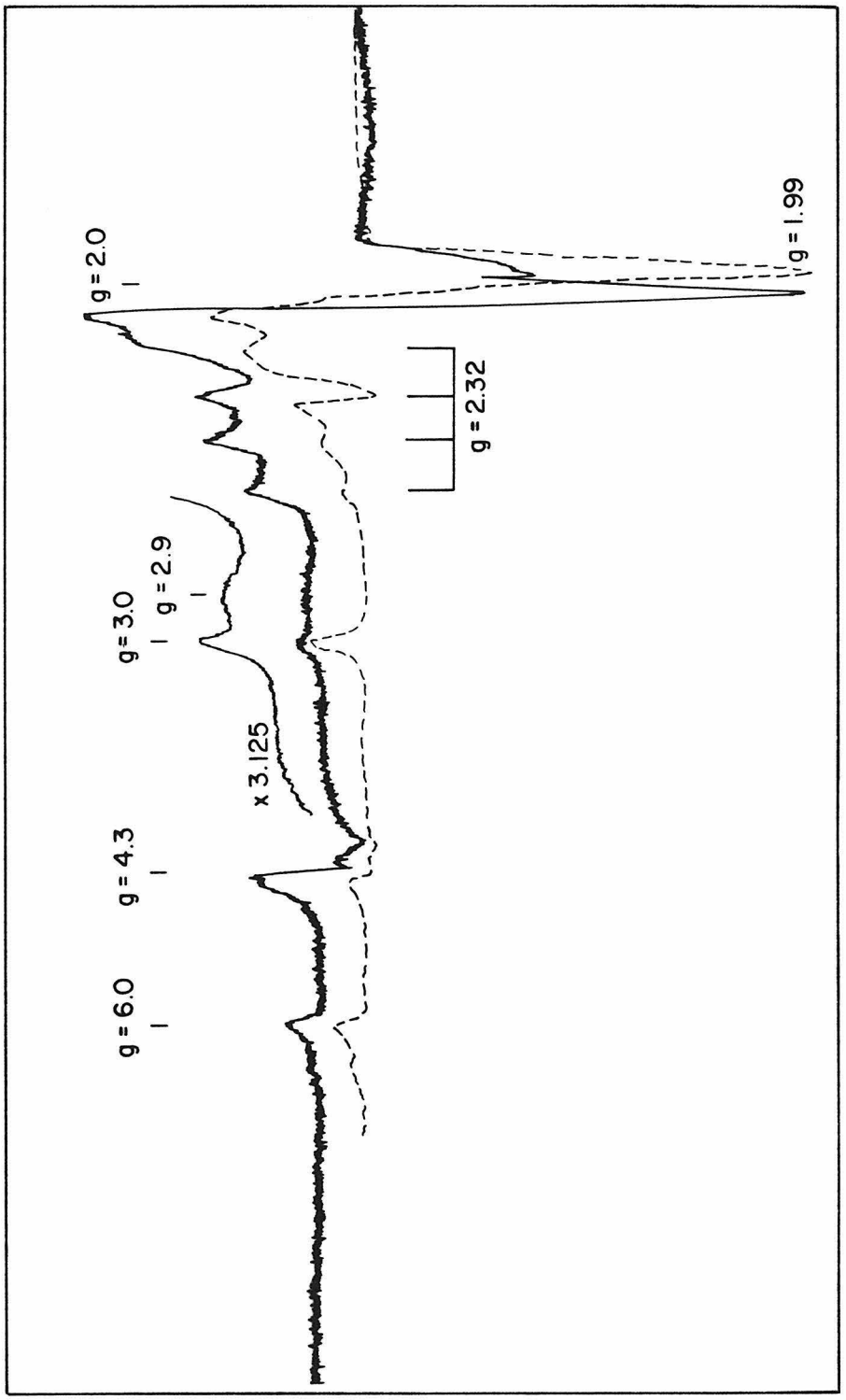
g = 2.0
g = 1.99
g = 2.32
g = 3.0
g = 2.9
x 3.125
g = 4.3
g = 6.0

oxidizing potentials are not reached (5,36). This system is well suited, because of its simplicity, to the study of interactions between these sites. Since cytochrome a_3 and Cu_B remain reduced during the course of these experiments, the slightly sigmoidal appearance and nonintegral slope of the data in Figure 3, 5, 7, and 11, if caused by intersite interaction, indicate that there is a previously unsuspected interaction between cytochrome *a* and Cu_A. Various alternatives to intramolecular site–site interactions may be proposed to explain these kinds of behavior, including electrostatic effects within a membrane-like aggregate (37) or intradimeric interactions (38). It is therefore important to test a particular interaction model in every way possible and to verify that the data are not systematically at variance with the predictions of the model. The data obtained in the long-path experiment are consistent with the proposed Fe_a/Cu_A interaction model in two key respects: first, the interaction potential ΔE inferred from the data on the iron site is the same, within experimental error, as that inferred from the data on the copper site; and second, the potentials of the copper site that are inferred from the computer fits to the iron data, while poorly determined by the fits and thus subject to considerable variation from one experiment to another, are in agreement with the Cu_A potentials determined directly from the copper data. Through the extensive study of beef heart cytochrome *a* using thin-layer spectroelectrochemistry, we found that the magnitude of the interaction was batch-dependent, but in the range from 20 to 40 mV. A similar magnitude of interaction between cytochrome *a* and Cu_A is also found for the yeast cytochrome oxidase (*cf.* Table 2).

The anticooperative interaction between cytochrome *a* and Cu_A could take place via either an electrostatic mechanism or a conformational mechanism. The electron spin relaxation study of Cu_A by Blair (19) suggested that the intersite distance is between 13 and 26 Å. Conceivably a 40-mV electrostatic interaction at this distance can be achieved if the dielectric constant for the

protein matrix is between 10 and 20. On the other hand, evidence of a conformational change is also present. The line shape of the Cu_A EPR resonance shows that one of its g values shifts slightly upon reduction of cytochrome a (39). This indicates that reduction of cytochrome a induces a minor structure change at the Cu_A site. Therefore neither mechanism can be ruled out completely as the cause of the anticooperative interaction. It is worth noting, however, that although the interaction potential measured in the yeast oxidase is of the same order as that in the beef heart enzyme, suggesting that the origin of this interaction is the same for both enzymes, the reduction potentials of cytochrome a and Cu_A in yeast oxidase are roughly 45 mV higher than those in beef heart oxidase. If the reduction potential is an indication of conformation difference, the constant interaction potential seems to favor the electrostatic mechanism.

The proposed redox interaction is likely to have implications for the behavior of the oxidase during turnover. The conventionally accepted electron transfer sequence from cytochrome c to dioxygen has been:

$$c \longrightarrow a \longrightarrow Cu_A \longrightarrow (a_3, Cu_B) \longrightarrow O_2. \qquad (5)$$

Because of the anticooperative interaction, cytochrome a and Cu_A will tend to accept only one electron between them, and it will be thermodynamically less likely for both sites to be reduced simultaneously. Previous reports (11,12) showed that the reduction potential of cytochrome a was substantially increased upon oxidation of Fe_{a_3}/Cu_B site. Our study on native beef heart enzyme (17) indicated that under such circumstances the reduction potential of cytochrome a increases to *ca.* 360 mV vs. NHE. On the other hand, no such interaction between Cu_A and the Fe_{a_3}/Cu_Bsite was inferred. Thus the effective reduction potential of cytochrome a will probably be significantly greater than that of Cu_A under turnover conditions (where the Fe_{a_3}/Cu_B site is mostly oxidized).

If electron transfer between cytochrome *a* and Cu_A is very fast, as is generally thought, these sites will be at redox equilibrium with each other. The equilibrium will be between the high-asymptotic reduction potentials of these sites, which is ~360 mV for cytochrome *a* versus ~285 mV for Cu_A in the case of beef heart enzyme. Thus we arrive at the conclusion that rapid electron transfer from cytochrome *a* to Cu_A is rather unfavorable and the equilibrium is not necessarily fast (40,41). The available kinetic data may be interpreted as well if it is postulated instead that Cu_A can accept electrons directly from cytochrome *c*. The presence of two different functional cytochrome *c* binding sites on the oxidase (42,43) and the proximity of Cu_A to residues that are involved in binding cytochrome *c* (44) are consistent with this proposal. We presented in Chapter 4 low temperature intermediate studies, which suggest that electrons can be transferred to the a_3 site from either cytochrome *a* or Cu_A. To summarize, the electron transfer scheme may thus be as follows,

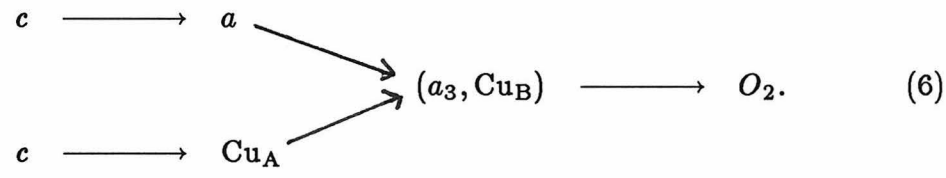

(6)

If electron transfer between cytochrome *a* and Cu_A is relatively slow, these two sites could each take on one of two different effective reduction potentials, depending upon the redox states of their respective interaction partners. In the reactant-pulse experiment, cytochrome *a* will be reduced first because it has a higher reduction potential. The pertinent reduction potential for Cu_A will be the lower asymptotic potential. On the other hand, in the mitochondrial steady state, where the metal centers are mostly oxidized, the higher of the two potentials measured here will most often be the pertinent one for both cytochrome *a* and Cu_A.

Comparison of Yeast and Beef Heart cytochrome a

Our measurement of the reduction potential of yeast cytochrome *a* represents the first quantitative effort to compare the redox properties of yeast and beef heart cytochrome oxidase. We employed CO to inhibit the a_3 site (the fact that CO reacts with the reduced form of both the high-spin and low-spin cytochrome a_3 was demonstrated in Chapter 3) in order to examine the reduction potential of cytochrome *a*. Yeast cytochrome *a* is found to have a reduction potential ~45 mV higher than that of beef heart cytochrome *a* at 10°C with the same pH and ionic strength. From Figures 9 & 10, it is clear that this potential is pertinent to the normal functioning cytochrome *a*. The same magnitude of the interaction potential between cytochrome *a* and Cu_A as that found for beef heart enzyme provides additional support for this suggestion. Considering that the homology of the three mitochondrially synthesized polypeptides (subunits I, II, & III) between beef heart and yeast enzyme is only 40% (45), we feel that a 45 mV difference in redox potential is not that surprising. It is frequently observed that analogous proteins from different organisms possess different reduction potentials; for example, the reduction potential of azurin from various sources varies from 230 to 308 mV vs. NHE (46).

Cytochrome *c*, the electron donor to cytochrome oxidase, on the other hand, does not exhibit such variability in reduction potential. Reduction potentials of cytochrome *c* isolated from yeast as well as from half a dozen other sources are reported to be around 260 mV vs. NHE (47). They also exhibit similar temperature-dependences. It may seem that the matching of reduction potentials for cytochrome *c* and cytochrome oxidase is less perfect in yeast than in beef heart. However, in the steady state in mitochondria, the pertinent reduction potential of beef heart cytochrome *a* is as high as 360 mV because of the interaction betweeen cytochrome *a* and a_3. In light of this, the 'mismatching' in yeast may not be severe.

The 'Inactive' Form of Yeast Cytochrome Oxidase

Before our study, Siedow *et al.* (48) reported that yeast cytochrome oxidase contained a fraction of reduced low-spin heme in the resting state without the presence of any exogenous or endogenous reductant. They thought the partial reduction was a consequence of a modification of cytochrome *a* leading to a substantial increase in its reduction potential. They suggested that the increased potential might constitute a block of electron transfer from *a* to a_3 to render the enzyme inactive, and this block of electron transfer was probably related to the well-known inactive species reported for beef heart cytochrome oxidase (49).

Our Mössbauer study (presented in Chapter 2) indicates, however, that the reduced heme, which is indeed low spin, results from a spin transition and autoreduction of cytochrome a_3. In this study, we examined carefully the high-potential spectra, including those measured after several cycles of oxidoreduction, and found no redox center with anomalously high reduction potential. On the contrary, as the enzyme became degraded after extensive titration, there was greater scattering in the Nernst plot, the interaction potential became ill-defined, and the overall reduction potential seemed to be lowered. All these phenomena were caused by the transition of some cytochrome *a* into low-potential redox sites. The heterogeneity of these low-potential sites are reflected by the extremely broad linewidth of the EPR band at $g = 2.9$, indicating a very wide distribution of crystal field splittings at these sites (50). Their reduction potentials are significantly lower than the normal yeast cytochrome *a* but cannot be measured precisely in this experiment. EPR measurement indicates that these sites are still low-spin hemes and also reveals substantial damage at the Cu_A (may be Cu_B also) site.

Taken together, the Mössbauer and spectroelectrochemical studies suggest the following description for the denaturation of yeast cytochrome oxidase: the

enzyme undergoes a conformation change that affects all metal centers. The reduction potentials of cytochrome *a* and Cu_A become too low for electrons to transfer from cytochrome *c* to cytochrome oxidase. On the other side of the enzyme, the cytochrome a_3/Cu_B site probably disrupts, and cytochrome a_3 is transformed into a reduced low-spin form. Presumably cytochrome a_3 has become six-coordinated and it no longer reduces dioxygen.

Whether these results bear on the inactivation of the beef heart enzyme is unclear. Vanneste and other researchers (49) detected the inactivation of the beef heart enzyme during steady-state turnover studies; unfortunately no absolute spectra are available for comparison. Partial reduction is often found in beef heart enzyme preparations, judging from the slightly higher α band than β band. Moreover, Lemberg (51) showed that, in some preparations, the beef heart enzyme contained a percentage of a heme that is not readily reduced, so that a shoulder remained in the region of 418-424 nm. Similar shoulders have been observed in some of our yeast oxidase preparations when reduced by ascorbate/PPD or NADH/PMS (data not shown). Interestingly, the inactive species was thought to be related to Vanneste's finding that, in the purified enzyme, less than 50% of the hemes reacted with CO (52). On the other hand, Van Gelder and Muijsers (53) thought that half of the 'hard to reduce' cytochrome oxidase could still react with CO. It is conceivable that the low-spin cytochrome a_3 (denatured heme) reacts with CO at a slower rate than the high-spin cytochrome a_3 because the former is six-coordinated. These observations about the beef heart enzyme seem understandable in terms of the proposed inactivation process for yeast cytochrome oxidase: in the damaged enzyme molecule, cytochrome *a* is not readily reduced; when eventually reduced by a strong reductant such as dithionite, the intensity increase is likely to be around 428 nm instead of 443 nm as Figure 12 suggests, while a concomitant conformational transition around a_3 site forces cytochrome a_3 to become low

spin and reduced, with a different reactivity towards CO than in the case of the normal enzyme.

Partial reduction of the resting enzyme was previously attributed to the low-spin cytochrome *a*, determined from the absorbance changes at 605 & 443 nm. Indeed, for the normal functioning enzyme, cytochrome *a* contributes most of the intensity at 605 nm, and both hemes share the intensity at 443 nm fairly equally (18,29). The degraded cytochrome a_3, however, becomes low spin and contributes to the 605 nm band significantly. The denatured cytochrome *a*, on the other hand, exhibits a very different spectrum in the Soret region from the normal ones. Using these spectroscopic criteria to determine the nature of the inactive material may therefore lead to misleading or erroneous conclusions.

REFERENCES

1. Minnaert, K. (1965). *Biochim. Biophys. Acta* **110**, 42–56.
2. Hinkle, P., & Mitchell, P. (1970). *J. Bioenerget.* **1**, 45–60.
3. Heineman, W.R., Kuwana, T., & Hartzell, C.R. (1972). *Biochem. Biophys. Res. Comm.* **49**, 1–8.
4. Vanderkooi, J., & Erecińska, M. (1974). *Arch. Biochem. Biophys.* **162**, 385–391.
5. Anderson, J.L., Kuwana, T., & Hartzell, C.R. (1976). *Biochemistry* **15**, 3847–3855.
6. Schroedl, N.A., & Hartzell, C.R. (1977). *Biochemistry* **16**, 4961–4965.
7. Schroedl, N.A., & Hartzell, C.R. (1977). *Biochemistry* **16**, 4966–4971.
8. Babcock, G.T., Vickery, L.E., & Palmer, G. (1978). *J. Biol. Chem.* **253**, 2400–2411.
9. Artzatbanov, V.Y., Konstantinov, A.A., & Skulachev, V.P. (1978). *FEBS Lett.* **87**, 180–185.
10. Carithers, R.P., & Palmer, G. (1981). *J. Biol. Chem.* **256**, 7967–7976.
11. Kojima, I., & Palmer, G. (1983). *J. Biol. Chem.* **258**, 14908–14913.
12. Goodman, G. (1984). *J. Biol. Chem.* **259**, 15094–15099.
13. Malmström, B.G. (1974). *Quart. Rev. Biophys.* **6**, 389–431.
14. Wikström, M.K.F., Harmon, H.J., Ingledew, W.J., & Chance, B. (1976). *FEBS Lett.* **65**, 259–277.
15. Ellis, W.R., Jr., Wang, H., Blair, D.F., Gray, H.B., & Chan, S.I. (1986). *Biochemistry* **25** 161–167.
16. Wang, H., Blair, D.F., Ellis, W.R., Jr., Gray, H.B., & Chan, S.I. (1986). *Biochemistry* **25** 167–171.
17. Blair, D.F., Ellis, W.R., Jr., Wang, H., Gray, H.B., & Chan, S.I. (1986). *J. Biol. Chem.* , 11524–11537.

18. Blair, D.F., Bocian, D.F., Babcock, G.T., & Chan, S.I. (1982). *Biochemistry* **21**, 6928–6935.

19. Blair, D.F. (1985). Ph.D. Thesis, California Institute of Technology.

20. Ellis, Jr., W.R. (1986). Ph.D. Thesis, California Institute of Technology.

21. Hartzell, C.R., & Beinert, H. (1974). *Biochim. Biophys. Acta* **368**, 318–338.

22. Lowry, O.H., Rosebrough, N.J., Farr, A.L., & Randall, R.J. (1951). *J. Biol. Chem.* **193**, 265–275.

23. van Gelder, B.F. & Slater, E.C. (1963). *Biochim. Biophys. Acta* **73**, 663–665.

24. van Gelder, B.F. (1966). *Biochim. Biophys. Acta* **118**, 36–46.

25. Pladziewicz, J.R., Meyer, T.J., Broomhead, S.A. & Taube, H. (1973). *Inorg. Chem.* **12**, 639–643.

26. Cummins, D., & Gray, H.B. (1977). *J. Am. Chem. Soc.* **99**, 5158–5167.

27. Taniguchi, V.T., Ellis, W.R., Jr., Cammarata, V., Webb, J., Anson, F.C., & Gray, H.B. (1982). In *Electrochemical and Spectrochemical Studies of Biological Redox Components* (Kadish, K.M., ed.), pp 51–68. American Chemical Society Advances in Chemistry Series No. 201, Washington, D.C.

28. Ives, D.J.G., & Janz, G.J. (1961). In *Reference Electrodes*, Academic Press, New York, p. 161.

28. Cornish-Bowden, A., & Koshland, D.E., Jr. (1975). *J. Mol. Biol.* **95**, 201–212.

30. Vanneste, W.H., & Vanneste, M.-T. (1965). *Biochem. Biophys. Res. Commun.* **19**, 182–186.

31. Beinert, H., Shaw, R.W., Hansen, R.E., & Hartzell, C.R. (1980). *Biochim. Biophys. Acta* **591**, 458–470.

32. Blair, D.F., Martin, C.T., Gelles, J., Wang, H., Brudvig, G.W., Stevens, T.H., & Chan, S.I. (1983). *Chemica Scripta* **21**, 43–53.

33. Hall, D.O., Rao, K.K., & Cammack, R. (1975). *Sci. Prog. Oxf.* **62**,

285–317.

34. van Steelandt-Frentrup, J., Salmeen, I., & Babcock, G.T. (1981). *J. Amer. Chem. Soc.* **103**, 5981–5982.
35. Carter, K. & Palmer, G. (1982). *J. Biol. Chem.* **257**, 13507–13514.
36. Wilson, D.F., & Nelson, D. (1982). *Biochim. Biophys. Acta* **680**, 233–241.
37. Walz, D. (1979). *Biochim. Biophys. Acta* **505**, 279–353.
38. Wikström, M., Krab, K., & Saraste, M. (1981). *Cytochrome Oxidase: A Synthesis*, Academic Press, London.
39. Brudvig, G.W., Blair, D.F., & Chan, S.I. (1984). *J. Biol. Chem.* **259**, 11001–11009.
40. Antalis, T.M., & Palmer, G. (1982). *J. Biol. Chem.* **257**, 6194–6206.
41. Wilson, M.T., Greenwood, C., Brunori, M., & Antonini, E. (1975). *Biochem. J.* **147**, 145–153.
42. Ferguson-Miller, S., Brautigan, D.L., & Margoliash, E. (1976). *J. Biol. Chem.* **251**, 1104–1115.
43. Wilms, J., Veerman, E.C.I., Konig, B.W., Dekker, H.L., & van Gelder, B.F. (1981). *Biochim. Biophys. Acta* **635**, 13–24.
44. Millett, F., Darley-Usmar, V.M., & Capaldi, R.A. (1982). *Biochemistry* **21**, 3857–3862.
45. Poyton, R.O. (1980). *Curr. Top. Cell. Regul.* **7**, 231–295.
46. Ainscough, E.W., Bingham, A.G., Brodie, A.M., Ellis, W.R., Jr., Gray, H.B., Loehr, T.M., Plowman, J.E., Norris, G.E., & Baker, E.N., submitted for publication.
47. Taniguchi, V.T., Sailasuta-Scott, N., Anson, F.C., & Gray, H.B. (1980). *Pure and Applied Chem.* **52**, 2275–2281.
48. Siedow, J.N., Miller, S., & Palmer, G. (1981). *J. Bioenerg. and Biomem.* **13** 171–179.
49. Vanneste, W.H., Ysebaert-Vanneste, M., & Mason, H.S. (1974). *J. Biol.*

Chem. **249**, 7390–7401.

50. Castner, T.G., Jr. (1959). *physiol. Rev.* Series 2, **115**, 1506-1515.
51. Lemberg, M.R. (1969). *Physiol. Rev.* **49**, 48–121.
52. Vanneste, H. (1966). *Biochemistry* **5**, 838–848.
53. van Gelder, B.F. & Muijsers (1966). *Biochim. Biophys. Acta* **118**, 47–57.

CONCLUSIONS

The incorporation of ^{57}Fe into the wild-type baker's yeast *Saccharomyces cerevisiae* made possible the study of the iron centers in cytochrome oxidase by Mössbauer spectroscopy. Through computer simulation, the spectral features of cytochrome *a* in the resting oxidized enzyme are resolved from the the rest of the spectrum. It is consistent with the picture of a low-spin heme in both the oxidized and reduced states. The simulation described the spectra of several samples quite well, although slight variations are observed, which suggest the presence of minor heterogeneity at this site.

On the other hand, at least three components were identified for cytochrome a_3 in the resting oxidized enzyme by Mössbauer spectroscopy: a functional coupled site, a high-spin ferric ion with the antiferromagnetic coupling between cytochrome a_3 and Cu_B disrupted, and a low-spin ferrous ion. The reduced heme is pobably a denatured form of cytochrome a_3. Yet it exists even in mitochondrial particles (1) and is probably intrinsic to yeast cells. The heterogeneity at the a_3 site was also revealed by flash photolysis experiments, which detected two cytochrome a_3 sites that exhibited drastically different CO-recombination behaviors. One site displayed a slow CO-rebinding process, which follows the Arrhenius behavior with an activation energy of 33 kJ/mol from 270 K to 160 K. This re-

sult is very similar to that observed in beef heart oxidase (2,3). As was pointed out by Fiamingo *et al.* (3), the large activation enthalpy is due to CO-ligation to Cu_B after CO is flashed off from cytochrome a_3. Therefore in the functional cytochrome oxidase, cytochrome a_3 and Cu_B are probably situated in the same pocket as illustrated in Scheme 1. The other site displayed a fast recombination kinetics and is related to the reduced low-spin heme that was detected in the resting oxidized enzyme by Mössbauer spectroscopy. The high-spin, uncoupled ferric hemes, apart from its low concentration (typically $< 5\%$ of the total iron), have relatively low redox potential and are not bound by CO. Therefore it was not detected by the CO-recombination studies.

The possibility that the functional cytochrome a_3 in the resting state is a ferryl ion as proposed by Seiter & Angelos (4) is dismissed on the ground of Mössbauer parameters. The spectral features of the coupled a_3 site indicate that a significant internal field is induced in the ground state by a small magnetic field. This cannot be explained by the Griffith model (5,6), which describes the widely accepted spin-coupling hypothesis. On the other hand, if a small, positive zero-field parameter D is assumed for the coupled $S = 2$ state, significant broadening in the simulated spectrum can be induced under a small field. Other researchers have also suggested a small D for this system (7,8). The small D model contradicts the current theory (the Griffith model) of the spin-coupling at the a_3 site, which derives the zero-field structure of the coupled a_3 site from that of the uncoupled cytochrome a_3. It is argued that the bridging ligand would have an additional chemical effect on the zero-field structure of cytochrome a_3 other than from the superexchange coupling. Therefore a small D is plausible. This approach was tested with an intermediate relaxation rate simulation program. The result is promising, although no satisfactory simulation has been obtained so far. Clearly it should be pursued further.

The spectrum of coupled cytochrome a_3 was also tested by other approaches.

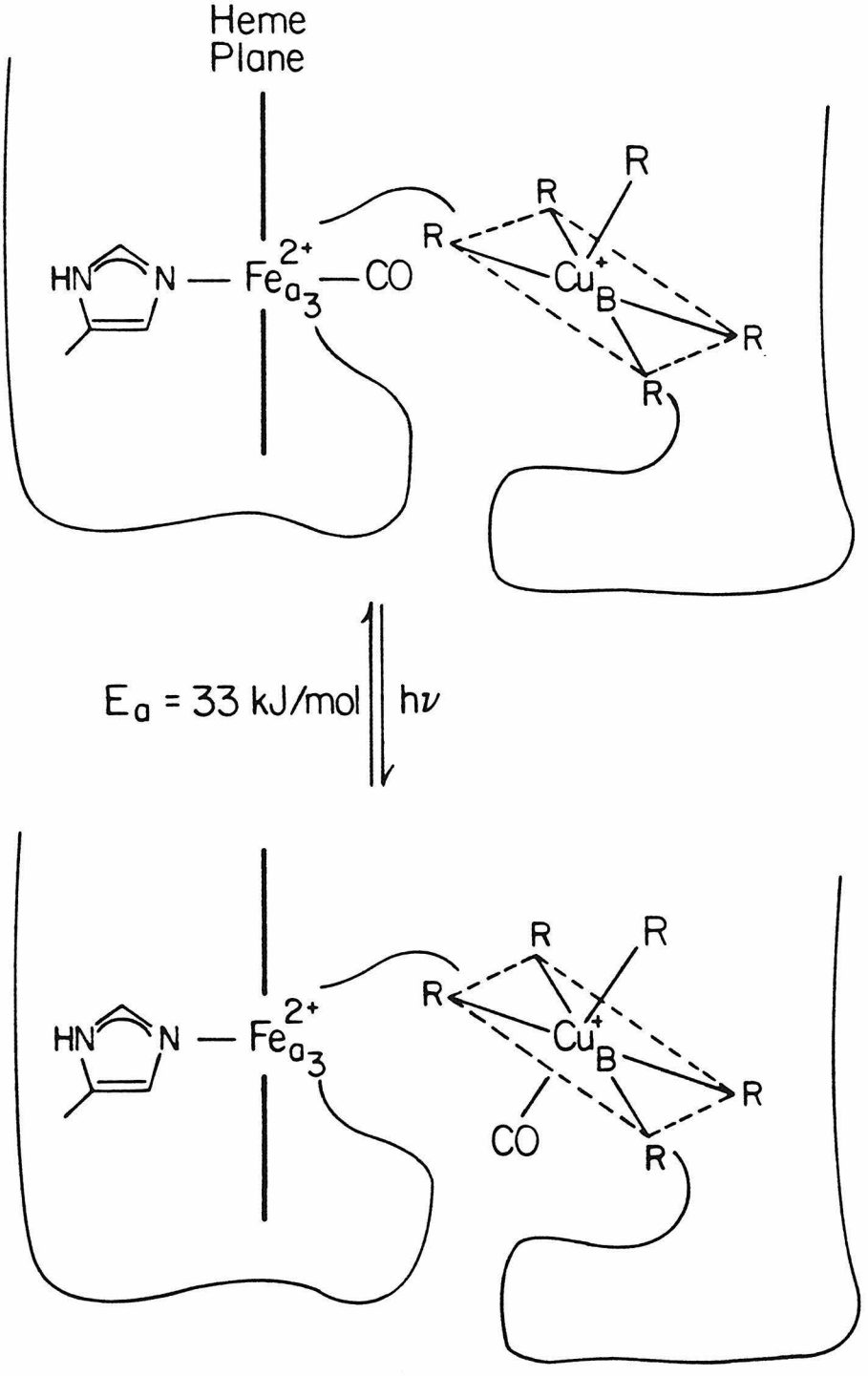

SCHEME 1

The negative D hypothesis is regarded as unlikely since it requires a very high rhombicity that has not been reported for hemeproteins. The potential of utilizing weak exchange to explain the spectra of oxidized cytochrome a_3 is demonstrated.

The reduced low-spin cytochrome a_3 that was detected in the resting oxidized yeast enzyme has exactly the same Mössbauer parameters as those for the reduced cytochrome *a*. This implies that the axial ligands of this cytochrome a_3 are probably also two histidines. Both Mössbauer and photolysis experiments indicate that this heme reacts with CO. The CO-recombination time at this site is in the order of msec at 120 K. The peak activation energy for this process is estimated to be 13 kJ/mol, not very different from that observed in myoglobin (9). This fast CO-recombination process is depicted in Scheme 2. In this denatured form of a_3 site, cytochrome a_3 and Cu_B are in separate pockets. (The redox potential of this Cu_B seems to be very low, as judged from EPR studies.) In this configuration, when CO is flashed off cytochrome a_3, the rebinding rate is very fast because CO is trapped in the iron pocket, possibly by histidine residue as was suggested for myoglobin (10).

The detection of the reduced material in the native enzyme by Mössbauer spectroscopy is the first direct evidence of such an inactive species in yeast cytochrome oxidase. Our results are in agreement with the results of a previous report by Siedow *et al.* (1) but argue forcibly against its being cytochrome *a*. It was thought previously that the denatured cytochrome *a* has a rather high redox potential that renders the enzyme inactive. Our spectroelectrochemical study on the CO-inhibited enzyme indicates, however, that the denatured cytochrome *a* exhibits a redox potential too low to accept electrons from cytochrome *c*. On the other hand, the normal functional cytochrome *a* has a redox potential roughly 45 mV higher than that of beef heart cytochrome *a*. The titrations of normal cytochrome *a* in both enzymes are well-described by a 2-site interaction model,

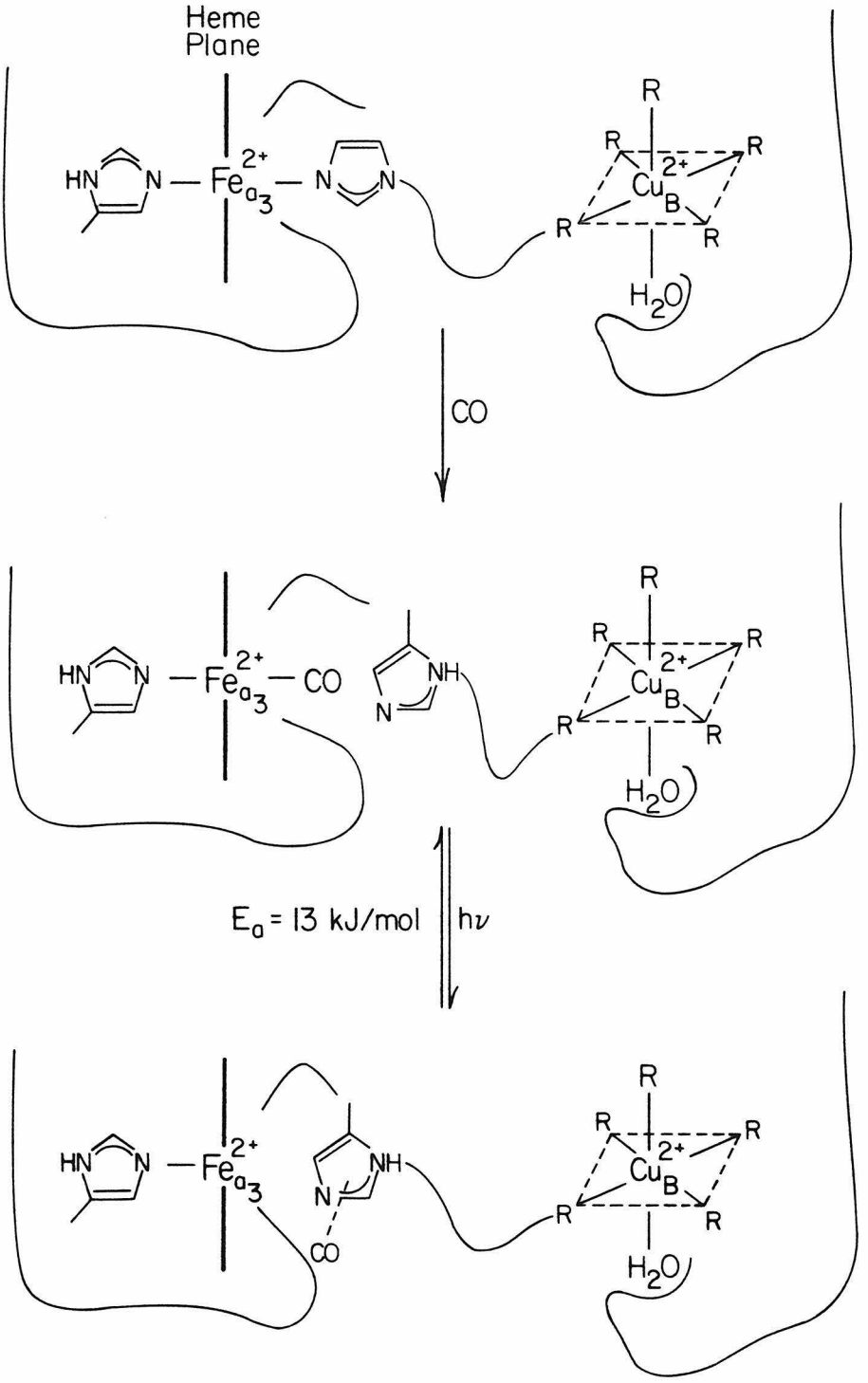
Heme
Plane
HN
N
Fe$_{a_3}^{2+}$
N
N
R
R
R
2+
Cu$_B$
R
R
H$_2$O
CO
HN
N
Fe$_{a_3}^{2+}$
CO
NH
N
R
R
R
2+
Cu$_B$
R
R
H$_2$O
E$_a$ = 13 kJ/mol
hν
HN
N
Fe$_{a_3}^{2+}$
NH
N
CO
R
R
R
2+
Cu$_B$
R
R
H$_2$O

SCHEME 2

which indicates a 40 mV interaction potential between cytochrome *a* and Cu_A.

Despite the presence of inactive materials and other minor contaminants in the yeast enzyme, a substantial amount of an 'unusual' copper EPR signal was produced using the 'triple-trapping' technique (11). This signal is associated with a reaction intermediate, which has the third elctron transferred from either cytochrome *a* or Cu_A to the oxygen binding site. The reoxidation course was followed by monitoring the EPR intensity of the cytochrome *a*, Cu_A, and the 'unusual' Cu_B signals. The present study of yeast oxidase agrees with the conclusions of previous studies on the beef heart enzyme (12,13) that, at the early stage of reoxidation, the reaction takes place via a 3-level, 4-intermediate mechanism. It also confirms the existence of two '$3e^-$-reduced' intermediates at the oxygen binding site. Therefore yeast cytochrome oxidase provided a unique opportunity to test the proposed structures for the intermediates by Mössbauer spectroscopy. A few intermediates are suggested by a preliminary Mössbauer study, which demonstrates a great potential in understanding the reoxidation mechanism of cytochrome oxidase.

REFERENCES

1. Siedow, J.N., Miller, S., and Palmer, G. (1981). *J. Bioenerg. Biomemb* **13** 171-179.
2. Sharrock, M. & Yonetani, T. (1977). *Biochim. Biophys. Acta* **462**, 718–730.
3. Fiamingo, F.G., Altschuld, R.A., Moh, P.P., & Alben, J.O. (1982). *J. Biol. Chem.* **257**, 1639–1650.
4. Seiter, C.H.A. & Angelos, S.G. (1980). *Proc. Nat. Acad. Sci., U.S.A.* **77**, 1806–1808.
5. Griffith, J.S. (1971). *Mol. Phys.* **21**, 141–143.
6. Buluggiu, E. (1980). *J. Phys. Chem. Solids* **41**, 43–45.
7. Hagen, W.R. (1982). *Biochim. Biophys. Acta* **708**, 82-98.
8. Dunham, W.R., Sands, R.H., Shaw, R.W., & Beinert, H. (1983). *Biochim. Biophys. Acta* **748**, 73–85.
9. Alberding, N., Austin, R.H., Chan, S.S., Eisenstein, L., Frauenfelder, H., Gunsalus, I.C., & Nordlund, T.M. (1976). *J. Chem. Phys.* **65**, 4701–4711.
10. Austin, R.H., Beeson, K.W., Eisenstein, L., Frauenfelder, H., & Gunsalus, I.C. (1975). *Biochemistry* **14**, 5355–5373.
11. Chance, B., Saronio, C., & Leigh, J.S., Jr. (1975). *J. Biol. Chem.* **250**, 9226–9237.
12. Clore, G.M., Andreasson, L.E., Karlsson, B., Aasa, R., & Malmstrom, B.G. (1980). *Biochem. J.* **185**, 139–154.
13. Blair, D.F., Witt, S.N., & Chan, S.I. (1985). *J. Amer. Chem. Soc.* **107**, 7389–7399.